REGULATION OF PROTEOLYSIS AND PROTEOME COMPOSITION IN PLANT RESPONSE TO ENVIRONMENTAL STRESS

EDITED BY: Mateusz Labudda, Zhiping Deng, Shaojun Dai and Ling Li

PUBLISHED IN: Frontiers in Plant Science

frontiers Research Topics

frontiers

ISSN 1664-8714
ISBN 978-2-83250-897-8
DOI 10.3389/978-2-83250-897-8

About Frontiers

Frontiers is more than just an open-access publisher of scholarly articles: it is a pioneering approach to the world of academia, radically improving the way scholarly research is managed. The grand vision of Frontiers is a world where all people have an equal opportunity to seek, share and generate knowledge. Frontiers provides immediate and permanent online open access to all its publications, but this alone is not enough to realize our grand goals.

Frontiers Journal Series

The Frontiers Journal Series is a multi-tier and interdisciplinary set of open-access, online journals, promising a paradigm shift from the current review, selection and dissemination processes in academic publishing. All Frontiers journals are driven by researchers for researchers; therefore, they constitute a service to the scholarly community. At the same time, the Frontiers Journal Series operates on a revolutionary invention, the tiered publishing system, initially addressing specific communities of scholars, and gradually climbing up to broader public understanding, thus serving the interests of the lay society, too.

Dedication to Quality

Each Frontiers article is a landmark of the highest quality, thanks to genuinely collaborative interactions between authors and review editors, who include some of the world's best academicians. Research must be certified by peers before entering a stream of knowledge that may eventually reach the public - and shape society; therefore, Frontiers only applies the most rigorous and unbiased reviews.
Frontiers revolutionizes research publishing by freely delivering the most outstanding research, evaluated with no bias from both the academic and social point of view. By applying the most advanced information technologies, Frontiers is catapulting scholarly publishing into a new generation.

What are Frontiers Research Topics?

Frontiers Research Topics are very popular trademarks of the Frontiers Journals Series: they are collections of at least ten articles, all centered on a particular subject. With their unique mix of varied contributions from Original Research to Review Articles, Frontiers Research Topics unify the most influential researchers, the latest key findings and historical advances in a hot research area! Find out more on how to host your own Frontiers Research Topic or contribute to one as an author by contacting the Frontiers Editorial Office: frontiersin.org/about/contact

REGULATION OF PROTEOLYSIS AND PROTEOME COMPOSITION IN PLANT RESPONSE TO ENVIRONMENTAL STRESS

Topic Editors:
Mateusz Labudda, Warsaw University of Life Sciences-SGGW, Poland
Zhiping Deng, Zhejiang Academy of Agricultural Sciences, China
Shaojun Dai, Shanghai Normal University, China
Ling Li, Mississippi State University, United States

Citation: Labudda, M., Deng, Z., Dai, S., Li, L., eds. (2022). Regulation of Proteolysis and Proteome Composition in Plant Response to Environmental Stress. Lausanne: Frontiers Media SA. doi: 10.3389/978-2-83250-897-8

Table of Contents

frontiers | Frontiers in Plant Science

TYPE Editorial
PUBLISHED 15 November 2022
DOI 10.3389/fpls.2022.1080083

OPEN ACCESS

EDITED AND REVIEWED BY
Martin Cerny,
Mendel University in Brno, Czechia

*CORRESPONDENCE
Mateusz Labudda
mateusz_labudda@sggw.edu.pl

SPECIALTY SECTION
This article was submitted to Plant Proteomics and Protein Structural Biology, a section of the journal Frontiers in Plant Science

RECEIVED 25 October 2022
ACCEPTED 07 November 2022
PUBLISHED 15 November 2022

CITATION
Labudda M, Dai S, Deng Z and Li L (2022) Editorial: Regulation of proteolysis and proteome composition in plant response to environmental stress.
Front. Plant Sci. 13:1080083.
doi: 10.3389/fpls.2022.1080083

Editorial: Regulation of proteolysis and proteome composition in plant response to environmental stress

Mateusz Labudda[1]*, Shaojun Dai[2], Zhiping Deng[3] and Ling Li[4]

[1]Department of Biochemistry and Microbiology, Institute of Biology, Warsaw University of Life Sciences-SGGW, Warsaw, Poland, [2]China Development Center of Plant Germplasm Resources, College of Life Sciences, Shanghai Normal University, Shanghai, China, [3]Institute of Virology and Biotechnology, Zhejiang Academy of Agricultural Sciences, Hangzhou, China, [4]Department of Biological Sciences, Mississippi State University, Mississippi State, MS, United States

KEYWORDS

abiotic stress, biotic stress, protease, signal transduction, protein post-translational modification

Editorial on the Research Topic
Regulation of proteolysis and proteome composition in plant response to environmental stress

Introduction

Because of their sedentary lifestyle, plants are susceptible to changing environmental conditions. They must cope with miscellaneous abiotic stresses usually enhanced by heavy industry (Labudda et al., 2022). Moreover, changes in climate conditions and agricultural systems are favourable to pests and pathogens gradation on plants (Nykiel et al., 2022; Skoracka et al., 2022). However, plants are not defenceless; they are equipped with a battery of multiple mechanisms (from molecular through biochemical-physiological to structural) that are activated by them to ensure further growth and development and the production of diasporas (Muszyńska and Labudda, 2019; Formela-Luboińska et al., 2020; Tokarz et al., 2020; Tokarz et al., 2021; Fidler et al., 2022; Miernicka et al., 2022). Among these mechanisms, the control of proteolysis and thereby the quality and composition of proteins and pool of amino acids are of fundamental significance (Muszyńska et al., 2019; Labudda et al., 2020; O'Conner et al., 2021; Pan et al., 2021; Szewińska et al., 2021; Tan et al., 2021; Sun et al., 2022; Tanvir et al., 2022; Xing et al., 2022).

Proteolysis is an elementary biochemical process indispensable for protein metabolism. A wide spectrum of proteolytic enzymes is involved in this process, including exopeptidases (amino and carboxypeptidases) and endopeptidases (serine, aspartic, metallo- and cysteine peptidases) (Godson and van der Hoorn, 2021; van der Hoorn and Klemenčič, 2021). As uncontrolled proteolysis can seriously damage plant cells, the activity of peptidases is accurately regulated by their endogenous inhibitors

(Prabucka et al., 2017; Kunert and Pillay, 2022). Thus, an understanding of the mechanisms assuring the accurate regulation of peptidase activity and the dynamic alterations in the proteome and amino acids of plants struggling with environmental stresses is an urgent task undertaken by numerous teams from all over the world.

This Research Topic aimed to widen the understanding on protein and amino acid metabolism mechanisms in plants using an interdisciplinary approach. The Research Topic contains ten papers from several fields across abiotic stress (acid rain, low and elevated temperatures, salt, osmotic, and abscisic acid (ABA) treatments, and phosphate starvation) and biotic stress (infection with *Verticillium dahliae*). Two review articles are a valuable addition to the experimental articles. The first review by Zhang et al. concerns the application of TurboID-based proximity labelling in studying the protein interaction network in plant response to abiotic stress, while the second by Mangena shows the pleiotropic effects of recombinant protease inhibitors in plants.

What new have we learned from this Research Topic?

As Topic Editors, it was our pleasure and honour to review and manage the submitted manuscripts. In this editorial, we recapitulate the main findings of the published articles.

One of the abiotic stress, acid rain (AR) may cause severe damage to plant functioning. This problem is especially noticeable in woody plants. Hu et al. investigated the response of *Taxus wallichiana* var. *mairei* to AR stress. These authors showed that, in *T. wallichiana* var. *mairei* plants grown under AR stress in the soil with low calcium (Ca) level, the net photosynthetic rate and activity of the superoxide dismutase, ascorbate peroxidase, guaiacol peroxidase, and catalase were decreased in leaves; however, these physiological parameters were enhanced in plants cultivated under high Ca level in the soil. Furthermore, the proteomic profiling revealed forty-four differentially abundant proteins in leaves of AR stress-exposed *T. wallichiana* var. *mairei* plants cultivated under different Ca amounts in the soil. Identified proteins were classified into seven groups related to processes such as signal transduction, protein modification and degradation, metabolism, photosynthesis and energy, cell rescue and defence, transcription and translation and unknown proteins.

Another important abiotic stress is low temperature. Liu et al. presented the results concerning the enzyme aminoacyl tRNA synthetase YLC3, which has been shown to take part in the regulation of amino acid homeostasis and chloroplast thylakoid development in *Oryza sativa* plants under low temperature. This article showed a thermo-sensitive rice mutant *yellow leaf chlorosis3* (*ylc3*) with decreased chlorophyll content, changed thylakoid structure, and increased amounts of aspartate, asparagine, and glutamine in leaves under low-temperature stress.

It is well- known that a plant's response to stress is governed by an intricate network of phytohormones. Among these hormones are auxins. Ma et al. published results on the *Arabidopsis thaliana* endoplasmic reticulum (ER)-localized MAIGO2 (MAG2) complex and its protein homologue MAG2-Like (MAL) as regulators of plant development and vesicle trafficking and auxin homeostasis with functional redundancy. Moreover, it has been proven that MAIGO2 and MAG2-like participated in stress response, and in more detail the salt, osmotic, and ABA treatments have been examined.

Another published article concerned phosphate (Pi) stress. Wang et al. presented changes in phosphorylation and succinylation of *Hordeum vulgare* root proteins in response to phosphate starvation and recovery. The study showed that, the phosphorylated proteins associated with purine, the mitogen-activated protein kinases (MAPKs), pyrimidine, and ATP-binding cassette (ABC) transporters were upregulated in both Pi starved and recovered barley plants. s regards the succinylome, proteins in nitrogen and phenylpropanoid metabolism were significantly upregulated; on the other hand, proteins in lysine and tryptophan metabolism in both Pi-starved and recovered barley plants were significantly downregulated.

Adamiec et al. took a closer look at the role of the *A. thaliana* chloroplast EGY3 pseudoprotease in response to high-light and high-temperature stresses. Based on the molecular, biochemical, and physiological experiments, these authors concluded that, EGY3 mediated plant response to high-light and high-temperature stresses, and its role was related to photosystem I and light-independent reactions of photosynthesis. Moreover, these authors made the conclusion that, EGY3 took part in the regulation of H_2O_2 level through stabilization of the copper/zinc superoxide dismutase 2. Therefore, this matched up, as the authors concluded, to retrograde chloroplast-nucleus signalling.

An important global environmental problem is the soil salinity. Chen et al. using the quantitative proteomics analysis investigated changes in cell wall proteins of *Solanum lycopersicum* root in response to salinity. Two *S. lycopersicum* genotypes were used in this experiment, the salt-tolerant IL8-3 and the salt-sensitive M82 plants. This approach allowed the authors to show the differential responses of two contrasting genotypes. The salinity-tolerant IL8-3 plants presented not only a remarkably decremented Na^+ level but also a clearly improved redox balance and cell wall lignification in response to salinity in comparison to the salt-sensitive M82 *S. lycopersicum*. The common response of plants from both lines was that the proteins involved in signal transduction and cell wall polysaccharides were upregulated in response to salt stress.

In addition to abiotic stresses, biotic stresses, including fungal infections, contribute to losses in crops of arable plants. Lu et al. performed a comparative proteomic analysis of two *Gossypium barbadense* cultivars differing in *V. dahliae* tolerance (susceptible XH7 and resistant XH21). It was clear from this study that, changes in reduced ascorbate (AsA) and H_2O_2 contents and the gene expression of ascorbate peroxidases (APX) were essential for *V. dahliae* resistance in *G. barbadense*. Compared to susceptible XH7 plants, the resistant XH21 plants presented consonantly higher AsA level and sharply induced the APX gene expression.

An article by Zhang et al. presented proteomic analysis of the ClpX proteolytic complex consisted of a hexameric ATPase ClpX and a tetradecameric peptidase ClpP in the model cyanobacterium *Synechocystis* sp. PCC 6803. One of the used experimental approaches was the comprehensive proteomic identification of proteins which were ClpX-regulated in *Synechocystis*. One hundred seventy-two ClpX-regulated proteins were detected. As the functional analysis showed, these proteins were engaged in glycolysis, nitrogen assimilation, photosynthetic electron transport, ATP-binding cassette (ABC) transporters, and signal transduction.

Taken together, this Research Topic clearly shows that, investigations of various aspects of proteolysis and proteome composition in plant responses to environmental stresses are conducted by numerous teams from all over the world. This topic is timely from the point of view of modern plant biology. Therefore, there is a strong need for further research in this area, not only in the field of responses to environmental stresses, but also in terms of plant growth and development regulation.

Author contributions

All authors listed have made a substantial, direct, and intellectual contribution to the work and approved it for publication.

Acknowledgments

Topic Editors deeply thank all the authors and reviewers who have participated in this Research Topic. We would also like to thank Professor Martin Černý from the Mendel University in Brno (Czech Republic), as the Associate Editor, finally edited this editorial.

Conflict of interest

The authors declare that the research was conducted in the absence of any commercial or financial relationships that could be construed as a potential conflict.

Publisher's note

References

Fidler, J., Graska, J., Gietler, M., Nykiel, M., Prabucka, B., Rybarczyk-Płońska, A., et al. (2022). PYR/PYL/RCAR receptors play a vital role in the abscisic-acid-dependent responses of plants to external or internal stimuli. *Cells* 11, 1352. doi: 10.3390/cells11081352

Formela-Luboińska, M., Chadzinikolau, T., Drzewiecka, K., Jeleń, H., Bocianowski, J., Kęsy, J., et al. (2020). The role of sugars in the regulation of the level of endogenous signaling molecules during defense response of yellow lupine to *Fusarium oxysporum*. *Int. J. Mol. Sci.* 21, 4133. doi: 10.3390/ijms21114133

Godson, A., and van der Hoorn, R. A. L. (2021). The front line of defence: a meta-analysis of apoplastic proteases in plant immunity. *J. Exp. Bot.* 72, 3381–3394. doi: 10.1093/jxb/eraa602

Kunert, K. J., and Pillay, P. (2022). Loop replacement design: a new way to improve potency of plant cystatins. *FEBS J.* 289, 1823–1826. doi: 10.1111/febs.16335

Labudda, M., Dziurka, K., Fidler, J., Gietler, M., Rybarczyk-Płońska, A., Nykiel, M., et al. (2022). The alleviation of metal stress nuisance for plants–a review of promising solutions in the face of environmental challenges. *Plants* 11, 2544. doi: 10.3390/plants11192544

Labudda, M., Różańska, E., Prabucka, B., Muszyńska, E., Marecka, D., Kozak, M., et al. (2020). Activity profiling of barley vacuolar processing enzymes provides new insights into the plant and cyst nematode interaction. *Mol. Plant Pathol.* 21, 38–52. doi: 10.1111/mpp.12878

Miernicka, K., Tokarz, B., Makowski, W., Mazur, S., Banasiuk, R., and Tokarz, K. M. (2022). The adjustment strategy of venus fytrap photosynthetic apparatus to UV-a radiation. *Cells* 11, 3030. doi: 10.3390/cells11193030

Muszyńska, E., and Labudda, M. (2019). Dual role of metallic trace elements in stress biology-from negative to beneficial impact on plants. *Int. J. Mol. Sci.* 20, 3117. doi: 10.3390/ijms20133117

Muszyńska, E., Labudda, M., and Hanus-Fajerska, E. (2019). Changes in proteolytic activity and protein carbonylation in shoots of *Alyssum montanum* ecotypes under multi-metal stress. *J. Plant Physiol.* 232, 61–64. doi: 10.1016/j.jplph.2018.11.013

Nykiel, M., Gietler, M., Fidler, J., Prabucka, B., Rybarczyk-Płońska, A., Graska, J., et al. (2022). Signal transduction in cereal plants struggling with environmental stresses: from perception to response. *Plants* 11, 1009. doi: 10.3390/plants11081009

O'Conner, S., Zheng, W., Qi, M., Kandel, Y., Fuller, R., Whitham, S. A., et al. (2021). GmNF-YC4-2 increases protein, exhibits broad disease resistance and expedites maturity in soybean. *Int. J. Mol. Sci.* 22, 3586. doi: 10.3390/ijms22073586

Pan, J., Li, Z., Wang, Q., Guan, Y., Li, X., Huangfu, Y., et al. (2021). Phosphoproteomic profiling reveals early salt-responsive mechanisms in two foxtail millet cultivars. *Front. Plant Sci.* 12. doi: 10.3389/fpls.2021.712257

Prabucka, B., Mielecki, M., Chojnacka, M., Bielawski, W., Czarnocki-Cieciura, M., and Orzechowski, S. (2017). Structural and functional characterization of the triticale (× *Triticosecale* wittm.) phytocystatin TrcC-8 and its dimerization-dependent inhibitory activity. *Phytochemistry* 142, 1–10. doi: 10.1016/j.phytochem.2017.06.008

Skoracka, A., Laska, A., Radwan, J., Konczal, M., Lewandowski, M., Puchalska, E., et al. (2022). Effective specialist or jack of all trades? experimental evolution of a crop pest in fluctuating and stable environments. *Evol. Appl.* 15, 1639–1652. doi: 10.1111/eva.13360

Sun, M., Qiu, L., Liu, Y., Zhang, H., Zhang, Y., Qin, Y., et al. (2022). Pto interaction proteins: critical regulators in plant development and stress response. *Front. Plant Sci.* 13. doi: 10.3389/fpls.2022.774229

Szewińska, J., Różańska, E., Papierowska, E., and Labudda, M. (2021). Proteolytic and structural changes in rye and triticale roots under aluminum stress. *Cells* 10, 3046. doi: 10.3390/cells10113046

Tanvir, R., Ping, W., Sun, J., Cain, M., Li, X., and Li, L. (2022). *AtQQS* orphan gene and *NtNF-YC4* boost protein accumulation and pest resistance in tobacco (Nicotiana tabacum). *Plant Sci.* 317, 111198. doi: 10.1016/j.plantsci.2022.111198

Tan, J., Zhou, Z., Feng, H., Xing, J., Niu, Y., and Deng, Z. (2021). Data-independent acquisition-based proteome and phosphoproteome profiling reveals early protein phosphorylation and dephosphorylation events in arabidopsis seedlings upon cold exposure. *Int. J. Mol. Sci.* 22, 12856. doi: 10.3390/ijms222312856

Tokarz, K. M., Wesołowski, W., Tokarz, B., Makowski, W., Wysocka, A., Jędrzejczyk, R. J., et al. (2021). Stem photosynthesis–a key element of grass pea (*Lathyrus sativus* l.) acclimatisation to salinity. *Int. J. Mol. Sci.* 22, 685. doi: 10.3390/ijms22020685

Tokarz, B., Wójtowicz, T., Makowski, W., Jędrzejczyk, R. J., and Tokarz, K. M. (2020). What is the difference between the response of grass pea (*Lathyrus sativus* l.) to salinity and drought stress?–a physiological study. *Agronomy* 10, 833. doi: 10.3390/agronomy10060833

van der Hoorn, R. A. L., and Klemenčič, M. (2021). Plant proteases: from molecular mechanisms to functions in development and immunity. *J. Exp. Bot.* 72, 3337–3339. doi: 10.1093/jxb/erab129

Xing, J., Tan, J., Feng, H., Zhou, Z., Deng, M., Luo, H., et al. (2022). Integrative proteome and phosphoproteome profiling of early cold response in maize seedlings. *Int. J. Mol. Sci.* 23, 6493. doi: 10.3390/ijms23126493

frontiers in Plant Science

ORIGINAL RESEARCH
published: 04 March 2022
doi: 10.3389/fpls.2022.847364

The Rice Aspartyl-tRNA Synthetase YLC3 Regulates Amino Acid Homeostasis and Chloroplast Development Under Low Temperature

Hongjia Liu[1], Xue Gong[1], Hui Deng[2], Jinjuan Tan[1], Yanqing Sun[3], Fang Wang[1], Wenjuan Wu[4], Zhongjing Zhou[1], Rumeng Xu[1], Haiyan He[1] and Clive Lo[5]*

[1] State Key Laboratory for Managing Biotic and Chemical Threats to the Quality and Safety of Agro-Products, Institute of Virology and Biotechnology, Zhejiang Academy of Agricultural Sciences, Hangzhou, China, [2] College of Life Sciences, Fujian Agriculture and Forestry University, Fuzhou, China, [3] Institute of Crop Science and Institute of Bioinformatics, Zhejiang University, Hangzhou, China, [4] Shanghai Key Laboratory of Plant Molecular Sciences, College of Life Sciences, Shanghai Normal University, Shanghai, China, [5] School of Biological Sciences, The University of Hong Kong, Hong Kong, Hong Kong SAR, China

OPEN ACCESS

Edited by:
Shaojun Dai,
Shanghai Normal University, China

Reviewed by:
Juanjuan Yu,
Henan Normal University, China
Xu Na Wu,
Yunnan University, China

***Correspondence:**
Hongjia Liu
lhjzju@aliyun.com

Specialty section:
This article was submitted to Plant Proteomics and Protein Structural Biology, a section of the journal Frontiers in Plant Science

Received: *02 January 2022*
Accepted: *31 January 2022*
Published: *04 March 2022*

Citation:
Liu H, Gong X, Deng H, Tan J, Sun Y, Wang F, Wu W, Zhou Z, Xu R, He H and Lo C (2022) The Rice Aspartyl-tRNA Synthetase YLC3 Regulates Amino Acid Homeostasis and Chloroplast Development Under Low Temperature. Front. Plant Sci. 13:847364. doi: 10.3389/fpls.2022.847364

Aminoacyl tRNA synthetases primarily function to attach specific amino acids to the corresponding tRNAs during protein translation. However, their roles in regulating plant growth and development still remain elusive. Here we reported a rice thermo-sensitive mutant *yellow leaf chlorosis3* (*ylc3*) with reduced chlorophyll content, altered thylakoid structure, and substantially elevated levels of free aspartate, asparagine and glutamine in leaves under low temperature condition. Map-based cloning identified that *YLC3* encodes an aspartyl-tRNA synthetase which is localized in cytosol and mitochondria. In addition, quantitative proteomics analysis revealed that both nuclear and chloroplast-encoded thylakoid proteins were significantly down-regulated in the mutant. On the other hand, proteins involved in amino acid metabolism and the process of protein synthesis were up-regulated in *ylc3*, particularly for key enzymes that convert aspartate to asparagine. Moreover, uncharged tRNA-Asp accumulation and phosphorylation of the translation initiation factor eIF2α was detected in the mutant, suggesting that YLC3 regulates the homeostasis of amino acid metabolism and chloroplast thylakoid development through modulation of processes during protein synthesis.

Keywords: rice, aspartyl-tRNA synthetase, chloroplast, amino acid metabolism, eiF2α

INTRODUCTION

Rice is one of the most important staple crops in the world, feeding more than half of Asia's population. Photosynthesis efficiency is a major determinant of crop productivities. Chloroplasts are the location not only for photosynthesis, but also for biosynthesis of many important metabolites. Originated from endosymbiotic cyanobacteria approximately 1 billion years ago, chloroplasts are semi-autonomous organelles capable of independent transcription and translation (Dyall et al., 2004; Jarvis and López-Juez, 2013). Over a long period of symbiotic evolution, the

majority of chloroplast genes had been transferred to the nuclear genome, and their encoded proteins are translated in cytosol and then translocated to chloroplasts (Woodson and Chory, 2008). Currently there are approximately 3,000 chloroplast proteins, among which only about 100 proteins are encoded by the chloroplast genome (Abdallah et al., 2000; Richardson et al., 2017). Signaling regulatory mechanisms exist between nuclear genes and chloroplast genes. There are numerous nuclear genes regulating the processes of transcription, post-transcriptional modification, and translation in chloroplasts (Fernández and Strand, 2008). On the other hand, chloroplasts are regulating nuclear gene expression through tetrapyrrole signals and its own redox status (Fernández and Strand, 2008). Meanwhile, mitochondria, as the cellular energy factories which generate a large amount of ATP, are important for chloroplast biogenesis and development. In the rice mutant *wp3*, mitochondrial functional deficiencies also resulted in inhibition of chloroplast development (Li et al., 2018). Hence, normal chloroplast development requires coordinated regulation by nucleus, chloroplasts, and mitochondria.

Homeostasis of amino acid metabolism is pivotal to cellular growth and development (Bröer and Bröer, 2017). During amino acid deficiencies, mammalian-specific protein kinases are activated and they phosphorylate the translation initiation factor eiF2α (Hinnebusch, 2005; Wek et al., 2006). Consequently, translation of most proteins is inhibited to reduce energy consumption. At the same time, the expression of genes encoding enzymes for amino acid biosynthesis is enhanced to ensure cellular survival by transcription factor GCN4 (General Control Non-derepressible-4) during nutritional deficiencies (Natarajan et al., 2001; Dever and Hinnebusch, 2005; Li and Lam, 2008). In yeast, the GCN2 (General Control Non-derepressible-2) kinase-mediated eIF2α phosphorylation is an important adaptation strategy for metabolic and physiological changes resulting from nutritional deficiencies (Dever et al., 1992). Interaction between GCN1 and GCN2 is a necessary condition for the activation of GCN2 (Marton et al., 1993; Sattlegger and Hinnebusch, 2005). The Arabidopsis AtGCN2 could complement the yeast *gcn2* mutant phenotypes, implicating functional conservation (Zhang et al., 2003). In addition, chemically-induced amino acid starvation, UV light, wounding, chilling, and hormone treatments in Arabidopsis could all cause AtGCN2-dependent eIF2α phosphorylation which requires AtGCN1 and AtGCN2 interactions (Lageix et al., 2008; Zhang et al., 2008; Li et al., 2013; Wang et al., 2017). Moreover, Arabidopsis *atgcn1-1* and *atgcn1-2* mutants are cold-stress sensitive with retarded chloroplast development (Zhang et al., 2017). A recent study in Arabidopsis revealed that change in reactive oxygen species (ROS) levels in chloroplasts could also initiate AtGCN2-mediated eIF2α phosphorylation (Lokdarshi et al., 2020). These results indicated that eIF2a phosphorylation is a cold-stress tolerance mechanism in plants through inhibition of protein translation.

Aminoacyl-tRNA synthetases (AARSs) are one of the key enzymes involved in protein synthesis by linking amino acids with their specific tRNA (Ibba and Soll, 2000; O'Donoghue and Luthey-Schulten, 2003). Plant proteins are synthesized in cytosol, mitochondria and chloroplasts which all have a complete set of AARSs. In plants, AARSs are all nuclear-encoded, translated in cytosol, and then translocated to cytosol, mitochondria, or chloroplasts. There are 45 AARSs identified in Arabidopsis and some of them are translocated to different organelles to ensure normal protein synthesis (Duchêne et al., 2005). It can be perceived that sharing of AARSs between organelles is imperative for regulation of translation since the activities of AARSs and tRNA charged state are the major control points for prokaryotic and eukaryotic translational systems (Duchêne et al., 2005).

Gene cloning and functional characterizations of AARS mutants in tobacco, Arabidopsis, and rice revealed the involvement of some mitochondrial- and chloroplast-targeted AARSs chloroplast development and their mutations resulted in chlorotic or albino phenotypes (Kim et al., 2005; Liu et al., 2007; Wang et al., 2016; Zhang et al., 2017; Fang et al., 2020). The glutamyl-tRNA synthetase encoded by rice *Os10g0369000* is localized in cytosol and mitochondria, showing anther-specific expression and participating in anther formation and development (Yang et al., 2018). In Arabidopsis, 21 out of the 45 known AARSs are necessary for endosperm formation and embryogenesis (Berg et al., 2005). For example, cysteinyl-tRNA synthetase is specifically expressed in central cells of female gametes, determining the fate of the adjacent accessory cells (Kägi et al., 2010). Meanwhile, the Arabidopsis aspartyl-tRNA synthetase (IBI1, Impaired in BABA-induced disease Immunity1) is a beta-aminobutyric acid-inducible receptor protein for broad-spectrum disease resistance. IBI1 is mainly localized in endoplasmic reticulum and cytoplasm. Its deficiency led to accumulation of uncharged tRNAs, which in turn promoted GCN2-dependent phosphorylation of eIF2α, thereby inhibiting plant growth and development (Luna et al., 2014). In addition, IBI1 can be localized in nucleus, interacting with the transcription factors VOZ1/2 (Vascular Plant One Zinc Finger1/2) and regulating the expression of cell-wall defense and abiotic stress-responsive genes through the abscisic acid signaling pathway (Schwarzenbacher et al., 2020). Plant AARSs are mainly affecting amino acid homeostasis, protein synthesis and abiotic stress (Luna et al., 2014; Yang et al., 2018; Schwarzenbacher et al., 2020). However, it remains largely elusive regarding the protein localization and expression pattern of most of the other AARSs and their roles in plant growth and development, particularly for those in monocot species like rice.

In the present study, we reported the function of a cytosol- and mitochondria-localized aspartyl-tRNA synthetase in rice. YLC3 functional deficiency disrupted amino acid homeostasis, initiated eIF2α phosphorylation, inhibited translation, and influenced chloroplast development under low temperature condition.

RESULTS

Phenotypic Characterization of the *ylc3* Mutant

From a population of ethyl methanesulfonate (EMS)-induced rice mutants, a yellow leaf mutant designated as *ylc3* (*yellow leaf chlorosis3*) was identified. At 19°C, 2-week-old *ylc3* mutant plants showed yellow leaves containing only 30% photosynthetic

pigments compared to wild-type plants. The photosynthetic pigments increased to 50 and 80% of wild-type levels at 24 and 30°C, respectively. In addition, chlorophyll a content was inhibited more pronouncedly than chlorophyll b in the mutant. These data indicated that *ylc3* is a thermo-sensitive mutant (**Figure 1**). In light growth chambers, plant growth was affected by different temperatures. Under field conditions, *ylc3* plants were slightly shorter than wild-type plants while heading period and seeding rate were both normal (**Figure 1**). Transmission electronic microscopy analysis revealed the impaired development of chloroplasts in *ylc3* growing at 19°C with substantially reduced number of thylakoid grana lamella (**Figure 2**).

Map-Based Cloning of the *YLC3* Gene

To study the genetics of the yellow leaf phenotype, *ylc3* was crossed separately with Nipponbare or Kasalath wild-type plants. Under low temperature condition, the F_2 population of the *ylc3* × Nipponbare cross showed a segregation ratio of 95:330 for yellow leaf vs. green leaf(1:3 ratio, $\chi^2 = 2.38 < \chi^2_{0.05} = 3.84$, $P > 0.05$); 129 of 409 plants showed yellow leaf phenotype in the F_2 generation of *ylc3* × Kasalath (1:3 ratio, $\chi^2 = 0.30 < \chi^2_{0.05} = 3.84$, $P > 0.05$). The above results indicate that the yellow leaf phenotype is conferred by a single recessive nuclear gene. F_2 population from the *ylc3* × Kasalath cross was then used for genetic mapping. In the preliminary mapping, 94 F_2 plants with yellow leaf phenotype were analyzed with 120 sequence-tagged site (STS) markers which are evenly distributed on 12 rice chromosomes. *YLC3* was initially mapped within a 950-kb region between the molecular markers STS2 and STS3 on chromosome 2. At the same time, F_2 population from the *ylc3* and Nipponbare cross was subject to whole-genome sequencing-based MutMap method to map *YLC3* (Abe et al., 2012; Lü et al., 2015). The mutation was identified to be a single-base substitution (G → A) in the aspartyl-tRNA synthetase-encoding gene located on chromosome 2 (*LOC_Os02g46130*), resulting in a single amino acid replacement (Arginine → Lysine) near the C-terminal region of YLC3 (**Figure 3**).

To validate that *LOC_Os02g46130* was the affected gene, we constructed the binary vector Pro:YLC3-NOS for *ylc3* transformation. A total of 20 independent transformants were obtained with wild-type phenotypes. Meanwhile, a gene-editing vector was constructed for Nipponbare transformation. A total of 22 positive transformants were obtained, 9 of which were homozygous for the G → A substitution and they all showed yellow leaf phenotype at low temperature condition. Phenotyping and genotyping analyses revealed the yellow leaf phenotype in

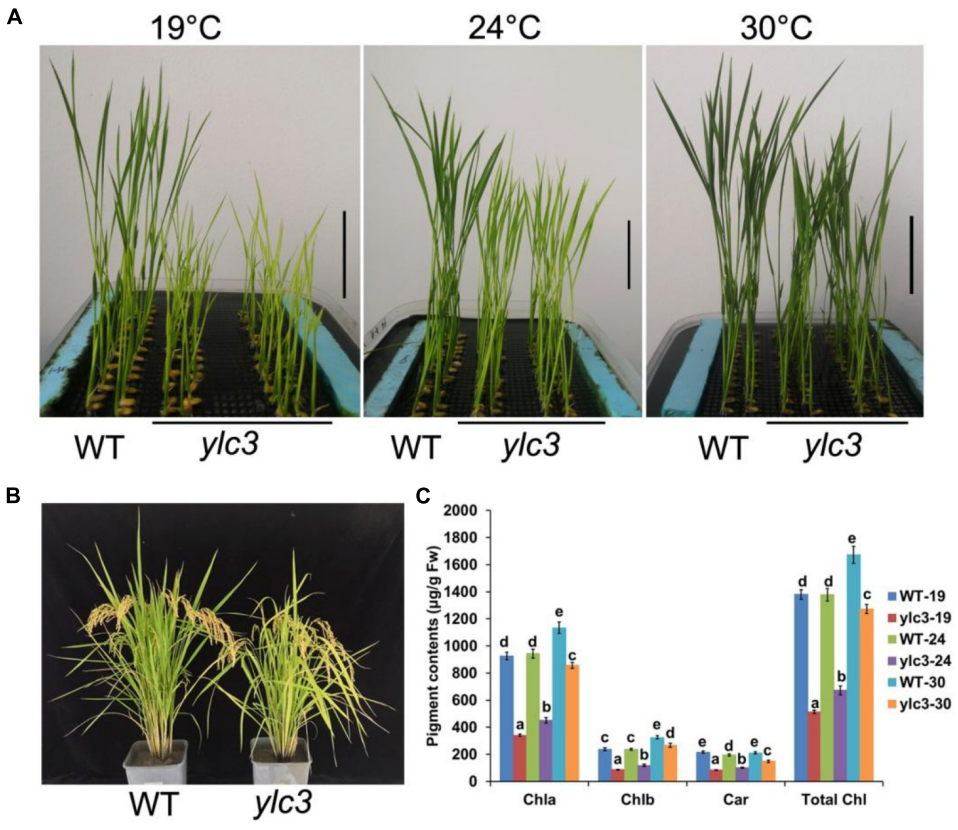

FIGURE 1 | Phenotypic analyses of *ylc3* mutant. **(A)** Phenotypes of the WT and *ylc3* seedlings (10-day-old) grown at different temperatures. Bar = 5 cm. **(B)** Heading stage. **(C)** Photosynthetic pigments of WT and *ylc3* (10-day-old) grown at different temperatures (°C). Error bars represent SD ($n = 5$). Bars with different letters indicate significant differences at $P < 0.05$, ANOVA.

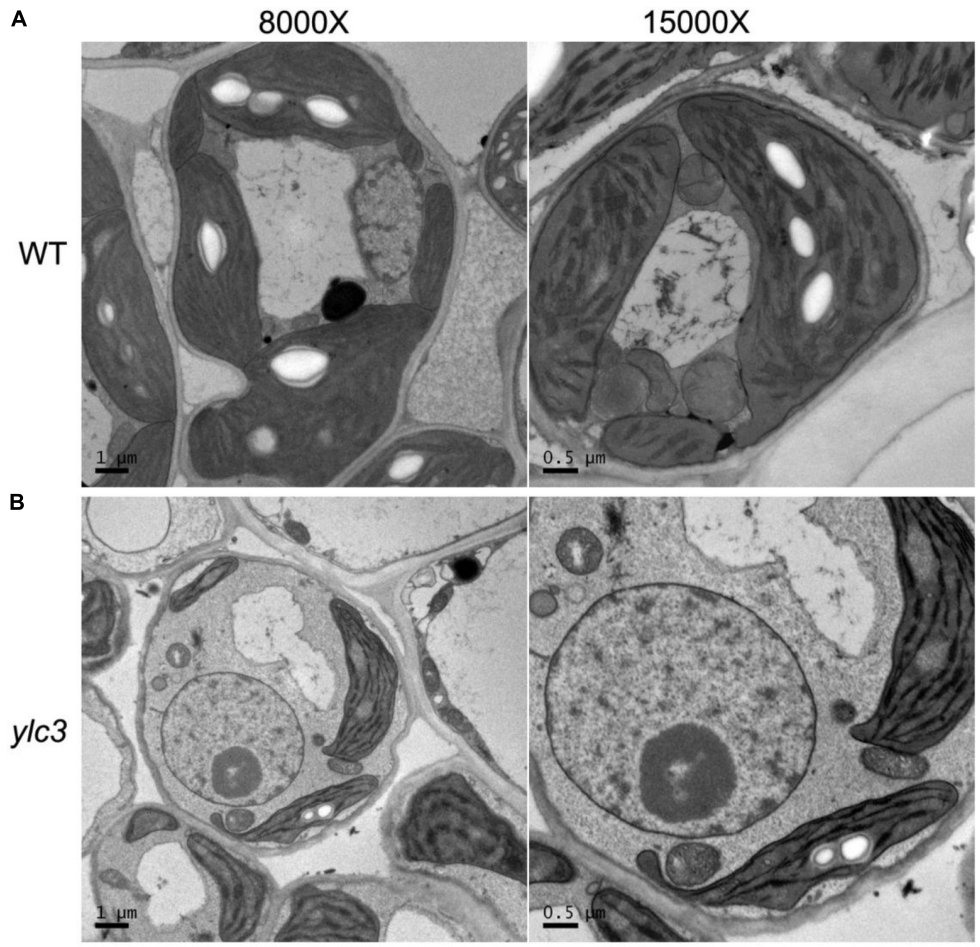

FIGURE 2 | Impaired thylakoid development in *ylc3* mutant. **(A)** WT chloroplasts showed well-developed thylakoids. **(B)** *ylc3* chloroplasts showed reduced number of thylakoid grana lamella.

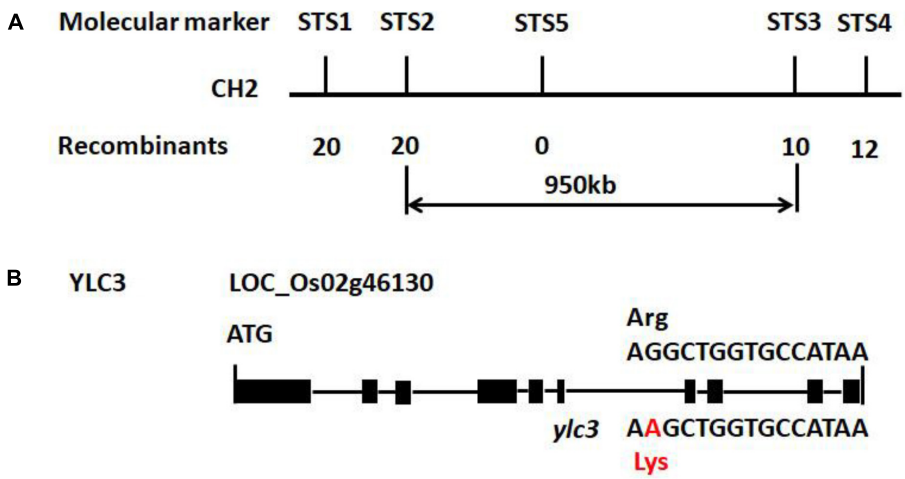

FIGURE 3 | Preliminary gene mapping and *ylc3* mutation. **(A)** InDel markers (STS1-5) used for preliminary mapping are indicated. Numbers of recombinants and F_2 mutants (n) are shown. **(B)** Gene structure of *YLC3* and the mutation site. The "A" in red indicates a one base-pair substitution in *ylc3*. Black rectangles represent exons.

the T_1 plants growing at lower temperatures. The above results established that the yellow leaf phenotype was conferred by the *ylc3* mutation in *LOC_Os02g46130* (**Figure 4**).

Sequence and Phylogenetic Analyses

Aminoacyl-tRNA synthetases are classified into two categories: eukaryotic-specific (clade I) and prokaryotic-originated (clade II). Sequence analysis of YLC3 revealed the presence of an N-terminal coiled coil functional domain and a C-terminal tRNA synthetase class II functional domain, hence YLC3 belongs to a clade II AARS. Clustering analysis further illustrated that YLC3 is very conserved among different species with highly homologous functional domain and motif. Among angiosperms, YLC3 shares higher homology with proteins from monocotyledons such as sorghum, barley and corn, with slightly lower homology with proteins from dicot species such as Arabidopsis, *Brassica napus* and soybean (**Figure 5**). Taken together, YLC3 is a highly conserved clade II aspartyl-tRNA synthetase.

Expression and Subcellular Localization Analyses

To examine the spatial expression of *YLC3*, a promoter: GUS binary vector was constructed and transformed into Nipponbare rice. GUS staining was performed in roots, stems, leaves, glumes, anthers, and pistils from the positive transformants. Results indicated that *YLC3* was expressed in all tissues examined. GUS staining was stronger in roots, stems, and leaves but weaker in anthers and pistils (**Figure 6**). Hence, *YLC3* is considered a constitutively expressed gene.

Aminoacyl-tRNA synthetases are mainly participating in protein synthesis and there is a complete set of AARSs in cytosol, mitochondria, and chloroplasts. To examine the subcellular localization of YLC3, a 35S promoter-driven YLC3:sGFP fusion expression vector was constructed. Transient expression of YLC3:sGFP in rice protoplasts revealed green fluorescent signals mainly in cytosol (**Figure 7**). After staining the transfected protoplasts with a mitochondrial specific dye (MitoTracker, Invitrogen, Carlsbad, CA, United States), some YLC3:sGFP green fluorescent signals were found to overlap with the red mitochondrial signals (**Figure 7**). These observations indicated that YLC3 is mainly localized in cytosol and mitochondria, but not in chloroplasts.

Analysis of Free Amino Acids in *ylc3* Mutant

YLC3 encodes an aspartyl-tRNA synthetase which catalyzes the reaction between aspartate and its specific tRNA. If aspartyl-tRNA synthetase is functionally deficient, it may result in the accumulation of free aspartate and uncharged tRNAs. Wild type plants, *ylc3* mutant plants and complementation lines were kept at low temperature (19°C) and high temperature (30°C) in light growth chambers and free amino acid contents in leaves were determined at 2-leaf stage. Under low temperature condition, *ylc3* mutant leaves showed 92% increase in aspartate, 10-fold increase in glutamine, and 78-fold increase in asparagine, when compared to wild-type plants and complementation lines (**Figure 8**). Under high temperature condition, contents of aspartate, glutamine, and asparagine were restored to normal levels in the *ylc3* mutant leaves (**Figure 8**). The above results demonstrated the changes in free amino acid contents in *ylc3* leaves, especially asparagine, under low temperature condition.

Quantitative Proteomics Analyses

Since AARSs are playing pivotal roles in protein synthesis while *ylc3* mutant showed severe inhibition of chlorophyll production and chloroplast development under low temperature condition, quantitative proteomics analyses were performed with *ylc3* and wild-type seedlings growing at 19°C. Using the high-throughput tandem mass tag method, a total of 9,212 proteins comprising 9143 nuclear-encoded proteins, 51 chloroplast-encoded proteins, and 18 mitochondrial-encoded proteins were detected (**Supplementary Table 1**). Among the mitochondrial-encoded proteins, 11 proteins were up-regulated in *ylc3* seedlings while the others were unaffected. All the

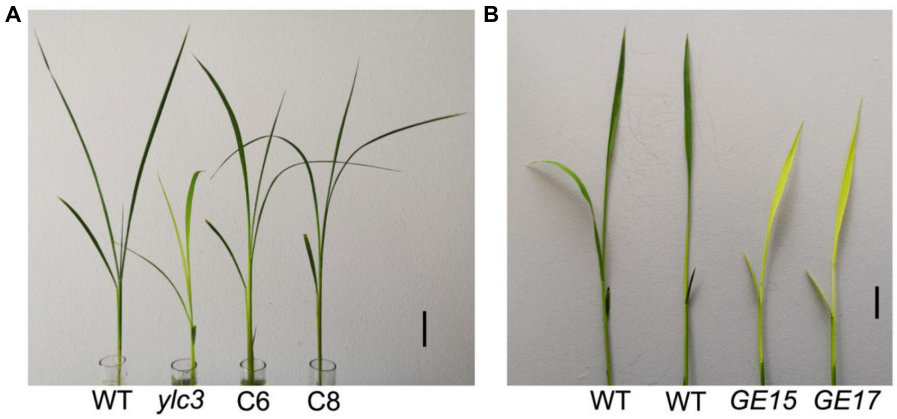

FIGURE 4 | Complementation and *YLC3* gene editing analysis. **(A)** The *ylc3* mutation was complemented by *YLC3* promoter expression of a full-length YLC3 coding sequence. Bar = 3 cm. **(B)** *YLC3* gene-editing transgenic seedlings showed the yellow leaf phenotype at low temperature. Bar = 1 cm.

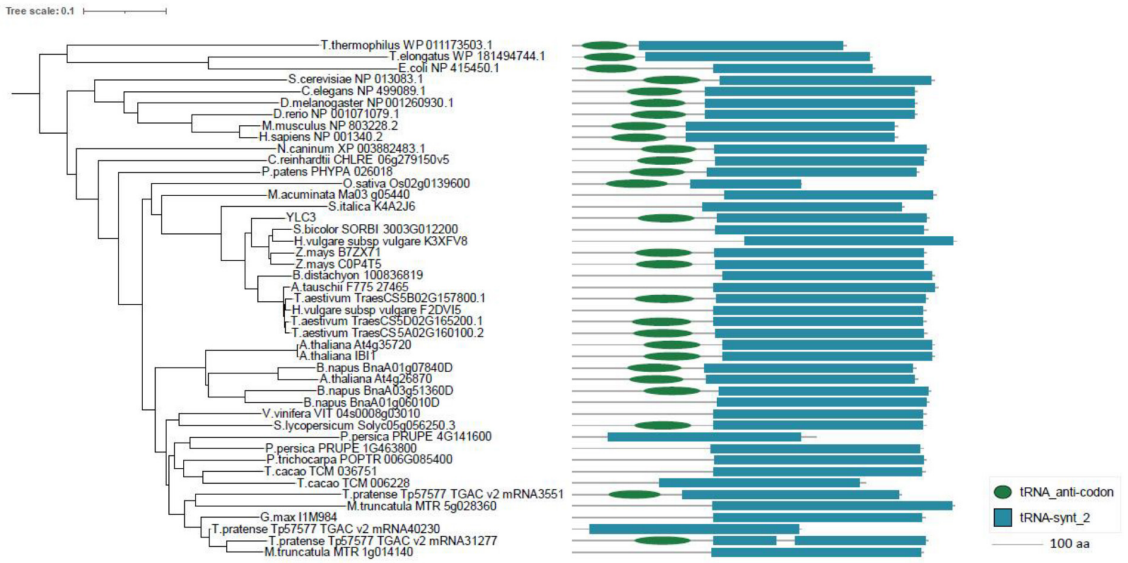

FIGURE 5 | Phylogenetic analysis and motif alignment. A phylogenetic tree was constructed with aligned full-length sequences of homologs of YLC3. Amino acid sequences from regions 101 to 188 and 223 to 544 in YLC3 were used for motif alignment by MEGA.

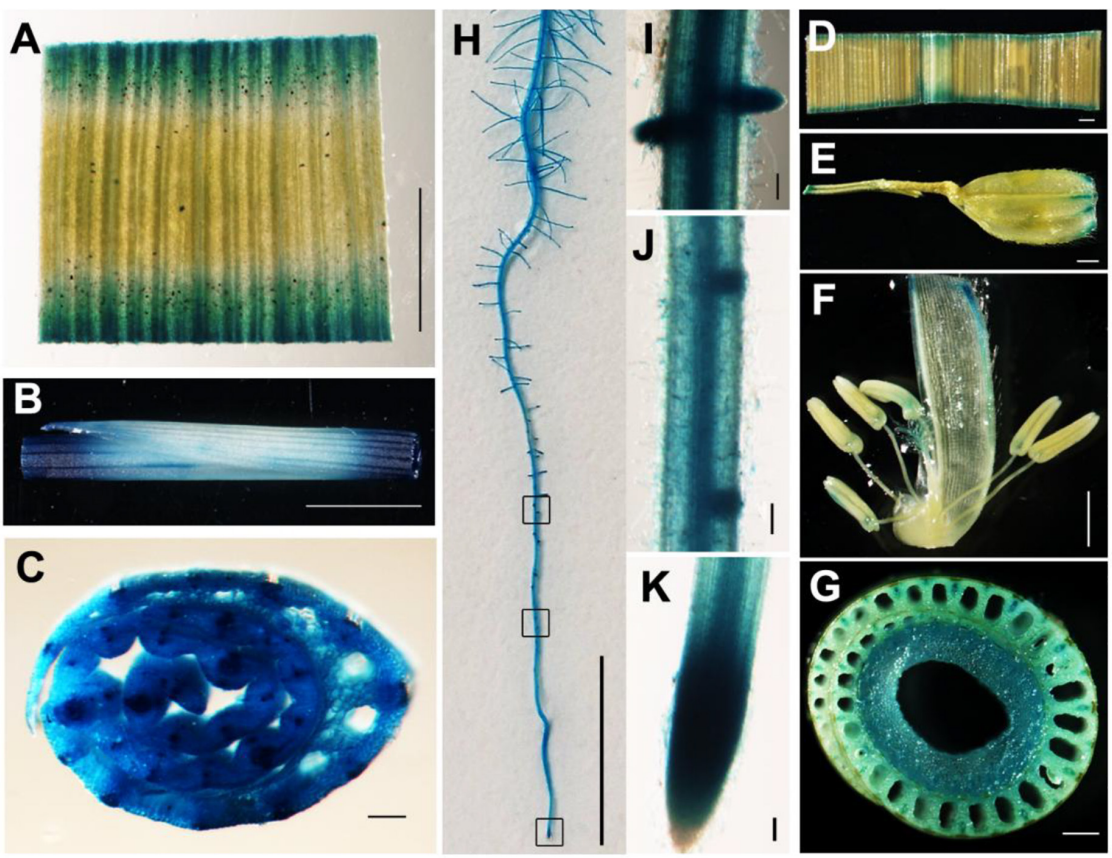

FIGURE 6 | Tissue expression pattern of *YLC3*. **(A–C,H–K)** GUS staining of 7-day-old ProYLC3:GUS transgenic seedlings. **(A)** Leaf. **(B)** Stem. **(C)** Cross section of stem. **(H)** Primary root. **(I)** Lateral root. **(J)** Lateral root primordium. **(K)** Root tip. **(D–G)** GUS staining of the heading stage of ProYLC3:GUS transgenic plants. **(D)** Leaf. **(E)** Glume. **(F)** Anthers and pistils. **(G)** Cross section of stem. Scale bars are 100 μm in **(C,D,E,I–K)**, 1 mm in **(A,B,F,G)**, and 1 cm in **(H)**.

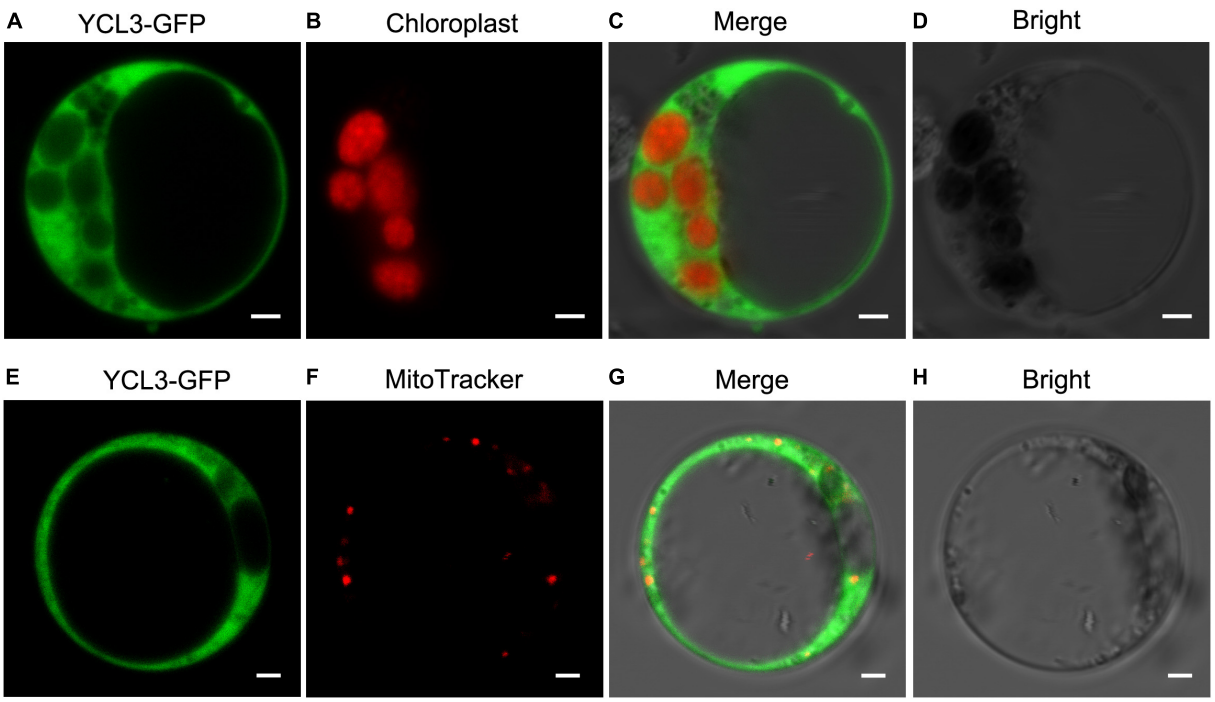

FIGURE 7 | Subcellular localization of YLC3-sGFP. **(A–D)** Transient expression of YLC3:sGFP in rice protoplasts. **(A)** GFP. **(B)** Chlorophyll autofluorescence. **(C)** Merged images of **(A,B)**. **(D)** Bright field. **(E–H)** Transient expression of YLC3:sGFP and MitoTracker staining of transfected protoplasts. **(E)** GFP. **(F)** Mitochondrial fluorescence staining by MitoTracker. **(G)** Merged images of **(E,F)**. **(H)** Bright field.

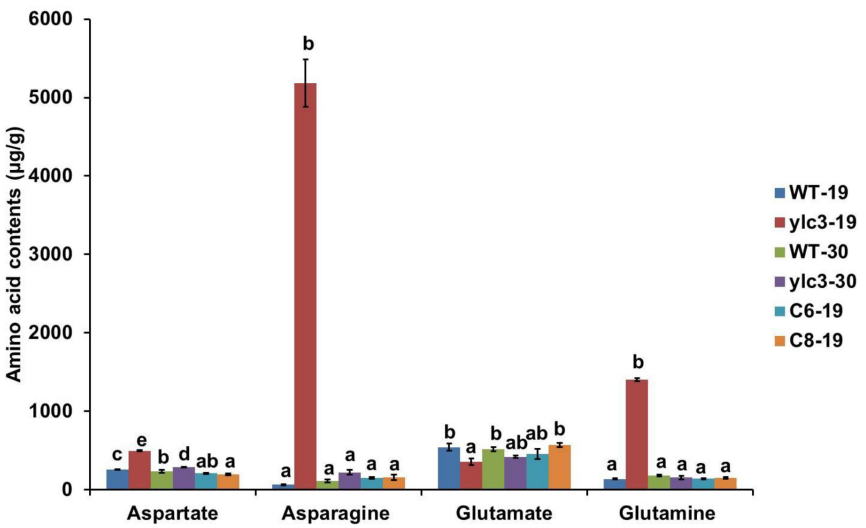

FIGURE 8 | Free amino acid analysis of 10-day-old WT and ylc3 seedlings grown at different temperatures. Error bars represent SD (n = 3). Bars with different letters indicate significant differences at $P < 0.05$, ANOVA.

25 chloroplast-encoded proteins in different thylakoid protein complexes such as Photosystem I, Photosystem II, cytochrome b_6f complex, and NADH dehydrogenase complex were down-regulated in the mutant (**Table 1**).

The KEGG analysis of 4,979 nuclear-encoded proteins revealed 1,384 differentially expressed proteins (>2-fold changes) with 154 proteins down-regulated and 1,230 proteins up-regulated (173 of them were up-regulated by more than threefold) in the *ylc3* mutant (**Supplementary Table 2**). The down-regulated proteins are enriched in photosynthesis-related proteins including 13 photosynthetic antenna proteins, 20 photosystem-related proteins, 14 photosynthetic carbon fixation

TABLE 1 | Chloroplast-encoded thylakoid protein with significant fold changes in *ylc3*.

Accession	Description	Pathway analysis	Ratio(M:W)	Adjust_*p*_value
1073625666	PetD (chloroplast) [*Oryza sativa*]	Electron transport system	0.246	1.91E-07
1073625664	PsbH (chloroplast) [*Oryza sativa*]	Photosystem II	0.282	9.97E-08
1073625661	PsbB (chloroplast) [*Oryza sativa*]	Photosystem II	0.334	3.18E-08
1073625622	PsbC (chloroplast) [*Oryza sativa*]	Photosystem II	0.377	8.04E-08
1073625653	PsbE (chloroplast) [*Oryza sativa*]	Photosystem II	0.445	2.09E-07
1073625621	PsbD (chloroplast) [*Oryza sativa*]	Photosystem II	0.499	3.34E-07
1073625651	PsbL (chloroplast) [*Oryza sativa*]	Photosystem II	0.624	3.92E-06
1073625616	PsbA (chloroplast) [*Oryza sativa*]	Photosystem II	0.573	5.52E-07
1073625649	PetA (chloroplast) [*Oryza sativa*]	Electron transport system	0.515	2.02E-07
1073625699	NdhA (chloroplast) [*Oryza sativa*]	Electron transport system	0.591	5.90E-07
1073625639	NdhJ (chloroplast) [*Oryza sativa*]	Electron transport system	0.626	5.54E-06
1073625640	NdhK (chloroplast) [*Oryza sativa*]	Electron transport system	0.678	4.16E-06
1073625691	NdhF (chloroplast) [*Oryza sativa*]	Electron transport system	0.681	6.36E-06
1073625684	NdhB (chloroplast) [*Oryza sativa*]	Electron transport system	0.727	0.000157
1073625698	NdhI (chloroplast) [*Oryza sativa*]	Electron transport system	0.729	1.62E-05
1073625700	NdhH (chloroplast) [*Oryza sativa*]	Electron transport system	0.740	2.92E-05
1073625695	PsaC (chloroplast) [*Oryza sativa*]	Photosystem I	0.349	1.99E-07
1073625636	PsaA (chloroplast) [*Oryza sativa*]	Photosystem I	0.399	1.70E-07
1073625635	PsaB (chloroplast) [*Oryza sativa*]	Photosystem I	0.499	1.76E-07
1073625631	AtpH (chloroplast) [*Oryza sativa*]	ATPase	0.383	4.25E-06
1073625630	AtpI (chloroplast) [*Oryza sativa*]	ATPase	0.393	1.39E-07
1073625632	AtpF (chloroplast) [*Oryza sativa*]	ATPase	0.452	2.61E-07
1073625642	AtpE (chloroplast) [*Oryza sativa*]	ATPase	0.479	1.41E-07
1073625643	AtpB (chloroplast) [*Oryza sativa*]	ATPase	0.471	1.32E-07
1073625633	AtpA (chloroplast) [*Oryza sativa*]	ATPase	0.522	3.76E-07

proteins, and 14 carbohydrate metabolism-related proteins (**Table 2**). Most of the nuclear-encoded and chloroplast-encoded thylakoid membranes were apparently down-regulated, which was probably the major cause for the reduced chlorophyll content, impaired thylakoid development, and yellow seedling phenotype in the *ylc3* mutant.

The KEEG analysis also identified 166 ribosomal proteins, 92 carbon metabolism-related proteins, 88 amino acid biosynthesis proteins, and 41 pyruvate metabolism-related proteins (**Figure 9**). Most of these proteins were significantly up-regulated in the *ylc3* mutant. For the aspartate metabolic pathways, asparagine synthetase, glutamine synthetase, and aspartate aminotransferase were all up-regulated while glutamate synthetase did not show any significant changes (**Table 3**). The above results suggested that ribosomal protein translation efficiencies were increased and amino acid biosynthesis was enhanced, especially for asparagine and glutamine, in the *ylc3* mutant under low temperature condition.

Uncharged tRNA-Asp Accumulation and Immunoblot Analysis of eif2α Phosphorylation

In Arabidopsis, aspartyl-tRNA synthetase deficiency resulted in accumulation of aspartate and uncharged tRNA, which in turn interacted with AtGCN2 and activated its kinase activities. The activated AtGCN2 then phosphorylated eIF2a, reduced protein translation efficiencies, and inhibited plant growth and development (Luna et al., 2014). Two aspartyl-tRNA genes (trnD-GUC, Id: 29141347; trnD-GTC, Id: 3950710) in rice were retrieved from the NCBI database. To check uncharged tRNA-Asp levels, northern-blot analysis was performed. Our results demonstrated that tRNA-trnD-GUC was obviously increased in *ylc3* seedlings under low temperature. However, we failed to detect the transcription of trnD-GTC in rice seedlings.

We speculated that the eif2α phosphorylation level might be increased in the *ylc3* mutant under low temperature condition. Accordingly, AtEIF2α, AtGCN1, and AtGCN2 protein sequences were searched against the NCBI rice database to retrieve the homologous proteins in rice as OsEIF2α (LOC_Os03g18510), OsGCN1 (LOC_Os03g51140) and OsGCN2 (LOC_Os04g41530), respectively. These three proteins were found to be up-regulated by onefold from the above quantitative proteomics analysis. Since the phosphorylation sites are identical between OsEIF2α and AtEIF2α (as revealed by sequence alignment), eif2α-specific phosphorylation antibody (Luna et al., 2014; Wang et al., 2017) could be utilized for immunoblot detection in rice plants. We found that eif2α was apparently phosphorylated in the *ylc3* mutant growing under low temperature condition when compared to the wild-type plants (**Figure 10**). Hence, under low temperature condition, *ylc3* mutation resulted in eif2α phosphorylation which could inhibit

TABLE 2 | Nuclear-encoded thylakoid protein with significant fold changes in *ylc3*.

Accession	Description	Gene_name	Pathway Analysis	Ratio (M:W)	Adjust_*p*_value
LOC_Os01g52240.1	Similar to type I chlorophyll a/b-binding protein b (fragment)	Lhcb1.1	Photosystem II	0.231	3.49E-08
LOC_Os04g38410.1	Similar to chlorophyll a/b-binding protein CP24, photosystem II (fragment)	CP24	Photosystem II	0.244	3.49E-08
LOC_Os02g37060.1	Similar to photosystem II 5 kD protein		Photosystem II	0.258	3.51E-08
LOC_Os08g01380.1	Ferredoxin I, chloroplast precursor (anti-disease protein 1)	Fd1	Photosystem II	0.2667	4.44E-07
LOC_Os01g64960.1	22-kDa photosystem II protein, photoprotection	PSBS1	Photosystem II	0.269	3.03E-08
LOC_Os05g22730.1	Similar to one helix protein		Photosystem II	0.274	8.19E-08
LOC_Os03g39610.1	Similar to photosystem II type II chlorophyll a/b binding protein (fragment)	LHCB	Photosystem II	0.277	2.82E-08
LOC_Os07g37240.1	Similar to chlorophyll a/b-binding protein CP29 precursor	CP29	Photosystem II	0.288	3.37E-08
LOC_Os07g37550.1	Similar to type III chlorophyll a/b-binding protein (fragment)		Photosystem II	0.297	3.89E-08
LOC_Os07g36080.1	Similar to oxygen-evolving enhancer protein 3-2, chloroplast precursor		Photosystem II	0.335	5.60E-08
LOC_Os08g10020.1	Similar to photosystem II 10 kDa polypeptide (fragment)	OsPsbR3	Photosystem II	0.335	6.37E-08
LOC_Os01g31690.1	Similar to photosystem II oxygen-evolving complex protein 1 (fragment)	PsbO	Photosystem II	0.368	1.48E-07
LOC_Os09g17740.1	Similar to chlorophyll a-b binding protein, chloroplast precursor (LHCII type I CAB) (LHCP)	CAB1R	Photosystem II	0.388	7.93E-08
LOC_Os02g10390.1	Chlorophyll a/b-binding protein type III (fragment)		Photosystem II	0.402	9.30E-08
LOC_Os07g04840.1	Similar to 23 kDa polypeptide of photosystem II	PsbP	Photosystem II	0.46	2.85E-07
LOC_Os03g19380.1	Similar to CP12 (fragment)	OsCP12	Photosystem II	0.507	1.61E-06
LOC_Os03g21560.1	Similar to photosystem II 11 kD protein		Photosystem II	0.508	5.22E-07
LOC_Os08g44680.1	Similar to Photosystem I reaction center subunit II, chloroplast precursor (photosystem I 20 kDa subunit) (PSI-D)	PsaD	Photosystem II	0.509	1.79E-07
LOC_Os09g26810.1	Similar to type II chlorophyll a/b binding protein from photosystem I precursor	Lhca6	Photosystem II	0.52	3.26E-07
LOC_Os03g17174.1	Similar to kinase binding protein (fragment)	PsbP	Photosystem II	0.529	2.34E-07
LOC_Os06g01210.1	Plastocyanin, chloroplast precursor	OsPC	Electron transport system	0.282	5.66E-07
LOC_Os01g01340.1	Light-regulated protein, regulation of light-dependent attachment of LEAF-TYPE FERREDOXIN-NADP + OXIDOREDUCTASE (LFNR) to the thylakoid membrane	LIR1	Electron transport system	0.325	5.35E-07
LOC_Os08g45190.1	Similar to PGR5	OsPGR5	Electron transport system	0.371	1.19E-07
LOC_Os02g01340.2	Leaf-type ferredoxin-NADP+-oxidoreductase, regulation of electron partitioning in the chloroplast	OsLFNR1	Electron transport system	0.508	2.40E-07
LOC_Os04g33830.1	Photosystem I PsaO domain containing protein	PsaO	Photosystem I	0.216	7.02E-08
LOC_Os09g30340.1	Similar to photosystem I reaction center subunit V	PsaG	Photosystem I	0.277	6.85E-08
LOC_Os06g21590.1	Similar to light-harvesting complex I (fragment)		Photosystem I	0.296	1.30E-07
LOC_Os12g23200.1	Similar to photosystem I reaction center subunit XI, chloroplast precursor (PSI- L) (PSI subunit V)	PsaL	Photosystem I	0.317	1.27E-07
LOC_Os12g08770.1	Similar to photosystem I reaction center subunit N, chloroplast precursor (PSI- N)	PsaN	Photosystem I	0.369	3.08E-06
LOC_Os08g33820.1	Similar to LHC I type IV chlorophyll binding protein (fragment)	cab	Photosystem I	0.398	1.19E-07
LOC_Os05g48630.2	Photosystem I reaction center subunit VI, chloroplast precursor (PSI- H) (light-harvesting complex I 11 kDa protein) (GOS5 protein)	PSAH	Photosystem I	0.409	1.99E-07
LOC_Os07g25430.1	Photosystem I reaction center subunit IV, chloroplast precursor (PSI- E) (photosystem I 10.8 kDa polypeptide)	PsaE	Photosystem I	0.426	2.11E-07
LOC_Os02g52650.1	Similar to Lhca5 protein		Photosystem I	0.427	1.92E-07
LOC_Os07g05480.1	Photosystem I protein-like protein	PsaK	Photosystem I	0.429	1.18E-06
LOC_Os03g56670.2	Similar to photosystem-1 F subunit	OsPS1-F	Photosystem I	0.44	1.01E-07
LOC_Os03g52130.1	Photosystem I reaction center subunit N family protein		Photosystem I	0.517	5.00E-05

the translation of thylakoid complex proteins, leading to impaired chloroplast development and yellow leaf phenotype.

DISCUSSION

Plant AARSs with different expression patterns and subcellular locations play key role in protein synthesis (Ibba and Soll, 2000; Duchêne et al., 2005). YLC3, a cytosol- and mitochondrial-localized aspartyl-tRNA synthetase, is required for free amino acid homeostasis in rice under low temperature condition. In addition, translation of thylakoid proteins is likely to be down-regulated by the GCN2-eif2α phosphorylation pathway in the *ylc3* seedlings.

YLC3 Encodes an Aspartyl-tRNA Synthetase

YLC3 is a constitutively expressed gene with stronger expression in roots, stem and leaves but weaker expression in anthers and pistils (**Figure 6**). YLC3 contains the typical aspartyl-tRNA catalytic domain and a coiled coil functional domain.

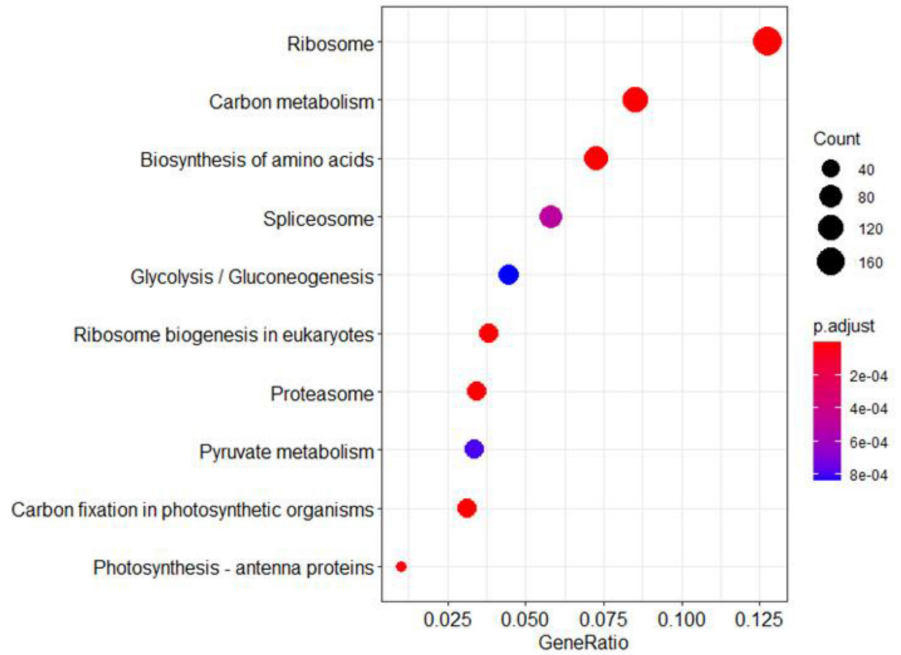

FIGURE 9 | KEGG pathway analysis. Differentially regulated proteins were used to perform KEGG analysis on clusterProfiler. Significant differences between *ylc3* and WT were detected for proteins related to photosynthesis. Pathways including carbon metabolism, pyruvate metabolism, carbon fixation in photosynthetic organisms and photosynthesis-antenna proteins were enriched (corrected *P*-value < 0.05).

TABLE 3 | Expression levels of aspartate metabolic pathway enzymes in *ylc3*.

Accession	Description	Gene name	Ratio (M:W)	Adjust_*p*_value
LOC_Os02g50240.1	Glutamine synthetase	OsGS1;1	1.418	9.96025E-06
LOC_Os02g50240.2	Glutamine synthetase	OsGS1;1	1.383	0.000125334
LOC_Os03g50490.1	Glutamine synthetase	OsGS1;3	1.991	9.37E-07
LOC_Os03g12290.1	Glutamine synthetase	OsGS1;2	1.503	5.85E-06
LOC_Os01g48960.1	Glutamate synthase	OsNADH-GOGAT1	0.998	0.955012272
LOC_Os05g48200.1	Glutamate synthase	OsNADH-GOGAT2	1.161	0.001536878
LOC_Os02g14110.1	Aminotransferase	Aspartate aminotransferase	1.594	1.78E-06
LOC_Os01g55540.1	Aminotransferase	Aspartate aminotransferase	2.363	1.19E-07
LOC_Os06g35540.1	Aminotransferase	Aspartate aminotransferase	2.318	1.77E-07
LOC_Os03g18130.1	Asparagine synthetase	Aspartate synthetase	2.704	5.93E-07

Phylogenetic analysis illustrated that YLC3 is highly conserved with reported aspartyl-tRNA synthetases including Arabidopsis IBI1 (Luna et al., 2014). Furthermore, free amino acid analyses revealed that aspartate level was increased in the *ylc3* mutant. Collectively, the enhanced aspartate level together with the protein functional domain and phylogenetic analyses strongly suggested that YLC3 is an aspartyl-tRNA synthetase.

The rice *ylc3* mutant is a thermo-sensitive chlorotic mutant and gene mapping identified a single amino acid substitution in the C-terminal region of YLC3. The substitution occurred outside the catalytic and coiled coil domains, indicating that the C-terminus is also critical for the activities of aspartyl-tRNA synthetase. The importance of this substitution was further supported by gene editing approach which generated transgenic rice lines with the same mutation and phenotype. On the other hand, chlorophyll and free amino acid contents are normal in *ylc3* plants under high temperature condition, indicating that the mutant YLC3 protein can be functional. Alternatively, as there are at least 3 aspartyl-tRNA synthetases in rice, it remains to be investigated whether the other isozymes are involved in restoration of chlorophyll and free amino acid contents under high temperature conditions.

There is a lack of an N-terminal signal peptide in YLC3 which is localized in cytosol and mitochondria, but not chloroplasts (**Figure 7**). Currently, all the known aminoacyl-tRNA synthetases participating in chloroplast development are chloroplast-localized. The Arabidopsis aspartyl-tRNA synthetase IBI1 is localized in endoplasmic reticulum and cytosol. During pathogen attack or low temperature stress, IBI1 is translocated

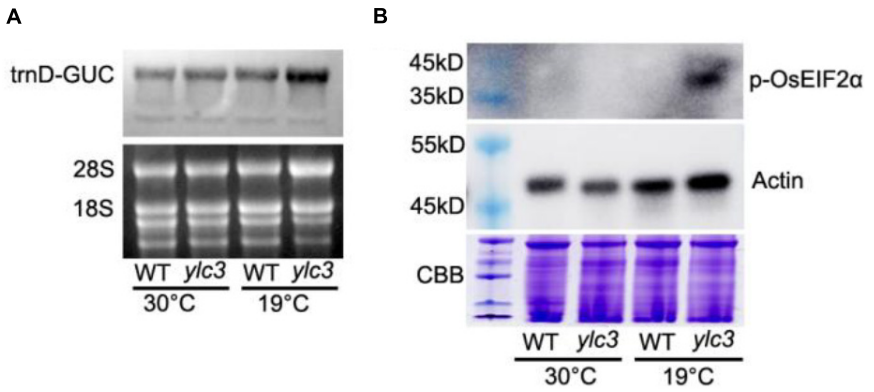

FIGURE 10 | Uncharged tRNA-Asp accumulation and phosphorylation of OsEIF2α at different growth temperatures. **(A)** Uncharged tRNA-Asp levels in WT and *ylc3* seedlings were analyzed by northern blot. The ethidium bromide-stained gel is shown as a loading reference. **(B)** Phosphorylation levels of OsEIF2α in WT and *ylc3* seedlings were monitored by immunoblot analysis. Upper and lower panels represent immunoblot results using antibodies against phosphorylated eIF2α and actin, respectively. Coomassie Brilliant Blue (CBB) staining is shown as a loading reference. Protein size marker is indicated.

to nucleus, inducing immunity responses in Arabidopsis (Schwarzenbacher et al., 2020). It cannot be excluded that YLC3 is translocated to chloroplasts to participate in chloroplast development under low temperature condition.

Changes of Amino Acid Homeostasis in *ylc3* Mutant

We have measured the 20 free amino acids in leaves of *ylc3* mutant growing under low temperature condition. Surprisingly, asparagine was increased by 78-fold, glutamine was increased by 10-fold while aspartate was only increased by 92% compared to wild-type plants. Meanwhile, Arabidopsis *ibi1* mutant showed 100% increase in aspartate (Luna et al., 2014). Rice *osers1* mutant anthers contain 144% more glutamate, 76% more aspartate, and 168% more histidine (Yang et al., 2018). According to the aspartate metabolic pathway, aspartate aminotransferase converts aspartate to glutamate and oxaloacetate, then glutamine synthetase converts glutamate to glutamine, and finally asparagine synthetase converts glutamine and aspartate to asparagine (**Figure 11**). Consistently, quantitative proteomics analysis demonstrated the up-regulation of the above enzymes with asparagine synthetase (ASN1) being most elevated. A previous study indicated that asparagine synthesis is mainly dependent on ASN1 (Ohashi et al., 2015; Luo et al., 2018). As the free amino acids were restored to normal levels in the *ylc3* complementation lines, the over-accumulation of glutamine and asparagine under low temperature condition represents a consequence of *ylc3* mutation. Consistently, the mutant showed normal levels of free amino acids under high temperature condition.

Apparently, the *ylc3* mutation resulted in functional deficiency of the encoded aspartyl-tRNA synthetase under low temperature condition. Consequently, aspartate and uncharged tRNA-ASP levels would be elevated (**Figure 10A**). We speculate that most of the excess aspartate had been converted to glutamine and asparagine which are the major storage form of organic nitrogen, some of them could be stored in xylem and phloem sap (Urquhart and Joy, 1981; Lea et al., 2007; Gaufichon et al., 2010, 2016). On the other hand, the conversion may relieve the inhibitory effects of high concentrations of aspartate (Schultz et al., 1998). Meanwhile, it is unknown whether over-accumulation of asparagine and glutamine may affect chloroplast development. Functional investigation of aspartyl-tRNA synthetases in different plant species may reveal whether there are conserved mechanisms for regulating aspartate metabolism and whether there are relationships between changes in free amino acid levels and chloroplast development.

Differential Regulation of Protein Abundances in *ylc3* Mutant

During amino acid starvation, the yeast GCN2 kinase inhibits protein translation and activates amino acid biosynthesis (Natarajan et al., 2001; Dever and Hinnebusch, 2005). This mechanism is at least partially conserved in the Arabidopsis homologous protein (Li et al., 2013; Luna et al., 2014). Amino acid starvation or AARS deficiencies could result in accumulation of uncharged tRNA. AtGCN2 interacts with uncharged tRNA and becomes activated, thereby phosphorylating the translation initiation factor AtEIF2α and leading to inhibition of protein translation (Luna et al., 2014). Under low temperature condition, aspartate accumulation in the *ylc3* mutant could lead to uncharged tRNA accumulation (**Figure 10A**). Hence, OsGCN2 would become activated to phosphorylate eif2α, leading to inhibition of protein translation (**Figure 10B**). In fact, there was no a GCN4 homolog in Arabidopsis (Halford et al., 2004; Halford, 2006). It is unclear which OsGCN2-regulated proteins are involved in the adaptation to amino acid starvation in rice. Under low temperature condition, the up-regulation of enzymes involved in amino acid biosynthesis and related pathways, such as those for pyruvate metabolism in *ylc3* mutant, is consistent with the transcriptional up-regulation of amino acid biosynthesis in yeast during amino acid starvation (Dever and Hinnebusch, 2005; Luna et al., 2014). Furthermore, up-regulation of aspartate metabolic enzymes could convert

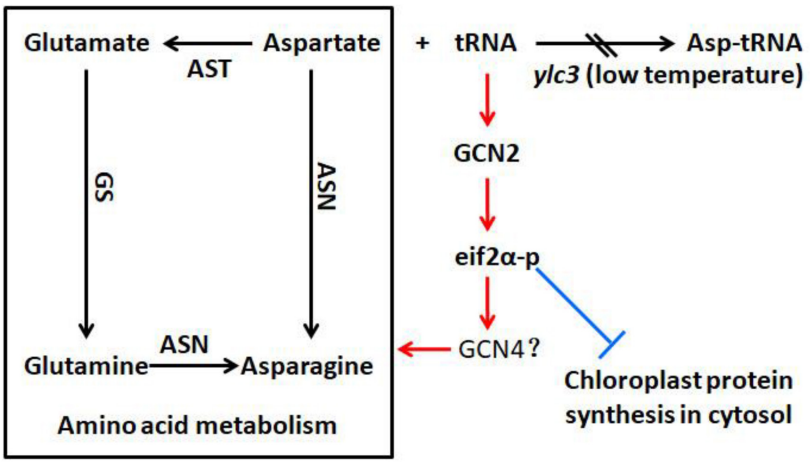

FIGURE 11 | Possible involvement of YLC3 in amino acid homeostasis and chloroplast development. Loss of YLC3 function leads to accumulation of uncharged tRNAs, which promote GCN2-dependent phosphorylation of eIF2α (eIF2α-p), thereby up-regulating amino acid synthesis and inhibiting chloroplast development. Consequently, excess free aspartate is converted to glutamine and asparagine for storage. Positive and negative regulatory effects are indicated in red and blue colors, respectively. ASN, asparagine synthetase; AST, aspartate aminotransferase; GS, glutamine synthetase.

some of the excess aspartate to asparagine and glutamine for storage, implicating a precise regulating mechanism during over-accumulation of aspartate. There was no significant down-regulation of chlorophyll biosynthesis enzymes, suggesting that the reduced chlorophyll content in the *ylc3* mutant was not due to their inhibition. On the other hand, thylakoid complex proteins are largely down-regulated in *ylc3* mutant under low temperature condition.

Translation of cytosolic mRNA is regulated at both global and mRNA-specific levels. For example, uncharged tRNAs-ASP accumulated and activated AtGCN2 in the Arabidopsis *ibi1* mutant (Li et al., 2013; Luna et al., 2014). Recently, inhibition of ribosome loading by activated GCN2 kinase was demonstrated for mRNAs functionally involved in mitochondrial ATP synthesis, chloroplast thylakoids, vesicle trafficking, and translation (Lokdarshi et al., 2020). In our study, the uncharged tRNAs-ASP level was increased and the translation initiation factor eIF2α was phosphorylated in *ylc3* seedlings under low temperature condition (**Figure 10**). Quantitative proteomics data also indicated that cytosolic mRNA translation of thylakoid proteins was suppressed specifically in the mutant. Overall, our results suggested that YLC3 deficiency could promote the GCN2-eif2α phosphorylation and impaired chloroplast development by suppressing cytosolic mRNA translation in rice (**Figure 11**). Further investigations are necessary in order to fully understand the functions of YLC3 and other aspartyl-tRNA synthetases in rice under different stress conditions.

MATERIALS AND METHODS

Plant Materials and Growth Conditions

The rice (*Oryza sativa* ssp. *japonica* cv. Nipponbare) *ylc3* mutant was isolated from an EMS-induced mutant population. Wild-type and *ylc3* mutant plants were grown in Kimura nutrient solution as described previously (Chen et al., 2013). They were kept in a light growth chamber (Panasonic MLR-352H-PC) with a 12 h-light/12 h-dark cycle at 70% relative humidity. Temperatures were set according to each specific treatment.

Genetic Analysis and Construction of F_2 Mapping Populations

The *ylc3* mutant was individually crossed with Nipponbare or Kasalath rice to generate the F_1 progenies which were self-pollinated to obtain the F_2 population. Using the F_1 and F_2 populations, genetic analysis and preliminary mapping were performed. From the F_2 population of the *ylc3* × Kasalath cross, 22 mutant plants were selected for preliminary mapping. The F_2 mutant number was increased to 94 during fine mapping. At the same time, genome sequencing and gene cloning were performed using the F_2 population from the *ylc3* × Nipponbare cross (Abe et al., 2012).

TEM Analysis of Chloroplast Structures and GUS Staining of Rice Tissues

Fifteen-day-old wild-type and *ylc3* seedlings kept in a light growth chamber at 19°C were used for chloroplast ultra-structural analysis. Leaves were cut into 2-mm sections and fixed using 2.5% glutaraldehyde in cacodylate buffer, following by secondary fixation in OsO_4. The fixed tissues were dehydrated by ethanol, embedded in epoxy resin, and sectioned for examination under an Hitachi H7650 TEM electron microscope. GUS staining was performed according to Jefferson et al. (1987). Roots, stems, and leaves from 7-day-old seedlings grown at 26°C in a light growth chamber as well as stems, leaves, and panicles from heading stage of mature plants grown in paddy field were collected. Stems and leaves were sliced into 2-mm sections and placed in GUS staining solution for vacuum infiltration (5–10 times) until the samples were completely submerged.

After staining at 37°C for 8 h, the tissues were decolored using 70% ethanol and then observed under a Nikon SMZ1000 stereomicroscope.

Complementation Analysis and Gene Editing Vector Construction

A complementation construct in the pCambia1300 binary vector harboring the YLC3 3.388-kb upstream sequence, the YLC3 1.846-kb cDNA containing the full coding region, and the NOS-3 terminator was generated and named as pCAMBIA1300-PR-YLC3-NOS. It was transformed into *Agrobacterium tumefaciens* EHA105 which was used to infect *ylc3* calluses for 3 days. Afterwards, the calluses were selected on hygromycin plates, followed by differentiation and tissue regeneration (Lee et al., 1999). For construction of the base editing vector, a 19-bp target-specific oligonucleotide initialized by "G" and a 5-bp adaptor were synthesized, annealed and ligated to a *Bsa*I-digested CBEmax-NGG vector (Wang et al., 2019). The constructed vector was confirmed by Sanger sequencing and used for *Agrobacterium*-mediated transformation of rice calluses. For the construction of YLC3 promoter-Gus vector, the 3.388-kb promoter region of YLC3 was fused with the GUS gene in the modified pCAMBIA1300-GUS vector. All primers used for constructing vectors are listed in **Supplementary Table 3**.

Subcellular Localization

The *YLC3* coding sequence without a stop codon and fused in-frame with sGFP was cloned into the pCAMBIA1301-35S-NOS vector and transiently expressed in rice protoplasts. Rice seedlings cultured on MS media for 10 days were digested with cellulases for protoplast preparation as described previously (Zhang et al., 2011). Protoplasts (100 μl) were transfected with the vector (5–10 μg) and dark-incubated at room temperature, following by examination of green fluorescence signals under a Zeiss confocal laser scanning microscope. For mitochondria co-localization, transfected protoplasts were stained using a mitochondria fluorescent dye (Mitotracker, Invitrogen, Carlsbad, CA, United States).

Phylogenetic Analysis and KEGG Analysis

A phylogenetic tree was constructed using aligned full-length sequences of homologs of YLC3. MEGA (version 10.1.7) (Kumar et al., 2018) and the neighbor-joining methods were used with a p-distance model, pairwise deletion and bootstrap (1,000 replicates). The maximum parsimony method of MEGA also was used to support the neighbor-joining tree using the default parameters. Amino acid sequences from regions 101 to 188 and 223 to 544 in YLC3 were used for motif alignment by MEGA. For GO and KEGG analysis, the differentiated expressed proteins were enriched with rice pathways and GO terms using clusterProfiler (Wu et al., 2021) and org.Osativa.eg.db. (Xu, 2019). The filtering criteria of p value Cutoff 0.05 and qvalueCutoff 0.1 were used.

Measurements of Free Amino Acid Contents

Free amino acid contents in rice leaves were measured using an Hitachi LA8080 automatic amino acid analyzer. Leaves (0.05 g) were placed in 2-ml centrifuge tubes, followed by addition of 1 ml 4% sulfosalicylic acid and two zirconia beads. Bead-beating was performed for 1 h at 1 time per 2 min until the samples became slurry. The samples were allowed to settle for 1 h, followed by centrifugation at 4°C for 10 min. Supernatant (500 μl) was taken, mixed with 500 μl 0.2 M HCl, and filtered through a 0.22 μl millipore filter. Finally, 20 μl sample was used for free amino acid analysis.

Quantitative Proteomics Analysis of Rice Seedlings

Protein Isolation

Crude proteins from rice seedling tissues were extracted by the modified phenol-methanol method as described (Deng et al., 2007). Extracted proteins were dissolved in lysis buffer [8 M urea, 50 mM triethylammonium bicarbonate (TEAB), pH 8.0] and quantified using a 2-D Quant kit (GE Healthcare, Piscataway, NJ, United States) with bovine serum albumin as a standard.

Tryptic Digestion, Peptide Labeling and Fractionation, LC-MS/MS Analysis

Tryptic digestion, TMT labeling, peptide fractionation and LC-MS/MS were performed as described (Zhu et al., 2022) unless otherwise stated. After tris(2carboxyethyl)phosphin (TCEP) and dithiothreitol (DTT) treatments, proteins were precipitated and dissolved in 50 mM TEAB buffer. Each sample (25 μg) was mixed with its respective 6-plex TMT reagent and incubated for 1 h at room temperature. Three biological replicates were labeled for each sample group, in which the Nipponbare samples were labeled with TMT reagents 126, 127, and 128, while *ylc3* samples were labeled with TMT reagents 129, 130, and 131, respectively. The labeling reactions were stopped by addition of hydroxylamine, then combined and dried by vacuum. The combined multiplexed TMT-labeled samples were separated on a Waters Acquity BEH C18 1.7 μm 2.1–100 mm column using H class UPLC system (Waters, Milford, MA, United States) at a flow rate of 300 μl/min. A total of 24 fractions were collected, then combined into 12 fractions and vacuum dried for LC-MS/MS analysis.

TMT-labeled samples were analyzed on an Ultimate 3000 nano UHPLC system (Thermo Scientific, Waltham, MA, United States) coupled online to a Q Exactive HF mass spectrometer (Thermo Scientific, Waltham, MA, United States) equipped with a Nanospray Flex Ion Source (Thermo Scientific, Waltham, MA, United States). Samples were separated by a binary buffer system of buffer A (0.1% formic acid) and buffer B (80% acetonitrile plus 0.1% formic acid). Peptides were eluted in a gradient of 5–8% solvent B in 2 min, 8–20% solvent B in 66 min, 20–40% solvent B in 33 min, and 40–90% solvent B in 4 min.

TMT Data Analysis

Raw data were processed using Proteome Discoverer 2.4.0.305 (Thermo Scientific, Waltham, MA, United States) with the SEQUEST HT search engine searching against a rice proteome database (Rice Genome Annotation Project[1], version 7.0, total 66,338 entries). Searches were configured with static modifications for the TMT reagents on lysine and N-termini, carbamidomethyl on cysteine, dynamic modifications for oxidation of methionine and acetylation of protein N-termini, precursor mass tolerance of 10 ppm, fragment mass tolerance of 0.02 Da, and trypsin cleavage (max 2 missed cleavages). Searches used a reversed sequence decoy strategy to control peptide false discovery and identifications were validated by Percolator software. Protein groups, peptide groups and PSMs were accepted at a false discovery rate (FDR) < 1%. Normalization was applied for the grand total reporter ion intensity for each channel within the 6-plex experiment. Further downstream analysis of the results was performed in the R scripting and statistical environment, using the limma package from Bioconductor[2]. The basic statistics used for significance analysis is the moderated t-statistics. Significantly expressed proteins were filtered for an average fold-change > 1.3 or <0.77, with *p*-values adjusted for multiple testing correction by FDR (Benjamini–Hochberg).

RNA Isolation and Northern-Blot Analysis

Total RNAs were extracted from 15-day-old seedlings grown at different temperatures using TRIzol reagent (Invitrogen, Carlsbad, CA, United States). RNA was precipitated by ethanol overnight at −20°C. Northern blot was performed as previously described (Huang et al., 2018). The sequences of biotinylated oligomer probes were listed as follows: trnD-GUC (Id: 29141347), 5′-TTGTAGTTCAATTGGTCAGAGCACC-3′; trnD(GTC) (Id: 3950710) 5′-GAAATAGCTCAGTTGGTTAGAGTG-3′.

Total Protein Extraction and Immunoblot Analysis

The first leaves were collected from WT and *ylc3* mutant seedlings grown at 19 or 30°C for immunoblot analysis. Total proteins were extracted using extraction buffer (containing 25 mM Tris-HCl [pH 7.5], 10 mM NaCl, 4 mM PMSF, 20 mM MG132, and protease inhibitor cocktail). Extracted proteins were subjected to sodium dodecyl sulfate polyacrylamide gel electrophoresis and immunoblotting. Immunoblotting was performed using a monoclonal antibody of phospho-eIF2α (Ser51) (Catalogue no. 9721, Cell Signalling, Danvers, MA, United States 1/1000 dilution) or a monoclonal antibody of Anti Plant Actin Mouse (Abbkine, A01050). Signals were detected using the Immobilon kit (Catalogue no WBKLS0500, Millipore) under standard conditions.

[1]http://rice.plantbiology.msu.edu/index.shtml

[2]http://www.bioconductor.org/

DATA AVAILABILITY STATEMENT

The proteomics data have been deposited to the ProteomeXchange Consortium. Link: https://www.iprox.cn/page/project.html?id=IPX0004037000; ProteomeXchange ID:PXD031497. The mass spectrometry proteomics data have been deposited to the ProteomeXchange Consortium (http://proteomecentral.proteomexchange.org) via the iProX partner repository (Ma et al., 2019) with the dataset identifier PXD031497.

AUTHOR CONTRIBUTIONS

HL and CL designed the experiments. HL, XG, HD, JT, FW, WW, ZZ, RX, and HH performed the experiments. YS, JT, ZZ, HL, and CL analyzed the data. HL and CL wrote the manuscript. All authors contributed to the article and approved the submitted version.

FUNDING

This work was supported by the National Natural Science Foundation of China (31571633).

ACKNOWLEDGMENTS

We thank Hui Zhang (Shanghai Normal University) for construction of the YLC3 gene editing vector, Yu Liu (Zhejiang University) for measurement of free amino acid contents.

SUPPLEMENTARY MATERIAL

The Supplementary Material for this article can be found online at: https://www.frontiersin.org/articles/10.3389/fpls.2022.847364/full#supplementary-material

Supplementary Figure 1 | GUS staining of 7-day-old ProYLC3::GUS transgenic seedlings grown at 19°C. Two independent ProYLC3::GUS transgenic lines (pr-1 and pr-4) was used to gus staining test. Bar = 1 cm.

Supplementary Figure 2 | Transcriptional expression of YLC3 was performed by Real-time PCR. Gene-specific primers is list below: YLC3-qpF, 5′-CTCCCTCAGCAAGGAATCAA-3′; YLC3-qpR, 5′-CACCTGAATCTCCACCTGCT-3′; Actin-qpF, 5′-GTGTGACAATGGAACTGGCA-3′; Actin-qpR 5′-CCACGATACTAGGGAAAACAGC-3′.

Supplementary Figure 3 | Subcellular localization analysis in YLC3::GFP transgenic rice. Two independent YLC3::GFP transgenic lines cultured on MS media for 10 days were digested with cellulases for protoplast preparation as described previously (Zhang et al., 2011). Green fluorescence signals was observed and captured by a Zeiss confocal laser scanning microscope. For mitochondria co-localization, protoplasts were stained in a mitochondria fluorescent dye (Mitotracker, Invitrogen, Carlsbad, CA, United States).

Supplementary Table 1 | 9,212 proteins from quantitative proteomics analysis.

Supplementary Table 2 | 4,979 proteins from KEGG analysis.

Supplementary Table 3 | Vector construction primers and indel primers.

REFERENCES

Abdallah, F., Salamini, F., and Leister, D. (2000). A prediction of the size and evolutionary origin of the proteome of chloroplasts of *Arabidopsis*. *Trends Plant Sci.* 5, 141–142. doi: 10.1016/s1360-1385(00)01574-0

Abe, A., Kosugi, S., Yoshida, K., Natsume, S., Takagi, H., Kanzaki, H., et al. (2012). Genome sequencing reveals agronomically important loci in rice using MutMap. *Nat. Biotechnol.* 30, 174–178. doi: 10.1038/nbt.2095

Berg, M., Rogers, R., Muralla, R., and Meinke, D. (2005). Requirement of aminoacyl-tRNA synthetases for gametogenesis and embryo development in *Arabidopsis*. *Plant J.* 44, 866–878. doi: 10.1111/j.1365-313X.2005.02580.x

Bröer, S., and Bröer, A. (2017). Amino acid homeostasis and signalling in mammalian cells and organisms. *Biochem. J.* 474, 1935–1963. doi: 10.1042/BCJ20160822

Chen, X., Shi, J., Hao, X., Liu, H., Shi, J., Wu, Y., et al. (2013). OsORC3 is required for lateral root development in rice. *Plant J.* 74, 339–350. doi: 10.1111/tpj.12126

Deng, Z., Zhang, X., Tang, W., Oses-Prieto, J. A., Suzuki, N., Gendron, J. M., et al. (2007). A proteomics study of brassinosteroid response in *Arabidopsis*. *Mol. Cell Proteomics* 6, 2058–2071. doi: 10.1074/mcp.M700123-MCP200

Dever, T. E., Feng, L., Wek, R. C., Cigan, A. M., Donahue, T. F., and Hinnebusch, A. G. (1992). Phosphorylation of initiation factor 2 alpha by protein kinase GCN2 mediates gene-specific translational control of GCN4 in yeast. *Cell* 68, 585–596. doi: 10.1016/0092-8674(92)90193-g

Dever, T. E., and Hinnebusch, A. G. (2005). GCN2 whets the appetite for amino acids. *Mol Cell* 18, 141–142. doi: 10.1016/j.molcel.2005.03.023

Duchêne, A. M., Giritch, A., Hoffmann, B., Cognat, V., Lancelin, D., Peeters, N. M., et al. (2005). Dual targeting is the rule for organellar aminoacyl-tRNA synthetases in *Arabidopsis thaliana*. *Proc. Natl. Acad. Sci. U. S. A.* 102, 16484–16489. doi: 10.1073/pnas.0504682102

Dyall, S. D., Brown, M. T., and Johnson, P. J. (2004). Ancient invasions: from endosymbionts to organelles. *Science* 304, 253–257. doi: 10.1126/science.1094884

Fang, G., Yang, S., Ruan, B., Liu, C., Zhang, A., Jiang, H., et al. (2020). Isolation of TSCD11 Gene for Early Chloroplast Development under High Temperature in Rice. *Rice* 13:49. doi: 10.1186/s12284-020-00411-6

Fernández, A. P., and Strand, A. (2008). Retrograde signaling and plant stress: plastid signals initiate cellular stress responses. *Curr. Opin. Plant Biol.* 11, 509–513. doi: 10.1016/j.pbi.2008.06.002

Gaufichon, L., Reisdorf-Cren, M., Rothstein, S. J., Chardon, F., and Suzukia, A. (2010). Biological functions of asparagine synthetase in plants. *Plant Sci.* 179, 141–153.

Gaufichon, L., Rothstein, S. J., and Suzuki, A. (2016). Asparagine Metabolic Pathways in *Arabidopsis*. *Plant Cell Physiol.* 57, 675–689. doi: 10.1093/pcp/pcv184

Halford, N. G. (2006). Regulation of carbon and amino acid metabolism, roles of sucrose nonfermenting-1-related protein kinase-1 and general control nonderepressible-2-related protein kinase. *Adv. Bot. Res.* 43, 93–142.

Halford, N. G., Hey, S., Jhurreea, J., Laurie, S., McKibbin, R. S., and Zhang, Y. (2004). Highly conserved protein kinases involved in the regulation of carbon and amino acid metabolism. *J. Exp. Bot.* 55, 35–42. doi: 10.1093/jxb/erh019

Hinnebusch, A. G. (2005). Translational regulation of GCN4 and the general amino acid control of yeast. *Annu. Rev. Microbiol.* 59, 407–450. doi: 10.1146/annurev.micro.59.031805.133833

Huang, W., Zhu, Y., Wu, W., Li, X., Zhang, D., and Yin, P. (2018). The Pentatricopeptide Repeat Protein SOT5/EMB2279 Is Required for Plastid rpl2 and trnK Intron Splicing. *Plant Physiol.* 177, 684–697. doi: 10.1104/pp.18.00406

Ibba, M., and Soll, D. (2000). Aminoacyl-tRNA synthesis. *Annu. Rev. Biochem.* 69, 617–650. doi: 10.1146/annurev.biochem.69.1.617

Jarvis, P., and López-Juez, E. (2013). Biogenesis and homeostasis of chloroplasts and other plastids. *Nat. Rev. Mol. Cell Biol.* 14, 787–802. doi: 10.1038/nrm3702

Jefferson, R. A., Kavanagh, T. A., and Bevan, M. W. (1987). GUS fusions: beta-glucuronidase as a sensitive and versatile gene fusion marker in higher plants. *EMBO J.* 6, 3901–3907.

Kägi, C., Baumann, N., Nielsen, N., Stierhof, Y. D., and Gross-Hardt, R. (2010). The gametic central cell of *Arabidopsis* determines the lifespan of adjacent accessory cells. *Proc. Natl. Acad. Sci. U. S. A.* 107, 22350–22355. doi: 10.1073/pnas.1012795108

Kim, Y. K., Lee, J. Y., Cho, H. S., Lee, S. S., Ha, H. J., Kim, S., et al. (2005). Inactivation of organellar glutamyl- and seryl-tRNA synthetases leads to developmental arrest of chloroplasts and mitochondria in higher plants. *J. Biol. Chem.* 280, 37098–37106. doi: 10.1074/jbc.M504805200

Kumar, S., Stecher, G., Li, M., Knyaz, C., and Tamura, K. (2018). MEGA X: molecular Evolutionary Genetics Analysis across Computing Platforms. *Mol. Biol. Evol.* 35, 1547–1549. doi: 10.1093/molbev/msy096

Lageix, S., Lanet, E., Pelissier, M. N., Espagnol, M. C., Robaglia, C., Deragon, J. M., et al. (2008). *Arabidopsis* eIF2alpha kinase GCN2 is essential for growth in stress conditions and is activated by wounding. *BMC Plant Biol.* 8:134. doi: 10.1186/1471-2229-8-134

Lea, P. J., Sodek, L., Parry, M. A. J., Shewry, P. R., and Halford, N. G. (2007). Asparagine in plants. *Ann. Appl. Biol.* 150, 1–26.

Lee, S., Jeon, J. S., Jung, K. H., and An, G. (1999). Binary vectors for efficient transformation of rice. *J. Plant Biol.* 42, 310–316.

Li, H., Ji, G., Wang, Y., Qian, Q., Xu, J., Sodmergen, et al. (2018). WHITE PANICLE3, a Novel Nucleus-Encoded Mitochondrial Protein, Is Essential for Proper Development and Maintenance of Chloroplasts and Mitochondria in Rice. *Front. Plant Sci.* 9:762. doi: 10.3389/fpls.2018.00762

Li, M. W., AuYeung, W. K., and Lam, H. M. (2013). The GCN2 homologue in *Arabidopsis thaliana* interacts with uncharged tRNA and uses *Arabidopsis* eIF2α molecules as direct substrates. *Plant Biol.* 15, 13–18. doi: 10.1111/j.1438-8677.2012.00606.x

Li, M. W., and Lam, H. M. (2008). Searching for nitrogen sensing systems in higher plants. *Dyn. Soil Dyn. Plant* 2, 13–22.

Liu, W., Fu, Y., Hu, G., Si, H., Zhu, L., Wu, C., et al. (2007). Identification and fine mapping of a thermo-sensitive chlorophyll deficient mutant in rice (*Oryza sativa* L.). *Planta* 226, 785–795. doi: 10.1007/s00425-007-0525-z

Lokdarshi, A., Guan, J., Urquidi Camacho, R. A., Cho, S. K., Morgan, P. W., Leonard, M., et al. (2020). Light Activates the Translational Regulatory Kinase GCN2 via Reactive Oxygen Species Emanating from the Chloroplast. *Plant Cell* 32, 1161–1178. doi: 10.1105/tpc.19.00751

Lü, Y., Cui, X., Li, R., Huang, P., Zong, J., Yao, D., et al. (2015). Development of genome-wide insertion/deletion markers in rice based on graphic pipeline platform. *J. Integr. Plant Biol.* 57, 980–991. doi: 10.1111/jipb.12354

Luna, E., Van Hulten, M., Zhang, Y., Berkowitz, O., López, A., Pétriacq, P., et al. (2014). Plant perception of beta-aminobutyric acid is mediated by an aspartyl-tRNA synthetase. *Nat. Chem. Biol.* 10, 450–456. doi: 10.1038/nchembio.1520

Luo, L., Qin, R., Liu, T., Yu, M., Yang, T., and Xu, G. (2018). OsASN1 Plays a Critical Role in Asparagine-Dependent Rice Development. *Int. J. Mol. Sci.* 20:130. doi: 10.3390/ijms20010130

Ma, J., Chen, T., Wu, S., Yang, C., Bai, M., Shu K., et al. (2019). iProX: an integrated proteome resource. *Nucleic Acids Res.* 47, D1211–D1217. doi: 10.1093/nar/gky869

Marton, M. J., Crouch, D., and Hinnebusch, A. G. (1993). GCN1, a translational activator of GCN4 in Saccharomyces cerevisiae, is required for phosphorylation of eukaryotic translation initiation factor 2 by protein kinase GCN2. *Mol. Cell Biol.* 13, 3541–3556. doi: 10.1128/mcb.13.6.3541-3556.1993

Natarajan, K., Meyer, M. R., Jackson, B. M., Slade, D., Roberts, C., Hinnebusch, A. G., et al. (2001). Transcriptional profiling shows that Gcn4p is a master regulator of gene expression during amino acid starvation in yeast. *Mol. Cell. Biol.* 21, 4347–4368. doi: 10.1128/MCB.21.13.4347-4368

O'Donoghue, P., and Luthey-Schulten, Z. (2003). On the evolution of structure in aminoacyl-tRNA synthetases. *Microbiol. Mol. Biol. Rev.* 67, 550–573. doi: 10.1128/MMBR.67.4.550-573

Ohashi, M., Ishiyama, K., Kojima, S., Konishi, N., Nakano, K., Kanno, K., et al. (2015). Asparagine synthetase1, but not asparagine synthetase2, is responsible for the biosynthesis of asparagine following the supply of ammonium to rice roots. *Plant Cell Physiol.* 56, 769–778. doi: 10.1093/pcp/pcv005

Richardson, L. G. L., Singhal, R., and Schnell, D. J. (2017). The integration of chloroplast protein targeting with plant developmental and stress responses. *BMC Biol.* 15:118. doi: 10.1186/s12915-017-0458-3

Sattlegger, E., and Hinnebusch, A. G. (2005). Polyribosome binding by GCN1 is required for full activation of eukaryotic translation initiation factor 2{alpha} kinase GCN2 during amino acid starvation. *J. Biol. Chem.* 280, 16514–16521. doi: 10.1074/jbc.M414566200

Schultz, C. J., Hsu, M., Miesak, B., and Coruzzi, G. M. (1998). *Arabidopsis* mutants define an in vivo role for isoenzymes of aspartate aminotransferase in plant nitrogen assimilation. *Genetics* 149, 491–499. doi: 10.1093/genetics/149.2.491

Schwarzenbacher, R. E., Wardell, G., Stassen, J., Guest, E., Zhang, P., Luna, E., et al. (2020). The IBI1 Receptor of β-Aminobutyric Acid Interacts with VOZ Transcription Factors to Regulate Abscisic Acid Signaling and Callose-Associated Defense. *Mol. Plant* 13, 1455–1469. doi: 10.1016/j.molp.2020.07.010

Urquhart, A. A., and Joy, K. W. (1981). Use of Phloem exudate technique in the study of amino Acid transport in pea plants. *Plant Physiol.* 68, 750–754. doi: 10.1104/pp.68.3.750

Wang, L., Li, H., Zhao, C., Li, S., Kong, L., Wu, W., et al. (2017). The inhibition of protein translation mediated by AtGCN1 is essential for cold tolerance in *Arabidopsis thaliana*. *Plant Cell Environ.* 40, 56–68. doi: 10.1111/pce.12826

Wang, M., Wang, Z., Mao, Y., Lu, Y., Yang, R., and Tao, X. (2019). Optimizing base editors for improved efficiency and expanded editing scope in rice. *Plant Biotechnol. J.* 17, 1697–1699. doi: 10.1111/pbi.13124

Wang, Y., Wang, C., Zheng, M., Lyu, J., Xu, Y., Li, X., et al. (2016). WHITE PANICLE1, a Val-tRNA Synthetase Regulating Chloroplast Ribosome Biogenesis in Rice, Is Essential for Early Chloroplast Development. *Plant Physiol.* 170, 2110–2123. doi: 10.1104/pp.15.01949

Wek, R. C., Jiang, H. Y., and Anthony, T. G. (2006). Coping with stress: eIF2 kinases and translational control. *Biochem. Soc. Trans.* 34, 7–11. doi: 10.1042/BST20060007

Woodson, J. D., and Chory, J. (2008). Coordination of gene expression between organellar and nuclear genomes. *Nat. Rev. Genet.* 9, 383–395. doi: 10.1038/nrg2348

Wu, T., Hu, E., Xu, S., Chen, M., Guo, P., Dai, Z., et al. (2021). clusterProfiler 4.0: a universal enrichment tool for interpreting omics data. *Innovation* 2:100141. doi: 10.1016/j.xinn.2021.100141

Xu, Z. (2019). *xuzhougeng/org.Osativa.eg.db v0.01 (Version v0.01)*. Geneva: Zenodo. doi: 10.5281/zenodo.3374105

Yang, X., Li, G., Tian, Y., Song, Y., Liang, W., and Zhang, D. (2018). A Rice Glutamyl-tRNA Synthetase Modulates Early Anther Cell Division and Patterning. *Plant Physiol.* 177, 728–744. doi: 10.1104/pp.18.00110

Zhang, Y., Dickinson, J. R., Paul, M. J., and Halford, N. G. (2003). Molecular cloning of an *Arabidopsis* homologue of GCN2, a protein kinase involved in coordinated response to amino acid starvation. *Planta* 217, 668–675. doi: 10.1007/s00425-003-1025-4

Zhang, Y., Su, J., Duan, S., Ao, Y., Dai, J., Liu, J., et al. (2011). A highly efficient rice green tissue protoplast system for transient gene expression and studying light/chloroplast-related processes. *Plant Methods* 7:30. doi: 10.1186/1746-4811-7-30

Zhang, Y., Wang, Y., Kanyuka, K., Parry, M. A., Powers, S. J., and Halford, N. G. (2008). GCN2-dependent phosphorylation of eukaryotic translation initiation factor-2alpha in *Arabidopsis*. *J. Exp. Bot.* 59, 3131–3141. doi: 10.1093/jxb/ern169

Zhang, Y. Y., Hao, Y. Y., Wang, Y. H., Wang, C. M., Wang, Y. L., Long, W. H., et al. (2017). Lethal albinic seedling, encoding a threonyl-tRNA synthetase, is involved in development of plastid protein synthesis system in rice. *Plant Cell Rep.* 36, 1053–1064. doi: 10.1007/s00299-017-2136-x

Zhu, Y., Qiu, W., Li, Y., Tan, J., Han, X., Wu, L., et al. (2022). Quantitative proteome analysis reveals changes of membrane transport proteins in Sedum plumbizincicola under cadmium stress. *Chemosphere* 287:132302. doi: 10.1016/j.chemosphere

Conflict of Interest: The authors declare that the research was conducted in the absence of any commercial or financial relationships that could be construed as a potential conflict of interest.

Publisher's Note: All claims expressed in this article are solely those of the authors and do not necessarily represent those of their affiliated organizations, or those of the publisher, the editors and the reviewers. Any product that may be evaluated in this article, or claim that may be made by its manufacturer, is not guaranteed or endorsed by the publisher.

frontiers in Plant Science

ORIGINAL RESEARCH
published: 16 March 2022
doi: 10.3389/fpls.2022.849532

MAG2 and MAL Regulate Vesicle Trafficking and Auxin Homeostasis With Functional Redundancy

*Xiaohui Ma[1†], Xiaonan Zhao[1,2†], Hailong Zhang[1], Yiming Zhang[1], Shanwen Sun[1], Ying Li[1], Zhengbiao Long[2], Yuqi Liu[1], Xiaomeng Zhang[1], Rongxia Li[3], Li Tan[3], Lixi Jiang[2], Jian-Kang Zhu[3] and Lixin Li[1]**

[1] Key Laboratory of Saline-Alkali Vegetation Ecology Restoration, College of Life Sciences, Ministry of Education, Northeast Forestry University, Harbin, China, [2] Institute of Crop Science, Zhejiang University, Hangzhou, China, [3] Shanghai Center for Plant Stress Biology, Center of Excellence in Molecular Plant Sciences, Chinese Academy of Sciences, Shanghai, China

Auxin is a central phytohormone and controls almost all aspects of plant development and stress response. Auxin homeostasis is coordinately regulated by biosynthesis, catabolism, transport, conjugation, and deposition. Endoplasmic reticulum (ER)-localized MAIGO2 (MAG2) complex mediates tethering of arriving vesicles to the ER membrane, and it is crucial for ER export trafficking. Despite important regulatory roles of MAG2 in vesicle trafficking, the *mag2* mutant had mild developmental abnormalities. MAG2 has one homolog protein, MAG2-Like (MAL), and the *mal-1* mutant also had slight developmental phenotypes. In order to investigate MAG2 and MAL regulatory function in plant development, we generated the *mag2-1 mal-1* double mutant. As expected, the double mutant exhibited serious developmental defects and more alteration in stress response compared with single mutants and wild type. Proteomic analysis revealed that signaling, metabolism, and stress response in *mag2-1 mal-1* were affected, especially membrane trafficking and auxin biosynthesis, signaling, and transport. Biochemical and cell biological analysis indicated that the *mag2-1 mal-1* double mutant had more serious defects in vesicle transport than the *mag2-1* and *mal-1* single mutants. The auxin distribution and abundance of auxin transporters were altered significantly in the *mag2-1* and *mal-1* single mutants and *mag2-1 mal-1* double mutant. Our findings suggest that MAG2 and MAL regulate plant development and auxin homeostasis by controlling membrane trafficking, with functional redundancy.

Keywords: MAG2 and MAL, vesicle trafficking, auxin homeostasis, plant development and stress response, proteomic analysis

OPEN ACCESS

Edited by:
Shaojun Dai,
Shanghai Normal University, China

Reviewed by:
Huazhong Shi,
Texas Tech University, United States
Caiji Gao,
South China Normal University, China

****Correspondence:***
Lixin Li
lixinli0515@nefu.edu.cn

† These authors have contributed equally to this work and share first authorship

Specialty section:
This article was submitted to Plant Proteomics and Protein Structural Biology, a section of the journal Frontiers in Plant Science

Received: *06 January 2022*
Accepted: *24 January 2022*
Published: *16 March 2022*

Citation:
Ma X, Zhao X, Zhang H, Zhang Y, Sun S, Li Y, Long Z, Liu Y, Zhang X, Li R, Tan L, Jiang L, Zhu J-K and Li L (2022) MAG2 and MAL Regulate Vesicle Trafficking and Auxin Homeostasis With Functional Redundancy. Front. Plant Sci. 13:849532. doi: 10.3389/fpls.2022.849532

INTRODUCTION

Auxin is a central phytohormone for almost all aspects of plant growth and development (reviewed in Gomes and Scortecci, 2021), and response to environmental stimuli (reviewed by Zhao, 2018). Auxin homeostasis regulated by coordination of auxin biosynthesis, catabolism, transport, conjugation, and deposition optimizes plant development and adaption to environmental stress (Bhalerao and Bennett, 2003; Blakeslee et al., 2019). Auxin gradients determine developmental outcomes (Leyser, 2005; Habets and Offringa, 2014; Zhao, 2018). Both roots and shoots exhibit

auxin gradients across longitudinal axes, and auxin levels are generally most concentrated in organ meristems and rapidly dividing tissues (Kramer and Bennett, 2006). Auxin transport is controlled mainly by AUXIN1 (AUX1), PIN-FORMED (PIN), and PIN-LIKES (PILS) family carriers. These proteins coordinately control auxin intercellular and intracellular transport and determine plant morphogenesis (Mravec et al., 2009; Barbez et al., 2012). Canonical PIN proteins such as AtPIN1-4 and AtPIN7 localize in the plasma membrane (PM) asymmetrically and play an overarching role in plant development by regulating directional cell-to-cell auxin transport (reviewed by Naramoto, 2017; Béziat and Kleine-Vehn, 2018). PILS proteins are observed to localize only in the endoplasmic reticulum (ER) (Barbez et al., 2012; Sauer and Kleine-Vehn, 2019), while, non-canonical PINs display diverse localization. For instance, AtPIN5 exhibits cell type-dependent localization, at the PM in aerial tissues and intracellular localization in root vascular cells (Ganguly et al., 2014); AtPIN6 shows dual localization in the ER and the PM (Simon et al., 2016; Ditengou et al., 2018); PIN8 is colocalized with PIN5 in the ER in pollen (Ding et al., 2012). Non-canonical PIN and PILS proteins likely sequester auxin in the ER and have an impact on cellular auxin signaling and homeostasis (Mravec et al., 2009; Barbez et al., 2012; Béziat et al., 2017; Middleton et al., 2018; Feraru et al., 2019; Sun et al., 2020).

After being synthesized and assembled in the ER (Borgese et al., 2006), canonical PIN proteins are delivered to the PM through the secretory pathway, and they maintain their homeostasis in the PM by the cycling machinery (Naramoto, 2017). Phosphorylation of PIN proteins, which appears to control both PIN directional delivery and activities, is regulated by kinases, D6 protein kinases (D6PKs), PINOID (PID), wavy root growth (WAG)1, WAG2, and protein phosphatese 2A (PP2As) (Friml et al., 2004; Michniewicz et al., 2007; Dhonukshe et al., 2010; Zourelidou et al., 2014; Weller et al., 2017; Barbosa et al., 2018; Zhou and Luo, 2018). The impact of PID and PP2As on PIN phosphorylation status determines PIN cycling and maintains PIN polar localization (Máthé et al., 2021).

The vesicle trafficking system maintains organelle identities and homeostasis to contribute to proper cellular activities. Recognition machineries of a donor with target membranes consist of tethering factors, Ras-related in brain (RABs), ADP-ribosylation factors (ARFs), guanine nucleotide exchange factors (GEFs), etc. (Lamber et al., 2019; Homma et al., 2021). Tethering factors mediate the first contact between arriving vesicles and target membrane (Grosshans et al., 2006), and transfer the machinery to downstream factors such as soluble *N*-ethylmalemide sensitive factor attachment protein receptors (SNAREs) (Wang et al., 2017). SNAREs facilitate membrane fusion of transport vesicles with target membranes. According to sequences of center amino acids in the SNARE motif, SNARE proteins are classified into Q-SANREs (including Qa-, Qb-, and Qc-SNAREs) and R-SNAREs. Specific combination of R- with Q-SNAREs forms a SNARE complex to drive membrane fusion (Fasshauer et al., 1998).

Tethering factors could be divided into two classes: long single coiled-coil proteins such as MAG4/Atp115 (Whyte and Munro, 2002; Takahashi et al., 2010), and multisubunit complexes (Bröcker et al., 2010; Vukašinović and Žárský, 2016; Ravikumar et al., 2017; Zhao et al., 2018). Different tethering factors localize in distinct compartments as specific recognition machineries (Vukašinović and Žárský, 2016; Ravikumar et al., 2017). For example, the exocyst complex mediates tethering of post-Golgi vesicles to the PM (Saeed et al., 2019). The yeast Dsl1 complex consisting of Dsl1p, Sec39p, and Tip20p is localized in the ER and regulates Golgi-to-ER retrograde transport (Andag and Schmitt, 2003; Ren et al., 2009). The downstream SNAREs are Use1p, Sec20p, and Ufe1p (Linders et al., 2019). Our previous study has demonstrated that the *Arabidopsis* homolog complex of the Dsl1 complex is the MAG2-MIP1-MIP2-MIP3 complex (Li et al., 2006, 2013; Zhao et al., 2018). The MAIGO2 (MAG2) complex cooperates with ER-localized SANRE complex components, Qa-AtSYP81 and Qc-AtSec20, and potentially regulates Golgi-to-ER vesicle trafficking (Li et al., 2006, 2013). The *mag2* and *mip1/2/3* mutants abnormally accumulated precursors of seed storage proteins (SSPs, e.g., 2S albumins and 12S globulins) inside the ER lumen in seed cells (Li et al., 2006, 2013). In addition to important regulatory roles in membrane trafficking, MAG2 and MAG2-interacting proteins (MIPs) are also involved in response to abiotic stress and hormone, such as salinity, heat shock and osmotic stress, and abscisic acid (ABA) and gibberellic acid (Zhao et al., 2013, 2018; Zhao and Lu, 2014).

Despite the important regulatory roles of MAG2 in vesicle transport and stress response, *mag2* mutants just exhibit mild developmental abnormalities. It is reported that MAG2 has a homolog protein, MAG2-like (MAG2-Like (MAL), *At1g08400*) (Zhao et al., 2013; Zhao and Lu, 2014). We isolated a T-DNA insertion mutant, *mal-1*, and found that it also had slight developmental phenotypes. In order to analyze MAG2 and MAL function in plant development, we generated a double mutant, *mag2-1 mal-1*. As expected, the *mag2-1 mal-1* double mutant had serious developmental defects such as decreased germination activities, dwarf and partial seed abortion, and abnormal response to salt and osmotic and ABA stress. SSP precursors also accumulated at a higher level in the double mutant seeds than in the single mutant seeds. Proteomic analysis revealed that signaling, metabolism, and stress response were affected in *mag2-1 mal-1*, especially membrane trafficking, auxin biosynthesis, signaling, and transport. Biochemical and cell biological analysis indicated that the *mag2-1 mal-1* double mutant had more serious defects on vesicle transport than the single mutants. Auxin distribution and auxin transporter accumulation were significantly altered in *mag2-1*, *mal-1*, and *mag2-1 mal-1*. Our findings suggested that MAG2 and MAL regulate plant development, auxin homeostasis, and stress response potentially by controlling vesicle trafficking, and that they are functionally redundant.

MATERIALS AND METHODS

Plant Materials and Growth Conditions

Arabidopsis thaliana ecotype Col-0 was used as wild-type plants. The T-DNA-tagged line (*mal-1*, GABI_kat_288E12) was provided by the *Arabidopsis* Biological Resource Center (ABRC) at Ohio State University. The *mag2-1* mutant was from our

previous study (Li et al., 2006, 2013; Zhao et al., 2018). Homozygous plants were obtained by PCR screening using gene-specific primers. *Arabidopsis* seeds were surface-sterilized and sown either on soil or in 0.8 or 1.2% agar with 1/2 Murashige and Skoog medium (PhytoTech, China) and 1% (w/v) sucrose. The plants were grown at 22°C under 16: 8-h/light: dark cycles.

Transgenic plants (Col-0 background) of overexpressing TAP-tagged *MAL* were generated using a modified pNTAPa vector described by Li et al. (2006, 2013) and Zhao et al. (2018).

RNA Extraction and RT-PCR Analysis

Total RNA was isolated using RNAiso Plus (9109; TAKARA, Japan). Total RNA 0.5–1 μg was reverse transcribed using PrimeScript™ RT Master Mix (Perfect Real Time) (RR036A; TAKARA, Japan). Semiquantitative RT-PCR and RT-qPCR were performed according to the manufacturer's instructions. *ACT2* was used as an endogenous control for RT-PCT.

Antibodies and Immunoblot Analysis

Sodium dodecyl sulfate polyacrylamide gel electrophoresis (SDS)–PAGE and immunoblot analysis were performed as described previously (Shimada et al., 2003). Antibody dilutions were as follows: anti-BiP (AS09 481; Agriser, Sweden) 1:2,000, anti-12S 1:20,000, anti-2S3P 1:5,000 (Li et al., 2006); anti-myc (9E10:sc-40; Santa Cruz Biotechnology, Inc., Shanghai, China) 1:2,000; anti-TUA (R0267-1a; Abiocode, CA, United States) 1:2,000. The dilution of horseradish peroxidase-conjugated rabbit antibodies raised against rabbit IgG (ZB2301, ZSGB-BIO, Beijing, China) was 1:5,000. Signals were detected using an enhanced chemiluminescence (ECL) detection system (LAS-4000; Fujifilm, Japan).

Yeast Two-Hybrid Assay

For the yeast two-hybrid assay, *AtSYP81*, *AtSEC20*, and *MAG2* constructs were generated as described in our previous study (Li et al., 2006). The cDNA of *MAL* was amplified and fused in-frame downstream of the GAL4 activation domain in the pGADT7 vector or downstream of the GAL4 DNA binding domain in the pGBKT7 vector. We introduced paired constructs into strain AH109 of *Saccharomyces cerevisiae* (Clontech, United States) and selected on SD/-Leu/-Trp (synthetic defined plate deficient in both Leu and Trp) plates. The interactions were examined on SD/-Leu/-Trp/-His/-Ade plates.

Preparation of Microsomal Proteins

Fractionation was performed basically as described previously (Li et al., 2006). Two grams of roots from 7-day-old seedlings were harvested and ground to fine powder in liquid nitrogen. Ground tissues were suspended in a homogenization buffer (50 mM Tris–HCl, 2 mM ethylene diamine tetraacetic acid (EDTA), 10 mMβ-mercaptoethanol, 250 mM sucrose, pH 7.5) and centrifuged at 8,000 × *g* for 15 min at 4°C to remove debris. The supernatant was recovered, and we repeated centrifugation. The resulting supernatant was ultracentrifuged (Optima™ L-100 XP Ultracentrifuge; Beckman Coulter, United States) at 100,000 × *g* for 1 h at 4°C. The pellet was surface washed with 80% cold acetone and subjected to proteomics analysis.

Label-Free Analysis

Label-free analysis was performed as described previously (Sheng et al., 2015), with modifications. The abundance of each protein in multiply samples was normalized by total intensity. Briefly, peptides were harvested by centrifugation, acidified with 1% CF3COOH, and subsequently dried with a refrigerated CentriVap concentrator (Labconco, Kansas, MO, United States). The dried peptide mixture powder from each digested sample was reconstituted with 30 μl 2 mM TEAB buffer (pH 8.5). Prior to mass spectrum (MS) analysis, samples were desalted onto an Empore C18 47-mm disk (3M) (Ishihama et al., 2006). The dried peptides were resuspended in 0.1% (v/v) formic acid solution and then analyzed with a Q Exactive mass spectrometer (Thermo Electron Finnigan, San Jose, CA, United States). The mass spectra were submitted to the Maxquant software (version1.4.1.2) for peptide identification, and searched against *A. thaliana* protein sequences (Tair) downloaded in 2014. The following parameters were used: carbamidomethylation of Cys was set as fixed modification, phospholation of STY, oxidation of M, and acetylation of protein N terminal were set as variable modifications, and a maximum of two missed cleavages was allowed. The false discovery rate for peptide, protein, and site identification was set to 1% (Cox et al., 2011). A total of 4,546 proteins were identified in both wild-type and *mag2-1 mal-1*, and 515 were differently accumulated proteins (DAPs) in the *mag2-1 mal-1* double mutant. The DAPs were filtered with change ratio >1.2 or $p \leq 0.05$, and 124 of the DAPs met the requirements.

β-glucuronidase Staining

Plant tissues were incubated in β-glucuronidase (GUS) staining solution [10 μl X-Gluc stock (50 mg X-Gluc in 1 ml DMF) (1270MG100; BioFroxx, Germany), add 990-μl base solution (98.9 ml 100 mM PBS (pH 7), 0.164625 g $K_3[Fe(CN)_6]$, 0.211195 g $K_4[Fe(CN)_6]\cdot 3H_2O$, 100 μl Triton X-100, 0.37224 g $Na_2EDTA\cdot 2H_2O$)] for 6–8 h (for DR5:GUS) or overnight (for PIN:GUS) at 37°C. The samples were cleared using 95, 70, 50, and 25% ethanol sequentially and finally rinsed with distilled water. All the samples were observed using a fluorescence microscope (BX41, Olympus, Japan).

1-Naphthylacetic Acid and N-1-naphthylphthalamic Acid Treatment

The seeds were sown on 1/2 MS medium with 50 nM 1-Naphthylacetic acid (NAA) (HY-18570; MedChemExpress, United States) or 3 μM N-1-naphthylphthalamic acid (NPA) (N131601; Aladdin, United States) and grew vertically for seven days. Root length in all the experiments was measured using ImageJ.

NaCl, Mannitol, and Abscisic Acid Treatment

The seeds were sown in a 1/2 MS medium with 125 mM NaCl (YongDa Chemical, Tianjin, China) and 200 mM mannitol (Sinopharm Chemical Reagent Co., Ltd., Shanghai, China) or 1 μM ABA (Yuanye Bio-Technology, Shanghai, China), and grew vertically for 7 days.

Gene Ontology Enrichment Analysis

For function enrichment analysis, Gene Ontology (GO) analysis was conducted on the identified differently expressed genes (DEGs) (Ashburner et al., 2000) using online OmicShare tools.[1] First, all the DEGs were mapped to GO terms in the Gene Ontology database,[2] gene numbers were calculated for every term, and significantly enriched GO terms in the DEGs compared to genome background were defined by hypergeometric test. Calculated *p*-values underwent FDR correction with FDR ≤ 0.05 as the threshold. Finally, we filter out excessive terms in the three main categories [biological process (BP), MC, and cellular component (CC)].

Accession Numbers

GenBank/EMBL accession numbers and *Arabidopsis* Genome Initiative locus identifiers for the genes mentioned in this article are as follows: *MAG2*, *At3g47700.1*; *MAL*, *At1g08400*; *AtSYP81*, *At1g51740*; *AtSec20*, *At3g24315*; *PIN4*, *At2g01420*; *PIN5*, *At5g16530*; *PIN7*, *At1g23080*; *AUX1*, *At2g38120*; *IAA1*, *At4g14560*; and *IAA3*, *At1g04240*.

RESULTS

MAIGO2 and MAG2-Like Play an Important Regulatory Role in Plant Growth and Development With Functional Redundancy

Our previous study demonstrated that MAG2 plays a crucial role in ER export (Li et al., 2006, 2013). MAG2 has a homologous protein, MAG2-like (MAL) (Zhao et al., 2013; Zhao and Lu, 2014). Both of them have similar gene structure (**Figure 1A**) and protein structure that contain a conserved RINT-1/TIP20 domain (**Figure 1B**). Tissue expression determination revealed that *MAL* was expressed in all tissues, with highest level in roots, followed by rosette leaves, inflorescences, and seedlings, and with lowest level in stems and siliques (**Figure 1C**).

In order to analyze the function of *MAL*, we isolated a T-DNA insertion mutant, *mal-1*, in which T-DNA was inserted in the fourth exon (**Figure 1A**). Northern blot and RT-PCR analysis indicated that *MAL* expression was depleted in *mal-1* and reduced in *mag2-1*, but that *MAG2* expression had no significant change in *mal-1* (**Figure 1D** and **Supplementary Figure 1A**). In order to investigate the regulatory function MAG2 and MAL in plant development, we crossed *mal-1* with *mag2-1* to generate a double mutant. We also generated *TAP-MAL* overexpression (*MAL*/OE) plants. RT-PCR and immunoblot analysis indicated higher expression levels of *MAL* in *MAL*/OE lines (**Supplementary Figures 1A,B**).

The germination ratio of *mal-1* and *mag2-1* single mutants did not have significant change compared with that of the wild type (**Figures 2A,B**), but green leaf ratio was lower than that of the wild type (**Figures 2C,D**). The germination ratio and green leaf ratio of the *mal-1 mag2-1* double mutant were significantly reduced, but those of *MAG2*/OE and *MAL*/OE did not change significantly compared with those of the wild type (**Figures 2A–D**). The primary root length of seven-day-old seedlings of *mag2-1*, *mal-1*, *mal-1 mag2-1* mutants and *MAL*/OE line was significantly shorter than that of wild type, especially *mal-1 mag2-1* double mutant. However, there was no significant difference between wild type and *MAG2*/OE (**Figures 2E,F**). Noticeably, the lateral root (LR) number of 14-day-old seedlings of the *mal-1 mag2-1*double mutant was higher than that of the wild type, but there was no significant difference among the other lines (**Figures 2G,H**). The LR length of *mal-1 mag2-1* and MAG2/OE and MAL/ OE lines were significantly longer than that of wild type, especially the double mutant was more than twice of wild type. However, there was no significant difference between the *mal-1* and *mag2-1* single mutants and the wild type (**Figure 2I**). The aerial part and rosette leaves of 36-day-old plants of *mag2-1*, *mal-1*, and *mal-1 mag2-1* were smaller than those of the wild type (**Figure 2J**), especially the double mutant, while the 70-day-old plant height of all the mutants and OE lines were shorter than that of the wild type, especially the double mutant (**Figures 2K,L**).

The seed number per silique of *mag2-1*, *mal-1*, and *mal-1 mag2-1* was significantly less than that of the wild type, especially *mal-1 mag2-1* (**Figures 2M,N**). The seed size of *mag2-1*, *mal-1*, and *mal-1 mag2-1* was smaller than that of the wild type, but that of *MAG2*/OE and *MAL*/OE was larger than that of the wild type (**Figure 2O**). Consistent with this, the thousand grain weight (TGW) of *mag2-1* and *mal-1 mag2-1* was significantly lower than that of the wild type, that of *MAG2*/OE and *MAL*/OE was significantly higher than that of the wild type, and that of *mal-1* was similar to that of the wild type (**Figure 2P**). The above results suggest that both MAG2 and MAL are involved in regulation of plant growth and development. The fact that the phenotypes of the *mal-1 mag2-1* double mutant were more serious than those of the *mal-1* and *mag2-1* single mutants suggest that both MAG2 and MAL play important roles in plant growth and development with functional redundancy.

MAIGO2 and MAG2-Like Regulate Protein Transport With Redundancy

Our previous research clarified that MAG2 forms a complex with MIP1, MIP2, and MIP3 to regulate Golgi-to-ER retrograde transport (Li et al., 2006, 2013). MAG2 also interacts with ER-localized Qa-SNARE AtSYP81 and Qb-SNARE AtSec20 to promote membrane fusion (Li et al., 2013). In the *mag2*, *mip1*, *mip2*, and *mip3* mutants, ER export of SSP precursors is blocked, which results in accumulation of proteins inside the ER and serious ER stress (Li et al., 2006, 2013; Zhao et al., 2018; Guan et al., 2021). In order to explore the role of MAL in vesicle transport, we first performed yeast two hybrid analysis to detect the interaction between MAL and SNARE and MAG2 complex subunits. The results indicated that MAL interacted with AtSYP81, AtSec20, MIP1, and MIP2, and that MAG2 interacted with AtSYP81, AtSec20, and MIP1 (**Figure 3A**), suggesting that MAL has the ability to form a complex with MIP subunits to regulate arriving vesicle tether to the ER membrane, maybe coordinately with SNAREs.

[1] www.omicshare.com/tools

[2] http://www.geneontology.org/

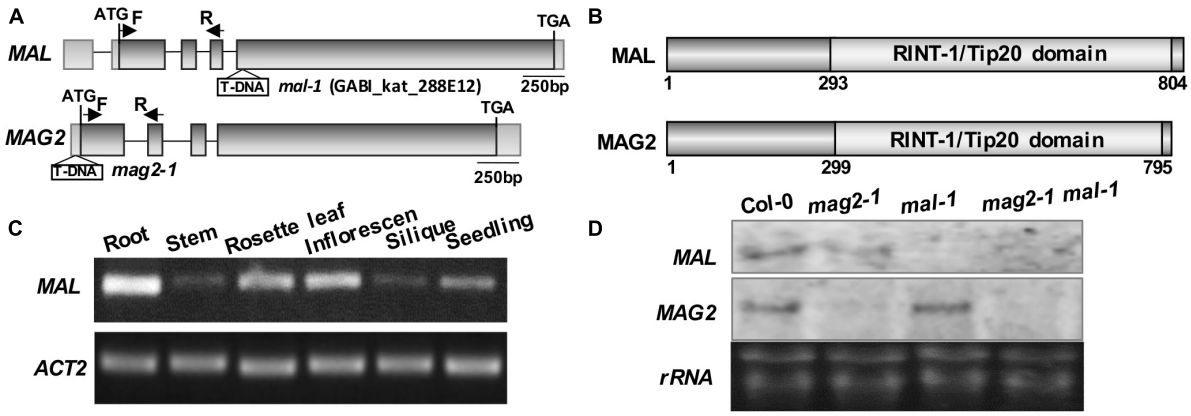

FIGURE 1 | Structural diagram of *MAL* and T-DNA insertion mutant. **(A)** *MAG2* and *MAL* gene structures and T-DNA insertion sites in the mutants. The arrows indicate the position of real-time (RT)-PCR primers. **(B)** MAL and MAG2 protein structures and conserved domains. **(C)** RT-PCR determination of the tissue expression pattern of *MAL*. **(D)** Northern blot detection of the expression levels of *MAL* and *MAG2*.

Immunoblot analysis revealed that a trace amount of SSP precursors accumulated in the *mal-1* seeds, and that numerous precursors accumulated in the double mutant seeds and were more than those in *mag2-1* (**Figures 3B,C**). This suggests that MAL plays a minor role in protein transport and that it is functionally redundant with MAG2. Since abnormal accumulation of proteins in the ER lumen induces ER stress (Li et al., 2006, 2013; Zhao et al., 2018; Guan et al., 2021), we detected the expression of ER stress markers. Western blot of BiP1/2, a common ER stress marker, indicated that their protein accumulation was significantly increased in all the mutants, especially in the *mal-1 mag2-1* double mutant (**Figure 3D**). Moreover, RT-PCR determination of *BiP3*, and ER stress-specific marker, indicated that the transcription of *BiP3* also increased significantly in all the mutants (**Figure 3E**). These results suggest that protein export from the ER is blocked, inducing ER stress in *mal-1*. To further clarify the function of MAL, we detected the protein accumulation of MAG2 complex subunits in the *mal-1* mutant. As shown in **Figure 3F**, in *mal-1*, the protein levels of MAG2 and MIP1 decreased, while that of MIP2 increased; in *mag2-1*, the protein levels of both MIP1 and MIP2 decreased; in the *mal-1 mag2-1* double mutant, MIP1 and MIP2 decreased more than in the single mutants, indicating that both MAG2 and MAL affect the stability of the MAG2 complex. The above results suggest that MAL also plays a role in protein transport, that MAG2 function is dominant, and that they are functionally redundant.

Proteomics Analysis of Microsomal Membrane Proteins in the *mag2-1 mal-1* Double Mutant

To further elucidate the effects of simultaneous depletion of MAG2 and MAL on cellular activities, we performed a proteomics analysis using extracted microsomal fraction from roots of 7-day-old seedlings by label-free identification. A total of 4,546 proteins from both the wild type and *mag2-1 mal-1* were identified, 515 of which were DAPs in *mag2-1 mal-1* compared with those in the wild type. The DAPs were filtered by a change ratio >1.2 or $p \leq 0.05$, and 124 DAPs met the requirements (**Supplementary Table 1**). Then, the set of 124 DAPs was subjected to GO analysis to achieve a broader functional characterization. As a result, the DAPs were classified into 40 subcategories within three main categories: 20 subcategories in BP, 13 in CC, and 7 in molecule function (MF) (**Figure 4A**). In total, 110 DAPs were associated with BP terms (GO:0008150), 115 DAPs were associated with CC terms (GO:0005575), and 107 DAPs were associated with MF terms (GO:0003674) (**Supplementary Table 2**). Among these, one DAP could be assigned to more than one category. In BP, the most enriched pathways were response to stimulus (GO:0050896) (54 DAPs), organonitrogen compound metabolic process (GO:1901564) (52 DAPs), response to chemical (GO:0042221) (36 DAPs), organonitrogen compound biosynthetic process (GO:1901566) (31 DAPs), peptide metabolic process (GO:0006518) (24 DAPs), and amino metabolic process (GO:0043603) (24 DAPs) (**Figure 4B**). In CC, the most enriched pathways were cell (GO:0005623) (113 DAPs), cell part (GO:0044464) (113 DAPs), cytoplasm (GO:0005737) (105 DAPs), cytoplasm part (GO:0044444) (101 DAPs), intracellular organelle part (GO:0044446) (69 DAPs), and organelle part (GO:0044422) (69 DAPs) (**Figure 4D**). In MF, the most enriched pathways were RNA binding (GO:0003723) (30 DAPs), mRNA binding (GO:0003729) (27 DAPs), structural molecule activity (GO:0005198) (21 DAPs), structural constituent of ribosome (GO:0003735) (20 DAPs), transition metal ion binding (GO:0046914) (15 DAPs), and cofactor binding (GO:0048037) (13 DAPs) (**Figure 4F**). The functional categories of GO terms of BP, CC, and MF were shown as a diagram (**Figures 4C,E,G**). These results indicate that metabolism, biosynthesis, signaling, and environmental response were affected in the *mag2-1 mal-1* double mutant.

Depletion of MAIGO2 and MAG2-Like Affects Intracellular Transport

We first extracted DAPs related to vesicle trafficking (**Supplementary Table 3**) and restored their functional location

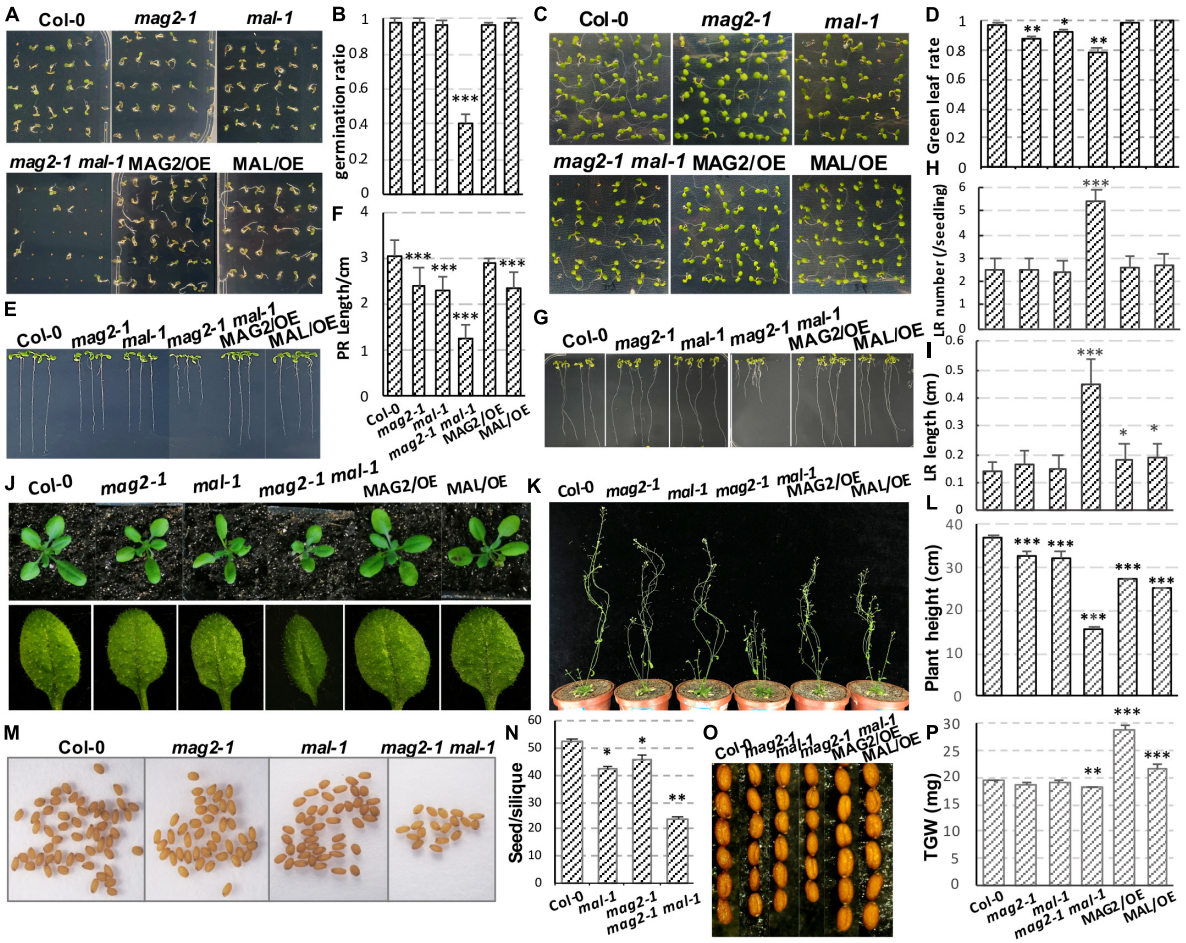

FIGURE 2 | MAG2 and MAL regulate plant growth and development with redundancy. **(A)** Three-day-old seedlings grown in the 1/2 Murashige and Skoog (MS) medium. **(B)** Statistics of germination ratio in panel **(A)**. Values are means ± SD; $n = 36$, three repeats per sample. **(C)** Six-day-old seedlings grown in the 1/2 MS medium. **(D)** Statistics of green leaf ratio in panel **(C)**. Values are means ± SD; $n = 36$, three repeats per sample. **(E)** Seven-day-old seedlings grown in the 1/2 MS medium vertically. **(F)** Statistics of primary root length in panel **(E)**. Values are means ± SD; $n = 30$, three repeats per sample. **(G)** Fourteen-day-old seedlings grown in the 1/2 MS medium vertically. **(H)** Statistics of lateral root number of seedlings in panel **(G)**. Values are means ± SD; $n = 10$ PR, three repeats per sample. **(I)** Statistics of lateral root length in panel **(G)**. Values are means ± SD; $n = 30$, three repeats per sample. **(J)** Thirty-six-day-old plants and their rosette leaves. **(K)** Seventy-day-old plants. **(L)** Statistics of plant height in panel **(K)**. **(M)** Seeds in one silique from indicated lines. **(N)** Statistics of seed number per silique of panel **(M)**. **(O)** Seed size comparison. **(P)** Statistics of thousand grain weight. PR, primary root; LR, lateral root; TGW, thousand grain weight. $^{*}p < 0.05$, $^{**}p < 0.01$, and $^{***}p < 0.001$. Significance was evaluated by Student's *t*-test using the IBM SPSS Statistics 26 software. The seeds used in this study were all newly harvested.

(**Figure 5A**). In ER-Golgi transport, the protein levels of SAR1 (initiates coat assembly in COPII vesicles) (Saito et al., 2017) in the anterograde pathway, and MIP2 and MIP3 (MAG2 complex subunits) (Li et al., 2006, 2013), and RTNLB3 and RTNLB8 (RTN) (RTN complex subunits) (Huang et al., 2018), in the retrograde pathway were decreased. In intra-Golgi trafficking, the protein level of conserved oligomric golgi complex 6 (COG6) (COG complex subunit) (Ungar et al., 2002; Zolov and Lupashin, 2005; Trahey and Hay, 2010) was decreased, while the protein levels of Golgi-localized galactose transporter GGLT1 (Sechet et al., 2018) and phosphate deficiency response 2 (PDR2) (mediates manganese transport into the ER) (Alvim Kamei et al., 2008) were increased. On the secretory and endocytic/recycling pathway, the protein levels of PRA1 (with multiple localization of ER, Golgi, and endosome, functioning in both secretory and endocytic pathways) (Alvim Kamei et al., 2008), the trans-Golgi network (TGN)-localized SM protein AtVPS45 (binds with Qa-AtTLG2 and Qb-AtVTI1b to mediate endosome-to-TGN transport) (Bassham et al., 2000), the PM-localized EXO84B (a subunit of exocyst complex that tethers Golgi/TGN-derived vesicles to the PM) (Heider and Munson, 2012; Saeed et al., 2019), and a clathrin light chain protein, CLC3,weredecreased; while the protein levels of CLC1, another CLC protein, RabA1b/BEX5, a TGN/EE-localized small GTPase (regulates TGN-to-PM trafficking) (Wang et al., 2013; Majeed et al., 2014), and BIG2/BEN3, an guanine-nucleotide exchange factor of ADP-ribosylation factor (ARF GEF) protein (regulates PIN1 secretion) (Kitakura et al., 2017), were increased. In the vacuole-targeting pathway, the protein levels of the Golgi-localized Qc-SNARE AtSTF12 (regulates Na^{+} sequestration in vacuoles under salt

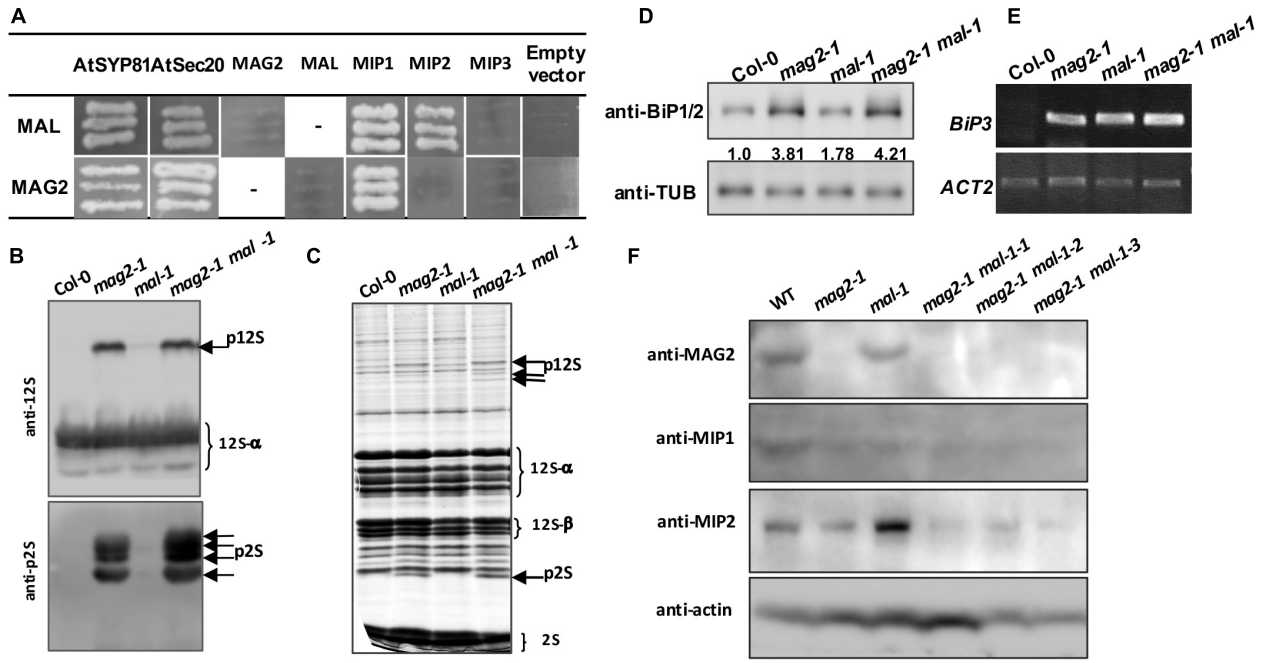

FIGURE 3 | MAG2 and MAL regulate protein export from the endoplasmic reticulum (ER). **(A)** Yeast two hybrid detection of MAL interactors. Detection of combinations of both *MAL/pGADT7* and *MAL/pGBKT7* with corresponding constructs was performed. AtSYP81 vs. AtSec20 served as positive control, whereas MAL/MAG2 vs. empty vectors served as negative control. −, Not performed. **(B)** Immunoblot detection of precursors of seed storage proteins. **(C)** Profile of whole seed proteins. **(D)** Immunoblot detection of BiP1/BiP2 proteins. Statistics of relative band concentration (presents protein abundance) is indicated in number below the bands (BiP/TUB, measured with ImageJ). **(E)** RT-PCR determination of *BiP3* expression. **(F)** Immunoblot detection of MAG2, MIP1, and MIP2 in 7-day-old seedlings of indicated lines. 12S, 12S globulins; 2S, 2S albumins; p12S, precursors of 12S globulins; p2S, precursors of 2S albumins.

and osmotic stress) (Tarte et al., 2015), PVC/MVB-localized ARA7 (a Rab5 homolog) (Lee et al., 2004), and R-SNARE VAMP713, which interacts with the vacuolar-tether complex HOPS to regulate vacuole targeting (Takemoto et al., 2018), and the vacuolar sorting receptor VSR3 (functions in vacuolar cargo sorting) (Lee et al., 2013; Ichino et al., 2014) were increased; while the Golgi-localized GFS9 (involved in proteins and phytochemical transport to vacuoles) (Ichino et al., 2014), MVB/PVC-localized ALIX, the bridge protein of ESCRT-I and ESCRT-III complexes (essential for vacuolar targeting) (Shen et al., 2016), RAB7 and a HOPS subunit, VPS33 (also a SM protein) (both proteins bind vacuolar SNARE complexes to facilitate membrane fusion) (Lobingier and Merz, 2012), were decreased. The protein level of trigalactosyldiacylglycerol 4 (TGD4), which is localized in ER-chloroplast membrane contact sites and mediates the transfer of lipid precursors from the ER to chloroplast for biogenesis of photosynthetic membranes (reviewed by Fan et al., 2015), was also decreased (**Figure 5B**). All the influences on diverse pathways suggest that blocking of protein export from the ER in *mag2-1 mal-1* affects subsequent vesicle trafficking processes.

MAIGO2 and MAG2-Like Deficiency Influenced Protein Quality Control

The ER is crucial for maintenance of cellular homeostasis, because its functions in various cellular processes, such as folding and initial modification of secretory and transmembrane proteins. Misfolded and unfolded proteins that accumulate in the ER lumen induce ER stress. To maintain ER homeostasis, several strategies have been evolved, including unfolded protein response (UPR), ER-associated degradation (ERAD), and ER-phagy (Chen et al., 2020). As shown in **Figure 5C**, the protein levels of ER-localized CDC48B ATPase (extracts unfolded/misfolded proteins from the ER lumen and membrane for targeting to proteasomes) (Wu and Rapoport, 2018) and MNS4 mannosidase (promotes BRI1-5 ubiquitylation and degradation) (Hüttner et al., 2014) in the ERAD pathway, and Sec62, an ER-phagy receptor (coordinates with ATG8e to engulf misfolded proteins into autophagosomes for vacuolar degradation) (Hu et al., 2020) were increased. These changes have probably resulted from blocking of protein export from the ER, suggesting that MAG2 and MAL are important for protein quality control. Interestingly, the quinolinic acid phosphoribosyl transferase (QPT), which is essential for pyridine nucleotide cycle and biosynthesis of alkaloid nicotine (Eads et al., 1997; Sinclair et al., 2000) decreased in *mag2-1 mal-1* (**Figure 5D**).

MAIGO2 and MAG2-Like Affect Abundance of Regulators Related to Auxin Biosynthesis, Transport, and Signaling

Since the growth and development of the *mag2-1 mal-1* double mutant were seriously affected, we then focused on auxin-related

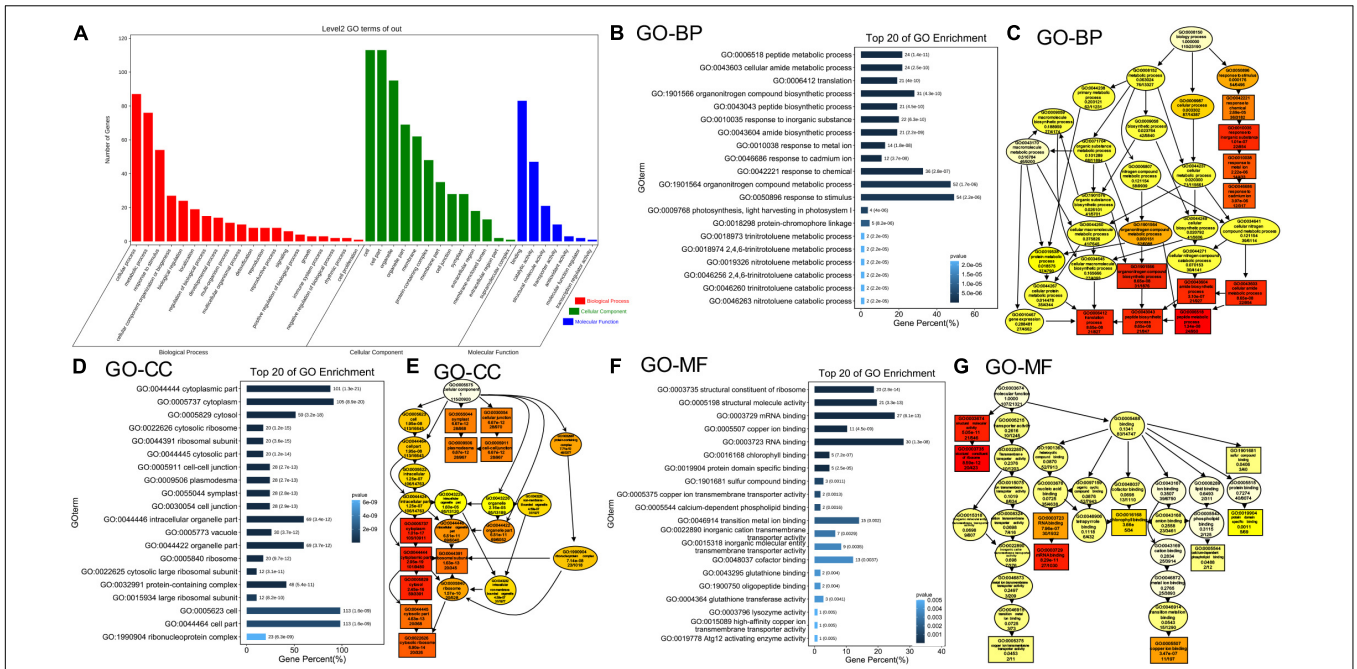

FIGURE 4 | Gene Ontology (GO) classification of the differently accumulated proteins (DAPs). **(A)** DAP distribution in three GO terms of biological process (BP), cellular component (CC), and molecular function (MF). X axis represents GO terms. Y axis represents number of genes. **(B)** Top 20 GO enrichment terms in BP. X axis represents gene percentage. Y axis represents GO terms. The number on each column indicates DAP number, followed by *p*-value in the brackets. The same in panel **(D,F)**. **(C)** The functional categories of GO terms in BP are shown as a diagram. **(D)** Top 20 GO enrichment terms in CC. **(E)** The functional categories of GO terms in CC. **(F)** Top 20 GO enrichment terms in MF. **(G)** The functional categories of GO terms in MF.

DAPs and plant phenotypic analysis. We first extracted auxin-related DAPs (**Supplementary Table 4**) and restored their function (**Figures 5E–G**).

In auxin transport pathways (**Figure 5E**), the protein levels of the phosphatase PP2A (works antagonistically with PINOID kinase in PIN cycling) (Feraru and Friml, 2008; Grones et al., 2018), PP2A-3, a catalytic subunit of PP2A holoenzymes (dephosphorylates ACR4, a PM-localized receptor kinase controlling WOX5 expression) (Kong et al., 2015; Yue et al., 2016), PILS3, an ER-localized auxin transporter, and MAB4, an interactor of PIN1 and PIN2 (coordinates with AGC kinases to regulate PIN polar localization) (Glanc et al., 2021) were decreased, while the protein level of the TGN/EE-localized BEX1, an ARF protein (facilitates PIN recycling to the PM) (Tanaka et al., 2014), was increased. These results suggest that MAG2 and MAL might affect auxin transport by influencing polar localization maintenance of auxin carriers.

In auxin signaling pathways (**Figure 5F**), the protein levels of TIR1/AFB2, a subunit of the SCF^{TIR1} complex (triggers proteasomal degradation of Aux/IAA to release ARFs for transcriptional activation of auxin-responsive genes such as *RSL4*) (Pires et al., 2013; Mangano et al., 2017), *PRX7*, a class III peroxidase activated by RSL4 (Vijayakumar et al., 2016; Marzol et al., 2017), STV1/RPL24, which regulates the expression of auxin responsive genes (Sessions et al., 1997; Hardtke and Berleth, 1998), and sAPX, the stromal APX regulated by GAP1/ANAC089 (Klein et al., 2012; Yang et al., 2014) which triggers production of nitric oxide (NO) to regulate auxin transport in a PIN1-dependent manner (Fernández-Marcos et al., 2011), were decreased, while the protein levels of CSN7, a subunit of the CSN complex regulating AUX/IAA degradation (Serino and Deng, 2003; Mergner and Schwechheimer, 2014), and SCI1, which affects the transcription of auxin-responsive genes such as *IAAs* (Serino and Deng, 2003; Mergner and Schwechheimer, 2014), were increased. In auxin biosynthesis pathways (**Figure 5G**), IAA is synthesized mainly from L-Trp precursors, which are generated *via* the shikimate pathway. ASA1, an anthranilate synthase subunit that catalyzes shikimate to produce anthranilate (ANT) (Radwanski and Last, 1995; Li et al., 2020), TSB2, a tryptophan synthase subunit that catalyzes the formation of Trp from indole (Wang et al., 2015; Li et al., 2020), CYP71B6, a monooxygenase that converts indole-3-acetonitrile (IAN) to ICA (Böttcher et al., 2014; Müller et al., 2019; Pastorczyk et al., 2020), and IBR10, which can convert IBA to IAA (reviewed by Strader and Bartel, 2011), were increased in *mag2-1 mal-1*. These results suggest that MAG2 and MAL might affect auxin signaling and biosynthesis by influencing the abundance of regulators.

Auxin Distribution Was Affected in Different Manner in *mag2-1* and *mal-1*

Then, we determined auxin distribution in the mutants using an auxin response marker, DR5:GUS, which was introduced into each mutant by crossing. Chemical staining indicated that DR5:GUS signal was distributed in quiescent cells (QCs) and

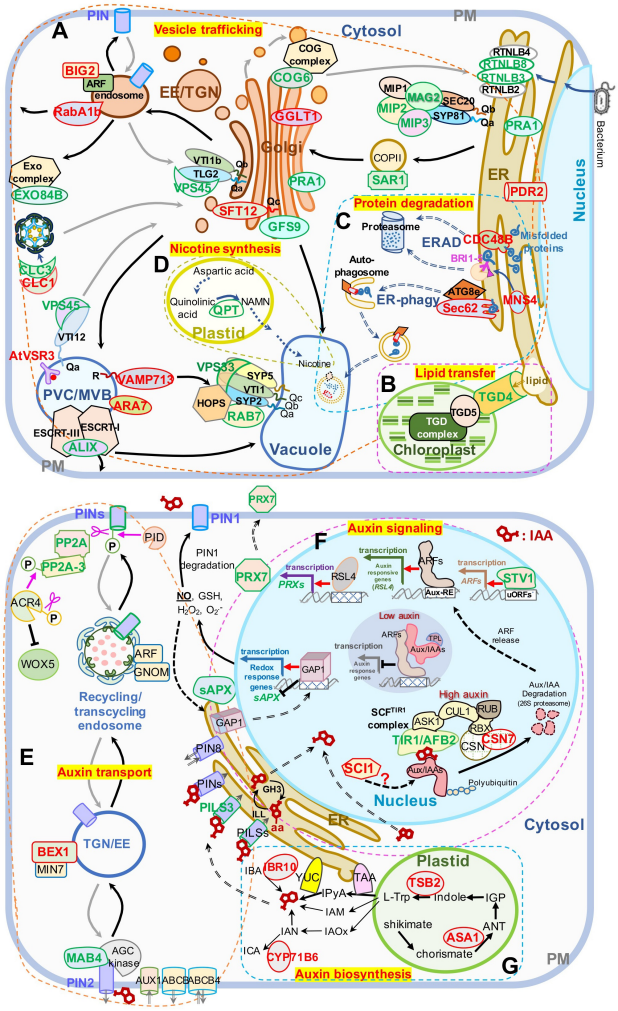

FIGURE 5 | Schematic presentation of DAPs enriched in panel **(A–D)** vesicle trafficking and **(E–G)** auxin-related pathways. **(A)** Intracellular vesicle trafficking pathways. **(B)** Lipid transfer pathways. **(C)** Protein degradation pathways including ERAD and ER-phagy. **(D)** Nicotine biosynthesis pathways. **(E)** Auxin transport pathways. **(F)** Auxin signaling pathways. **(G)** Auxin biosynthesis pathways. Protein names in red and green represent increased and decreased DAP abundances, respectively. The ranges of panel **(A–G)** are defined by frames with dashed lines. AUX1, auxin resistant 1; ABCA, ATP binding cassette; ANT, anthranilate; AUX/IAAs, auxin/indole-3-acetic acid proteins; ARFs, auxin response factors; Aux-RE, auxin response element; ASK1, *Arabidopsis* serine/threonine kinase 1; ACR4, *Arabidopsis* crinkly 4; ATG8e, autophagy 8e; ALIX, ALG-2 interacting protein-X; BEX1/MIN7, bfa-visualized exocytic trafficking defective1/hopm interactor 7; CSN, COP9 signalosome subunit 7; CUL1, cullin 1; CYP71B6, cytochrome p450 71 B6; CDC48B, cell division cycle 48 B; COG6, conserved oligomric Golgi complex 6; CLC1, clathrin light chain 1; CLC3, clathrin light chain 3; EXO84B, exocyst complex component 84 B; EE, early endosomes; ER, endoplasmic reticulum; ERAD, endoplasmic reticulum (ER)-associated degradation; GAP1, GTPase-activating protein 1; GFS9, green fluorescent seed 9; GGLT1, golgi GDP-L-galactose transporter 1; IGP, indole-3-glycerol phosphate; IAOx, indole-3-acetaldoxime; IAM, indole-3-acetamide; IPyA, indole-3-pyruvic acid; ICA, indole-3-carboxaldehyde; IAN, indole-3-acetonitrile; IBA, indole-3-butyric acid; IBR10, indol-3-butyric acid response 10; L-Trp, L-tryptophan; MAB4, macchi-bou 4; MNS4, mannosidase 4; PIN, PIN-FORMED; PRX7, peroxidase 7; PILS3, PIN-LIKES 3; PP2A, protein phosphatase 2A; PID, PINOID; PRA1, prenylated rab acceptor 1; PDR2, phosphate deficiency response 2; QPT, (Continued)

FIGURE 5 | quinolinate phoshorbosyl transferase; RBX, ring-box 1; RUB, ubiquitin-related protein; RSL4, root hair defective 6-like 4; RTNLB3, reticulon-like protein B3; reticulon-like protein B8; RABA1B, rab GTPase homolog A1B; RTNL3, reticulon 3; sAPX, stromal ascorbate peroxidase; SCI, stigma/style cell-cycle inhibitor 1; TGN, trans-Golgi network; TIR1/AFB2, transport inhibitor response 1/auxin signaling F-box 2; TPL, topless; TSB2, tryptophan synthase beta-subunit 2; TAA, tryptophan aminotransferase of *Arabidopsis*; TGD4, trigalactosyldiacylglycerol 4; uORF, upstream open reading frame; WEI2, weak ethylene insensitive 2; VSR3, vacuolar sorting receptor 3; VPS45, vacuolar protein sorting 45; VPS33, vacuolar protein sorting 33; YUC, YUCCA flavin-containing monooxygenases; YUC4, YUCCA4. A "P" in a circle indicates phosphorylation; pink scissors represent dephosphorylation; the pink arrow represents phosphorylation; the red arrows represent transcriptional activation; the black T-shape indicates transcriptional inhibition; the white blocks with lattices represent regulatory cis-elements; the red structural formula represents IAA molecule, and the one with –aa represents IAA–amino acid conjugates; right-angled arrows represent transcription products; the long gray and black arrows represent cycling transport pathways.

columella cells in primary and lateral root tips, lateral root primordium, cotyledon veins and margin, and true leaf tips in the wild type. However, in *mag2-1*, the DR5:GUS signal was significantly reduced, only observed in a few columella cells in primary root tips. Unexpectedly, the expression pattern of DR5:GUS in *mal-1* was completely different. In *mal-1* primary roots, the DR5:GUS signal increased significantly not only in QCs and columella cells but also in stele cells. Moreover, increased GUS signals were also observed in lateral root tips, lateral root primordium, cotyledon veins and margin, and true leaf tips, while in the *mag2-1 mal-1* double mutant, DR5:GUS distribution was similar to that in *mag2-1* (**Figure 6A**). These results suggest that knockout of MAG2 and MAL affects auxin level and distribution, but that the two homolog proteins might play different regulatory roles in auxin distribution.

We further detected the auxin response of the mutants and OE lines. Application of 50 nM of NAA, a synthetic auxin analog, inhibited the growth of primary roots of 7-day-old seedlings. In the wild type, root length decreased by more than 20%, while the reduction in the root length of mutants and OE lines was much less than that in the wild type (**Figures 6B–D**). These results suggest that MAG2 and MAL are involved in auxin response.

Then, we checked polar auxin transport (PAT). Application of 3 μM of NPA, an auxin transport inhibitor, inhibited the growth of primary roots of 7-day-old seedlings. Reduction in the root length of the *mag2-1* and *mal-1* single mutants and the OE lines was less than that of the wild type, while the root growth of the *mag2-1 mal-1* double mutant was not sensitive to the inhibition of 3 μM NPA treatment (**Figures 6B–D**). These results suggest that PAT was affected in the mutants and OE lines, especially in the *mag2-1 mal-1* double mutant.

PIN-FORMED Abundance Was Affected in the Mutants

To clarify the mechanisms underlying MAG2 and MAL regulation in auxin transport, we introduced the cassettes of PIN1:GUS, PIN1-GFP, PIN2:GUS, PIN2-GFP, PIN3:GUS, and PIN3-GFP into the mutants by crossing, and we observed their

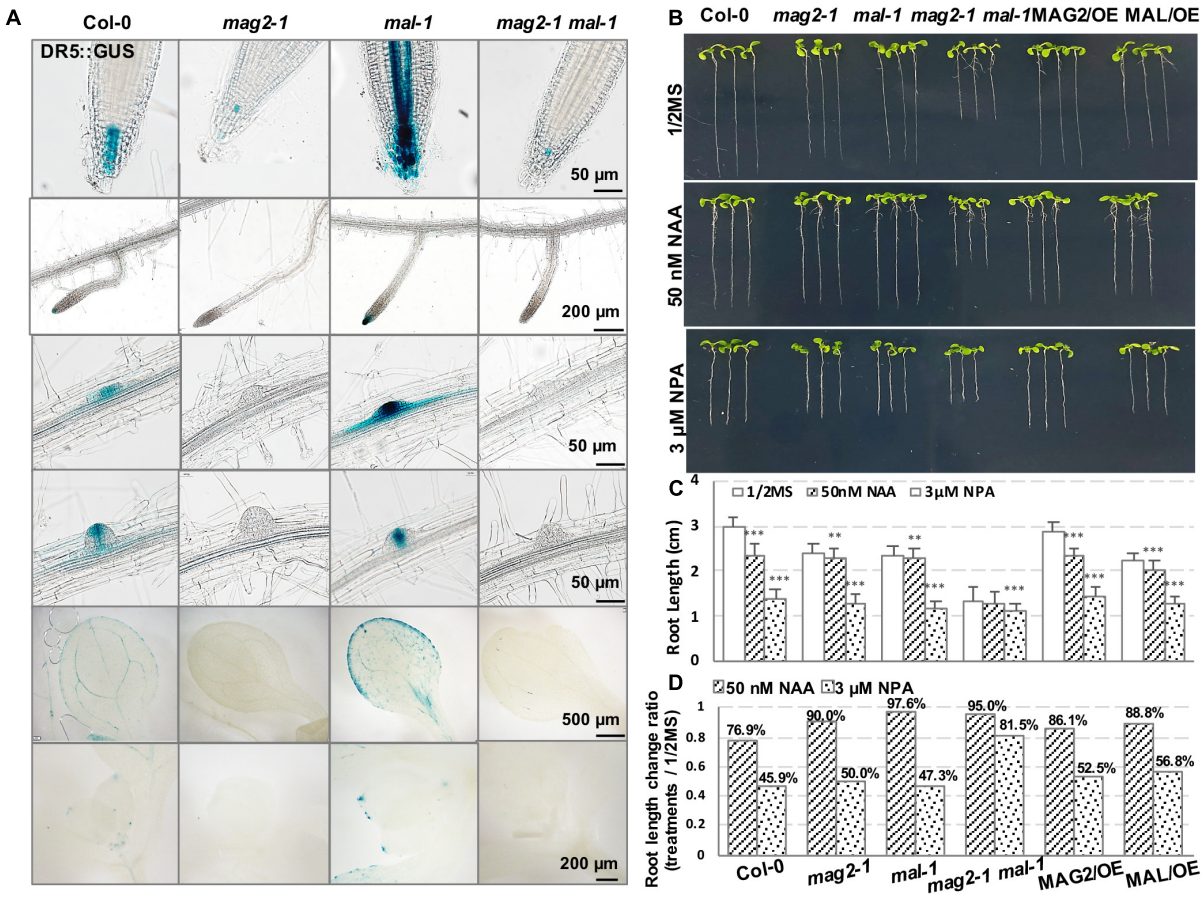

FIGURE 6 | MAG2 and MAL regulate auxin distribution. **(A)** Tissue expression pattern of DR5:GUS. Bars are as shown. **(B)** Seven-day-old seedlings grown in the 1/2 MS medium with 50 nm NAA or 3 μM NPA. **(C)** Statistics of root length in panel **(B)**. Values are means ± SD; $n = 30$, three repeats per sample. **(D)** Statistics of root length ratio before and after treatment in panel **(C)**. $^{**}p < 0.01$, and $^{***}P < 0.001$. Significance was evaluated by Student's *t*-test using IBM SPSS Statistics 26.

distribution. PIN1 is localized on cell basal side in root stele and stem vascular tissue, as well as lateral root primordium (LRP) (Omelyanchuk et al., 2016). Compared with the wild type, PIN1-GFP signals decreased significantly in stele cells in *mag2-1*, *mal-1*, and *mag2-1 mal-1*, especially in the *mag2-1 mal-1* double mutant (**Figure 7A**). PIN1:GUS in stele cells of primary roots decreased significantly in *mag2-1*, *mal-1*, and *mag2-1 mal-1*, especially in *mag2-1 mal-1*. Interestingly, PIN1:GUS expression increased in QC cells in primary roots of *mag2-1* and *mal-1*, especially *mag2-1*. No signal was observed in the *mag2-1 mal-1* double mutant (**Figure 7B**). In wild-type LRP, PIN1:GUS evenly distributed in all cells, but in *mag2-1* LRP, PIN1:GUS signals increased in the basal layer. Conversely, in *mal-1* LRP, PIN1:GUS signals decreased in the outer layer. No signals were detected in the *mag2-1 mal-1* double mutant (**Figure 7B**). PIN2 is mainly expressed in cortical and epidermal cells in root tips and is involved lateral root development (Chen et al., 1998; Zhou and Luo, 2018). In *mag2-1* and *mal-1*, PIN2-GFP localization and abundance did not change significantly, but in the *mag2-1 mal-1* double mutant, PIN2-GFP abundance likely increased (**Figure 7C**). PIN2:GUS signals increased in cortical and epidermal cells in primary and lateral root tips of *mag2-1* and *mag2-1 mal-1* but decreased in *mal-1* (**Figure 7D**). In the early LR development stage, PIN2:GUS in *mag2-1* tended to accumulate in basal layers compared with that in the wild type, but in *mal-1*, PIN2:GUS signals became weaker, whereas in the *mag2-1 mal-1* double mutant, GUS signals became higher and diffused (**Figure 7D**). PIN3 is distributed in root columella and stele cells (Li et al., 2015), participating in primary root development and lateral root formation in early steps (Zhou and Luo, 2018). In *mag2-1*, *mal-1*, and *mag2-1 mal-1*, PIN3-GFP abundance in columella and stele cells reduced, especially in the *mag2-1 mal-1* double mutant (**Figure 7E**). PIN3:GUS was expressed in stele, columella, and LRP cells in the wild type, but almost no signal was detected in all the mutants (**Figure 7F**). We further determined the expression of *AUX1*, part of *PIN* and *IAA* genes. The results indicate that the expression of *IAA1* increased and that of *IAA3* reduced slightly (**Supplementary Figure 1C**). The alteration in abundance of PIN1, PIN2, and PIN3, and expression of *IAAs* in the mutants might lead to abnormal auxin transport and distribution and affect lateral root development. Combined with the proteomics results, it is

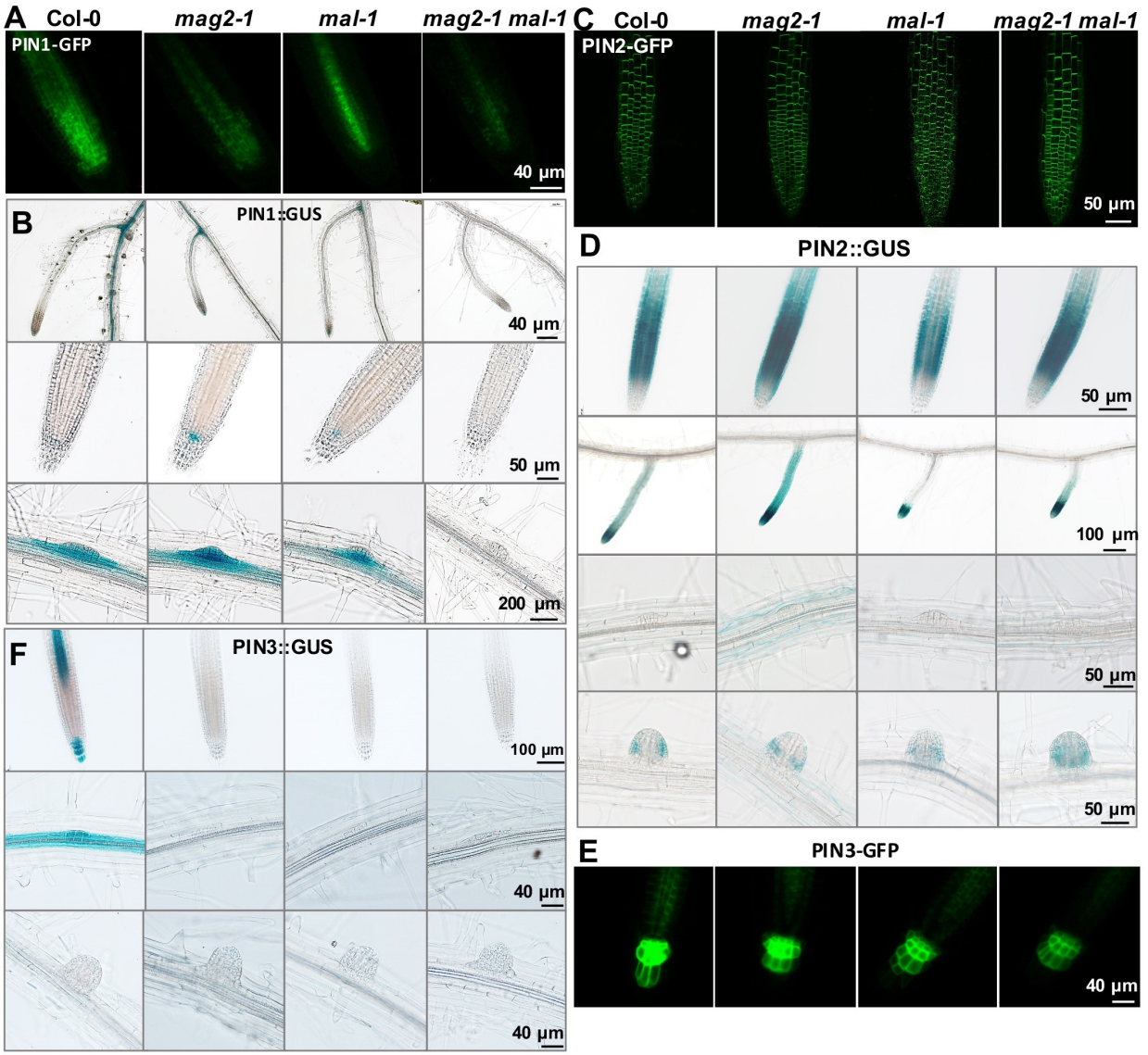

FIGURE 7 | MAG2 and MAL regulate the expression of auxin transporters. Confocal images of **(A)** PIN1-GFP, **(C)** PIN2-GFP, and **(E)** PIN3-GFP in primary roots. **(B,D,F)** Expression pattern of **(B)** PIN1:GUS, **(D)** PIN2:GUS, and **(F)** PIN3:GUS in 7-day-old seedlings grown in 1/2MS medium tissues. Bars are as shown.

suggested that auxin transport and signaling are disturbed in MAG2- and MAL-deficient mutants.

MAIGO2 and MAG2-Like Are Involved in Plant Stress Response

It was observed that in the early stage of germination, the seedlings of *mag2-1*, *mal-1*, *mag2-1 mal-1*, *MAG2*/OE, and *MAL*/OE lines accumulated higher levels of anthocyanins than those of the wild type (**Supplementary Figure 1D**). Anthocyanins are antioxidants that protect plants from growth inhibition and cell death by scavenging abiotic stress-induced ROS, thereby enabling plant adaption to abiotic stress (Naing and Kim, 2021). The higher accumulation of anthocyanins suggested loss of ROS homeostasis in the mutants and OE plants.

In order to explore the function of MAG2 and MAL in plant response to environmental stress, we performed salt, osmotic, and ABA treatments. In the 125-mM NaCl treatment, reduction of root length of the mutants was more than that of the wild type, but that of the OE lines was less than that of the wild type (**Figures 8A–C**). In the 200-mM mannitol treatment, reduction of root length of the mutants and OE lines was less than that of the wild type (**Figures 8A–C**). In the 1-μM ABA treatment, reduction of root length of the mutants was higher, and that the OE lines was less than that of the wild type (**Figures 8D–F**). Since ABA signaling was disrupted in *mag2-1* (Zhao et al., 2018), we checked the expression levels of *ABI3* and *ABI4* in *mag2-1 mal-1*. As shown in **Figure 8G**, the expression of *ABI3* and *ABI4* was significantly elevated in *mag2-1 mal-1*. All these results suggest

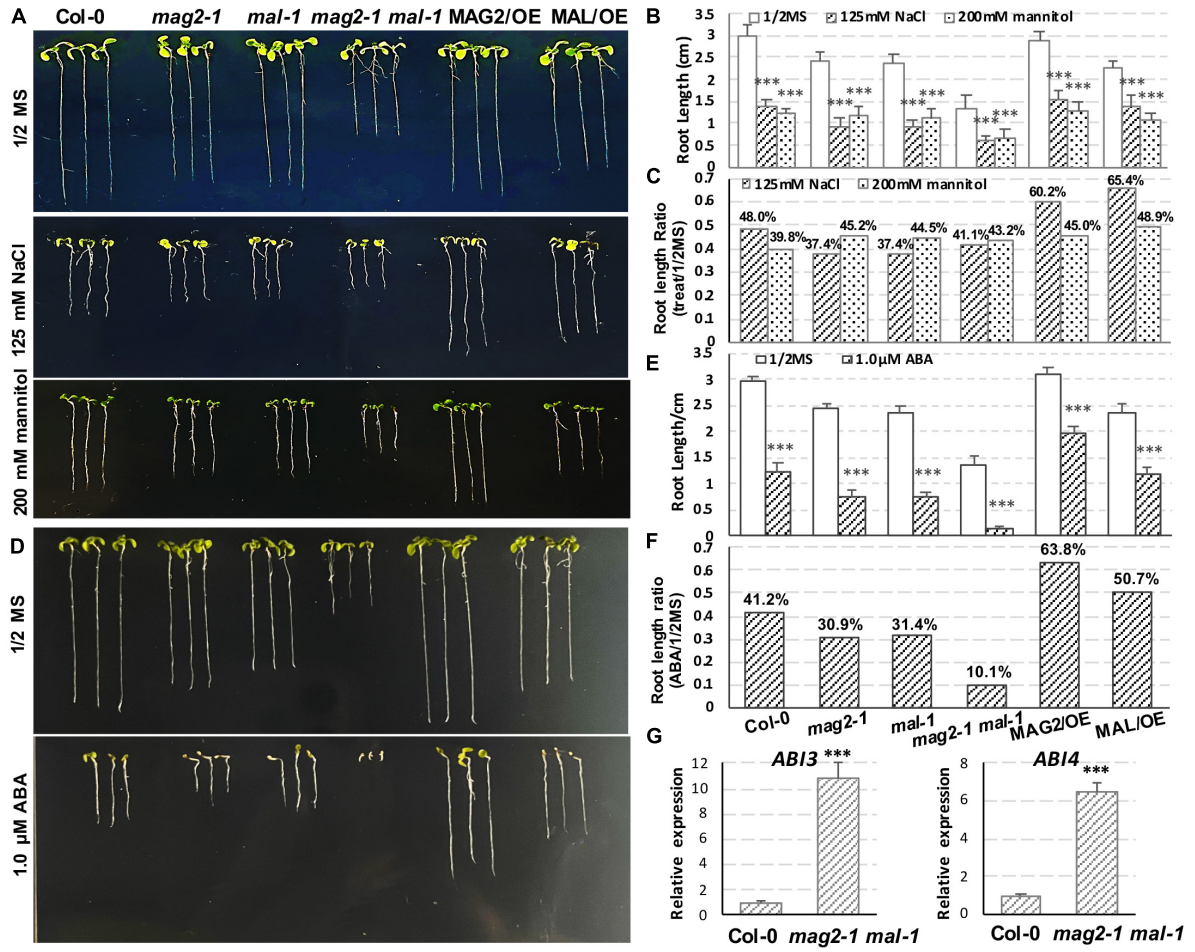

FIGURE 8 | MAG2 and MAL regulate plant stress response. **(A)** Seven-day-old seedlings grown in the 1/2 MS medium with 125 mM NaCl or 200 mM mannitol. **(B)** Statistics of root length in panel **(A)**. Values are means ± SD; $n = 30$, three repeats per sample. **(C)** Statistics of root length ratio before and after treatment in panel **(C)**. **(D)** Seven-day-old seedlings grown in the 1/2 MS medium with 1 μM ABA. **(E)** Statistics of root length in panel **(D)**. Values are means ± SD; $n = 30$, three repeats per sample. **(F)** Statistics of root length ratio before and after treatment in panel **(E)**. **(G)** RT-qPCR determination of relative expression level of *ABI3* and *ABI4*. Two independent experiments per sample, and three repeats per experiment. $^{*}p < 0.05$, $^{**}p < 0.01$, and $^{***}p < 0.001$. Significance was evaluated by Student's *t*-test using IBM SPSS Statistics 26.

that MAG2 and MAL play important roles in regulation of plant stress response.

DISCUSSION

MAIGO2 and MAG2-Like Play Important Roles in Plant Development With Functional Redundancy and Division

Our previous study clarified that MAG2 forms a tethering complex with MIP1, MIP2, and MIP3 to regulate protein export from the ER. Deficiency of any subunit of the complex leads to the formation of a novel cell structure (we call it "*mag* Body"), which contains precursors of SSPs and the ER, BiP, and PDI. *mag* Bodies are trapped inside the ER lumen and induce severe ER stress (Li et al., 2006, 2013; Zhao et al., 2018). In this study, we investigate the function of MAL and compared it with that of its homologs protein, MAG2. As expected, MAL also plays roles in vesicle trafficking, plant development, and environmental stress response, and it was functionally redundant with MAG2. MAL and MAG2 deficiency significantly affected the stability of the MAG2 complex (**Figure 3F**), indicating that MAL might form a complex with MIP proteins to regulate vesicle transport when MAG2 is deficient, or in different developmental stages or tissues.

One observation that attracted our attention was the different performance of MAL and MAG2 on auxin transport. The DR5:GUS signals were reduced significantly in *mag2-1* but, conversely, were elevated substantially in *mal-1*, and the *mag2-1 mal-1* double mutant displayed a trend similar to *mag2-1* (**Figure 6**). Similarly, the opposite phenotypes were also observed in PIN2:GUS distribution in roots. The PIN2:GUS signals were increased significantly in *mag2-1*, while they were decreased markedly in *mal-1* in root elongation zones. The *mag2-1 mal-1*

double mutant displayed a trend similar to *mag2-1* (**Figure 7D**). Also, PIN1:GUS expression level in LRP in *mag2-1* was elevated but reduced in *mal-1* (**Figure 7B**). These phenotypes suggest that MAL and MAG2 have a functional division in regulating auxin transport, and that their functions might be opposite: MAG2 plays a positive role, while MAL plays a negative role, and MAG2 is dominant. However, the speculation needs more evidence to be confirmed.

The *mag2* and *mip* single mutants as well as their double mutants such as *mag2-1 mip3-1* and *mip2-1 mip3-1* have a distorted response to environmental stresses (Zhao et al., 2018). The single and double mutant seeds have reduced protein qualities, germination activities, and longevity, since they have reduced content of mature SSPs, which could protect cell components and cell structures from oxidative stress during deposition. The blocking of vesicle transport in the *mag2* and *mip* single and double mutants disturb endomembrane function and ABA signaling. The expression levels of *ABI3*, *ABI4*, and *ABI5* was altered significantly compared with that of the wild type under normal and stress conditions (Zhao et al., 2018). Consistent with these, the expression of *ABI3* and *ABI4* in *mag2-1 mal-1* was also altered significantly (**Figure 8G**), suggesting that serious blocking of ER export is bound to affect ABA signaling.

MAIGO2 and MAG2-Like Regulate Auxin Homeostasis by Controlling Golgi-to-Endoplasmic Reticulum Vesicle Trafficking

Since ER export is blocked in *mag2-1*, the function of ER is seriously disrupted. Numerous newly synthesized proteins are trapped inside the ER lumen and form a novel cell structure, *mag* Body, and subsequently induce severe ER stress (Li et al., 2006, 2013; Zhao et al., 2018). The *mag2-1 mal-1* double mutant has more serious transport defects such as more SSP precursors and higher ER stress than the *mag2-1* single mutant, thus ER function disorder should be more serious. A large amount of DAPs in vesicle trafficking pathways represent the severity of the disorder (**Figure 5A**). The DAPs were distributed not only in the ER-Golgi COPI- and COPII-mediated pathways but also in the late secretion and recycling pathways as well as vacuole targeting pathways. This reflected the close correlation among the transport pathways. The ER is the initial point of secretory pathway and is important for ion homeostasis, quality control of newly synthesized proteins, lipid biosynthesis and transfer, and organelle communication (Borgese et al., 2006). The serious protein export jam and ER stress in *mag2-1 mal-1* double mutant definitely disrupted ER homeostasis and functions, and affected the abundance of regulators of vesicle trafficking (**Figure 5A**), ERAD and ER-phagy pathways (**Figure 5B**), and lipid transfer system (**Figure 5C**). As a consequence, cellular function and integrity as well as plant development were seriously affected.

Another spectacular change was the large amount of DAPs in auxin transport, signaling, and biosynthesis pathways (**Figures 5E–G**). Auxin homeostasis is coordinately regulated by multiple processes such as IAA biosynthesis, conjugation, transport, and signaling as. However, the controlling mechanisms of IAA homeostasis is elusive because of the complexity of combination of diverse pathways and spatiotemporal (different organs and developmental stages) and environmental factors. The two-step pathway converting tryptophan (Trp) to IAA is a highly conserved auxin biosynthetic pathway. TAA aminotransferases catalyze tryptophan to IPyA, and then YUC monooxygenases convert IPyA to IAA (Stepanova et al., 2008; Cao et al., 2019). Flower-specific YUC4.2 is the first reported ER membrane-anchored monooxygenase (Kriechbaumer et al., 2012). In *Arabidopsis* and maize, about half of TAA/TAR and YUC family enzymes such as TAR2, YUC3, YUC5, YUC7, YUC8, and YUC9, are localized in the ER membrane (Kriechbaumer et al., 2015, 2016). These enzymes are actively involved in auxin biosynthesis (Kriechbaumer et al., 2016; Poulet and Kriechbaumer, 2017). Moreover, about 20% of the total IAA biosynthetic activity was detected in a purified microsomal membrane fraction (Kriechbaumer et al., 2015, 2016). Thus, the ER could be considered as a platform for auxin biosynthesis. The abnormal protein accumulation inside the ER in the *mag2-1 mal-1* double mutant will definitely affect the function of these auxin biosynthesis-related proteins.

Endoplasmic reticulum-localized PIN5, PILS2, and PILS5 are suggested to transport auxin from the cytosol to the ER (Mravec et al., 2009; Wabnik et al., 2011). PILS2 and PILS5 are proposed to regulate auxin metabolism and signaling by increasing IAA conjugates and simultaneously decreasing nuclear auxin signaling, presumably by confining IAA in the ER (Barbez et al., 2012), whereas the pollen-specific PIN8 decreases IAA ER-compartmentation antagonistically (Dal Bosco et al., 2012; Ding et al., 2012). Therefore, these ER-localized auxin carriers affect auxin conjugation and link IAA transport to metabolism and signaling (Barbez and Kleine-Vehn, 2013; Kriechbaumer et al., 2015). In addition, the auxin-deconjugation, ILL2, IAR3, and ILR1, have been shown to localize in the ER where they are likely to produce free IAA by amidohydrolyzing IAA–amino acid conjugates (Ludwig-Müller, 2011; Sanchez Carranza et al., 2016). Considering the above clues, it is speculated that auxin conjugation could happen in the ER (Kriechbaumer et al., 2015). It is predicted that the ER functions as the main conduit for nuclear auxin uptake (Sauer and Kleine-Vehn, 2019). Given all of that, the ER serves not only as a platform for auxin biosynthesis but also as an auxin deposit and cycling hub (Friml et al., 2003). The disordered ER homeostasis and functions in the *mag2-1 mal-1* double mutant might affect auxin deposition and cycling.

In *mag2-1* cells, protein abundance of the phosphatase PP2A, which works antagonistically with kinase PID to regulate PIN cycling and activity, was decreased (**Figure 5A**). Breaking of balance of two enzymes with opposite functions will definitely influence PIN homeostasis in the PM. As a result, the protein abundance of PIN-GFP and PIN:GUS was altered significantly (**Figure 7**) and subsequently affected auxin transport and response in the *mag2-1 mal-1* double mutant (**Figure 6**).

Endoplasmic reticulum and auxin homeostasis maintenance by MAG2/MAL-mediated vesicle trafficking is essential for auxin transport and plant development, especially under stress

conditions. Our study unveiled a novel perspective of membrane trafficking regulatory role in auxin homeostasis.

DATA AVAILABILITY STATEMENT

The datasets presented in this study can be found in online repositories. The names of the repository/repositories and accession number(s) can be found in the article/**Supplementary Material**.

AUTHOR CONTRIBUTIONS

LL and J-KZ conceived the project. LL and XNZ designed the experiments. XM, XMZ, HZ, ZL, YLiu, and XNZ conducted the experiments. XM, YZ, SS, YLi, and RL conducted the proteomics data analysis. HZ and LT conducted the confocal observation. LJ contributed reagents, materials, and analytical platform. LL and XM wrote the manuscript. All authors commented on the manuscript and approved the submitted version.

FUNDING

This work was supported by National Natural Science Foundation of China (Grant Nos. 31570246 and 32170279), and the Fundamental Research Funds for the Central Universities (Grant No. 2572019CT03).

ACKNOWLEDGMENTS

We thank Chuanyou Li (Institute of Genetics and Developmental Biology, Chinese Academy of Sciences, Beijing) for donating the PIN1-GFP, PIN2-GFP, and PIN3-GFP marker lines. We also thank Xugang Li (Shandong Agricultural University) for donating the PIN1:GUS, PIN2:GUS, and PIN3:GUS marker lines.

SUPPLEMENTARY MATERIAL

The Supplementary Material for this article can be found online at: https://www.frontiersin.org/articles/10.3389/fpls.2022.849532/full#supplementary-material

Supplementary Table 1 | Proteomic analysis of microsomal fraction of the *mag2-1 mal* double mutant.

Supplementary Table 2 | Gene Ontology (GO) enrichment analysis of differently accumulated proteins (DAPs).

Supplementary Table 3 | Vesicle trafficking-related DAPs.

Supplementary Table 4 | Auxin-related DAPs.

Supplementary Table 5 | Primers and probes used in this study.

REFERENCES

Alvim Kamei, C. L., Boruc, J., Vandepoele, K., Van den Daele, H., Maes, S., Russinova, E., et al. (2008). The PRA1 gene family in *Arabidopsis*. *Plant Physiol.* 147, 1735–1749. doi: 10.1104/pp.108.122226

Andag, U., and Schmitt, H. D. (2003). Dsl1p, an essential component of the Golgi-endoplasmic reticulum retrieval system in yeast, uses the same sequence motif to interact with different subunits of the COPI vesicle coat. *J. Biol. Chem.* 278, 51722–51734. doi: 10.1074/jbc.M308740200

Ashburner, M., Ball, C. A., Blake, J. A., Botstein, D., Butler, H., Cherry, J. M., et al. (2000). Gene ontology: tool for the unification of biology. The Gene Ontology Consortium. *Nat. Genet.* 25, 25–29. doi: 10.1038/75556

Barbez, E., and Kleine-Vehn, J. (2013). Divide Et Impera–cellular auxin compartmentalization. *Curr. Opin. Plant Biol.* 16, 78–84. doi: 10.1016/j.pbi.2012.10.005

Barbez, E., Kubeš, M., Rolèík, J., Béziat, C., Pìnèík, A., Wang, B., et al. (2012). A novel putative auxin carrier family regulates intracellular auxin homeostasis in plants. *Nature* 485, 119–122. doi: 10.1038/nature11001

Barbosa, I. C. R., Hammes, U. Z., and Schwechheimer, C. (2018). Activation and polarity control of PIN-FORMED auxin transporters by phosphorylation. *Trends Plant Sci.* 23, 523–538. doi: 10.1016/j.tplants.2018.03.009

Bassham, D. C., Sanderfoot, A. A., Kovaleva, V., Zheng, H., and Raikhel, N. V. (2000). AtVPS45 complex formation at the trans-Golgi network. *Mol. Biol. Cell* 11, 2251–2265. doi: 10.1091/mbc.11.7.2251

Béziat, C., and Kleine-Vehn, J. (2018). The road to auxin-dependent growth repression and promotion in apical hooks. *Curr. Biol.* 28, R519–R525. doi: 10.1016/j.cub.2018.01.069

Béziat, C., Barbez, E., Feraru, M. I., Lucyshyn, D., and Kleine-Vehn, J. (2017). Light triggers PILS-dependent reduction in nuclear auxin signalling for growth transition. *Nat. Plants* 3:17105. doi: 10.1038/nplants.2017.105

Bhalerao, R. P., and Bennett, M. J. (2003). The case for morphogens in plants. *Nat. Cell Biol.* 5, 939–943. doi: 10.1038/ncb1103-939

Blakeslee, J. J., Spatola Rossi, T., and Kriechbaumer, V. (2019). Auxin biosynthesis: spatial regulation and adaptation to stress. *J. Exp. Bot.* 70, 5041–5049. doi: 10.1093/jxb/erz283

Borgese, N., Francolini, M., and Snapp, E. (2006). Endoplasmic reticulum architecture: structures in flux. *Curr. Opin. Cell Biol.* 18, 358–364. doi: 10.1016/j.ceb.2006.06.008

Böttcher, C., Chapman, A., Fellermeier, F., Choudhary, M., Scheel, D., and Glawischnig, E. (2014). The biosynthetic pathway of indole-3-carbaldehyde and indole-3-carboxylic acid derivatives in *Arabidopsis*. *Plant Physiol.* 165, 841–853. doi: 10.1104/pp.114.235630

Bröcker, C., Engelbrecht-Vandré, S., and Ungermann, C. (2010). Multisubunit tethering complexes and their role in membrane fusion. *Curr. Biol.* 20, R943–R952. doi: 10.1016/j.cub.2010.09.015

Cao, X., Yang, H., Shang, C., Ma, S., Liu, L., and Cheng, J. (2019). The roles of auxin biosynthesis YUCCA gene family in plants. *Int. J. Mol. Sci.* 20:6343. doi: 10.3390/ijms20246343

Chen, Q., Yu, F., and Xie, Q. (2020). Insights into endoplasmic reticulum-associated degradation in plants. *New Phytol.* 226, 345–350. doi: 10.1111/nph.16369

Chen, R., Hilson, P., Sedbrook, J., Rosen, E., Caspar, T., and Masson, P. H. (1998). The *Arabidopsisthaliana* AGRAVITROPIC 1 gene encodes a component of the polar-auxin-transport efflux carrier. *Proc. Natl. Acad. Sci. U.S.A.* 95, 15112–15117. doi: 10.1073/pnas.95.25.15112

Cox, J., Neuhauser, N., Michalski, A., Scheltema, R. A., Olsen, J. V., and Mann, M. (2011). Andromeda: a peptide search engine integrated into the MaxQuant environment. *J. Proteome Res.* 10, 1794–1805. doi: 10.1021/pr101065j

Dal Bosco, C., Dovzhenko, A., Liu, X., Woerner, N., Rensch, T., Eismann, M., et al. (2012). The endoplasmic reticulum localized PIN8 is a pollen-specific auxin carrier involved in intracellular auxin homeostasis. *Plant J.* 71, 860–870. doi: 10.1111/j.1365-313X.2012.05037.x

Dhonukshe, P., Huang, F., Galvan-Ampudia, C. S., Mähönen, A. P., Kleine-Vehn, J., Xu, J., et al. (2010). Plasma membrane-bound AGC3 kinases phosphorylate PIN auxin carriers at TPRXS(N/S) motifs to direct apical PIN recycling. *Development* 137, 3245–3255. doi: 10.1242/dev.052456

Ding, Z., Wang, B., Moreno, I., Dupláková, N., Simon, S., Carraro, N., et al. (2012). ER-localized auxin transporter PIN8 regulates auxin homeostasis and male gametophyte development in *Arabidopsis*. *Nat. Commun.* 3:941. doi: 10.1038/ncomms1941

Ditengou, F. A., Gomes, D., Nziengui, H., Kochersperger, P., Lasok, H., Medeiros, V., et al. (2018). Characterization of auxin transporter PIN6 plasma membrane targeting reveals a function for PIN6 in plant bolting. *New Phytol.* 217, 1610–1624. doi: 10.1111/nph.14923

Eads, J. C., Ozturk, D., Wexler, T. B., Grubmeyer, C., and Sacchettini, J. C. (1997). A new function for a common fold: the crystal structure of quinolinic acid phosphoribosyltransferase. *Structure* 5, 47–58. doi: 10.1016/s0969-2126(97)00165-2

Fan, J., Zhai, Z., Yan, C., and Xu, C. (2015). *Arabidopsis* trigalactosyldiacylglycerol5 Interacts with TGD1. TGD2, and TGD4 to Facilitate Lipid Transfer from the Endoplasmic Reticulum to Plastids. *Plant Cell* 27, 2941–2955. doi: 10.1105/tpc.15.00394

Fasshauer, D., Sutton, R. B., Brunger, A. T., and Jahn, R. (1998). Conserved structural features of the synaptic fusion complex: SNARE proteins reclassified as Q- and R-SNAREs. *Proc. Natl. Acad. Sci. U.S.A.* 95, 15781–15786. doi: 10.1073/pnas.95.26.15781

Feraru, E., and Friml, J. (2008). PIN polar targeting. *Plant Physiol.* 147, 1553–1559. doi: 10.1104/pp.108.121756

Feraru, E., Feraru, M. I., Barbez, E., Waidmann, S., Sun, L., Gaidora, A., et al. (2019). PILS6 is a temperature-sensitive regulator of nuclear auxin input and organ growth in *Arabidopsisthaliana*. *Proc. Natl. Acad. Sci. U.S.A.* 116, 3893–3898. doi: 10.1073/pnas.1814015116

Fernández-Marcos, M., Sanz, L., Lewis, D. R., Muday, G. K., and Lorenzo, O. (2011). Nitric oxide causes root apical meristem defects and growth inhibition while reducing PIN-FORMED 1 (PIN1)-dependent acropetal auxin transport. *Proc. Natl. Acad. Sci. U.S.A.* 108, 18506–18511. doi: 10.1073/pnas.1108644108

Friml, J., Vieten, A., Sauer, M., Weijers, D., Schwarz, H., Hamann, T., et al. (2003). Efflux-dependent auxin gradients establish the apical-basal axis of *Arabidopsis*. *Nature* 426, 147–153. doi: 10.1038/nature02085

Friml, J., Yang, X., Michniewicz, M., Weijers, D., Quint, A., Tietz, O., et al. (2004). A PINOID-dependent binary switch in apical-basal PIN polar targeting directs auxin efflux. *Science* 306, 862–865. doi: 10.1126/science.1100618

Ganguly, A., Park, M., Kesawat, M. S., and Cho, H. T. (2014). Functional analysis of the hydrophilic loop in intracellular trafficking of *Arabidopsis* PIN-FORMED proteins. *Plant Cell* 26, 1570–1585. doi: 10.1105/tpc.113.118422

Glanc, M., Van Gelderen, K., Hoermayer, L., Tan, S., Naramoto, S., Zhang, X., et al. (2021). AGC kinases and MAB4/MEL proteins maintain PIN polarity by limiting lateral diffusion in plant cells. Curr. Biol. 31, 1918-1930.e5. doi: 10.1016/j.cub.2021.02.028

Gomes, G. L. B., and Scortecci, K. C. (2021). Auxin and its role in plant development: structure, signalling, regulation and response mechanisms. *Plant Biol. (Stuttg)* 23, 894–904. doi: 10.1111/plb.13303

Grones, P., Abas, M., Hajný, J., Jones, A., Waidmann, S., Kleine-Vehn, J., et al. (2018). PID/WAG-mediated phosphorylation of the *Arabidopsis* PIN3 auxin transporter mediates polarity switches during gravitropism. *Sci. Rep.* 8:10279. doi: 10.1038/s41598-018-28188-1

Grosshans, B. L., Ortiz, D., and Novick, P. (2006). Rabs and their effectors: achieving specificity in membrane traffic. *Proc. Natl. Acad. Sci. U.S.A.* 103, 11821–11827. doi: 10.1073/pnas.0601617103

Guan, L., Yang, S., Li, S., Liu, Y., Liu, Y., Yang, Y., et al. (2021). AtSEC22 regulates cell morphogenesis via affecting cytoskeleton organization and stabilities. *Front. Plant Sci.* 12:635732. doi: 10.3389/fpls.2021.635732

Habets, M. E. J., and Offringa, R. (2014). PIN-driven polar auxin transport in plant developmental plasticity: a key target for environmental and endogenous signals. *New Phytol.* 203, 362–377. doi: 10.1111/nph.12831

Hardtke, C. S., and Berleth, T. (1998). The *Arabidopsis* gene MONOPTEROS encodes a transcription factor mediating embryo axis formation and vascular development. *Embo J.* 17, 1405–1411. doi: 10.1093/emboj/17.5.1405

Heider, M. R., and Munson, M. (2012). Exorcising the exocyst complex. *Traffic* 13, 898–907. doi: 10.1111/j.1600-0854.2012.01353.x

Homma, Y., Hiragi, S., and Fukuda, M. (2021). Rab family of small GTPases: an updated view on their regulation and functions. *FEBS J.* 288, 36–55. doi: 10.1111/febs.15453

Hu, S., Ye, H., Cui, Y., and Jiang, L. (2020). AtSec62 is critical for plant development and is involved in ER-phagy in *Arabidopsisthaliana*. *J. Integr. Plant Biol.* 62, 181–200. doi: 10.1111/jipb.12872

Huang, F. C., Fu, B. J., Liu, Y. T., Chang, Y. R., Chi, S. F., Chien, P. R., et al. (2018). *Arabidopsis* RETICULON-LIKE3 (RTNLB3) and RTNLB8 participate in agrobacterium-mediated plant transformation. *Int. J. Mol. Sci.* 19:638. doi: 10.3390/ijms19020638

Hüttner, S., Veit, C., Vavra, U., Schoberer, J., Liebminger, E., Maresch, D., et al. (2014). *Arabidopsis* Class I α-Mannosidases MNS4 and MNS5 Are involved in endoplasmic reticulum-associated degradation of misfolded glycoproteins. *Plant Cell* 26, 1712–1728. doi: 10.1105/tpc.114.123216

Ichino, T., Fuji, K., Ueda, H., Takahashi, H., Koumoto, Y., Takagi, J., et al. (2014). GFS9/TT9 contributes to intracellular membrane trafficking and flavonoid accumulation in *Arabidopsisthaliana*. *Plant J.* 80, 410–423. doi: 10.1111/tpj.12637

Ishihama, Y., Rappsilber, J., and Mann, M. (2006). Modular stop and go extraction tips with stacked disks for parallel and multidimensional Peptide fractionation in proteomics. *J. Proteome Res.* 5, 988–994. doi: 10.1021/pr050385q

Kitakura, S., Adamowski, M., Matsuura, Y., Santuari, L., Kouno, H., Arima, K., et al. (2017). BEN3/BIG2 arf gef is involved in brefeldin a-sensitive trafficking at the trans-golgi network/early endosome in *Arabidopsisthaliana*. *Plant Cell Physiol.* 58, 1801–1811. doi: 10.1093/pcp/pcx118

Klein, P., Seidel, T., Stöcker, B., and Dietz, K. J. (2012). The membrane-tethered transcription factor ANAC089 serves as redox-dependent suppressor of stromal ascorbate peroxidase gene expression. *Front. Plant Sci.* 3:247. doi: 10.3389/fpls.2012.00247

Kong, X., Lu, S., Tian, H., and Ding, Z. (2015). WOX5 is shining in the root stem cell niche. *Trends Plant Sci.* 20, 601–603. doi: 10.1016/j.tplants.2015.08.009

Kramer, E. M., and Bennett, M. J. (2006). Auxin transport: a field in flux. *Trends Plant Sci.* 11, 382–386. doi: 10.1016/j.tplants.2006.06.002

Kriechbaumer, V., Botchway, S. W., and Hawes, C. (2016). Localization and interactions between *Arabidopsis* auxin biosynthetic enzymes in the TAA/YUC-dependent pathway. *J. Exp. Bot.* 67, 4195–4207. doi: 10.1093/jxb/erw195

Kriechbaumer, V., Seo, H., Park, W. J., and Hawes, C. (2015). Endoplasmic reticulum localization and activity of maize auxin biosynthetic enzymes. *J. Exp. Bot.* 66, 6009–6020. doi: 10.1093/jxb/erv314

Kriechbaumer, V., Wang, P., Hawes, C., and Abell, B. M. (2012). Alternative splicing of the auxin biosynthesis gene YUCCA4 determines its subcellular compartmentation. *Plant J.* 70, 292–302. doi: 10.1111/j.1365-313X.2011.04866.x

Lamber, E. P., Siedenburg, A. C., and Barr, F. A. (2019). Rab regulation by GEFs and GAPs during membrane traffic. *Curr. Opin. Cell Biol.* 59, 34–39. doi: 10.1016/j.ceb.2019.03.004

Lee, G. J., Sohn, E. J., Lee, M. H., and Hwang, I. (2004). The *Arabidopsis* rab5 homologs rha1 and ara7 localize to the prevacuolar compartment. *Plant Cell Physiol.* 45, 1211–1220. doi: 10.1093/pcp/pch142

Lee, Y., Jang, M., Song, K., Kang, H., Lee, M. H., Lee, D. W., et al. (2013). Functional identification of sorting receptors involved in trafficking of soluble lytic vacuolar proteins in vegetative cells of *Arabidopsis*. *Plant Physiol.* 161, 121–133. doi: 10.1104/pp.112.210914

Leyser, O. (2005). Auxin distribution and plant pattern formation: how many angels can dance on the point of PIN? *Cell* 121, 819–822. doi: 10.1016/j.cell.2005.06.005

Li, K., Kamiya, T., and Fujiwara, T. (2015). Differential Roles of PIN1 and PIN2 in root meristem maintenance under low-b conditions in *Arabidopsisthaliana*. *Plant Cell Physiol.* 56, 1205–1214. doi: 10.1093/pcp/pcv047

Li, L., Shimada, T., Takahashi, H., Koumoto, Y., Shirakawa, M., Takagi, J., et al. (2013). MAG2 and three MAG2-INTERACTING PROTEINs form an ER-localized complex to facilitate storage protein transport in *Arabidopsisthaliana*. *Plant J.* 76, 781–791. doi: 10.1111/tpj.12347

Li, L., Shimada, T., Takahashi, H., Ueda, H., Fukao, Y., Kondo, M., et al. (2006). MAIGO2 is involved in exit of seed storage proteins from the endoplasmic reticulum in *Arabidopsisthaliana*. *Plant Cell* 18, 3535–3547. doi: 10.1105/tpc.106.046151

Li, R., Jiang, J., Jia, S., Zhu, X., Su, H., and Li, J. (2020). Overexpressing broccoli tryptophan biosynthetic genes BoTSB1 and BoTSB2 promotes biosynthesis of IAA and indole glucosinolates. *Physiol. Plant* 168, 174–187. doi: 10.1111/ppl.12933

Linders, P. T., Horst, C. V., Beest, M. T., and van den Bogaart, G. (2019). Stx5-Mediated ER-Golgi transport in mammals and yeast. *Cells* 8:780. doi: 10.3390/cells8080780

Lobingier, B. T., and Merz, A. J. (2012). Sec1/Munc18 protein Vps33 binds to SNARE domains and the quaternary SNARE complex. *Mol. Biol. Cell* 23, 4611–4622. doi: 10.1091/mbc.E12-05-0343

Ludwig-Müller, J. (2011). Auxin conjugates: their role for plant development and in the evolution of land plants. *J. Exp. Bot.* 62, 1757–1773. doi: 10.1093/jxb/erq412

Majeed, S. R., Vasudevan, L., Chen, C. Y., Luo, Y., Torres, J. A., Evans, T. M., et al. (2014). Clathrin light chains are required for the gyrating-clathrin recycling pathway and thereby promote cell migration. *Nat. Commun.* 5:3891. doi: 10.1038/ncomms4891

Mangano, S., Denita-Juarez, S. P., Choi, H. S., Marzol, E., Hwang, Y., Ranocha, P., et al. (2017). Molecular link between auxin and ROS-mediated polar growth. *Proc. Natl. Acad. Sci. U.S.A.* 114:5289. doi: 10.1073/pnas.1701536114

Marzol, E., Borassi, C., Denita Juárez, S. P., Mangano, S., and Estevez, J. M. (2017). RSL4 Takes Control: multiple signals, one transcription factor. *Trends Plant Sci.* 22, 553–555. doi: 10.1016/j.tplants.2017.04.007

Máthé, C. M. M. H., Freytag, C., and Garda, T. (2021). The protein phosphatase PP2A plays multiple roles in plant development by regulation of vesicle traffic-facts and questions. *Int. J. Mol. Sci.* 22:975. doi: 10.3390/ijms22020975

Mergner, J., and Schwechheimer, C. (2014). The NEDD8 modification pathway in plants. *Front. Plant Sci.* 5:103. doi: 10.3389/fpls.2014.00103

Michniewicz, M., Zago, M. K., Abas, L., Weijers, D., Schweighofer, A., Meskiene, I., et al. (2007). Antagonistic regulation of PIN phosphorylation by PP2A and PINOID directs auxin flux. *Cell* 130, 1044–1056. doi: 10.1016/j.cell.2007.07.033

Middleton, A. M., Dal Bosco, C., Chlap, P., Bensch, R., Harz, H., Ren, F., et al. (2018). Data-driven modeling of intracellular auxin fluxes indicates a dominant role of the ER in controlling nuclear auxin uptake. *Cell Rep.* 22, 3044–3057. doi: 10.1016/j.celrep.2018.02.074

Mravec, J., Skùpa, P., Bailly, A., Hoyerová, K., Krecek, P., Bielach, A., et al. (2009). Subcellular homeostasis of phytohormone auxin is mediated by the ER-localized PIN5 transporter. *Nature* 459, 1136–1140. doi: 10.1038/nature08066

Müller, T. M., Böttcher, C., and Glawischnig, E. (2019). Dissection of the network of indolic defence compounds in *Arabidopsisthaliana* by multiple mutant analysis. *Phytochemistry* 161, 11–20. doi: 10.1016/j.phytochem.2019.01.009

Naing, A. H., and Kim, C. K. (2021). Abiotic stress-induced anthocyanins in plants: their role in tolerance to abiotic stresses. *Physiol. Plant.* 172, 1711–1723. doi: 10.1111/ppl.13373

Naramoto, S. (2017). Polar transport in plants mediated by membrane transporters: focus on mechanisms of polar auxin transport. *Curr. Opin. Plant Biol.* 40, 8–14. doi: 10.1016/j.pbi.2017.06.012

Omelyanchuk, N. A., Kovrizhnykh, V. V., Oshchepkova, E. A., Pasternak, T., Palme, K., and Mironova, V. V. (2016). A detailed expression map of the PIN1 auxin transporter in *Arabidopsisthaliana* root. *BMC Plant Biol.* 16(Suppl. 1):5. doi: 10.1186/s12870-015-0685-0

Pastorczyk, M., Kosaka, A., Piślewska-Bednarek, M., López, G., Frerigmann, H., Kułak, K., et al. (2020). The role of CYP71A12 monooxygenase in pathogen-triggered tryptophan metabolism and *Arabidopsis* immunity. *New Phytol.* 225, 400–412. doi: 10.1111/nph.16118

Pires, N. D., Yi, K., Breuninger, H., Catarino, B., Menand, B., and Dolan, L. (2013). Recruitment and remodeling of an ancient gene regulatory network during land plant evolution. *Proc. Natl. Acad. Sci. U.S.A.* 110, 9571–9576. doi: 10.1073/pnas.1305457110

Poulet, A., and Kriechbaumer, V. (2017). Bioinformatics analysis of phylogeny and transcription of TAA/YUC auxin biosynthetic genes. *Int. J. Mol. Sci.* 18:1791. doi: 10.3390/ijms18081791

Radwanski, E. R., and Last, R. L. (1995). Tryptophan biosynthesis and metabolism: biochemical and molecular genetics. *Plant Cell* 7, 921–934. doi: 10.1105/tpc.7.7.921

Ravikumar, R., Steiner, A., and Assaad, F. F. (2017). Multisubunit tethering complexes in higher plants. *Curr. Opin. Plant Biol.* 40, 97–105. doi: 10.1016/j.pbi.2017.08.009

Ren, Y., Yip, C. K., Tripathi, A., Huie, D., Jeffrey, P. D., Walz, T., et al. (2009). A structure-based mechanism for vesicle capture by the multisubunit tethering complex Dsl1. *Cell* 139, 1119–1129. doi: 10.1016/j.cell.2009.11.002

Saeed, B., Brillada, C., and Trujillo, M. (2019). Dissecting the plant exocyst. *Curr. Opin. Plant Biol.* 52, 69–76. doi: 10.1016/j.pbi.2019.08.004

Saito, K., Maeda, M., and Katada, T. (2017). Regulation of the Sar1 GTPase cycle is necessary for large cargo secretion from the endoplasmic reticulum. *Front. Cell Dev. Biol.* 5:75. doi: 10.3389/fcell.2017.00075

Sanchez Carranza, A. P., Singh, A., Steinberger, K., Panigrahi, K., Palme, K., Dovzhenko, A., et al. (2016). Hydrolases of the ILR1-like family of *Arabidopsisthaliana* modulate auxin response by regulating auxin homeostasis in the endoplasmic reticulum. *Sci. Rep.* 6:24212. doi: 10.1038/srep24212

Sauer, M., and Kleine-Vehn, J. (2019). PIN-FORMED and PIN-LIKES auxin transport facilitators. *Development* 146:dev168088. doi: 10.1242/dev.168088

Sechet, J., Htwe, S., Urbanowicz, B., Agyeman, A., Feng, W., Ishikawa, T., et al. (2018). Suppression of *Arabidopsis* GGLT1 affects growth by reducing the L-galactose content and borate cross-linking of rhamnogalacturonan-II. *Plant J.* 96, 1036–1050. doi: 10.1111/tpj.14088

Serino, G., and Deng, X. W. (2003). The COP9 signalosome: regulating plant development through the control of proteolysis. *Annu. Rev. Plant Biol.* 54, 165–182. doi: 10.1146/annurev.arplant.54.031902.134847

Sessions, A., Nemhauser, J. L., McColl, A., Roe, J. L., Feldmann, K. A., and Zambryski, P. C. (1997). ETTIN patterns the *Arabidopsis* floral meristem and reproductive organs. *Development* 124, 4481–4491.

Shen, J., Gao, C., Zhao, Q., Lin, Y., Wang, X., Zhuang, X., et al. (2016). AtBRO1 Functions in ESCRT-I complex to regulate multivesicular body protein sorting. *Mol. Plant.* 9, 760–763. doi: 10.1016/j.molp.2016.02.005

Sheng, Q., Li, R., Dai, J., Li, Q., Su, Z., Guo, Y., et al. (2015). Preprocessing significantly improves the peptide/protein identification sensitivity of high-resolution isobarically labeled tandem mass spectrometry data. *Mol. Cell Proteomics* 14, 405–417. doi: 10.1074/mcp.O114.041376

Shimada, T., Fuji, K., Tamura, K., Kondo, M., Nishimura, M., and Hara-Nishimura, I. (2003). Vacuolar sorting receptor for seed storage proteins in *Arabidopsisthaliana*. *Proc. Natl. Acad. Sci. U.S.A.* 100, 16095–16100. doi: 10.1073/pnas.2530568100

Simon, S., Skùpa, P., Viaene, T., Zwiewka, M., Tejos, R., Klíma, P., et al. (2016). PIN6 auxin transporter at endoplasmic reticulum and plasma membrane mediates auxin homeostasis and organogenesis in *Arabidopsis*. *New Phytol.* 211, 65–74. doi: 10.1111/nph.14019

Sinclair, S. J., Murphy, K. J., Birch, C. D., and Hamill, J. D. (2000). Molecular characterization of quinolinate phosphoribosyltransferase (QPRtase) in Nicotiana. *Plant Mol. Biol.* 44, 603–617. doi: 10.1023/a:1026590521318

Stepanova, A. N., Robertson-Hoyt, J., Yun, J., Benavente, L. M., Xie, D. Y., Dolezal, K., et al. (2008). TAA1-mediated auxin biosynthesis is essential for hormone crosstalk and plant development. *Cell* 133, 177–191. doi: 10.1016/j.cell.2008.01.047

Strader, L. C., and Bartel, B. (2011). Transport and metabolism of the endogenous auxin precursor indole-3-butyric acid. *Mol. Plant* 4, 477–486. doi: 10.1093/mp/ssr006

Sun, L., Feraru, E., Feraru, M. I., Waidmann, S., Wang, W., Passaia, G., et al. (2020). PIN-LIKES Coordinate Brassinosteroid Signaling with Nuclear Auxin Input in *Arabidopsisthaliana*. *Curr. Biol.* 30, 1579.e–1588.e. doi: 10.1016/j.cub.2020.02.002

Takahashi, H., Tamura, K., Takagi, J., Koumoto, Y., Hara-Nishimura, I., and Shimada, T. (2010). MAG4/Atp115 is a golgi-localized tethering factor that mediates efficient anterograde transport in *Arabidopsis*. *Plant Cell Physiol.* 51, 1777–1787. doi: 10.1093/pcp/pcq137

Takemoto, K., Ebine, K., Askani, J. C., Krüger, F., Gonzalez, Z. A., Ito, E., et al. (2018). Distinct sets of tethering complexes, SNARE complexes, and Rab GTPases mediate membrane fusion at the vacuole in *Arabidopsis*. *Proc. Natl. Acad. Sci. U.S.A.* 115, E2457–E2466. doi: 10.1073/pnas.1717839115

Tanaka, H., Nodzyłski, T., Kitakura, S., Feraru, M. I., Sasabe, M., Ishikawa, T., et al. (2014). BEX1/ARF1A1C is required for BFA-sensitive recycling of PIN auxin transporters and auxin-mediated development in *Arabidopsis*. *Plant Cell Physiol.* 55, 737–749. doi: 10.1093/pcp/pct196

Tarte, V. N., Seok, H. Y., Woo, D. H., Le, D. H., Tran, H. T., Baik, J. W., et al. (2015). *Arabidopsis* Qc-SNARE gene AtSFT12 is involved in salt and osmotic stress responses and Na(+) accumulation in vacuoles. *Plant Cell Rep.* 34, 1127–1138. doi: 10.1007/s00299-015-1771-3

Trahey, M., and Hay, J. C. (2010). Transport vesicle uncoating: it's later than you think. *F1000 Biol. Rep.* 2:47. doi: 10.3410/b2-47

Ungar, D., Oka, T., Brittle, E. E., Vasile, E., Lupashin, V. V., Chatterton, J. E., et al. (2002). Characterization of a mammalian Golgi-localized protein complex,

COG, that is required for normal Golgi morphology and function. *J. Cell Biol.* 157, 405–415. doi: 10.1083/jcb.200202016

Vijayakumar, P., Datta, S., and Dolan, L. (2016). Root Hair Defective Six-Like4 (RSL4) promotes root hair elongation by transcriptionally regulating the expression of genes required for cell growth. *New Phytol.* 212, 944–953. doi: 10.1111/nph.14095

Vukašinović, N., and Žárský, V. (2016). Tethering complexes in the *Arabidopsis* endomembrane system. *Front. Cell Dev. Biol.* 4:46. doi: 10.3389/fcell.2016.00046

Wabnik, K., Kleine-Vehn, J., Govaerts, W., and Friml, J. (2011). Prototype cell-to-cell auxin transport mechanism by intracellular auxin compartmentalization. *Trends Plant Sci.* 16, 468–475. doi: 10.1016/j.tplants.2011.05.002

Wang, B., Chu, J., Yu, T., Xu, Q., Sun, X., Yuan, J., et al. (2015). Tryptophan-independent auxin biosynthesis contributes to early embryogenesis in *Arabidopsis*. *Proc. Natl. Acad. Sci. U.S.A.* 112, 4821–4826. doi: 10.1073/pnas.1503998112

Wang, C., Yan, X., Chen, Q., Jiang, N., Fu, W., Ma, B., et al. (2013). Clathrin light chains regulate clathrin-mediated trafficking, auxin signaling, and development in *Arabidopsis*. *Plant Cell* 25, 499–516. doi: 10.1105/tpc.112.108373

Wang, T., Li, L., and Hong, W. (2017). SNARE proteins in membrane trafficking. *Traffic* 18, 767–775. doi: 10.1111/tra.12524

Weller, B., Zourelidou, M., Frank, L., Barbosa, I. C., Fastner, A., Richter, S., et al. (2017). Dynamic PIN-FORMED auxin efflux carrier phosphorylation at the plasma membrane controls auxin efflux-dependent growth. *Proc. Natl. Acad. Sci. U.S.A.* 114, E887–E896. doi: 10.1073/pnas.1614380114

Whyte, J. R., and Munro, S. (2002). Vesicle tethering complexes in membrane traffic. *J. Cell Sci.* 115, 2627–2637.

Wu, X., and Rapoport, T. A. (2018). Mechanistic insights into ER-associated protein degradation. *Curr. Opin. Cell Biol.* 53, 22–28. doi: 10.1016/j.ceb.2018.04.004

Yang, Z. T., Wang, M. J., Sun, L., Lu, S. J., Bi, D. L., Sun, L., et al. (2014). The membrane-associated transcription factor NAC089 controls ER-stress-induced programmed cell death in plants. *PLoS Genet.* 10:e1004243. doi: 10.1371/journal.pgen.1004243

Yue, K., Sandal, P., Williams, E. L., Murphy, E., Stes, E., Nikonorova, N., et al. (2016). PP2A-3 interacts with ACR4 and regulates formative cell division in the *Arabidopsis* root. *Proc. Natl. Acad. Sci. U.S.A.* 113, 1447–1452. doi: 10.1073/pnas.1525122113

Zhao, P., and Lu, J. (2014). MAIGO2 is involved in gibberellic acid, sugar, and heat shock responses during germination and seedling development in *Arabidopsis*. *Acta Physiol. Plant.* 36, 315–321. doi: 10.1007/s11738-013-1412-9

Zhao, P., Liu, F., Zhang, B., Liu, X., Wang, B., Gong, J., et al. (2013). MAIGO2 is involved in abscisic acid-mediated response to?abiotic stresses and Golgi-to-ER retrograde transport. *Physiol. Plant.* 148, 246–260. doi: 10.1111/j.1399-3054.2012.01704.x

Zhao, X., Guo, X., Tang, X., Zhang, H., Wang, M., Kong, Y., et al. (2018). Misregulation of ER-Golgi Vesicle Transport Induces ER Stress and Affects Seed Vigor and Stress Response. *Front. Plant Sci.* 9:658. doi: 10.3389/fpls.2018.00658

Zhao, Y. (2018). Essential roles of local auxin biosynthesis in plant development and in adaptation to environmental changes. *Annu. Rev. Plant Biol.* 69, 417–435. doi: 10.1146/annurev-arplant-042817-040226

Zhou, J. J., and Luo, J. (2018). The PIN-FORMED auxin efflux carriers in plants. *Int. J. Mol. Sci.* 19:2759. doi: 10.3390/ijms19092759

Zolov, S. N., and Lupashin, V. V. (2005). Cog3p depletion blocks vesicle-mediated Golgi retrograde trafficking in HeLa cells. *J. Cell Biol.* 168, 747–759. doi: 10.1083/jcb.200412003

Zourelidou, M., Absmanner, B., Weller, B., Barbosa, I. C., Willige, B. C., Fastner, A., et al. (2014). Auxin efflux by PIN-FORMED proteins is activated by two different protein kinases, D6 PROTEIN KINASE and PINOID. *Elife* 3:e02860. doi: 10.7554/eLife.02860

Conflict of Interest: The authors declare that the research was conducted in the absence of any commercial or financial relationships that could be construed as a potential conflict of interest.

Publisher's Note: All claims expressed in this article are solely those of the authors and do not necessarily represent those of their affiliated organizations, or those of the publisher, the editors and the reviewers. Any product that may be evaluated in this article, or claim that may be made by its manufacturer, is not guaranteed or endorsed by the publisher.

frontiers in Plant Science

ORIGINAL RESEARCH
published: 21 March 2022
doi: 10.3389/fpls.2022.845107

Physiological, Proteomic Analysis, and Calcium-Related Gene Expression Reveal *Taxus wallichiana* var. *mairei* Adaptability to Acid Rain Stress Under Various Calcium Levels

Wen-Jun Hu[1], Ting-Wu Liu[2], Chun-Quan Zhu[3], Qian Wu[4], Lin Chen[1], Hong-Ling Lu[1], Chen-Kai Jiang[1], Jia Wei[1], Guo-Xin Shen[1]* and Hai-Lei Zheng[4]**

[1] Zhejiang Academy of Agricultural Sciences, Hangzhou, China, [2] School of Life Science, Huaiyin Normal University, Huai'an, China, [3] State Key Laboratory of Rice Biology, China National Rice Research Institute, Hangzhou, China, [4] Key Laboratory for Subtropical Wetland Ecosystem Research of Ministry of Education (MOE), College of the Environment and Ecology, Xiamen University, Xiamen, China

OPEN ACCESS

Edited by:
Mateusz Labudda, Warsaw University of Life Sciences – SGGW, Poland

Reviewed by:
Juan Chen, Northwest A&F University, China
Biswojit Debnath, Sylhet Agricultural University, Bangladesh

***Correspondence:**
Wen-Jun Hu
guyuexingshi@163.com
Guo-Xin Shen
guoxin.shen@ttu.edu
Hai-Lei Zheng
zhenghl@xmu.edu.cn

Specialty section:
This article was submitted to Plant Proteomics and Protein Structural Biology, a section of the journal Frontiers in Plant Science

Received: *29 December 2021*
Accepted: *07 February 2022*
Published: *21 March 2022*

Citation:
Hu W-J, Liu T-W, Zhu C-Q, Wu Q, Chen L, Lu H-L, Jiang C-K, Wei J, Shen G-X and Zheng H-L (2022) Physiological, Proteomic Analysis, and Calcium-Related Gene Expression Reveal Taxus wallichiana var. mairei Adaptability to Acid Rain Stress Under Various Calcium Levels. Front. Plant Sci. 13:845107. doi: 10.3389/fpls.2022.845107

As one of the serious environmental problems worldwide, acid rain (AR) has always caused continuous damage to the forestry ecosystem. Studies have shown that AR can leach calcium ions from plants and soil. Calcium (Ca) is also a crucial regulator of the plant stress response, whereas there are few reports on how Ca regulates the response of AR-resistant woody plants to AR stress. In this study, by setting different exogenous Ca levels, we study the physiological and molecular mechanism of Ca in regulating the *Taxus wallichiana* var. *mairei* response to AR stress. Our results showed that low Ca level leads to photosynthesis, and antioxidant defense system decreases in *T. wallichiana* var. *mairei* leaves; however, these negative effects could be reversed at high Ca level. In addition, proteomic analyses identified 44 differentially expressed proteins in different Ca level treatments of *T. wallichiana* var. *mairei* under AR stress. These proteins were classified into seven groups, which include metabolic process, photosynthesis and energy pathway, cell rescue and defense, transcription and translation, protein modification and degradation, signal transduction, etc. Furthermore, the study found that low Ca level leads to an obvious increase of Ca-related gene expression under AR stress in *T. wallichiana* var. *mairei* using qRT-PCR analyses and however can be reversed at high Ca level. These findings would enrich and extend the Ca signaling pathways of AR stress in AR-resistant woody plants and are expected to have important theoretical and practical significance in revealing the mechanism of woody plants tolerating AR stress and protecting forestry ecosystem in soil environment under different Ca levels.

Keywords: plant proteomics, acid rain, calcium, *Taxus wallichiana var. mairei*, soil, tree species

INTRODUCTION

As a serious environmental problem, acid rain (AR) affects seriously normal growth and development of forest tree species, which includes balance of leaf nutrient, growth indices, chlorosis, and necrosis in leaves, chlorophyll content, restrict photosynthesis, and the antioxidant enzyme activity (Liu and Diamond, 2005; Larssen et al., 2006; Hu et al., 2014a, 2016, 2021;

Huang et al., 2019; Liu M. et al., 2019; Grennfelt et al., 2020; Zhang et al., 2020). Furthermore, AR can interfere with the material metabolism, transcriptional factors, and secondary metabolites genes, further cause metabolic disorders and inhibit the plant growth and development, and even cause plant death in severe cases (Lee et al., 2006; Hu et al., 2016; Debnath and Ahammed, 2020; Debnath et al., 2020, 2021). In addition, recent studies have found that AR severely affects woody plant vegetation growth through leaching away calcium (Ca) element from plant and soil (Likens et al., 1996; Malakoff, 2010; Liu et al., 2011c). Further studies have also revealed that AR can disturb mineral ion absorption, deplete soil base Ca ion from pools, and limit the Ca uptake in woody plant (Liu et al., 2011c; Hu et al., 2014c; Shu et al., 2019). Many studies have demonstrated that Ca plays important roles in plants responding to environmental stresses, and exogenous Ca level regulates cytosolic Ca concentration and enhances antioxidant defense, thus serving as a source of nutrition and structure, regulatory agent to further modulate signaling functions (Reddy and Reddy, 2004; Hepler, 2005; Juice et al., 2006; Zhang et al., 2021). On the other hand, our previous studies also indicated that exogenous Ca level played a key role in the response process of AR stress in AR-sensitive woody plants (Hu et al., 2014c, 2016). Ma et al. (2021) also found that exogenous Ca enhances antioxidant defense to simulated AR stress in rice. However, the AR-resistant woody plants in response to AR stress at different Ca levels have not been reported in forest tree species.

Taxus wallichiana var. *mairei* is a well-known gymnosperm with great ornamental and medicinal value (Gao et al., 2007; Cheng et al., 2021; Xiong et al., 2021). As an AR-resistant tree species, *T. wallichiana* var. *mairei* is distributed over large areas of southern China, where AR is relatively serious (Gao et al., 2007; Hu et al., 2014a). Some physiological and biochemical changes and growth response to simulated AR have been reported in *T. wallichiana* var. *mairei* (Liu K. et al., 2007; Liu et al., 2012). Our previous study also found that *T. wallichiana* var. *mairei* is an AR-tolerant species under normal Ca condition (Hu et al., 2014a). However, the molecular mechanisms of AR resistance remain poorly understood in *T. wallichiana* var. *mairei* under different Ca conditions.

As responses of different Ca levels to AR stress are very complex processes, and further investigations are needed to clarify the molecular mechanism in AR-resistant species. Although our recent study revealed that there are rescue effects of exogenous Ca against AR stress in AR-sensitive species (Hu et al., 2014c, 2016), the underlying mechanisms remain unclear in AR-tolerant species at various Ca levels. To better understand the extent to which biological and environmental factors shape AR resistance of *T. wallichiana* var. *mairei* at different Ca levels, proteomics and Ca-related gene expression in *T. wallichiana* var. *mairei* response to AR stress at different Ca levels is one of powerful ways to identify the molecular mechanism. A recent study has presented a reference genome of *T. wallichiana* var. *mairei*, which will provide genetic resources and serve as a platform for identification and decoding of the AR resistance pathway in various Ca conditions in the future (Cheng et al., 2021; Xiong et al., 2021). In this study, we conduct proteomic study to clarify the molecular mechanisms of various Ca levels in *T. wallichiana* var. *mairei* under AR treatment. The objective of this study was to characterize the AR-responsive proteins in *T. wallichiana* var. *mairei* at different Ca levels, combined with the physiological and gene expression data, and further to establish the molecular metabolism in Ca-mediated AR resistance in AR-resistant woody plants.

MATERIALS AND METHODS

Soil Pretreatment

In our experiment, the substrate soil was lateritic soil, and the soil samples were collected from in southern forest areas of China where AR is much too harmful. Ca content in the soil was leached for 6 months of simulated AR, and the specific soil leaching process is referred to Liu J. X. et al. (2007) and Liu et al. (2011c). According to Hu et al. (2014c), Ca content was analyzed using ICP-MS (PerkinElmer Inc., Elan DRC-e, Waltham, MA, United States). Soil nutrients were recovered by a Hoagland nutrient solution, which contains one of the three Ca concentrations (20.0, 2.0, or 0.1 mmol L^{-1}), respectively (Liu et al., 2011c). The final soil exchangeable Ca level was high Ca level (107.08 mmol kg^{-1}), medium Ca level (19.65 mmol kg^{-1}), and low Ca level (1.85 mmol kg^{-1}).

Plant Materials and Experimental Procedure

The 6-month-old and size-identical *T. wallichiana* var. *mairei* seedlings (the aerial part length was 6.3 ± 0.5 cm) were transplanted into plastic pots. The seedlings were grown in a greenhouse with a light–dark regime of 16/8 h, temperature of 27/21°C (day/night), relative humidity of 60–70%, and photosynthetically active radiation of 210 μmol m^{-2} s^{-1}. After 2 weeks of recovery, the *T. wallichiana* var. *mairei* seedlings were sprayed once each day with simulated AR solution (pH 3.0) with medium Ca level as control group and low or high Ca level for treatment group as described by the previous study (Hu et al., 2014c). After 2-month AR treatment, the fresh leaves of *T. wallichiana* var. *mairei* seedlings were collected for further experiments, which include physiological and proteomic research and qRT-PCR analysis.

Measurements of Physiological and Growth Indexes

Chlorophyll in *T. wallichiana* var. *mairei* leaves was extracted using ice-cold 80% v/v acetone according to the study by Hu et al. (2014c). Net photosynthetic rate (*P*n) was performed with a portable photosynthesis system (Li-6400, Li-Cor, Lincoln, NE, United States) as described by Chen et al. (2013). At least eight saplings were randomly selected from the control group or the treatment group for *P*n measurements. For Ca element analysis, T. wallichiana var. mairei leaf tissue was dried at 80°C for 72 h. Ca concentration in the leaves was measured using ICP-MS (PerkinElmer Inc., Elan DRC-e, Waltham, MA, United States), following the study by Hu et al. (2014c).

Assay of Lipid Peroxidation, Reactive Oxygen Species Production, and Antioxidant Enzyme Activity

Soluble protein, proline, H_2O_2, and $O2^{\bullet -}$ content were measured as described by Chen et al. (2013). According to Liu et al. (2011a), lipid peroxidation in leaves was measured by estimating the content of malondialdehyde (MDA) using thiobarbituric acid (TBA) reaction. Superoxide dismutase (SOD) activity, ascorbic peroxidase (APX) activity, peroxidase (POD) activity, and catalase (CAT) activity were measured following the methods of Hu et al. (2014b).

Protein Extraction, Two-Dimensional Electrophoresis, and Data Analysis

Protein in *T. wallichiana* var. *mairei* leaves was extracted using the method of phenol extraction according to the study of Hu et al. (2014a). Three independent biological repetitions were performed for each treatment. According to the manufacturer's instructions of GE Healthcare Amersham Bioscience, protein concentration of the lysates was measured using a 2-D Quant Kit.

Two-dimensional electrophoresis (2-DE) was conducted according to the study of Hu et al. (2014a). Ettan IPGphor isoelectric focusing system (GE Healthcare Amersham Bioscience, Little Chalfont, United Kingdom) was used for isoelectric focusing (IEF). After IEF, gel strips were equilibrated as described by Hu et al. (2014c). For the second-dimension electrophoresis, it was conducted using a protein apparatus (Bio-Rad), the proteins were separated on 12.5% SDS polyacrylamide gels according to the manufacturer's instructions (Hu et al., 2014c). The 2-DE gels were stained using Coomassie Brilliant Blue R-250, and an image scanner (Uniscan M3600, China) was used for gel images at 600 dots per inch resolution. The 2-D gel images were analyzed using PDQuest software (Version 8.01, Bio-Rad, Hercules, CA, United States). The intensity of protein spots changed more than twofold and passed the Student's *t*-test ($p < 0.05$), which were considered for mass spectrometry analysis.

Protein Identification and Protein Classification

Protein digestion and protein identification in *T. wallichiana* var. *mairei* was performed according to the study of Hu et al. (2014a). The identified tryptic peptide masses in *T. wallichiana* var. *mairei* were searched against the National Center for Biotechnology Information non-redundant (NCBInr) database, and the taxonomy of green plants was selected using the MASCOT interface (Version 2.5; Matrix Science, London, United Kingdom). The following parameters were used for database search: no molecular weight restriction, permitting one missed cleavage, fixed modification of cysteine by carbamidomethylation, oxidation (Met) as a variable modification, the peptide tolerance of 100 ppm, and fragment ion mass tolerance of ±0.3 Da. At least three peptides were matched for protein identification, and the protein scores of MOWSE threshold were set greater than 73 with the NCBInr database ($p < 0.05$). As described by Hu et al. (2014a), the functions and subcellular localization of identified proteins were searched for the NCBI protein database,[1] UniProt,[2] and published literature.

Hierarchical Cluster Analysis

Hierarchical clustering was performed on density value of differentially expressed proteins according to the study of Hu et al. (2014c). Input value was calculated by dividing volume percentage of each protein spot at the high Ca-AR level and low Ca-AR level by the corresponding protein spot at the medium Ca-AR level. Complete linkage algorithm was enabled, and the results of hierarchical cluster were plotted using TreeView software version 1.1.3.

RNA Extraction and qRT-PCR Analysis

Total RNA from *T. wallichiana* var. *mairei* leaves (0.1 g) was extracted using RNA purification reagent (Invitrogen Inc., CA, United States) in liquid nitrogen according to the study of Hu et al. (2014c). The M-MLV reverse transcriptase (TaKaRa, Dalian, China) was used for the synthesis of the first-strand cDNAs as described by the previous study (Hu et al., 2014c). Gene primers were designed for cloning the fragments of Ca-related genes in *T. wallichiana* var. *mairei* (**Supplementary Table 1**). The Ca-related gene abundance was analyzed using the Rotor-gene-6000 real-time PCR system (Corbett Research, Mortlake, NSW, Australia) as described by Hu et al. (2014c) with minor modifications. The following temperature program was used for qRT-PCR analysis: 94°C for 10 min, followed 94°C for 30 s by 40 cycles, primer annealing at 52–56°C for 30 s (**Supplementary Table 2**), and extension at 72°C for 20 s. The glyceraldehyde-3-phosphate dehydrogenase gene (*GAPDH*) in *T. wallichiana* var. *mairei* was used as the internal control for each sample. Three independent biological replicates were performed for each sample.

Statistical Analysis

All data were presented as the mean ± SE of three replicated samples. The statistical significance was analyzed using a univariate analysis of variance (one-way ANOVA; SPSS, version 22.0, Inc., Chicago, IL, United States). Statistical significance was considered at $p < 0.05$.

RESULTS

Effects of Acid Rain Stress on Physiological Parameters of *Taxus wallichiana* var. *mairei* at Different Calcium Levels

To study the responses of woody plant to AR stress at different Ca levels, *T. wallichiana* var. *mairei* was treated with simulated AR (pH 3.0) for 2 months. Physiological changes are shown in **Figure 1**, and Ca content of the leaf, chlorophyll content, and photosynthetic activity (*P*n) were also tested and analyzed. After 2-month AR treatment, Ca content and *P*n were significantly

[1] http://www.ncbi.nlm.nih.gov

[2] http://www.uniprot.org

decreased in *T. wallichiana* var. *mairei* leaves at low Ca level; however, high Ca treatment can reverse the decline of the physiological indicators.

Effects of Acid Rain Stress on Antioxidant System Response in *Taxus wallichiana* var. *mairei* at Different Calcium Levels

As shown in **Figures 2A,B**, there was an obvious increase in soluble protein content and proline content in AR-treated *T. wallichiana* var. *mairei* at high Ca level. We found that the levels of MDA, H_2O_2, and $O2^{\bullet -}$ were significantly stimulated by low Ca treatment (**Figures 2C–E**). It found that SOD, APX, POD, and CAT showed a significant increase in *T. wallichiana* var. *mairei* leaves at high Ca level (**Figures 2F–I**).

Protein Profile and Functional Classification in *Taxus wallichiana* var. *mairei* Leaves Response to Acid Rain Stress at Different Calcium Levels

To further explore the proteome changes in *P*inus *massoniana* and *T. wallichiana* var. *mairei* leaves under AR treatment, 2-DE was performed in this study.

A total of 44 protein spot in *T. wallichiana* var. *mairei* leaves response to AR stress with different Ca treatments (**Figure 3A** and **Table 1**). Close-up views of representative different protein spots are shown in **Figure 3B**. To analyze which biological processes the identified differential proteins are involved in, the identified 44 proteins were analyzed in appropriate functional pathways (**Figure 4**). The differentially expressed proteins were divided into seven groups based on their biological functions. The largest protein group was sorted to photosynthesis and energy pathway (27.2%), followed by transcription and translation (20.5%), cell rescue and defense (18.2%), signal transduction (11.4%), metabolic process (9.1%), and protein modification and degradation (4.5%) (**Figure 4A**). As shown in **Figure 4B**, the subcellular localization analysis found that 44 differentially expressed proteins were located in the cytoplasm (25.0%), chloroplast (22.7%), mitochondrion (11.4%), membrane (11.4%), nucleus (9.0%), extracellular (4.5%), endoplasmic reticulum (2.3%), and vacuole (2.3%).

In addition, we used a hierarchical cluster analysis to find the regular pattern of different protein expression changes during AR stress in *T. wallichiana* var. *mairei* leaves with different Ca treatments. As shown in **Figure 5**, the differentially expressed proteins are mainly distributed into two branches in *T. wallichiana* var. *mairei*. We found that the expression abundance of cell defense-related proteins (spots 21, 22, and 24) showed a downward trend with the increase of Ca concentration under AR stress. Signal transduction-related proteins (spots 3, 37, and 39) showed a significant upregulation trend under low Ca-AR treatment. The expression trend of these proteins was

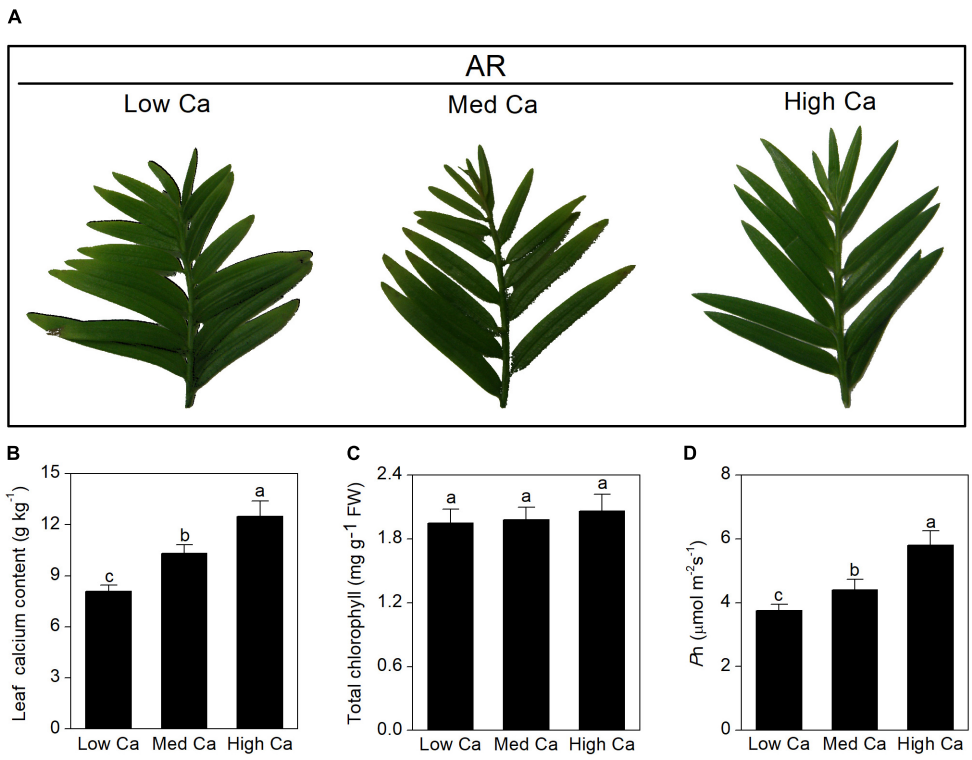

FIGURE 1 | Effects of different Ca treatments on morphological and physiological parameters of *T. wallichiana* var. *mairei* leaves under AR stress. **(A)** Phenotype on plant leaves. **(B)** Leaf Ca content. **(C)** Chlorophyll content. **(D)** Net photosynthetic rate (*Pn*). Different letters above columns indicate significant difference at $p < 0.05$.

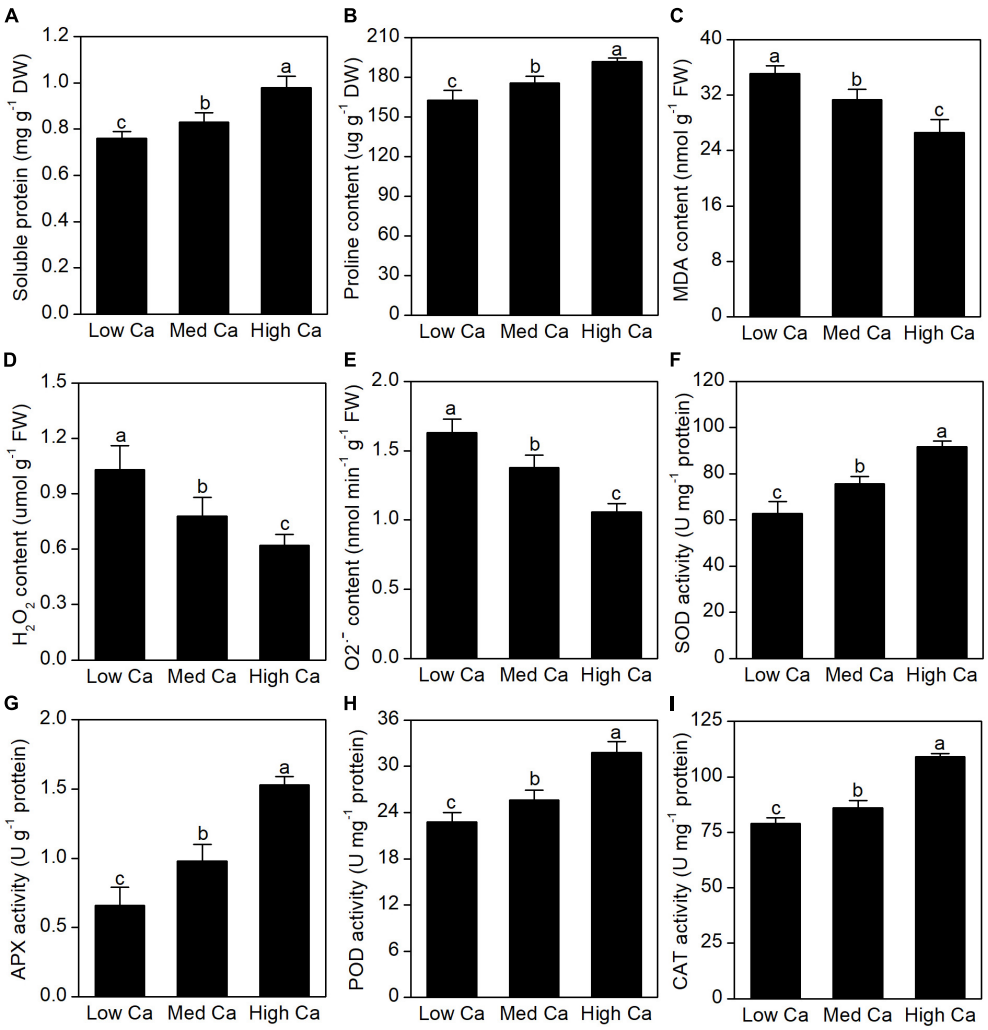

FIGURE 2 | Effects of different Ca treatments on lipid peroxidation, ROS production, and antioxidant enzyme activity under simulated AR stress in *T. wallichiana* var. *mairei* leaves. The soluble protein content **(A)**, proline content **(B)**, MDA content **(C)**, H_2O_2 content **(D)**, $O2^{\bullet-}$ content **(E)**, SOD activity **(F)**, APX activity **(G)**, POD activity **(H)**, and CAT activity **(I)**. Columns labeled by different letters indicate significant differences at $p < 0.05$.

reversed to downregulated with the increase in Ca concentration. More interestingly, we found that a protein (spot 17, light-harvesting complex II protein Lhcb1) related to photosynthesis process was significantly downregulated in low Ca condition, but turned to upregulated in high Ca condition, which indicates that high Ca treatment helps to improve *T. wallichiana* var. *mairei* leaves photosynthesis, which is one of the ways to enhance plant resistance to AR stress. The specific information of the differential proteins is listed in **Table 1**.

Protein Abundance Analysis by Western Blot

The proteomics results revealed that the abundance of ribulose-1, 5-bisphosphate carboxylase–oxygenase large subunit (spot 16), and ATP synthase (spots 7, 8, and 10) was increased in high Ca-AR-treated *T. wallichiana* var. *mairei* (**Table 1**). As shown in **Figure 6**, protein abundance levels of rubulose-1, 5-bisphoshate carboxylase–oxygenase large subunit (Rubisco LSU), and ATP synthase (ATPase) were significantly increased with high Ca treatment.

Calcium-Related Gene Expression Analysis

To evaluate the expression abundances of the Ca-related genes at different Ca levels in AR-treated *T. wallichiana* var. *mairei*, we further analyze calmodulin gene (*CaM1*), touch 3 gene (*TCH3*), calreticulin 3 gene (*CRT3*), CDPK-related kinase gene (*CDPK1*), glutamate dehydrogenase 2 gene (*GDH2*), calcineurin B-like calcium sensor protein 1 gene (*CBL1*), calnexin 1 gene (*CNX1*), and respiratory burst oxidase homolog A gene (*RbohA*). As shown in **Figure 7**, under AR stress, the expression abundance of most Ca-related genes increased obviously at low Ca level; however, this expression trend can be reversed at high Ca level.

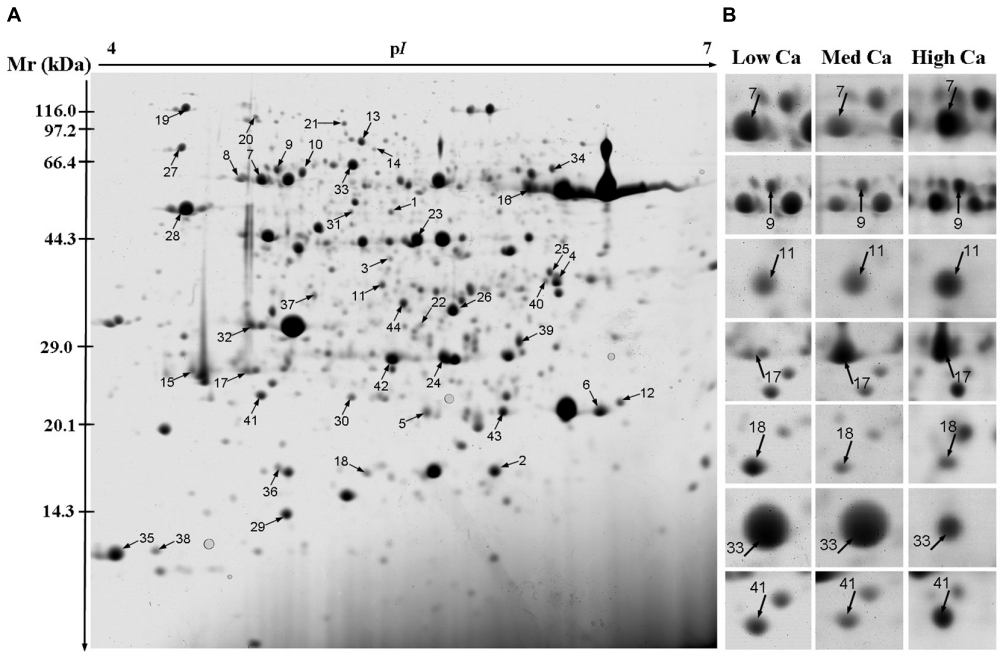

FIGURE 3 | Two-dimensional electrophoresis analysis of proteins extracted from the leaves of *T. wallichiana* var. *mairei* treated at different Ca levels under AR stress. The numbers are assigned to the protein spots correspond to those listed in **Table 1**. **(A)** Representative CBB R250-stained 2D gel of total proteins. Arrows indicate 44 spots showing at least twofold changes ($p < 0.05$) analyzed by MALDI-TOF/TOF MS. **(B)** The enlarged window represents some differentially expressed protein spots after AR treatment at different Ca levels.

DISCUSSION

Metabolic Process, Protein Modification, and Degradation-Related Proteins

The environmental stresses severely affect the material metabolism of plants (Liu et al., 2011a; Chen et al., 2014). UDP-glucose pyrophosphorylase is the precursor of carbohydrate formation (Chen et al., 2019). Our results showed that Ca application reduced AR-induced increases in protein abundance of UDP-glucose pyrophosphorylase (spot 2) in *T. wallichiana* var. *mairei* (**Table 1**). Under AR stress, our previous study indicates that high Ca level enhances the carbohydrate metabolism in *L*iquidambar *formosana* (Hu et al., 2016). It has been showed that woody plants against environmental stresses with a complex manner, which results in similar protein expressions (Hu et al., 2014c; Liu Y. et al., 2019). In this study, our finding is consistent with the results from the study of how exogenous Ca affects other woody plants to AR stress. These results showed that Ca application helps in alleviating the adverse effects of AR stress by accelerating the carbohydrate metabolism. On the other hand, Chen et al. (2019) found that UDP-glucose pyrophosphorylase plays an important role in cell wall metabolism and the synthesis of cellulase and hemicellulose. Carbohydrates act as a cytoskeleton and compose the cell wall as the first physical barrier defending against all types of AR stress (Liu et al., 2011b). We speculate that the protecting role of Ca can be explained by the upregulated carbohydrate metabolism-related protein under AR stress. S-adenosylmethionine synthase catalyzes the formation of S-adenosylmethionine from methionine and ATP, which is the critical enzymes in ethylene biosynthetic process (Peleman et al., 1989; Wang et al., 2002). In this study, protein abundances of S-adenosylmethionine synthase (spot 4) increased after low Ca treatment (**Figure 5**), which indicates that Ca-mediated ethylene biosynthetic process might make effect in AR tolerance in *T. wallichiana* var. *mairei*. Additionally, the abundance of S-adenosylmethionine synthase increases in high Ca-AR-treated *L. formosana* (Hu et al., 2016). These findings indicate that exogenous Ca plays different roles in AR-resistant tree species (*T. wallichiana* var. *mairei*) and AR-sensitive tree species (*L. formosana* and *P. massoniana*) in response to AR stress. Further study is needed to clarify the different metabolic processes at various Ca levels in AR-tolerance woody plants.

Aspartyl aminopeptidase is likely to play an important role in intracellular protein proteolysis and peptide metabolism (Park et al., 2017). In addition, F-box/kelch-repeat protein is involved in the pathway of protein ubiquitination, which is a part of protein modification. F-box/kelch-repeat protein may mediate the ubiquitination and subsequent proteasomal degradation of target proteins (González-Carranza et al., 2007). In this study, our proteomic analysis has detected increased abundance of probable aspartyl aminopeptidase (spot 6) and F-box/kelch-repeat protein (spot 36) at low Ca level in *T. wallichiana* var. *mairei* response to AR stress; however, this expression trend can be reversed at high Ca level (**Table 1**). It should be noted that the previous proteome analysis reveals the significantly elevated abundance of

TABLE 1 | Differentially expressed proteins of *Taxus wallichiana* var. *mairei* in response to AR stress under different calcium levels.

Spot[a]	NCBI accession[b]	Protein identity[c]	Thero. kDa/pI[d]	Exper. kDa/pI[e]	Pep. Count[f]	Score[g]
Metabolic process						
1	gi| 2500930	Cell wall beta-fructosidase 1	62.90/7.07	46.39/5.49	6	94
2	gi| 158705664	UDP-glucose pyrophosphorylase	51.97/5.34	11.69/5.91	6	90
4	gi| 223635315	S-adenosylmethionine synthase	43.61/5.55	25.36/6.17	7	107
5	gi| 77556698	Phytoene synthase	44.99/8.64	15.91/5.67	5	81
Photosynthesis and energy pathway						
7	gi| 138277483	ATP synthase beta subunit	51.67/5.11	62.61/4.99	18	164
8	gi| 138277483	ATP synthase beta subunit	51.67/5.11	63.61/4.90	18	170
9	gi| 4388533	F1-ATP synthase beta subunit	49.22/5.25	67.99/5.04	16	174
10	gi| 226493589	ATP synthase beta chain	59.06/5.90	65.39/5.14	12	125
11	gi| 7592732	Plasma membrane H^+-ATPase	22.04/8.92	31.30/5.47	6	102
12	gi| 372486191	NADH-plastoquinone oxidoreductase subunit 7	46.04/5.78	25.36/6.53	6	81
13	gi| 311893429	ATP-dependent zinc metalloprotease ThFtsH8	73.83/6.33	83.00/5.37	10	108
14	gi| 356517518	ATP-dependent zinc metalloprotease FTSH	74.58/5.93	77.61/5.42	14	134
15	gi| 3293555	Chlorophyll *a/b* binding protein	28.35/5.47	20.90/4.74	6	93
16	gi| 91177512	Ribulose-1,5-bisphosphate carboxylase/oxygenase large subunit	51.99/6.23	25.36/6.04	16	150
17	gi| 224114357	Light-harvesting complex II protein Lhcb1	28.09/5.29	20.55/4.94	7	96
18	gi| 3913651	Ferredoxin-NADP reductase	40.71/8.37	11.75/5.40	6	88
Cell rescue and defense						
19	gi| 255570990	Heat shock protein	75.43/5.35	120.00/4.69	8	92
20	gi| 392465167	Heat shock protein 70	71.46/5.14	107.67/4.97	17	178
21	gi| 357493781	Thioredoxin-related protein	32.06/7.74	98.05/5.30	5	91
22	gi| 110808557	Trypsin inhibitor AeTI	2.24/4.55	25.13/5.63	3	85
23	gi| 153865891	Alcohol dehydrogenase 1	21.73/6.23	39.43/5.60	5	96
24	gi| 327342604	Glutathione S-transferase	25.52/6.34	21.12/5.71	6	96
25	gi| 335346406	Abscisic acid 8-hydroxylase	53.18/8.77	25.36/6.17	7	88
26	gi| 302815799	2-Oxoglutarate-iron(II)-dependent oxygenase	40.96/5.76	26.72/5.75	6	90
Transcription and translation						
27	gi| 14579025	Maturase K	60.80/9.56	85.64/4.67	10	99
28	gi| 56744289	Putative transposon MuDR mudrA-like protein	85.62/8.03	49.90/4.69	9	106
29	gi| 67968326	Ribosomal protein L14	13.07/10.40	10.00/5.10	5	90
30	gi| 62733886	Retrotransposon protein	64.07/7.58	17.28/5.35	7	87
31	gi| 379054892	Initiation factor 4A-3-like protein	43.02/6.30	46.73/5.33	10	123
32	gi| 359494561	Transcription factor JUNGBRUNNEN 1	32.65/6.67	26.35/4.95	6	89
33	gi| 159480324	Mitochondrial transcription termination factor	25.87/9.46	68.05/5.34	6	106
34	gi| 77551510	Transposon protein	81.78/9.17	25.36/6.13	10	112
35	gi| 334183835	Small subunit ribosomal protein S1	56.63/5.06	8.46/4.47	8	96
Protein modification and degradation						
6	gi| 385178691	Probable aspartyl aminopeptidase	54.33/6.36	25.36/6.37	6	88
36	gi| 357469355	F-box/kelch-repeat protein	48.50/6.29	11.99/5.08	7	100
Signal transduction						
3	gi| 269980525	IAA-amino acid hydrolase	47.90/5.95	35.80/5.48	6	96
37	gi| 195627742	Membrane steroid-binding protein 1	10.99/5.35	30.34/5.20	4	84
38	gi| 356516069	2A phosphatase-associated protein of 46 kDa	45.15/5.39	8.59/4.58	11	111
39	gi| 307939386	Lectin	9.86/9.23	25.36/6.02	4	81
40	gi| 356573251	Calcium-binding protein KIC-like	14.00/4.18	25.36/6.13	7	112
Unknown protein						
41	gi| 116782579	Unknown	15.71/6.30	17.74/5.01	4	74
42	gi| 356566253	Uncharacterized protein LOC100799858	38.98/6.01	20.96/5.52	6	98
43	gi| 296087931	Unnamed protein product	79.30/7.32	15.63/5.96	11	106
44	gi| 20198271	Hypothetical protein	13.97/7.88	28.14/5.54	5	91

[a] *Spot is the unique differentially expressed protein spot number.*
[b] *Database accession numbers according to NCBInr.*
[c] *The name of the proteins identified by MALDI-TOF/TOF MS.*
[d] *Theoretical mass (kDa) and pI of identified proteins.*
[e] *Experimental mass (kDa) and pI of identified proteins.*
[f] *Number of the matched peptides.*
[g] *The Mascot searched score against the database NCBInr.*

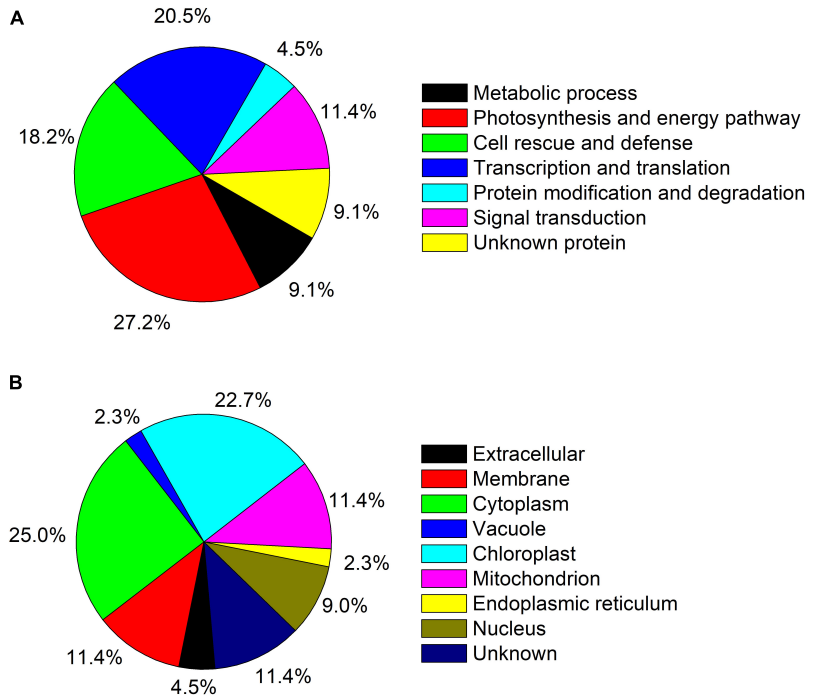

FIGURE 4 | (A) Functional category distribution of the identified proteins in AR-treated *T. wallichiana* var. *mairei* at low, medium, and high Ca levels. **(B)** Protein subcellular locations of all 44 identified and quantified proteins in AR-treated *T. wallichiana* var. *mairei* at low, medium, and high Ca levels.

F-box family protein in AR-treated woody plant, which suggests that AR stress affects the biosynthesis and refolding of proteins and exacerbated protein degradation (Chen et al., 2014; Hu et al., 2014a). The findings provide informative clues regarding the protein modification and degradation mechanisms for the negative regulation of exogenous Ca level during *T. wallichiana* var. *mairei* response to AR stress. It is reasonable to speculate that AR stress leads to more serious protein degradation in low Ca condition, and high expression of degraded proteins system needs to be activated to maintain the stability of the protein metabolism in *T. wallichiana* var. *mairei*; high Ca condition has effective protection mechanism, low expression, or without degradation of protein fragments damaged by AR stress. AR stress can damage the homeostasis of protein metabolism between biosynthesis and degradation (Hu et al., 2014a). Most of these proteins play important roles in linking change of Ca concentration and the subsequent metabolic adaptation to AR stress in woody plants (Hu et al., 2014c, 2016), but the specific details of the mechanism need to be further studied in the future.

Photosynthesis and Energy Pathway-Related Proteins

Photosynthesis is a key metabolic process of woody plants, which is sensitive to AR stress (Liu et al., 2011a; Chen et al., 2013). In addition, our previous studies found that photosynthesis is greatly affected by simulated AR stress under low Ca level (Hu et al., 2014c, 2016). In this study, physiological analysis found that the photosynthesis is inhibited with low Ca-AR treatment, but significantly increased with high Ca-AR treatment in *T. wallichiana* var. *mairei* leaves (**Figure 1C**). Consistent with the results of physiological data, our proteomic data analysis showed that high Ca level can remarkably improve photosynthetic capacity of *T. wallichiana* var. *mairei* with AR treatment. For instance, we found that chlorophyll *a*/*b*-binding protein (spot 15), ribulose-1,5-bisphosphate carboxylase–oxygenase large subunit (spot 16), light-harvesting complex II protein Lhcb1 (spot 17), and ferredoxin-NADP reductase (spot 18) were decreased in protein expression abundance with low Ca-AR treatment and increased with high Ca-AR treatment in *T. wallichiana* var. *mairei* (**Table 1**). These results indicated that high Ca level could restore the impaired photosynthetic function in AR-treated *T. wallichiana* var. *mairei* seedlings.

The protective role of exogenous Ca may lie in the increased upregulation of photosynthesis and energy pathway, which enhances AR tolerance in *T. wallichiana* var. *mairei*. This inference is supported by our previous studies, in which we demonstrated that exogenous Ca supply improved photosynthesis in woody plants against AR stress (Hu et al., 2014c, 2016).

On the other hand, sufficient ATP is necessary for *T. wallichiana* var. *mairei* responding to AR stress in plants. ATP synthase and ATPase are the key enzymes in energy production and conversion (Liu et al., 2011b; Hu et al., 2014a). Previous evidence indicates that enough ATP is necessary for plants in response to environmental stress (Jiang et al., 2007). Our results found that a large number of enzymes were involved in this process that include ATP synthase beta subunit

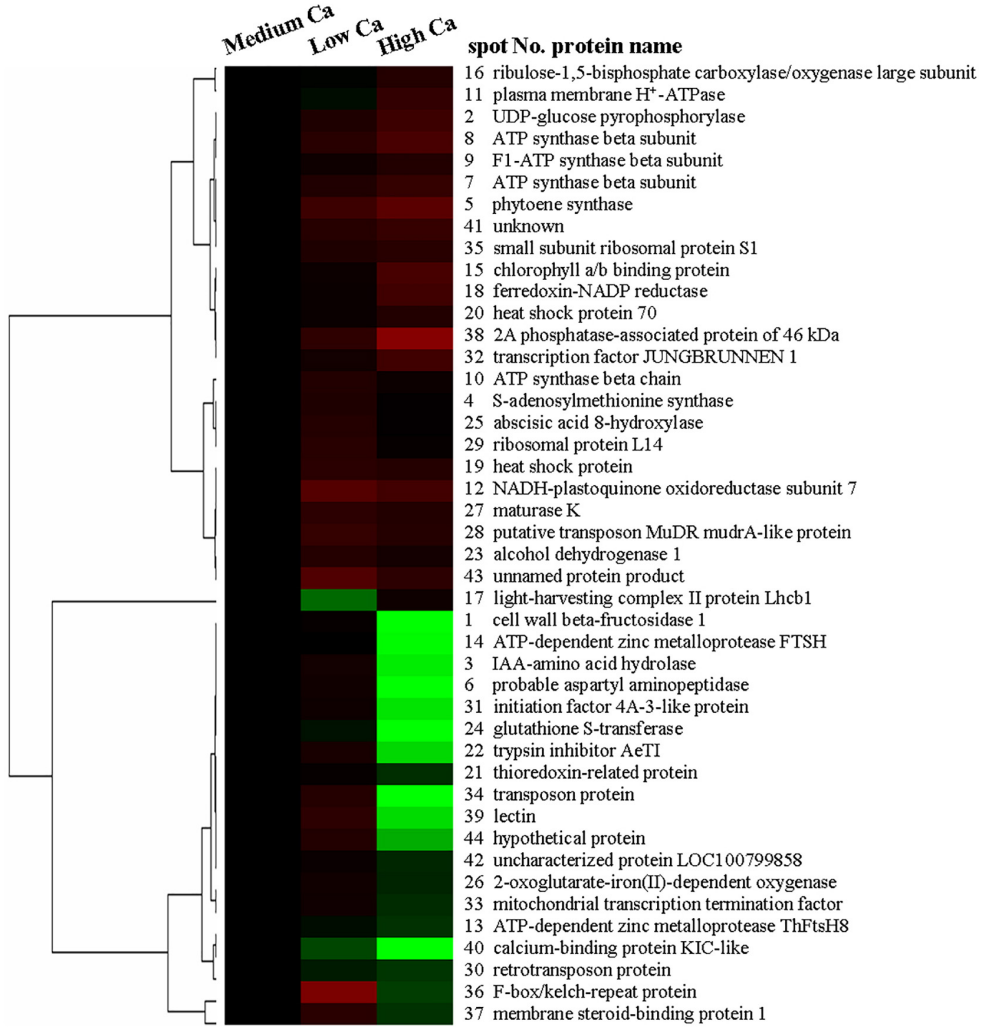

FIGURE 5 | Hierarchical clustering analyses of the 44 AR-responsive proteins expression profiles at different Ca levels in *T. wallichiana* var. *mairei*.

(spots 7, 8), F1-ATP synthase beta subunit (spot 9), and ATP synthase beta chain (spot 10). Our previous studies found that AR-sensitive tree species (*L. formosana* and *P. massoniana*) have the increased abundance of energy production-related proteins with high Ca-AR treatment (Hu et al., 2014c, 2016). In this study, we also find a similar pattern in *T. wallichiana* var. *mairei*. Additionally, western blot analysis showed that relative abundance levels of the Rubisco LSU and ATPase were increased with high Ca treatment (**Figure 6**), and western blot result is consistent with the selected protein of our proteomic data at various Ca levels in AR-treated *T. wallichiana* var. *mairei*. Besides, as a membrane-bound protein located in thylakoids, ATP-dependent zinc metalloprotease-related proteins involve in the removal of a damaged D1 protein from PSII in plants (Hu et al., 2014a). Expression abundance of ATP-dependent zinc metalloprotease ThFtsH8 (spot 13) and ATP-dependent zinc metalloprotease FTSH (spot 14) was downregulated in high Ca-AR-treated *T. wallichiana* var. *mairei*. This change meant that less damaged protein is produced in high Ca condition, by which we furthermore find that the recovered photosynthesis decline caused by AR stress. Moreover, H^+-ATPase plays an important role in the maintenance of ion homeostasis and nutrient uptake in plants (Liu et al., 2011b; Chen et al., 2019). Our study also showed that plasma membrane H^+-ATPase (spot 11) was upregulated by high Ca level with AR treatment. Based on these results, high Ca condition may stimulate the resistance of *T. wallichiana* var. *mairei* to AR stress by modulating special energy-related pathway. These findings indicate that with high Ca-AR treatment, the mechanisms of energy pathway in AR-resistant tree species (*T. wallichiana* var. *mairei*) are different from AR-sensitive tree species (*L. formosana* and *P. massoniana*). Further investigations are needed to clarify the different energy pathways in AR-tolerance woody plants.

Cell Rescue and Defense-Related Proteins

Acid rain stress has negative effects on plant growth and development, and also the internal functional components. Low

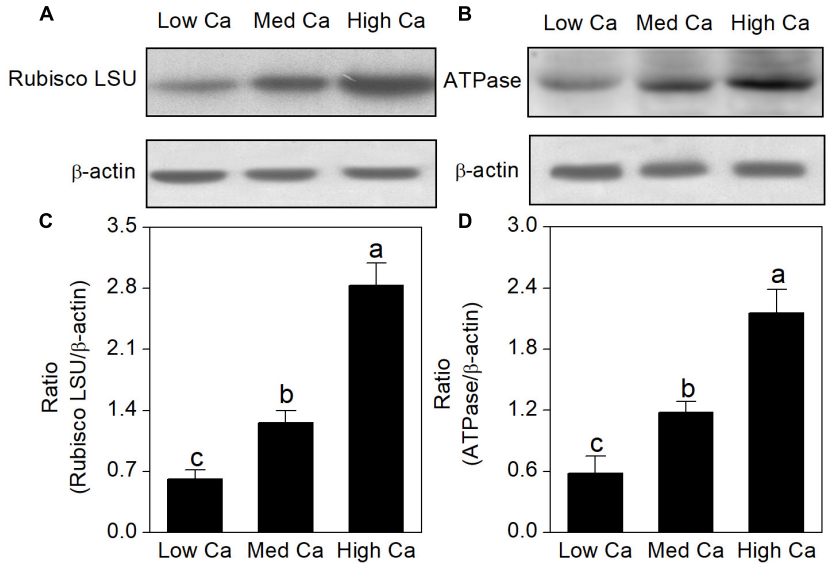

FIGURE 6 | Effects of different Ca levels on rubulose-1, 5-bisphoshate carboxylase–oxygenase large subunit (Rubisco LSU) **(A)**, ATP synthase (ATPase) **(B)** in *T. wallichiana* var. *mairei* under AR stress using western blot. Relative expression levels of Rubisco LSU **(C)** and ATPase **(D)** were analyzed with the Quantity One software. β-Actin was used as the internal control. Bars with different letters are significantly different from each other ($p < 0.05$).

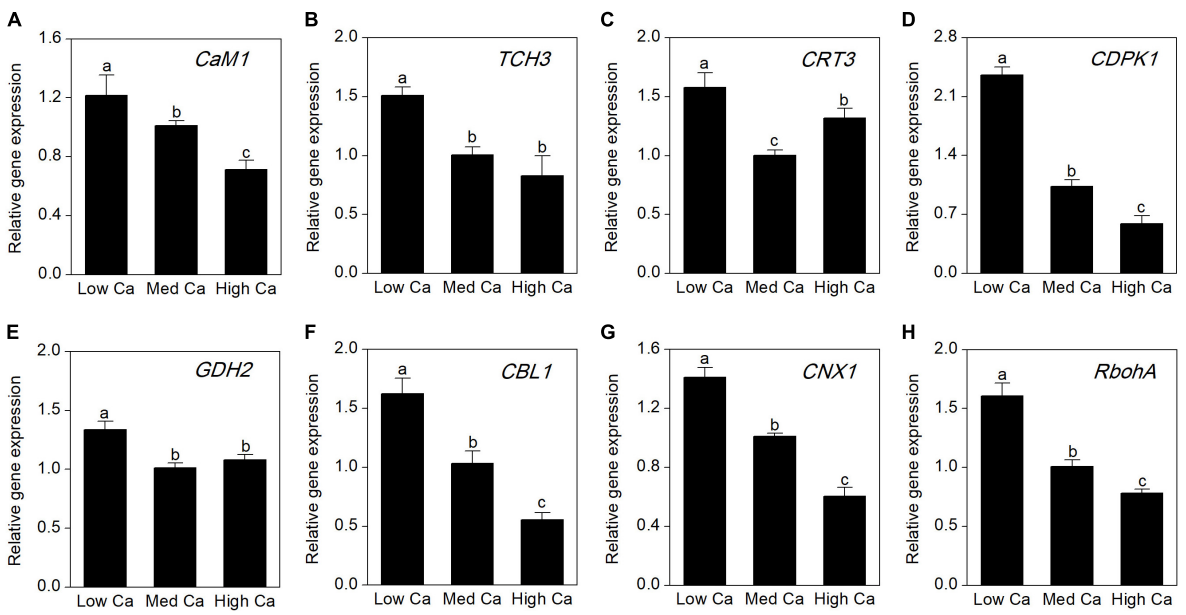

FIGURE 7 | Expression analysis by qRT-PCR of eight Ca-related genes in *T. wallichiana* var. *mairei* treated at different Ca levels under AR stress. **(A)** Calmodulin 1 (*CaM1*), **(B)** touch 3 gene (*TCH3*), **(C)** calreticulin 3 gene (*CRT3*), **(D)** calcium-dependent protein kinase 1 (*CDPK1*), **(E)** glutamate dehydrogenase 2 gene (*GDH2*), **(F)** calcineurin B-like calcium sensor protein 1 gene (*CBL1*), **(G)** calnexin 1 gene (*CNX1*), **(H)** respiratory burst oxidase homolog A gene (*RbohA*). Bars represent the mean value ± SE ($n = 3$). Bars with different letters are significantly different from each other ($p < 0.05$).

Ca-AR treatment increased the content of MDA and reactive oxygen radicals [reactive oxygen species (ROS), e.g., H_2O_2 and $O2^{\bullet-}$], which suggests the ROS enrichment in *T. wallichiana* var. *mairei*; however, high Ca supplementation can reverse these effects (**Figure 2**). In addition, we observed that soluble protein content, proline content, SOD, APX, POD, and CAT activity showed a significant increase in *T. wallichiana* var. *mairei* leaves with high Ca treatment, which implies that antioxidant defense system was provoked by high Ca supplementation in AR-treated *T. wallichiana* var. *mairei*. These changes of physiological and biochemical findings indicated the protective role in exogenous Ca being against AR stress in *T. wallichiana* var. *mairei*.

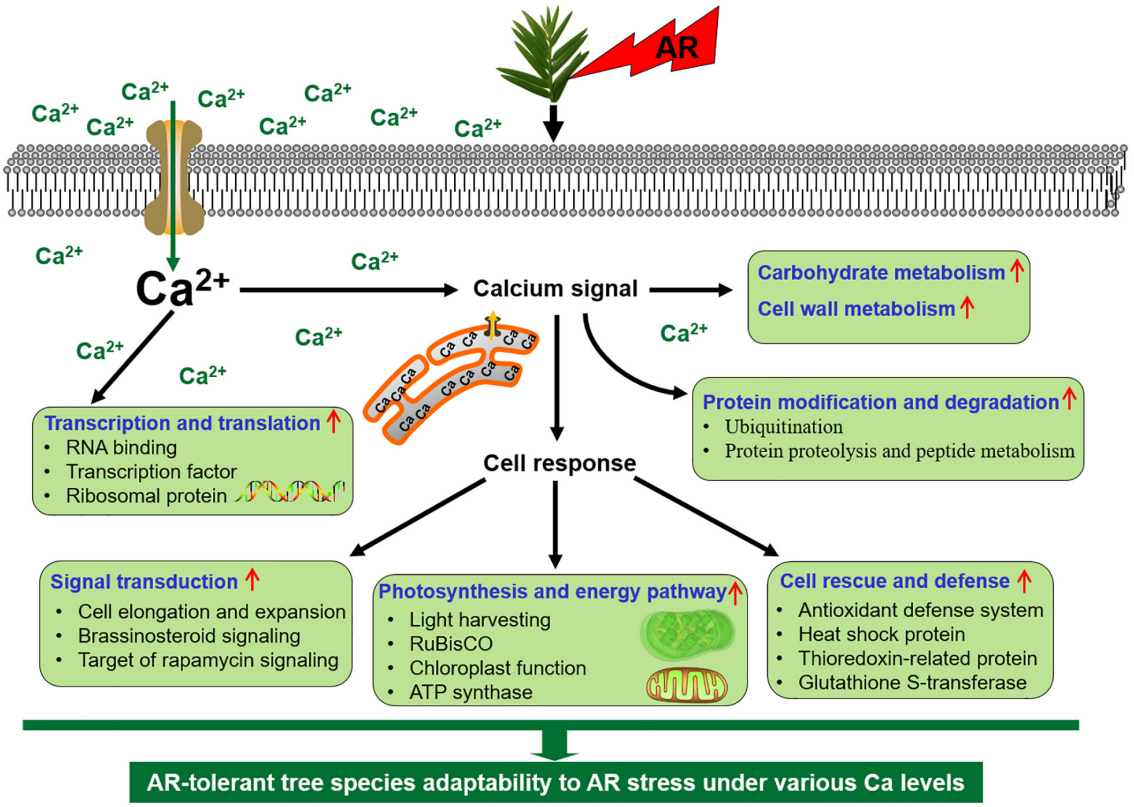

FIGURE 8 | An adaptive strategy of *T. wallichiana* var. *mairei* leaves response to AR stress under different Ca levels.

To further reveal the different strategies to cope with AR stress at various Ca levels, many cell rescue and defense-related proteins were also identified by proteomic analysis in this study. As stress response proteins and heat shock proteins can be induced by many abiotic stresses (Wang et al., 2004, 2013), our study showed that exogenous Ca addition enhanced the abundance of heat shock protein (spot 19) and heat shock protein 70 (spot 20). Additionally, heat shock proteins are also considered as an important part in stabilizing protein folding and play important roles in the cellular stress response (Chen et al., 2019). The increased abundance of the heat shock-related proteins in high Ca-AR treatment set indicated the multidimensional role of external Ca supply in the alleviation of AR stress in *T. wallichiana* var. *mairei*.

In this study, decreased expressions of thioredoxin-related protein (spot 21) and glutathione S-transferase (spot 24) were also observed at high Ca levels. It was reported that thioredoxin can reduce intramolecular disulfide bridges of target proteins, maintain suppression of apoptosis, and supply reducing equivalents to the antioxidant systems (Tada et al., 2008; Liu et al., 2011b). Under both low and high Ca levels, elevated abundance of thioredoxin superfamily protein was described in *L. formosana* seedlings in response to AR stress (Hu et al., 2016). In addition, glutathione S-transferases are associated with stress tolerance, which can catalyze the addition of glutathione to electrophilic compounds and resist various cellular damages (Frova, 2003; Aloui et al., 2009). Previous studies reported the enhanced expressions of glutathione S-transferase in *Arabidopsis* response to AR stress and low Ca-AR-treated *P. massoniana* seedlings (Hu et al., 2014c, 2016). As an antioxidative protein, glutathione S-transferase can be strongly induced by biotic and abiotic stresses (Dixon et al., 2002). In this study, downregulation of these proteins indicates that high Ca level has the potential to protect *T. wallichiana* var. *mairei* from oxidative stress caused by AR stress, which suggests that AR-resistant tree species has developed different defense strategies against AR stress under high Ca condition.

Transcription and Translation-Related Proteins

Transcription and translation regulate the expression level of stress responsive genes, which are important for plants response to environmental stresses (Jiang et al., 2007; Chen et al., 2014; Hu et al., 2014c). In this study, we have successfully identified nine proteins related to transcription and translation. In plants, maturase K catalyzes intron RNA binding and affects gene expression at the transcriptional level (Ji et al., 2009). The expression level of maturase K is complex in plants response to abiotic stress, which depends on plant species and the type of environmental stresses (Pandey et al., 2008; Chen et al., 2014).

In this study, the abundance of maturase K (spot 27) increases in both low Ca-AR and high Ca-AR-treated *T. wallichiana* var. *mairei*, which suggests that expression changes in maturase K may play a part in linking change of Ca level under AR stress. Moreover, Chen et al. (2019) showed that a transcription factor displayed an elevated expression pattern in Arabidopsis of exogenous Ca-alleviated Al toxicity. We also found that exogenous high Ca enhances the abundance of transcription factor JUNGBRUNNEN 1 (spot 32) in *T. wallichiana* var. *mairei.* In addition, Hu et al. (2016) found that an increase in ribosomal protein S1 was detected in high Ca-AR-treated woody plant. Consistent with previous research, protein synthesis machinery was also affected by high Ca treatment as increased expression level of ribosomal protein L14 (spot 29) and small subunit ribosomal protein S1 (spot 35) has been detected in *T. wallichiana* var. *mairei* under AR stress. Transcription and translation control the expression of stress responsive genes, which play crucial roles in plants in response to various abiotic stresses (Amme et al., 2006). We detected increased abundance of series transcription and translation-related proteins in *T. wallichiana* var. *mairei* under high Ca-AR treatment, and the results indicated that Ca-regulated transcription and translation mediate *T. wallichiana* var. *mairei* adaptation to AR stress. The complex AR-responsive signaling pathways are associated with stress sensing and activation of defense pathways, which involves in calcium-regulated proteins crosstalk among various transcription factors. Under AR stress, future work on these transcription and translation-related proteins are needed to clarify the specific functions in various Ca conditions.

Signal Transduction-Related Proteins

Under environmental stresses, woody plants initiate multiple signaling pathways through sensing and transducting several stress signals, further regulate the expression level of many functional proteins, and finally exhibit corresponding physiological response to against the abiotic stresses (Hu et al., 2014a; Liu Y. et al., 2019). Membrane steroid-binding protein 1 (MSBP1) can bind steroids and negatively regulates cell elongation and expansion, and also photomorphogenesis and brassinosteroid signaling (Yang et al., 2005; Song et al., 2009; Shi et al., 2011). In this study, we found that the abundance of membrane steroid-binding protein 1 (spot 37) was significantly increased at low Ca level; however, it can reverse the increased abundance of MSBP1 in *T. wallichiana* var. *mairei* at high Ca level, which provides informative hints on interactions between Ca and membrane steroid-binding protein. This finding suggested the specific relationship between Ca and steroid-binding protein in the BR signaling pathway. Protein phosphatase 2A plays an important role in plant development and growth through a functional link with the target of rapamycin (TOR) signaling pathway (Ahn et al., 2015). The TOR signaling pathway integrates multiple signals transduction, such as energy, nutrients, growth factors, and environmental conditions, to regulate plant cell metabolism and growth (Wullschleger et al., 2006; Xiong et al., 2013). We found that the expression level of 2A phosphatase-associated protein of 46 kDa (spot 38) was significantly upregulated in *T. wallichiana* var. *mairei* with high Ca-AR treatment. On the other hand, it should be noted that the abundance of 2A phosphatase-associated protein of 46 kDa was decreased in *P. massoniana* under high Ca-AR treatment (Hu et al., 2014c), which suggests that 2A phosphatase-associated protein of 46 kDa could play a specific role in woody plants response to AR stress. These results implied the different expression patterns and coping response strategies between AR-sensitive (*P. massoniana*) and AR-resistant (*T. wallichiana* var. *mairei*) tree species under high Ca condition; however, further studies are needed to elucidate the specific function of the signal transduction-related proteins in AR-stressed tree species.

Moreover, Ca plays an important role in plants coping with a series of environmental stresses (Reddy et al., 2011). In the cytoplasm, free cytosolic Ca^{2+} level is a universal second messenger of signal transduction in plants in response to environmental stresses (Kudla et al., 2018). Ca-binding-related proteins regulated modulation of intracellular Ca^{2+} levels (Hu et al., 2014a, 2016). In this study, expression level of calcium-binding protein KIC-like (spot 40) showed declines in *T. wallichiana* var. *mairei* with high Ca-AR treatment. It has been observed that Ca-binding proteins are regarded as crosstalk key nodes for environmental stress signaling pathways (Hepler, 2005; Liu Y. et al., 2019). These findings suggest that calcium-binding proteins participate in adaptation responses to AR stress in *T. wallichiana* var. *mairei*, which provides informative hints on interactions between Ca-associated signal transduction and AR tolerance. In **Figure 7**, our result provided additional evidence that the expression abundance of eight Ca-related genes (CaM1, TCH3, CRT3, CDPK1, GDH2, CBL1, CNX1, and RbohA) increased obviously at low Ca level, whereas this expression trend can be reversed at high Ca level under AR stress. Plants respond to environmental stresses through altering gene expression and adaptive responses associated with stress sensing and activation of defense pathways, such as expression of stress adaptive proteins, synthesis of oxidative stress protectors, calcium-regulated proteins, and signal pathway (Hasegawa et al., 2000; Hu et al., 2014a). In this study, these findings indicate that Ca-dependent signal transduction could induce upregulated expression of Ca-related genes and further interact with various biological processes to against AR stress in *T. wallichiana* var. *mairei*.

CONCLUSION

In this study, physiological and proteomic evidence is carried out to clarify that Ca plays an important role in AR-resistant tree species *T. wallichiana* var. *mairei* response to simulated AR treatment. Our data reveal that low Ca treatment activated the cell rescue- and defense-related proteins and Ca-related gene level to respond to AR stress in *T. wallichiana* var. *mairei*. These proteins might operate in a dynamic network in the response of AR-resistant tree species under AR stress, and these identified proteins might be useful in revealing insights into the different defense mechanisms of AR-resistant tree species to AR stress. In addition, exogenous Ca supply against AR stress by increasing the

abundance of the proteins involved in photosynthesis and energy pathway, translational factors, which suggest that AR-tolerant woody plants can equip themselves better to respond to AR stress by provoking related proteins and gene expression. As shown in **Figure 8**, we proposed a scheme associated with different defense mechanisms of *T. wallichiana* var. *mairei* responding to AR damage at different Ca levels. These results would deepen insights into the adaptation strategies of AR-resistant tree species under AR stress at different Ca levels and furthermore provide theoretical support for the scientific prevention of AR stress.

DATA AVAILABILITY STATEMENT

The original contributions presented for this study are included in the article/supplementary material. For details, please refer to **Supplementary Table S3** and **Supplementary Datasheet**.

AUTHOR CONTRIBUTIONS

H-LZ, W-JH, and G-XS: conceptualization and funding acquisition. W-JH and QW: methodology. T-WL: software and visualization. C-KJ: validation. JW: formal analysis. QW and H-LL: investigation. LC: resources. C-QZ: data curation. W-JH and C-QZ: writing – original draft preparation. H-LZ and G-XS: writing, reviewing, and editing, and project administration. H-LZ: supervision. All authors have read and agreed to the published version of the manuscript.

FUNDING

This research was funded by the Key Research and Development Program of Zhejiang Province (No. 2021C02002), the Key Technologies R&D Program for Crop Breeding of Zhejiang Province (No. 2021C02072-6), the National Natural Science Foundation of China (Nos. 32001104, 31870581, 32171740, and 30930076), the Open Project of State Key Laboratory of Rice Biology of China (No. 20190402), and the Project of Science and Technology Program of Quzhou (No. 2021K34).

SUPPLEMENTARY MATERIAL

The Supplementary Material for this article can be found online at: https://www.frontiersin.org/articles/10.3389/fpls.2022.845107/full#supplementary-material

REFERENCES

Ahn, C. S., Ahn, H.-K., and Pai, H.-S. (2015). Overexpression of the PP2A regulatory subunit Tap46 leads to enhanced plant growth through stimulation of the TOR signalling pathway. *J. Exp. Bot.* 66, 827–840. doi: 10.1093/jxb/eru438

Aloui, A., Recorbet, G., Gollotte, A., Robert, F., Valot, B., Gianinazzi-Pearson, V., et al. (2009). On the mechanisms of cadmium stress alleviation in *Medicago truncatula* by arbuscular mycorrhizal symbiosis: a root proteomic study. *Proteomics* 9, 420–433. doi: 10.1002/pmic.200800336

Amme, S., Matros, A., Schlesier, B., and Mock, H. P. (2006). Proteome analysis of cold stress response in *Arabidopsis thaliana* using DIGE-technology. *J. Exp. Bot.* 57, 1537–1546. doi: 10.1093/jxb/erj129

Chen, J., Duan, R.-X., Hu, W.-J., Zhang, N.-N., Lin, X.-Y., Zhang, J.-H., et al. (2019). Unravelling calcium-alleviated aluminium toxicity in *Arabidopsis thaliana*: insights into regulatory mechanisms using proteomics. *J. Proteomics* 199, 15–30. doi: 10.1016/j.jprot.2019.02.013

Chen, J., Hu, W.-J., Wang, C., Liu, T.-W., Chalifour, A., Chen, J., et al. (2014). Proteomic analysis reveals differences in tolerance to acid rain in two broad-leaf tree species, *Liquidambar formosana* and *Schima superba*. *PLoS One* 9:e102532. doi: 10.1371/journal.pone.0102532

Chen, J., Wang, W.-H., Liu, T.-W., Wu, F.-H., and Zheng, H.-L. (2013). Photosynthetic and antioxidant responses of *Liquidambar formosana* and *Schima superba* seedlings to sulfuric-rich and nitric-rich simulated acid rain. *Plant Physiol. Biochem.* 64, 41–51. doi: 10.1016/j.plaphy.2012.12.012

Cheng, J., Wang, X., Liu, X., Zhu, X., Li, Z., Chu, H., et al. (2021). Chromosome-level genome of Himalayan yew provides insights into the origin and evolution of the paclitaxel biosynthetic pathway. *Mol. Plant* 14, 1199–1209. doi: 10.1016/j.molp.2021.04.015

Debnath, B., and Ahammed, G. J. (2020). "Effect of acid rain on plant growth and development: physiological and molecular interventions," in *Contaminants in Agriculture*, eds M. Naeem, A. Ansari, and S. Gill (Berlin: Springer), 103–114.

Debnath, B., Li, M., Liu, S., Pan, T., Ma, C., and Qiu, D. (2020). Melatonin-mediate acid rain stress tolerance mechanism through alteration of transcriptional factors and secondary metabolites gene expression in tomato. *Ecotox. Environ. Saf.* 200:110720. doi: 10.1016/j.ecoenv.2020.110720

Debnath, B., Sikdar, A., Islam, S., Hasan, K., Li, M., and Qiu, D. (2021). Physiological and molecular responses to acid rain stress in plants and the impact of melatonin, glutathione and silicon in the amendment of plant acid rain stress. *Molecules* 26:862. doi: 10.3390/molecules26040862

Dixon, D. P., Lapthorn, A., and Edwards, R. (2002). Plant glutathione transferases. *Genome Biol.* 3:REVIEWS3004.

Frova, C. (2003). The plant glutathione transferase gene family: genomic structure, functions, expression and evolution. *Physiol. Plant.* 119, 469–479. doi: 10.1046/j.1399-3054.2003.00183.x

Gao, L., Möller, M., Zhang, X. M., Hollingsworth, M., Liu, J., Mill, R., et al. (2007). High variation and strong phylogeographic pattern among cpDNA haplotypes in *Taxus wallichiana* (Taxaceae) in China and North Vietnam. *Mol. Ecol.* 16, 4684–4698. doi: 10.1111/j.1365-294X.2007.03537.x

González-Carranza, Z. H., Rompa, U., Peters, J. L., Bhatt, A. M., Wagstaff, C., Stead, A. D., et al. (2007). HAWAIIAN skirt: an F-box gene that regulates organ fusion and growth in Arabidopsis. *Plant Physiol.* 144, 1370–1382. doi: 10.1104/pp.106.092288

Grennfelt, P., Engleryd, A., Forsius, M., Hov, O., Rodhe, H., and Cowling, E. (2020). Acid rain and air pollution: 50 years of progress in environmental science and policy. *Ambio* 49, 849–864. doi: 10.1007/s13280-019-01244-4

Hasegawa, P. M., Bressan, R. A., Zhu, J. K., and Bohnert, H. J. (2000). Plant cellular and molecular responses to high salinity. *Annu. Rev. Plant Biol.* 51, 463–499. doi: 10.1146/annurev.arplant.51.1.463

Hepler, P. K. (2005). Calcium: a central regulator of plant growth and development. *Plant Cell* 17, 2142–2155. doi: 10.1105/tpc.105.032508

Hu, H., Hua, W., Shen, A., Zhou, H., Sheng, L., Lou, W., et al. (2021). Photosynthetic rate and chlorophyll fluorescence of barley exposed to simulated acid rain. *Environ. Sci. Pollut. R.* 28, 42776–42786. doi: 10.1007/s11356-021-13807-8

Hu, W. J., Chen, J., Liu, T. W., Simon, M., Wang, W. H., Chen, J., et al. (2014a). Comparative proteomic analysis of differential responses of *Pinus massoniana* and *Taxus wallichiana* var. *mairei* to simulated acid rain. *Int. J. Mol. Sci.* 15, 4333–4355. doi: 10.3390/ijms15034333

Hu, W. J., Chen, J., Liu, T. W., Wu, Q., Wang, W. H., Liu, X., et al. (2014c). Proteome and calcium-related gene expression in *Pinus massoniana* leaves in response to acid rain under different calcium levels. *Plant Soil* 380, 285–303. doi: 10.1007/s11104-014-2086-9

Hu, W. J., Chen, J., Liu, T. W., Liu, X., Wu, F. H., Wang, W. H., et al. (2014b). Comparative proteomic analysis on wild type and nitric oxide-overproducing mutant (*nox1*) of *Arabidopsis thaliana*. *Nitric Oxide* 36, 19–30. doi: 10.1016/j.niox.2013.10.008

Hu, W. J., Wu, Q., Liu, X., Shen, Z., Chen, J., Liu, T., et al. (2016). Comparative proteomic analysis reveals the effects of exogenous calcium against acid rain stress in *Liquidambar formosana* Hance leaves. *J. Proteome Res.* 15, 216–228. doi: 10.1021/acs.jproteome.5b00771

Huang, J., Wang, H., Zhong, Y., Huang, J., Fu, X., Wang, L., et al. (2019). Growth and physiological response of an endangered tree, *Horsfieldia hainanensis* merr., to simulated sulfuric and nitric acid rain in southern China. *Plant Physiol. Biochem.* 144, 118–126. doi: 10.1016/j.plaphy.2019.09.029

Ji, X. L., Gai, Y. P., Zheng, C. C., and Mu, Z. M. (2009). Comparative proteomic analysis provides new insights into mulberry dwarf responses in mulberry (*Morus alba* L.). *Proteomics* 9, 5328–5339. doi: 10.1002/pmic.200900012

Jiang, Y., Yang, B., Harris, N. S., and Deyholos, M. K. (2007). Comparative proteomic analysis of NaCl stress-responsive proteins in Arabidopsis roots. *J. Exp. Bot.* 58, 3591–3607. doi: 10.1093/jxb/erm207

Juice, S. M., Fahey, T. J., Siccama, T. G., Driscoll, C. T., Denny, E. G., Eagar, C., et al. (2006). Response of sugar maple to calcium addition to northern hardwood forest. *Ecology* 87, 1267–1280. doi: 10.1890/0012-9658(2006)87[1267:rosmtc]2.0.co;2

Kudla, J., Becker, D., Grill, E., Hedrich, R., Hippler, M., Kummer, U., et al. (2018). Advances and current challenges in calcium signaling. *New Phytol.* 218, 414–431. doi: 10.1111/nph.14966

Larssen, T., Lydersen, E., Tang, D., He, Y., Gao, J., Liu, H., et al. (2006). Acid rain in China. *Environ. Sci. Technol.* 40, 418–425.

Lee, Y., Park, J., Im, K., Kim, K., Lee, J., Lee, K., et al. (2006). Arabidopsis leaf necrosis caused by simulated acid rain is related to the salicylic acid signaling pathway. *Plant Physiol. Biochem.* 44, 38–42. doi: 10.1016/j.plaphy.2006.01.003

Likens, G. E., Driscoll, C. T., and Buso, D. C. (1996). Long-term effects of acid rain: response and recovery of a forest ecosystem. *Science* 272, 244–245. doi: 10.1016/j.scitotenv.2021.149626

Liu, J. X., Zhou, G. Y., and Zhang, D. Q. (2007). Effects of acidic solutions on element dynamics in monsoon evergreen broad-leaved forest at Dinghushan, China. *Environ. Sci. Pollut. R.* 14, 123–129. doi: 10.1065/espr2006.07.325

Liu, J., and Diamond, J. (2005). China's environment in a globalizing world. *Nature* 435, 1179–1186. doi: 10.1038/4351179a

Liu, J., Yang, C., and Wang, M. (2012). Effect of simulated acid rain on physiological characteristics in *Taxus chinensis* var. *Mairei. Chinese J. Trop. Crop.* 33, 1046–1050.

Liu, K., Yu, F., Peng, S., Fang, Y., and Li, F. (2007). Effects of simulated acid on saplings of Taxus species. *Ecol. Env.* 16, 309–312.

Liu, M., Huang, X., Song, Y., Tang, J., Cao, J., Zhang, X., et al. (2019). Ammonia emission control in China would mitigate haze pollution and nitrogen deposition, but worsen acid rain. *Proc. Natl. Acad. Sci. U. S. A.* 116, 7760–7765. doi: 10.1073/pnas.1814880116

Liu, T. W., Wu, F. H., Wang, W. H., Chen, J., Li, Z. J., Dong, X. J., et al. (2011c). Effects of calcium on seed germination, seedling growth and photosynthesis of six forest tree species under simulated acid rain. *Tree Physiol.* 31, 402–413. doi: 10.1093/treephys/tpr019

Liu, T. W., Fu, B., Niu, L., Chen, J., Wang, W.-H., He, J.-X., et al. (2011a). Comparative proteomic analysis of proteins in response to simulated acid rain in Arabidopsis. *J. Proteome Res.* 10, 2579–2589. doi: 10.1021/pr200056a

Liu, T. W., Jiang, X., Shi, W., Chen, J., Pei, Z., and Zheng, H. (2011b). Comparative proteomic analysis of differentially expressed proteins in β-aminobutyric acid enhanced *Arabidopsis thaliana* tolerance to simulated acid rain. *Proteomics* 11, 2079–2094. doi: 10.1002/pmic.201000307

Liu, Y., Ji, D., Turgeon, R., Chen, J., Lin, T., Huang, J., et al. (2019). Physiological and proteomic responses of Mulberry Trees (*Morus alba*. L.) to combined salt and drought stress. *Int. J. Mol. Sci.* 20:2486. doi: 10.3390/ijms20102486

Ma, Y., Ren, X., and Liang, C. (2021). Exogenous Ca^{2+} enhances antioxidant defense in rice to simulated acid rain by regulating ascorbate peroxidase and glutathione reductase. *Planta* 254, 1–16. doi: 10.1007/s00425-021-03679-0

Malakoff, D. (2010). Taking the sting out of acid rain. *Science* 330, 910–911. doi: 10.1126/science.330.6006.910

Pandey, A., Chakraborty, S., Datta, A., and Chakraborty, N. (2008). Proteomics approach to identify dehydration responsive nuclear proteins from chickpea (*Cicer arietinum* L.). *Mol. Cell Proteomics* 7, 88–107. doi: 10.1074/mcp.M700314-MCP200

Park, S. Y., Scranton, M. A., Stajich, J. E., Yee, A., and Walling, L. L. (2017). Chlorophyte aspartyl aminopeptidases: ancient origins, expanded families, new locations, and secondary functions. *PLoS One* 12:e0185492. doi: 10.1371/journal.pone.0185492

Peleman, J., Boerjan, W., Engler, G., Seurinck, J., Botterman, J., Alliotte, T., et al. (1989). Strong cellular preference in the expression of a housekeeping gene of *Arabidopsis thaliana* encoding S-adenosylmethionine synthetase. *Plant Cell* 1, 81–93. doi: 10.1105/tpc.1.1.81

Reddy, A. S., Ali, G. S., Celesnik, H., and Day, I. S. (2011). Coping with stresses: roles of calcium-and calcium/calmodulin-regulated gene expression. *Plant Cell* 23, 2010–2032. doi: 10.1105/tpc.111.084988

Reddy, V. S., and Reddy, A. S. (2004). Proteomics of calcium-signaling components in plants. *Phytochemistry* 65, 1745–1776. doi: 10.1016/j.phytochem.2004.04.033

Shi, Q. M., Yang, X., Song, L., and Xue, H. W. (2011). Arabidopsis MSBP1 is activated by HY5 and HYH and is involved in photomorphogenesis and brassinosteroid sensitivity regulation. *Mol. Plant* 4, 1092–1104. doi: 10.1093/mp/ssr049

Shu, X., Zhang, K., Zhang, Q., and Wang, W. (2019). Ecophysiological responses of *Jatropha curcas* L. seedlings to simulated acid rain under different soil types. *Ecotox. Environ. Saf.* 185:109705. doi: 10.1016/j.ecoenv.2019.109705

Song, L., Shi, Q.-M., Yang, X.-H., Xu, Z.-H., and Xue, H.-W. (2009). Membrane steroid-binding protein 1 (MSBP1) negatively regulates brassinosteroid signaling by enhancing the endocytosis of BAK1. *Cell Res.* 19, 864–876. doi: 10.1038/cr.2009.66

Tada, Y., Spoel, S. H., Pajerowska-Mukhtar, K., Mou, Z., Song, J., Wang, C., et al. (2008). Plant immunity requires conformational charges of NPR1 via S-nitrosylation and thioredoxins. *Science* 321, 952–956. doi: 10.1126/science.1156970

Wang, K. L., Li, H., and Ecker, J. R. (2002). Ethylene biosynthesis and signaling networks. *Plant Cell* 14, 131–151. doi: 10.1105/tpc.001768

Wang, W., Vinocur, B., Shoseyov, O., and Altman, A. (2004). Role of plant heat-shock proteins and molecular chaperones in the abiotic stress response. *Trends Plant Sci.* 9, 244–252.

Wang, X., Liu, Z., Niu, L., and Fu, B. (2013). Long-term effects of simulated acid rain stress on a staple forest plant, *Pinus massoniana* Lamb: a proteomic analysis. *Trees* 27, 297–309. doi: 10.1007/s00468-012-0799-z

Wullschleger, S., Loewith, R., and Hall, M. N. (2006). TOR signaling in growth and metabolism. *Cell* 124, 471–484.

Xiong, X., Gou, J., Liao, Q., Li, Y., Zhou, Q., Bi, G., et al. (2021). The Taxus genome provides insights into paclitaxel biosynthesis. *Nat. Plants* 7, 1026–1036. doi: 10.1038/s41477-021-00963-5

Xiong, Y., Mccormack, M., Li, L., Hall, Q., Xiang, C., and Sheen, J. (2013). Glucose–TOR signalling reprograms the transcriptome and activates meristems. *Nature* 496, 181–186. doi: 10.1038/nature12030

Yang, X. H., Xu, Z. H., and Xue, H.-W. (2005). Arabidopsis membrane steroid binding protein 1 is involved in inhibition of cell elongation. *Plant Cell* 17, 116–131. doi: 10.1105/tpc.104.028381

Zhang, C., Yi, X., Gao, X., Wang, M., Shao, C., Lv, Z., et al. (2020). Physiological and biochemical responses of tea seedlings (*Camellia sinensis*) to simulated acid rain conditions. *Ecotox. Environ. Saf.* 192:110315. doi: 10.1016/j.ecoenv.2020.110315

Zhang, H., Zhu, J., Gong, Z., and Zhu, J.-K. (2021). Abiotic stress responses in plants. *Nat. Rev. Genet.* 23, 104–119.

Conflict of Interest: The authors declare that the research was conducted in the absence of any commercial or financial relationships that could be construed as a potential conflict of interest.

Publisher's Note: All claims expressed in this article are solely those of the authors and do not necessarily represent those of their affiliated organizations, or those of the publisher, the editors and the reviewers. Any product that may be evaluated in this article, or claim that may be made by its manufacturer, is not guaranteed or endorsed by the publisher.

frontiers | Frontiers in Plant Science

ORIGINAL RESEARCH
published: 19 May 2022
doi: 10.3389/fpls.2022.877146

Comparative Proteomic Analysis Reveals the Ascorbate Peroxidase-Mediated Plant Resistance to *Verticillium dahliae* in *Gossypium barbadense*

Tianxin Lu[1†], Liping Zhu[1†], Yuxuan Liang[2,3], Fei Wang[1], Aiping Cao[1], Shuangquan Xie[1], Xifeng Chen[1], Haitao Shen[1], Beini Wang[3], Man Hu[3], Rong Li[1], Xiang Jin[1,2,3]* and Hongbin Li[1]**

[1] Key Laboratory of Xinjiang Phytomedicine Resource and Utilization of Ministry of Education, Key Laboratory of Oasis Town and Mountain-Basin System Ecology of Xinjiang Production and Construction Corps, College of Life Sciences, Shihezi University, Shihezi, China, [2] Research Center for Wild Animal and Plant Resource Protection and Utilization, Qiongtai Normal University, Haikou, China, [3] Ministry of Education Key Laboratory for Ecology of Tropical Islands, Key Laboratory of Tropical Animal and Plant Ecology of Hainan Province, College of Life Sciences, Hainan Normal University, Haikou, China

OPEN ACCESS

Edited by:
Shaojun Dai,
Shanghai Normal University, China

Reviewed by:
Shamim Hasan,
University of Bonn, Germany
David D. Fang,
Agricultural Research Service, United States Department of Agriculture, United States

***Correspondence:**
Rong Li
lirong@shzu.edu.cn
Xiang Jin
jinx@hainnu.edu.cn
Hongbin Li
lihb@shzu.edu.cn

[†] These authors have contributed equally to this work

Specialty section:
This article was submitted to Plant Proteomics and Protein Structural Biology, a section of the journal Frontiers in Plant Science

Received: *16 February 2022*
Accepted: *29 April 2022*
Published: *19 May 2022*

Citation:
Lu T, Zhu L, Liang Y, Wang F, Cao A, Xie S, Chen X, Shen H, Wang B, Hu M, Li R, Jin X and Li H (2022) Comparative Proteomic Analysis Reveals the Ascorbate Peroxidase-Mediated Plant Resistance to Verticillium dahliae in Gossypium barbadense. Front. Plant Sci. 13:877146. doi: 10.3389/fpls.2022.877146

In previous research on the resistance of cotton to Verticillium wilt (VW), *Gossypium hirsutum* and *G. barbadense* were usually used as the susceptible and resistant cotton species, despite their different genetic backgrounds. Herein, we present data independent acquisition (DIA)-based comparative proteomic analysis of two *G. barbadense* cultivars differing in VW tolerance, susceptible XH7 and resistant XH21. A total of 4,118 proteins were identified, and 885 of them were differentially abundant proteins (DAPs). Eight co-expressed modules were identified through weighted gene co-expression network analysis. GO enrichment analysis of the module that significantly correlated with *V. dahliae* infection time revealed that oxidoreductase and peroxidase were the most significantly enriched GO terms. The last-step rate-limiting enzyme for ascorbate acid (AsA) biosynthesis was further uncovered in the significantly enriched GO terms of the 184 XH21-specific DAPs. Additionally, the expression of ascorbate peroxidase (*APX*) members showed quick accumulation after inoculation. Compared to XH7, XH21 contained consistently higher AsA contents and rapidly increased levels of *APX* expression, suggesting their potential importance for the resistance to *V. dahliae*. Silencing *GbAPX1/12* in both XH7 and XH 21 resulted in a dramatic reduction in VW resistance. Our data indicate that APX-mediated oxidoreductive metabolism is important for VW resistance in cotton.

Keywords: ***Gossypium barbadense*, *Verticillium dahliae*, comparative proteomics, reactive oxygen species, ascorbate peroxidase**

INTRODUCTION

Verticillium dahliae Kleb is the fungal pathogen of Verticillium wilt (VW) that commonly causes dramatic reductions in the production of crops such as cotton, tomato, and tobacco (Song et al., 2020). *V. dahliae* was first reported in Virginia, United States, in 1914 and spread to many cotton-producing regions in China during the 1930s (Shaban et al., 2018). To date, more than half of the cotton fields in China contain *V. dahliae* pathogen and VW can lead to 30–50% yield reduction, sometimes even causes total yield loss (Zhang et al., 2020). VW usually causes more

severe damage in *G. hirsutum* than in *G. barbadense* (Ma et al., 1999). Little progress has been made in cotton breeding for VW resistance, either in *G. hirsutum* or in *G. barbadense* (Liu et al., 2018b).

The virulence mechanism exhibited by *V. dahliae* is predominantly induced through propagation in the vascular system, and finally leads to xylem vessel blockage, resulting in severe leaf chlorosis and wilting, leaf and boll abscission, and even plant death (Klosterman et al., 2009). For decades, efforts have been made by researchers to investigate the molecular mechanisms of VW-defense in cotton. It has been demonstrated that the resistance of cotton to VW primarily depends on preformed defense structures, such as thick cuticles, accumulation of phenolic compounds and structures delaying or hindering the expansion of the invader (Shaban et al., 2018). The proteins that are responsible for the resistance of cotton to *V. dahlia* have been identified, and these proteins include immune-related proteins, receptor-like kinases, and transcription factors, such as apoplastic thioredoxin protein (GbNRX1), the receptor-like kinase suppressor of BIR1-1 (GbSOBIR1) and MYB transcription factors (GhMYB108) (Cheng et al., 2016; Li et al., 2016; Zhou et al., 2019). Proteins that play various roles in cell wall modification and/or development, such as proline-rich protein GbHyPRP1 (which can thicken cell walls), are also involve in VW resistance (Yang et al., 2018). When the lignification of cell walls is increased and pectin methylesterase is inhibited, the resistance to VW is enhanced (Liu et al., 2018a). Furthermore, researchers have even identified cotton proteins that can directly degrade chitin in fungal cell walls to facilitate immune recognition (Han et al., 2019).

Reactive oxygen species (ROS) are important signaling molecules that have significant roles in plant development, signal transduction and environmental stress responses (Mittler et al., 2004; Li et al., 2007). Hydrogen peroxide (H_2O_2) is the major form of ROS in plants and is mainly produced in peroxisomes, chloroplasts and mitochondria; in addition, a high content of H_2O_2 in apoplast, which is the extracellular space between the plasma membrane and cell wall, is toxic to plant cells (Smirnoff and Arnaud, 2019). Higher plants have at least four types of peroxidases, glutathione peroxidases (GPX), catalase (CAT), ascorbate peroxidase (APX, class I peroxidase, intracellular) and plant-specific class III peroxidase (Prx, secreted) (Hiraga et al., 2001). Numerous studies have shown that Prxs are involved in plant defense, mainly through the reinforcement of cell walls, ROS metabolism, and the production of anti-microbial metabolites (Passardi et al., 2004; Okazaki et al., 2007). It has been reported that redox homeostasis is important for the elongation of fiber in cotton (Guo et al., 2016; Tao et al., 2018). Moreover, ROS scavenging is also considered important for VW resistance in cotton; for instance, a novel cluster of glutathione S-transferase genes was reported to provide VW resistance in cotton (Li et al., 2019). An NBS-LRR protein from *G. barbadense* was also identified to enhance VW resistance in *Arabidopsis* through the activation of ROS production and the ethylene signaling pathway (Li et al., 2018). Thus, investigating the potential roles of APX (class I) and Prx (class III) peroxidases in cotton resistance to VW will improve our understanding of redox homeostasis in the plant pathogen response.

Proteomics is frequently used for investigations on VW resistance in various plants and provides useful information for understanding the molecular mechanisms of disease resistance (Wang et al., 2018; Hu et al., 2019; Wu et al., 2019). In *V. dahliae*-inoculated *G. thurberi*, 6,533 proteins were identified in the roots, and salicylic acid was found to be significantly accumulated (Fang et al., 2015). Proteomics analysis of xylem sap in cotton showed that most of the over-accumulated proteins belonged to pathogenesis-related and cell wall proteins, while the under-accumulated and absent proteins were principally related to plant growth and development (Yang et al., 2020). Two-dimensional gel electrophoresis (2-DE)-based proteomic techniques have been applied for almost four decades since the 1980s, while liquid chromatography coupled to tandem mass spectrometry (LC–MS/MS) gel-free proteomic approaches have been predominant in recent years due to their high sensitivity and throughput (Roe and Griffin, 2006). Data-independent acquisition (DIA), an attractive MS analysis method, has recently emerged as a powerful approach for label-free relative protein quantification at the whole proteome level. With the DIA approach, thousands of proteins could be identified and quantified without performing fractionation, and only a few micrograms of the protein sample was needed (Pino et al., 2020).

Previous research on cotton VW resistance usually used *G. hirsutum* as a susceptible cotton species and *G. barbadense* as a resistant one, despite their different genetic backgrounds. To eliminate genetic background variation, we performed a DIA proteomics analysis of two *G. barbadense* varieties, susceptible XH7 and resistant XH21. A total of 4,118 proteins were identified, of which 885 proteins were differentially abundant proteins (DAPs) under the threshold of 1.5-fold change and $p < 0.05$. Weighted gene co-expression network analysis (WGCNA) showed that peroxidase activity was the most significantly enriched gene ontology term from the module that showed the most significant correlation with the time of fungal infection. In addition, one enzyme that is crucial for the biosynthesis of ascorbate acid (AsA) was observed in the most significantly enriched GO terms of XH21-specific DAPs. The expression levels of ascorbate peroxidase (*APX*) members were induced when the content of H_2O_2 increased during *V. dahliae* infection. Silencing *GbAPX1* and *GbAPX12* using virus-induced gene silencing (VIGS) in both XH7 and XH21 resulted in a dramatic reduction in VW tolerance. Our data provide the proteome profiles of *G. barbadense* varieties with different resistances to *V. dahliae* and reveal that the key members of the *APX* family are important for *V. dahliae* resistance in Pima cotton.

MATERIALS AND METHODS

Cotton Material and Fungal Treatment

XH7 and XH21 cotton plants were cultured in sterilized soil in an artificial climate room under 70% humidity, 30°C and a 16/8 h light/dark cycle. Four-week-old seedlings were used for inoculation with *V. dahliae*. The *V. dahliae* strain V592 was activated using potato-agar medium and then grown on Czapek's medium (30 g/L sucrose, 3 g/L $NaNO_3$, 0.5 g/L $MgSO_4$-$7H_2O$, 0.5 g/L KCl, 100 mg/L $FeSO_4$-$7H_2O$, 1 g/L K_2HPO_4,

pH 7.2) under 25°C for 5 days. Fungus spores were filtered using four-layer gauze to remove mycelium, and then the spore concentration was adjusted to 10^7 per milliliter in liquid medium. The cotton seedlings were incubated with fungi at 25°C and shaken at 200 rpm for 50 min. The cotton seedlings were then transferred into Hoagland's nutrient solution (Hoagland, 1920) for 3 weeks before phenotype identification. For high-throughput proteomic analysis, cotton roots from XH7 and XH21 were collected at 0, 6, and 24 h after incubation with *V. dahliae* and immediately frozen in liquid nitrogen before storage at –80°C. Three independent treatment replicates were performed for each time point.

Protein Extraction and Liquid Chromatography Coupled to Tandem Mass Spectrometry

The roots from ten cotton plants were used for protein extraction using an improved protein extraction method as previously reported (Jin et al., 2019). Protein quantification was performed following the Bradford method (Bradford, 1976) using a UV-160 spectrophotometer (Shimadzu, Kyoto, Japan). After concentration determination, 100 μg of total protein from each sample was used for trypsin digestion as previously described (Jin et al., 2019). After digestion, iRT (Escher et al., 2012) and digested peptides were mixed in a 1:10 volume ratio. Then, samples were recovered in phase A [2% acetonitrile (ACN), pH 10] and injected into an Agilent 1100 HPLC system (Agilent Technologies, Santa Clara, CA, United States). The samples were then fractionated into 10 fractions using an Agilent Zorbax Extend-C18 column under a 50 min gradient of phase B (90% ACN, pH 10) with a 300 μL/min flow rate. The fractions were then vacuum freeze dried and subjected to the subsequent nanoLC–MS/MS experiment, which was carried out using a DIA method (Bruderer et al., 2017) on the orbitrap Fusion Lumos platform (Thermo Fisher Scientific, Rockford, IL, United States). Positive ion and high-resolution (120,000 resolution at m/z 200 with automatic gain control target of $3e^6$) modes were used for MS/MS data collection. The mass spectra scan range was set to 350–1,650 m/z. The isolation window for MS2 was set to 26 m/z, and the normalized collision energy was 28%.

DIA spectra were analyzed using Spectronaut pulsar 13.7.190916 (Bernhardt et al., 2012) against the protein database derived from the genome sequence of *G. barbadense* (Wang et al., 2019) with the following settings: missed cleavage, 2; fixed modification, carbamidomethyl; variable modification, oxidation; and protein FDR cut-off, 0.05. The DIA configuration was as follows: precursor *q*-value cut-off: 0.01; protein *q*-value cut-off: 0.01; normalization strategy: local normalization; and quantity MS-Level: MS2. Proteins that were observed in at least two out of three replicates were considered high-quality identified proteins. Proteins specifically found in only one cotton variety were defined as variety-specific proteins. For common proteins that could be observed in all samples, fold change ratios of over 1.5 with a p-value < 0.05 were considered DAPs.

Bioinformatics Analyses

For further bioinformatic analyses, a heatmap was constructed using Heatmapper[1] (Babicki et al., 2016). Protein co-expression network analysis was performed with the R package WGCNA as previously described (Langfelder and Horvath, 2008). The GO analysis of DAPs was performed using the Cytoscape plug-in ClueGO (Gabriela et al., 2009), while GO analysis for cotton variety-specific DAPs was carried out using agriGO 2.0 (Tian et al., 2017).

RNA Extraction and Polymerase Chain Reaction

Total RNA was extracted from XH7 and XH21 cotton roots at 0, 6, and 24 h after a treatment with *V. dahliae* using an RNA extraction Kit (DP441, Tiangen, Beijing, China). cDNA was synthesized using a Takara reverse transcription Kit (K1622, Takara, Kusatsu, Japan). Semiquantitative polymerase chain reaction (PCR) was carried out using agarose gel electrophoresis by normalizing the housekeeping gene *GbUBQ*. Real-time quantitative PCR (qRT-PCR) was performed using SYBR green real-time PCR master premix (Applied Biosystems, Foster, CA, United States). The relative expression level of each tested gene was calculated using the $2^{-\triangle Ct}$ method with *GbUBQ* set to 1 unless otherwise stated. All qRT–PCR results are shown as the mean ± SD from three independent biological replicates. The primers used in this work are provided in **Supplementary Table 1**.

H_2O_2 and Ascorbate Acid Measurement

The content of H_2O_2 of cotton root was determined using a Micro Hydrogen Peroxide Assay Kit (BC3590, Solarbio, Beijing, China) and AsA was measured using an Ascorbic Acid Assay Kit (BC1230, Solarbio, Beijing, China) based on the methods in Wu et al. (2017).

3,3′-Diaminobenzidine Staining

DAB (3,3′-diaminobenzidine) staining of cotton leaves was performed according to Zheng et al. (2021). Briefly, cotton leaves were incubated in 1 mg/ml DAB-HCl, pH 3.8, in the dark for 8 h. The leaves were then cleared of pigment by boiling in an ethanol/acetic acid/glycerin mixture (3:1:1 v/v/v) for 20 min before imaging.

Virus Induced Gene Silencing

A VIGS system (Burch-Smith et al., 2004) was used to validate the functions of *GbAPX1/12* in cotton *V. dahliae* tolerance. The conserved fragments of target genes were cloned into the pTRV2 vector (TRV:*GbAPX1/12*) using the *Asc*I and *Spe*I restriction sites. TRV:*GbCLA* was also constructed as a positive marker, in which white leaves are observed in gene silencing transformants. Empty vector TRV:00 was used as a negative control. All vectors were introduced into the Agrobacterium GV3101. After injection into cotton cotyledons, the plants were placed in the dark for 24 h before being exposed to normal growth conditions. After 2 weeks, the successful silencing of target genes was verified by qRT–PCR, and positive plants were selected for *V. dahliae* tolerance analyses.

[1] http://www.heatmapper.ca/expression/

Statistical Analysis

All statistical analyses in this work were performed using SPSS 20.0 with one-way ANOVA and least significant difference methods. The asterisks represent statistical significance: $^{*}p < 0.05$; $^{**}p < 0.01$.

RESULTS

Phenotypes of XH7 and XH21 After Infection and Weighted Gene Co-expression Network Analysis of Differentially Abundant Proteins

Compared to XH21, XH7 exhibited more severe disease symptoms with more wilting leaves and smaller plants, as well as higher disease indexes at 3 weeks after infection by *V. dahliae* (**Figure 1A** and **Supplementary Figure 1**). Total proteins of the XH7 and XH21 roots at 0, 6, and 24 h after fungal treatment were extracted, and DIA proteomics analysis was performed with three biological replicates each. The Venn diagrams of all replicates showed a high consistency among the three replicates (**Supplementary Figure 2**). A total of 4,118 proteins were identified with high confidence. Furthermore, the proteins with a signal intensity fold change of over 1.5 compared to that at 0 h separately in XH7 or XH21 were considered DAPs that responded to *V. dahliae* infection (**Supplementary Figure 3**).

A total of 885 DAPs were determined with the threshold of fold change over 1.5 and $p < 0.05$, which were then used for subsequent bioinformatic analyses (**Figure 1B** and **Supplementary Table 2**). Eight co-expression modules were observed for the WGCNA of all the DAPs. The turquoise (0.88) and blue (–0.8) modules showed the most positive and negative relationships with the time point, while the black (0.76) and red (–0.71) modules showed the most significant relationships with varieties (**Supplementary Figure 4A**). The interactions among these modules are shown in Topological Overlap Matrix (**Supplementary Figure 4B**), suggesting that the modules were relatively independent.

Pathway Enrichment Analyses and Polymerase Chain Reaction Validation of the Module With the Highest Time Correlation and XH21-Specific Differentially Abundant Proteins

To investigate the enriched pathways, DAPs from the turquoise module were then subjected to a Cytoscape plug-in ClueGo (Gabriela et al., 2009). For the biological process category, 255 DAPs of the turquoise module were enriched in three clusters, in which the GO terms of organonitrogen compound biosynthetic process, oxidoreductase activity and peroxidase activity were the most enriched GO terms (**Supplementary Figure 5A**). Moreover, intracellular non-membrane-bounded organelle, cytosol and chloroplast stroma were the most enriched GO terms for the cellular component category, while carbon-oxygen lyase activity, coenzyme binding and RNA binding were the most enriched for the molecular function category (**Supplementary Figures 5B,C**). We noticed that nine peroxidases were significantly enriched in the GO term peroxidase activity for both biological process and molecular function categories. Thus, qPCR assays were performed to validate whether the mRNA levels of these peroxidases changed. Of the nine peroxidases-coding genes, the expressions of *GbPrx72* and *GbPrx* were extremely low. Seven detectable genes showed significantly up-regulated mRNA levels after *V. dahliae* infection in both XH7 and XH21 (**Figure 2**). Together, the proteomics and qPCR data showed that the majority of class III peroxidases were significantly up-regulated at both the mRNA and protein levels after *V. dahliae* infection in both high- and low-susceptibility *G. barbadense* cultivars, indicating that extracellular redox homeostasis might be important for cotton *V. dahliae* resistance.

In addition to the common DAPs, this study also provided insights into the XH21-specific DAPs, which were probably responsible for the high tolerance to *V. dahliae* in XH21. A total of 184 XH21-specific DAPs were identified, and the detailed information is provided in **Supplementary Table 3**. Furthermore, GO enrichment analysis of the 184 XH21-specific DAPs was performed using software AgriGO. For the molecular function category, the significantly enriched end-terms of the tree-view were structural constituent of ribosome (GO:0003735), lyase activity (GO:0016829), protein heterodimerization activity (GO:0046982), RNA binding (GO:0003723) and coenzyme binding (GO:0050662) (**Supplementary Figure 6**). The end-terms for the biological process category were translation (GO:0006412) and glycolytic process (GO:0006069) (**Supplementary Figure 7**), while the end-terms for the cellular component category were ribosome subunit (GO:0044391) and nucleosome (GO:0000786) (**Supplementary Figure 8**). Through qPCR, we further examined the expression levels of nine genes that were enriched in the GO term coenzyme binding (GO:0050662). Seven genes exhibited mRNA expression levels that were consistent with the protein accumulation patterns between XH7 and XH21 (*GbYUCCA10*, *GbAcox1*, *GbDFR*, *GbPDC*, *GbAKHSD*, *GbPDC2*, and *GbGLDH*) (**Supplementary Figure 9**, gene names and primers are provided in **Supplementary Table 1**). Notably, one of the validated genes, *GbGLDH*, was considered the rate-limiting enzyme for the biosynthesis of AsA (Mellidou and Kanellis, 2017), which is one of the key metabolites that reduces H_2O_2 by the catalysis of ascorbate peroxidases (APXs). Collectively, we found that redox homeostasis-related proteins were significantly enriched in DAPs that were common to both XH7 and XH21, and XH21-specific accumulated proteins.

Ascorbate Acid and H_2O_2 Contents and the Expression of Ascorbate Peroxidases Are Important for *Verticillium dahliae* Resistance in Cotton

To further confirm the influence of AsA and H_2O_2 on the susceptibility of different *G. barbadense* cultivars, we examined the contents of AsA and H_2O_2 in the roots of XH7 and XH21 at 0, 6, and 24 h post-infection. The AsA contents of both cultivars

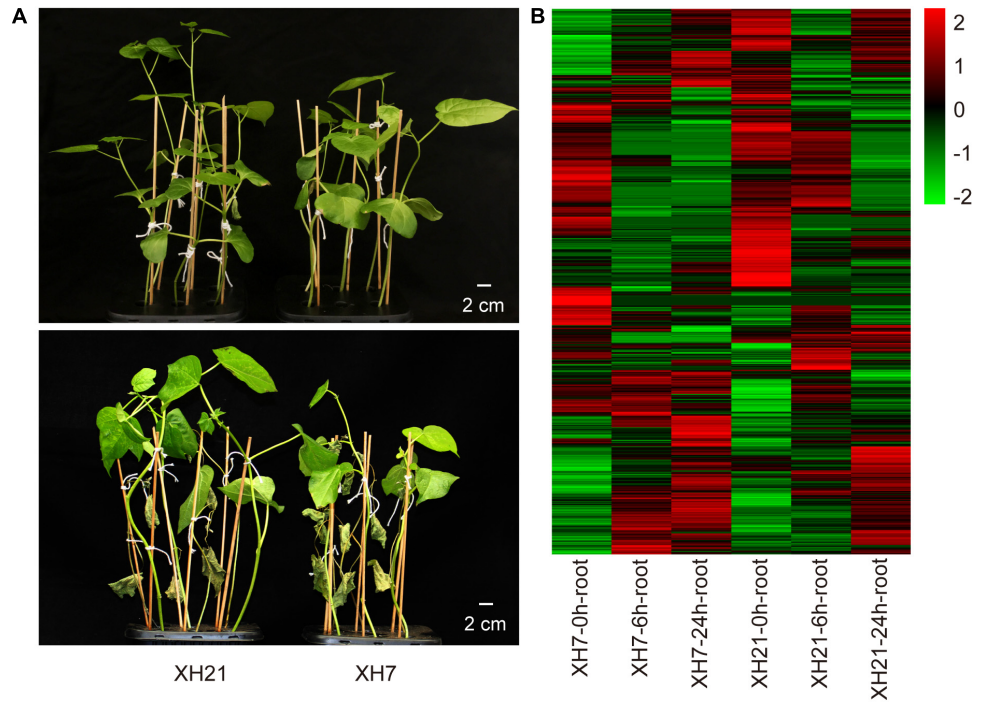

FIGURE 1 | Symptoms of Verticillium wilt disease and heatmap of differentially abundant proteins (DAPs). **(A)** Representative seedlings of XH21 and XH7 before (upper panel) and 21 days after (lower panel) incubation with *Verticillium dahliae*. Four-week-old seedlings were infected with *V. dahliae* and were photographed after 3 weeks. $N = 18$ for each group. **(B)** Heatmap of 885 DAPs. The Log_2 value of the expression levels of DAPs was used to produce the heatmap.

were similar before inoculation with *V. dahliae*; however, the AsA contents in XH21 were significantly higher than those in XH7 after treatment with *V. dahliae* ($p < 0.01$, **Figure 3A**). Correspondingly, the contents of H_2O_2 increased shortly after infection (6 h) but then decreased at 24 h post-fungal treatment (**Figure 3B**). The susceptible cultivar XH7 had a significantly higher ($p < 0.01$) H_2O_2 content than that of XH21 at 6 h, and the result was consistent with the lower level of AsA in XH7 at 6 h (**Figures 3A,B**). To visualize the H_2O_2 distribution, DAB staining was performed in cotton leaves from XH7 and XH21 at 0, 6, and 24 h after inoculation with *V. dahliae*. High levels of H_2O_2 predominantly accumulated at 6 h in both XH7 and XH21, with a stronger staining signal (dark brown) in XH7 (**Figures 3D,G**). Exogenous application of AsA onto XH7 and XH21 leaves significantly improved the disease resistance of cotton plants, indicating that extracellular ROS scavenging by peroxidases might be crucial for *V. dahliae* resistance in *G. barbadense* (**Supplementary Figure 10**).

Thus, we further investigated the mRNA expression levels of *APX* genes, which are considered the only enzymes that catalyze the reduction of H_2O_2 using AsA as a specific electron donor. Based on our previous work (Tao et al., 2018) and a transcriptome analysis of *G. barbadense* at different times after *V. dahliae* infection (**Supplementary Figure 11**, NCBI accession number: PRJNA234454), eight homologs of the *GbAPX* family that were predominantly expressed were selected for qPCR assays (*GbAPX1A/D*, *GbAPX2A/D*, *GbAPX3A/D*, and *GbAPX12A/D*). The results showed that the mRNA levels of partial *GbAPX* homologs were slightly increased in XH21 (no more than twofold change), while most *APX* homologs that were tested here exhibited significantly up-regulated expression levels in XH7, especially *GbAPX1A/D* and *GbAPX12A/D* (**Figure 4**).

Silencing *GbAPX1* and *GbAPX12* Compromises the Resistance of Cotton to *Verticillium dahliae*

To validate the functions of the predominant *GbAPX* members in *V. dahliae* resistance, conserved fragments of *GbAPX1A/D* and *GbAPX12A/D* were used to construct a VIGS vector (TRV:*GbAPX1/12*). Successful silencing of the positive control and target genes was confirmed by semi and real-time quantitative PCR (**Supplementary Figure 12** and **Figures 5A,B**). The *V. dahliae* accumulation in the stem of *GbAPX1/12*-silenced transformants was more severe than that in the TRV:00 control at 14 days after *V. dahliae* inoculation in both XH7 and XH21, and more dark brown streaks were observed in the stems (**Figure 5C**). In the fungal recovery assays, more hyphae around stem sections were observed with the *GbAPX1/12*-silenced plants than with the TRV:00 controls (**Figure 5D**). As a result, the disease symptoms observed for the TRV:00 plants were similar to those of regular wild type plants (XH7 is susceptible and XH21 is resistant), while TRV:*GbAPX1/12* plants of both XH7 and XH21 showed similar disease symptoms, and these symptoms were much more severe than those of TRV:00 (**Figure 5E**). Together, silencing

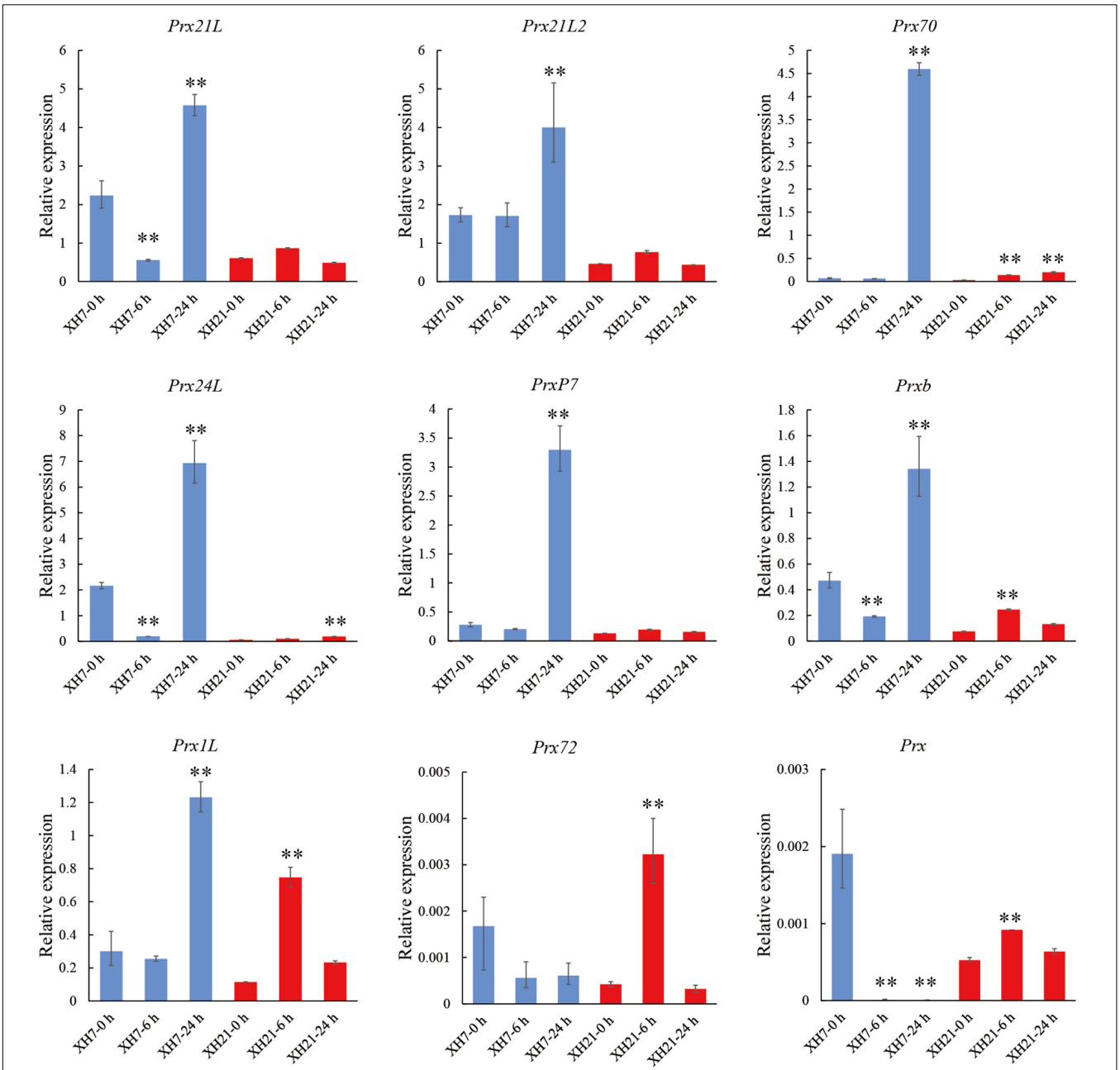

FIGURE 2 | Transcriptional expression analysis of nine peroxidases. Relative expression levels of nine peroxidases identified in GO enrichment analysis. *GbUBQ* was used as an internal control and set to 1. Three independent replicates were performed for each PCR assay. $^{**}p < 0.01$.

predominantly expressed APX family members in Pima cotton compromises the resistance to *V. dahliae*.

DISCUSSION

In total, 885 DAPs were identified at 0, 6, and 24 h after infection in XH7 and XH21, and a much higher number of DAPs were observed than those identified in 2-DE based studies (Witzel et al., 2017). Benefiting from the high sensitivity, many novel DAPs have been identified, such as low-abundant transcript factors (nuclear transport factor 2 -like protein, transcription factor RF2a, GATA transcription factor 26 -like protein) and very small molecular weight peptides (malate dehydrogenase-2C mitochondrial, cytochrome b-c1 complex subunit 9), which are very difficult to be detected by 2-DE based proteomic techniques (**Supplementary Table 2**). The WGCNA and pathway enrichment analyses of the module with the highest module-trait relationship revealed the key pathways that are involved in VW resistance in *G. barbadense* (**Supplementary Figures 4, 5**). Some

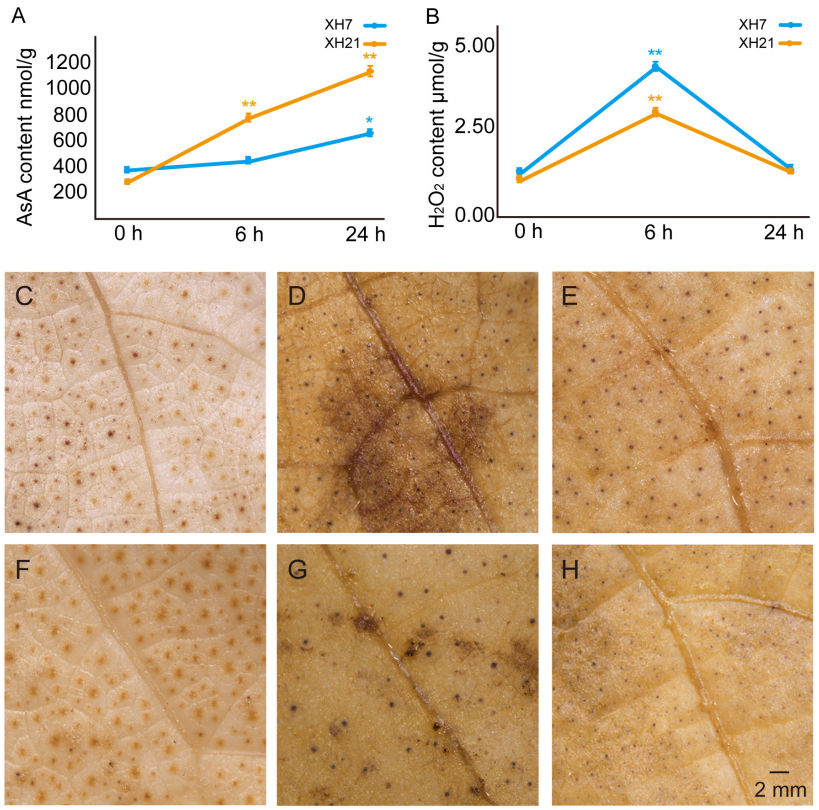

FIGURE 3 | Detection of the AsA and H_2O_2 contents in XH7 and XH21 after *V. dahliae* incubation. AsA **(A)** and H_2O_2 **(B)** contents were determined in XH7 and XH21 roots treated with *V. dahliae* for 0, 6, and 24 h, respectively. $^*p < 0.05$; $^{**}p < 0.01$. DAB staining of leaves of XH7 **(C–E)** and XH21 **(F–H)** after *V. dahliae* treatment for 0 h **(C,F)**, 6 h **(D,G)**, and 24 h **(E,H)** are shown. The stained H_2O_2 is indicated with a brown color. Bar = 2 mm.

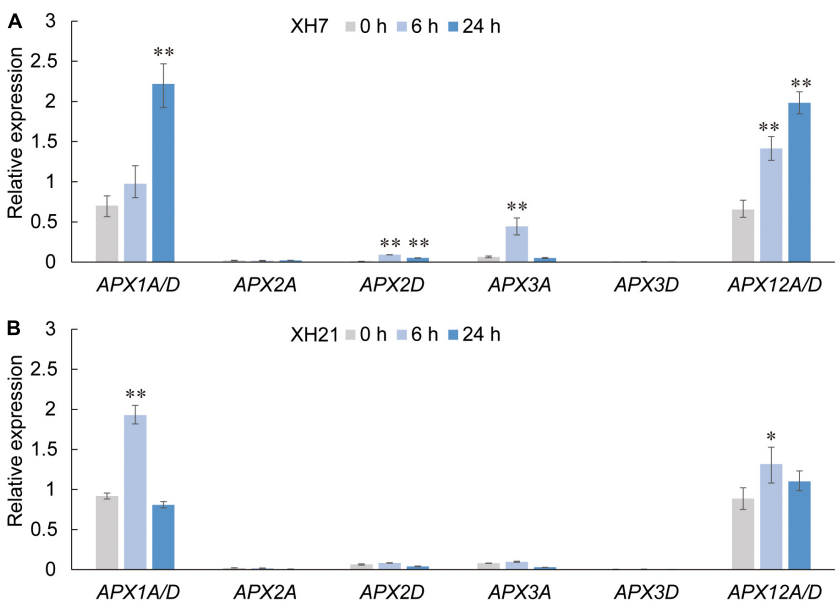

FIGURE 4 | Relative expression levels of *APX* family members in Pima cotton roots of XH7 **(A)** and XH21 **(B)** at 0, 6, and 24 h after *V. dahliae* incubation. Genes with extremely high nucleotide similarity that could not be distinguished by primers were detected using identical primers (*APX1A/D* and *APX12A/D*). *GbUBQ* was used as a reference gene and set to 1. Three independent replicates were performed for each qPCR assay. Significance was analyzed using one-Way ANOVA. $^*p < 0.05$; $^{**}p < 0.01$.

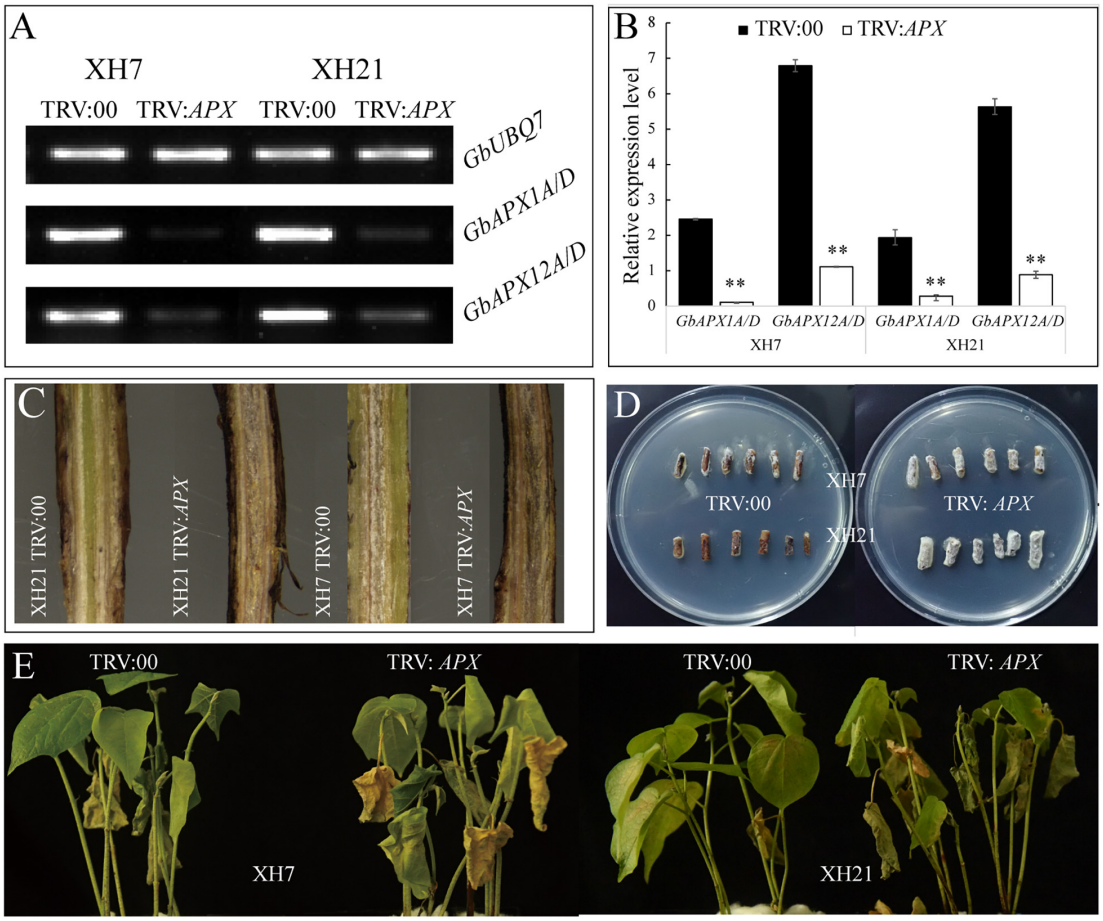

FIGURE 5 | The resistance of VIGS plants to *V. dahlia* was compromised. Semi-quantitative **(A)** and real-time quantitative **(B)** PCR were used to select successfully silenced transformants. Three replicates were performed for each transformed plant. $^{**}p < 0.01$. **(C)** Fungal accumulation in the stems of TRV:*00* and TRV:*GbAPX1/12* plants. **(D)** Fungal hyphae recovery assays of the *V. dahlia*-infected cotton. The stem sections were plated on PDA medium, incubated at 25°C, and photographed at 5 days post-plating. **(E)** Disease symptoms for the representative plants of TRV:00 and TRV:*GbAPX1/12* at 14 days after inoculation. $N = 18$ for each treatment.

of the enriched pathways were mentioned in previous works, such as the response to oxidative stress (Hu et al., 2019). In addition to the common DAPs, DAPs that are specific to the resistant cotton XH21 also represented biological significance for cotton VW resistance. Both pathway enrichment analyses of common and XH21-specific DAPs revealed that ROS-related pathways, especially the biological processes related to H_2O_2 scavenging, were significantly enriched (**Supplementary Figures 5, 6**). Ribosomal protein GaRPL18 contributes significantly to cotton resistance (Gong et al., 2017). In this study, ribosomal-related pathways were also observed to be significantly enriched pathways and can be studied for the function of these proteins in cotton disease resistance in future investigations.

Ascorbate acid has been demonstrated to play various important roles in cotton, including fiber development and stress response (Ma et al., 2019; Pan et al., 2019; Song et al., 2019). It is well known that the antioxidant system is important for improving plant resistance to abiotic or biotic stress; however, few studies have reported the functions of AsA in *V. dahliae* resistance in *G. barbadense*. Here, we examined the AsA and H_2O_2 contents in resistant and susceptible cultivars, showing that higher AsA contents and lower H_2O_2 levels were closely correlated with the disease resistance (**Figure 3**). The different levels of AsA and H_2O_2 between high- and low-resistance *G. barbadens* cultivars could be partly explained by our data for the XH21-speicific accumulated protein *GLDH* (**Supplementary Figure 9**), which is responsible for AsA biosynthesis, and by the higher expression levels of the class I peroxidase *APX* in XH7 (**Figure 4**). Exogenous application of AsA onto XH7 and XH21 plants significantly improved their VW syptoms (**Supplementary Figure 10**).

Ascorbate peroxidase are necessary for cotton fiber development (Li et al., 2007; Guo et al., 2016); however, thus far, no study has linked APX to pathogen resistance in cotton species, although several investigations have shown that APX activity is important for the tolerance of rice and wheat to pathogens (Gou et al., 2015; Jiang et al., 2016). Our data showed that APXs might be related to cotton VW resistance

by regulating redox homeostasis. The qPCR of *APXs*, coupled with the AsA and H_2O_2 content assays, might provide a possible explanation for the high *V. dahliae* resistance of XH21, which was mainly attributed to the high activity of AsA biosynthesis and the high levels of AsA in XH21. In contrast, the AsA levels in XH7 were much lower than those in XH21, possibly because of the low level of *GbGLDH* and significantly increased expression of *GbAPX*, which consumes AsA as an electron donor. This was further confirmed by gene silencing experiments. TRV:00 transformants exhibited disease symptoms similar to those of their original phenotypes; cultivar XH7 was susceptible and XH21 was resistant. However, by knocking down *GbAPX1/12* expression, the transformants of TRV:*GbAPX1/12* exhibited a significantly decreased resistance to *V. dahliae* in both XH7 and XH21 (**Figure 5E**).

CONCLUSION

In summary, we identified many novel DAPs by using a DIA-based high-throughput proteomic analysis in two *G. barbadense* varieties with different VW resistance. WGCNA and pathway enrichment analyses revealed the key pathways that are involved in VW resistance in *G. barbadense.* Increased AsA level, decreased H_2O_2 content, were observed in VW resistant variety XH21. Knocking down *GbAPX1/12* expression in *G. barbadense* resulted in significantly decreased resistance to *V. dahlia* in both XH7 and XH21. Our results provide effective proteomic references for elucidating the VW resistance mechanism and genetic improvement of VW resistant cotton germplasms.

DATA AVAILABILITY STATEMENT

The datasets presented in this study can be found in online repository ProteomeXchange Consortium (http://proteomecentral.proteomexchange.org) under the identifier PXD017527.

AUTHOR CONTRIBUTIONS

RL, XJ, and HL contributed to conception and design of the study. TL, LZ, YL, FW, AC, SX, XC, HS, BW, and MH performed the experiment and data analyses. TL and LZ performed the statistical analysis. TL and XJ wrote the first draft of the manuscript. LZ, RL, XJ, and HL wrote sections of the manuscript. All authors contributed to manuscript revision, read, and approved the submitted version.

FUNDING

This research was funded by the National Natural Science Foundation of China (Grant Number 31960413); the Science and Technology Project of Shihezi University (Grant Numbers CXPY202017 and RCZK201905); and the Specific Research Fund of the Innovation Platform for Academicians of Hainan Province (Grant Nos. YSPTZX202023 and YSPTZX202211).

ACKNOWLEDGMENTS

The authors want to thank to the support from the academician workstation of Hainan Province and thank to the National Mid-term GenBank for cotton at the Institution of Cotton Research of Chinese Academy of Agriculture Sciences (ICR, CAAS) for providing the germplasm resources used in this study.

SUPPLEMENTARY MATERIAL

The Supplementary Material for this article can be found online at: https://www.frontiersin.org/articles/10.3389/fpls.2022.877146/full#supplementary-material

Supplementary Figure 1 | Disease index of XH7 and XH21 after *V. dahliae* incubation. The number of four represented the highest disease index when the whole plant died, and the number of zero indicated the lowest disease index with no visible wilting. The numbers zero to four are also presented by different colors for visualization.

Supplementary Figure 2 | Venn diagram for three replicates of proteomics data. The diagram shows the distribution of the identified proteins in three independent experiments, indicating a high repetitiveness of three replicates in each group.

Supplementary Figure 3 | Statistical analysis of DAPs. Venn diagram of DAPs at 6 and 24 h compared to 0 h in XH7 **(A)** and XH21 **(D)**. The red and green numbers indicate up- and down-regulated protein respectively. Volcano plots of DAPs at 6 h compared to 0 h in XH7 **(B)** and XH21 **(E)**; volcano plots of DAPs of 24 h compared to 0 h in XH7 **(C)** and XH21 **(F)**; the red and green dots represented increased and decreased abundant proteins, respectively, and the blue dots represent proteins without significance.

Supplementary Figure 4 | Weighted gene co-expression network analysis of 885 DAPs. **(A)** Network heatmap of DAPs. Recognized modules are indicated by different colors. The light color represents a low overlap, and darker red indicates a higher overlap between proteins. **(B)** Module-trait relationship of eight well-coexpression modules. The depth of color corresponds to the correlation. Positive correlations are indicated in red color, and negative correlations are represented in blue color. Significance (*p*-value) of each module to time or variety presented in parentheses.

Supplementary Figure 5 | GO enrichment of the 255 DAPs from the turquoise module, which showed the most significant positive relationships with infection time. **(A)** Biological Process. **(B)** Cellular Component. **(C)** Molecular Function. The sphere size indicates the number of genes in the corresponding term; the color corresponds to different correct *p*-value ranges. Gray lines connect the terms with related functional enrichment.

Supplementary Figure 6 | Tree-view of GO terms for the molecular function category enriched by 184 XH21-specific DAPs. The depth of color corresponds to the *p* value of significance. The GO ID, *p*-value, annotation and the numbers of DAPs for each GO term are shown inside the boxes. The GO ID with red color font indicates the subsequent experimental verification term selected in this study.

Supplementary Figure 7 | Tree-view of GO terms for the biological process category enriched by the 184 XH21-specific DAPs. The white box represents GO category terms. The depth of color corresponds to the statistical significance. The GO ID, *p*-value, annotation and the numbers of DAPs for each GO term are shown inside the boxes. Stars indicate that the terms are not on the key nodes of the tree.

Supplementary Figure 8 | Tree-view of GO terms for the cellular component category enriched by the 184 XH21-specific DAPs. The white box represents GO category terms. The depth of color corresponds to the statistical significance. The GO ID, *p*-value, annotation and the numbers of DAPs for each GO term are shown inside the boxes. Stars indicate that the terms are not on the key nodes of the tree.

Supplementary Figure 9 | qRT–PCR validation of the expression levels of the nine proteins in GO:0050662, coenzyme binding. The transcriptional expression

levels of the nine proteins distributed in the coenzyme binding category of GO:0050662, including flavin-containing monooxygenase YUCCA10-like protein (*YUCCA10*), peroxisomal acyl-coenzyme A oxidase 1-like protein (*Acox1*), FAD/NAD(P)-binding oxidoreductase family protein isoform 1 (*FAD*), dihydroflavonol-4-reductase (*DFR*), thiamine pyrophosphate dependent pyruvate decarboxylase family protein (*PDC*), bifunctional aspartokinase (*AKHSD*), thiamine pyrophosphate dependent pyruvate decarboxylase family protein (*PDC2*), glucose-6-phosphate 1-dehydrogenase-2C chloroplastic (*G6PD1*), and l-galactono-1,4-lactone dehydrogenase-2C mitochondrial-like protein (*GLDH*), were measured by qRT–PCR with relative expression levels to the reference gene of *UBQ*. Finally, the fold change between the infected groups and the control is shown, and the expression level in the 0 h samples is set to 1. Three independent replicates were performed for each qPCR assay. $*p < 0.05$; $**p < 0.01$.

Supplementary Figure 10 | Disease index of XH7 and XH21 with or without exogenous AsA application after *V. dahliae* treatment. The exogenous applications of 0.5 mM AsA were performed when the cotton seedlings were exposed to *V. dahliae*, and H_2O was used as a control. The fungal treatment time was extended to 3 days. Then, the seedlings were transferred into Hoagland's nutrient solution to measure the disease index. The number four was the highest disease index when the whole plant died, and zero indicated the lowest disease index with no visible wilting. The numbers zero to four are also illustrated by different colors for visualization.

Supplementary Figure 11 | Heatmap of transcriptional expression levels of all *G. barbadense APX* genes deduced from public transcriptome data of *V. dahlia*-treated roots. The transcriptome data of *G. barbadense* roots after *V. dahliae* treatment were obtained from the public online database at NCBI (accession number: PRJNA234454). The colors of yellow, black, and blue indicate high, moderate, and low transcriptional expression levels, respectively. The heatmap was produced by the value of Log_2 of FPKM by Heatmapper (http://www.heatmapper.ca/expression/). The *APX* genes of red fonts were selected for further analysis of qRT–PCR validation.

Supplementary Figure 12 | Phenotypes and qPCR assays of the positive control. TRV:*GbCLA* was used as a positive control for VIGS. Silencing of *GbCLA* will prevent the biosynthesis of chlorophyll and result in write leaves [**(A)** for XH7 and **(B)** for XH21]. qPCR of *GbCLA* showed a significant decrease of expression level in transformed plants **(C)**.

Supplementary Table 1 | Primers used in this work.

Supplementary Table 2 | Detailed information for the 885 DAPs.

Supplementary Table 3 | Detailed information for the 184 XH21-specific DAPs.

REFERENCES

Babicki, S., Arndt, D., Marcu, A., Liang, Y., Grant, J. R., Maciejewski, A., et al. (2016). Heatmapper: web-enabled heat mapping for all. *Nucleic Acids Res.* 44, 147–153. doi: 10.1093/nar/gkw419

Bernhardt, O. M., Selevsek, N., Gillet, L. C., Rinner, O., Picotti, P., Aebersold, R., et al. (2012). "Spectronaut: a fast and efficient algorithm for MRM-like processing of data independent acquisition (SWATH-MS) data," in *Proceedings of the 60th ASMS Conference on Mass Spectrometry and Allied Topics*, Vancouver.

Bradford, M. M. (1976). A rapid and sensitive method for the quantitation of microgram quantities of protein utilizing the principle of protein–dye binding. *Anal. Biochem.* 72, 248–254. doi: 10.1006/abio.1976.9999

Bruderer, R., Bernhardt, O. M., Gandhi, T., Xuan, Y., Sondermann, J., Schmidt, M., et al. (2017). Optimization of experimental parameters in data-independent mass spectrometry significantly increases depth and reproducibility of results. *Mol. Cell. Proteomics* 16, 2296–2309. doi: 10.1074/mcp.RA117.000314

Burch-Smith, T. M., Anderson, J. C., Martin, G. B., and Dinesh-Kumar, S. P. (2004). Applications and advantages of virus-induced gene silencing for gene function studies in plants. *Plant J.* 39, 734–746. doi: 10.1111/j.1365-313X.2004.02158.x

Cheng, H. Q., Han, L. B., Yang, C. L., Wu, X. M., Zhong, N. Q., Wu, J. H., et al. (2016). The cotton MYB108 forms a positive feedback regulation loop with CML11 and participates in the defense response against *Verticillium dahliae* infection. *J. Exp. Bot.* 67, 1935–1950. doi: 10.1093/jxb/erw016

Escher, C., Reiter, L., MacLean, B., Ossola, R., Herzog, F., Chilton, J., et al. (2012). Using iRT, a normalized retention time for more targeted measurement of peptides. *Proteomics* 12, 1111–1121. doi: 10.1002/pmic.201100463

Fang, W., Xie, D., Zhu, H., Li, W., Xu, Z., Yang, L., et al. (2015). Comparative proteomic analysis of *Gossypium thurberi* in response to *Verticillium dahliae* inoculation. *Int. J. Mol. Sci.* 16, 25121–25140. doi: 10.3390/ijms161025121

Gabriela, B., Bernhard, M., Hubert, H., Pornpimol, C., Marie, T., Amos, K., et al. (2009). Cluego: a cytoscape plug-in to decipher functionally grouped gene ontology and pathway annotation networks. *Bioinformatics* 8, 1091–1093. doi: 10.1093/bioinformatics/btp101

Gong, Q., Yang, Z., Wang, X., Butt, H. I., Chen, E., and He, S. (2017). Salicylic acid-related cotton (*Gossypium arboreum*) ribosomal protein *GaRPL18* contributes to resistance to *Verticillium dahliae*. *BMC Plant Biol.* 17:59. doi: 10.1186/s12870-017-1007-5

Gou, J. Y., Li, K., Wu, K., Wang, X., Lin, H., Cantu, D., et al. (2015). Wheat stripe rust resistance protein wks1 reduces the ability of the thylakoid-associated ascorbate peroxidase to detoxify reactive oxygen species. *Plant Cell* 27, 1755–1770. doi: 10.1105/tpc.114.134296

Guo, K., Du, X., Tu, L., Tang, W., Wang, P., Wang, M., et al. (2016). Fibre elongation requires normal redox homeostasis modulated by cytosolic ascorbate peroxidase in cotton (*Gossypium hirsutum*). *J. Exp. Bot.* 67, 3289–3301. doi: 10.1093/jxb/erw146

Han, L. B., Li, Y. B., Wang, F. X., Wang, W. Y., Liu, J., Wu, J. H., et al. (2019). The cotton apoplastic protein CRR1 stabilizes chitinase 28 to facilitate defense against the fungal pathogen *Verticillium dahliae*. *Plant Cell* 31, 520–536. doi: 10.1105/tpc.18.00390

Hiraga, S., Sasaki, K., Ito, H., Ohashi, Y., and Matsui, H. (2001). A large family of class III plant peroxidases. *Plant Cell Physiol.* 42, 462–468. doi: 10.1093/pcp/pce061

Hoagland, D. R. (1920). Optimum nutrient solutions for plants. *Science* 52, 562–564. doi: 10.1126/science.52.1354.562

Hu, X., Puri, K. D., Gurung, S., Klosterman, S. J., Wallis, C. M., Britton, M., et al. (2019). Proteome and metabolome analyses reveal differential responses in tomato -*Verticillium dahliae*-interactions. *J. Proteomics* 207:103449. doi: 10.1016/j.jprot.2019.103449

Jiang, G., Yin, D., Zhao, J., Chen, H., Guo, L., and Zhu, L. (2016). The rice thylakoid membrane-bound ascorbate peroxidase *OsAPX8* functions in tolerance to bacterial blight. *Sci. Rep.* 6:26104. doi: 10.1038/srep26104

Jin, X., Zhu, L., Tao, C., Xie, Q., Xu, X., Chang, L., et al. (2019). An improved protein extraction method applied to cotton leaves is compatible with 2-DE and LC-MS. *BMC Genomics* 20:285. doi: 10.1186/s12864-019-5658-5

Klosterman, S. J., Atallah, Z. K., Vallad, G. E., and Subbarao, K. V. (2009). Diversity, pathogenicity, and management of *Verticillium* species. *Annu. Rev. Phytopathol.* 47, 39–62. doi: 10.1146/annurev-phyto-080508-081748

Langfelder, P., and Horvath, S. (2008). WGCNA: an R package for weighted correlation network analysis. *BMC Bioinformatics* 9:559. doi: 10.1186/1471-2105-9-559

Li, H. B., Qin, Y. M., Pang, Y., Song, W. Q., Mei, W. Q., and Zhu, Y. X. (2007). A cotton ascorbate peroxidase is involved in hydrogen peroxide homeostasis during fibre cell development. *New Phytol.* 175, 462–471. doi: 10.1111/j.1469-8137.2007.02120.x

Li, N. Y., Zhou, L., Zhang, D. D., Klosterman, S. J., Li, T. G., Gui, Y. J., et al. (2018). Heterologous expression of the cotton NBS-LRR gene *GbaNA1* enhances *Verticillium* wilt resistance in *Arabidopsis*. *Front. Plant Sci.* 9:119. doi: 10.3389/fpls.2018.00119

Li, Y. B., Han, L. B., Wang, H. Y., Zhang, J., Sun, S. T., Feng, D. Q., et al. (2016). The thioredoxin *GbNRX1* plays a crucial role in homeostasis of apoplastic reactive oxygen species in response to *Verticillium dahliae* infection in cotton. *Plant Physiol.* 170, 2392–2406. doi: 10.1104/pp.15.01930

Li, Z. K., Chen, B., Li, X. X., Wang, J. P., Zhang, Y., Wang, X. F., et al. (2019). A newly identified cluster of glutathione S-transferase genes provides *Verticillium* wilt resistance in cotton. *Plant J.* 98, 213–227. doi: 10.1111/tpj.14206

Liu, N., Sun, Y., Wang, P., Duan, H., Ge, X., and Li, X. (2018b). Mutation of key amino acids in the polygalacturonase-inhibiting proteins *CkPGIP1* and *GhPGIP1* improves resistance to *Verticillium* wilt in cotton. *Plant J.* 96, 546–561. doi: 10.1111/tpj.14048

Liu, N., Sun, Y., Pei, Y., Zhang, X., Wang, P., Li, X., et al. (2018a). A pectin methylesterase inhibitor enhances resistance to *Verticillium* wilt. *Plant Physiol.* 176, 2202–2220. doi: 10.1104/pp.17.01399

Ma, R., Song, W., Wang, F., Cao, A., Xie, S., Chen, X., et al. (2019). A cotton (*Gossypium hirsutum*) *Myo*-inositol-1-phosphate synthase (*GhMIPS1D*) gene promotes root cell elongation in *Arabidopsis*. *Int. J. Mol. Sci.* 20:1224. doi: 10.3390/ijms20051224

Ma, Z., Wang, X., Zhang, G., Liu, S., Sun, J., and Liu, J. (1999). Genetic studies of *Verticillium* wilt resistance among different types of sea island cottons. *Zuo Wu Xue Bao* 26, 321–345.

Mellidou, I., and Kanellis, A. K. (2017). Genetic control of ascorbic acid biosynthesis and recycling in horticultural crops. *Front. Chem.* 5:50. doi: 10.3389/fchem.2017.00050

Mittler, R., Vanderauwera, S., Gollery, M., and Van Breusegem, F. (2004). Reactive oxygen gene network of plants. *Trends Plant Sci.* 9, 490–498. doi: 10.1016/j.tplants.2004.08.009

Okazaki, Y., Ishizuka, A., Ishihara, A., Nishioka, T., and Iwamura, H. (2007). New dimeric compounds of avenanthramide phytoalexin in oats. *J. Org. Chem.* 72, 3830–3839. doi: 10.1021/jo0701740

Pan, Z., Chen, L., Wang, F., Song, W., Cao, A., Xie, S., et al. (2019). Genome-wide identification and expression analysis of the ascorbate oxidase gene family in *Gossypium hirsutum* reveals the critical role of *GhAO1A* in delaying dark-induced leaf senescence. *Int. J. Mol. Sci.* 20:6167. doi: 10.3390/ijms20246167

Passardi, F., Penel, C., and Dunand, C. (2004). Performing the paradoxical: how plant peroxidases modify the cell wall. *Trends Plant Sci.* 9, 534–540. doi: 10.1016/j.tplants.2004.09.002

Pino, L. K., Just, S. C., MacCoss, M. J., and Searle, B. C. (2020). Acquiring and analyzing data independent acquisition proteomics experiments without spectrum libraries. *Mol. Cell. Proteomics* 19, 1088–1103. doi: 10.1074/mcp.P119.001913

Roe, M. R., and Griffin, T. J. (2006). Gel-free mass spectrometry-based high throughput proteomics: tools for studying biological response of proteins and proteomes. *Proteomics* 6, 4678–4687. doi: 10.1002/pmic.200500876

Shaban, M., Miao, Y., Ullah, A., Khan, A. Q., Menghwar, H., Khan, A. H., et al. (2018). Physiological and molecular mechanism of defense in cotton against *Verticillium dahliae*. *Plant Physiol. Biochem.* 125, 193–204. doi: 10.1016/j.plaphy.2018.02.011

Smirnoff, N., and Arnaud, D. (2019). Hydrogen peroxide metabolism and functions in plants. *New Phytol.* 221, 1197–1214. doi: 10.1111/nph.15488

Song, R., Li, J., Xie, C., Jian, W., and Yang, X. (2020). An overview of the molecular genetics of plant resistance to the *Verticillium* wilt pathogen *Verticillium dahliae*. *Int. J. Mol. Sci.* 21:E1120.

Song, W., Wang, F., Chen, L., Ma, R., Zuo, X., Cao, A., et al. (2019). *GhVTC1*, the key gene for ascorbate biosynthesis in *Gossypium hirsutum*, involves in cell elongation under control of ethylene. *Cells* 8:1039. doi: 10.3390/cells8091039

Tao, C., Jin, X., Zhu, L., Xie, Q., Wang, X., and Li, H. (2018). Genome-wide investigation and expression profiling of *APX* gene family in *Gossypium hirsutum* provide new insights in redox homeostasis maintenance during different fiber development stages. *Mol. Genet. Genomics* 293, 685–697. doi: 10.1007/s00438-017-1413-2

Tian, T., Liu, Y., Yan, H., You, Q., Yi, X., Du, Z., et al. (2017). agriGO v2.0: a GO analysis toolkit for the agricultural community, 2017 update. *Nucleic Acids Res.* 45, 122–129. doi: 10.1093/nar/gkx382

Wang, F. X., Luo, Y. M., Ye, Z. Q., Cao, X., Liang, J. N., Wang, Q., et al. (2018). iTRAQ-based proteomics analysis of autophagy-mediated immune responses against the vascular fungal pathogen *Verticillium dahliae* in *Arabidopsis*. *Autophagy* 14, 598–618. doi: 10.1080/15548627.2017.1423438

Wang, M., Tu, L., Yuan, D., Zhu, D., Shen, C., Li, J., et al. (2019). Reference genome sequences of two cultivated allotetraploid cottons, *Gossypium hirsutum* and *Gossypium barbadense*. *Nat. Genet.* 51, 224–229. doi: 10.1038/s41588-018-0282-x

Witzel, K., Buhtz, A., and Grosch, R. (2017). Temporal impact of the vascular wilt pathogen *Verticillium dahliae* on tomato root proteome. *J. Proteomics* 169, 215–224. doi: 10.1016/j.jprot.2017.04.008

Wu, L. B., Ueda, Y., Lai, S. K., and Frei, M. (2017). Shoot tolerance mechanisms to iron toxicity in rice (*Oryza sativa* L.). *Plant Cell Environ.* 40, 570–584. doi: 10.1111/pce.12733

Wu, X., Yan, J., Wu, Y., Zhang, H., Mo, S., Xu, X., et al. (2019). Proteomic analysis by iTRAQ-PRM provides integrated insight into mechanisms of resistance in pepper to *Bemisia tabaci* (Gennadius). *BMC Plant Biol.* 19:270. doi: 10.1186/s12870-019-1849-0

Yang, J., Wang, X., Xie, M., Wang, G., Li, Z., Zhang, Y., et al. (2020). Proteomic analyses on xylem sap provides insights into the defense response of *Gossypium hirsutum* against *Verticillium dahliae*. *J. Proteomics* 213:103599. doi: 10.1016/j.jprot.2019.103599

Yang, J., Zhang, Y., Wang, X., Wang, W., Li, Z., Wu, J., et al. (2018). *HyPRP1* performs a role in negatively regulating cotton resistance to *V. dahliae* via the thickening of cell walls and ROS accumulation. *BMC Plant Biol.* 18:339. doi: 10.1186/s12870-018-1565-1

Zhang, X., Cheng, W., Feng, Z., Zhu, Q., Sun, Y., Li, Y., et al. (2020). Transcriptomic analysis of gene expression of *Verticillium dahliae* upon treatment of the cotton root exudates. *BMC Genomics* 21:155. doi: 10.1186/s12864-020-6448-9

Zheng, Y., Xu, J., Wang, F., Tang, Y., Wei, Z., Ji, Z., et al. (2021). Mutation types of CYP71P1 cause different phenotypes of mosaic spot lesion and premature leaf senescence in rice. *Front. Plant Sci.* 12:641300. doi: 10.3389/fpls.2021.641300

Zhou, Y., Sun, L., Wassan, G. M., He, X., Shaban, M., Zhang, L., et al. (2019). GbSOBIR1 confers *Verticillium* wilt resistance by phosphorylating the transcriptional factor *GbHLH171* in *Gossypium barbadense*. *Plant Biotechnol. J.* 17, 152–163. doi: 10.1111/pbi.12954

Conflict of Interest: The authors declare that the research was conducted in the absence of any commercial or financial relationships that could be construed as a potential conflict of interest.

Publisher's Note: All claims expressed in this article are solely those of the authors and do not necessarily represent those of their affiliated organizations, or those of the publisher, the editors and the reviewers. Any product that may be evaluated in this article, or claim that may be made by its manufacturer, is not guaranteed or endorsed by the publisher.

frontiers | Frontiers in Plant Science

TYPE Original Research
PUBLISHED 22 July 2022
DOI 10.3389/fpls.2022.965143

OPEN ACCESS

EDITED BY
Mateusz Labudda,
Warsaw University of Life Sciences-SGGW, Poland

REVIEWED BY
Jan Smalle,
University of Kentucky, United States
Małgorzata Janicka,
University of Wrocław, Poland
Beata Prabucka,
Warsaw University of Life Sciences, Poland

*CORRESPONDENCE
Małgorzata Adamiec
msolin@amu.edu.pl

SPECIALTY SECTION
This article was submitted to Plant Abiotic Stress, a section of the journal Frontiers in Plant Science

RECEIVED 09 June 2022
ACCEPTED 04 July 2022
PUBLISHED 22 July 2022

CITATION
Adamiec M, Dobrogojski J, Wojtyla Ł and Luciński R (2022) Stress-related expression of the chloroplast EGY3 pseudoprotease and its possible impact on chloroplasts' proteome composition.
Front. Plant Sci. 13:965143.
doi: 10.3389/fpls.2022.965143

Stress-related expression of the chloroplast EGY3 pseudoprotease and its possible impact on chloroplasts' proteome composition

Małgorzata Adamiec[1]*, Jędrzej Dobrogojski[2], Łukasz Wojtyla[1] and Robert Luciński[1]

[1]Department of Plant Physiology, Faculty of Biology, Institute of Experimental Biology, Adam Mickiewicz University in Poznań, Poznań, Poland, [2]Department of Biochemistry and Biotechnology, Faculty of Agronomy, Horticulture and Bioengineering, University of Life Sciences, Poznań, Poland

The EGY3 is a pseudoprotease, located in the thylakoid membrane, that shares homology with the family of site-2-proteases (S2P). Although S2P proteases are present in the cells of all living organisms, the EGY3 was found only in plant cells. The sequence of the pseudoprotease is highly conserved in the plant kingdom; however, little is known about its physiological importance. Results obtained with real-time PCR indicated that the expression of the *EGY3* gene is dramatically induced during the first few hours of exposure to high light and high-temperature stress. The observed increase in transcript abundance correlates with protein accumulation level, which indicates that EGY3 participates in response to both high-temperature and high light stresses. The lack of the pseudoprotease leads, in both stresses, to lower concentrations of hydrogen peroxide. However, the decrease of chloroplast copper/zinc superoxide dismutase 2 level was observed only during the high light stress. In both analyzed stressful conditions, proteins related to RubisCO folding, glycine metabolism, and photosystem I were identified as differently accumulating in *egy3* mutant lines and WT plants; however, the functional status of PSII during analyzed stressful conditions remains very similar. Our results lead to a conclusion that EGY3 pseudoprotease participates in response to high light and high-temperature stress; however, its role is associated rather with photosystem I and light-independent reactions of photosynthesis.

KEYWORDS

***Arabidopsis thaliana*, chloroplast, EGY3, high light stress, high-temperature stress, pseudoprotease**

Introduction

Pseudoenzymes are proteins sharing sequence homology with enzyme families but proven or predicted to be inactive due to mutations in amino acid motives crucial for catalytic activity. They are present in all kingdoms of life and are conserved in numerous protein families (Murphy et al., 2017). The pseudoenzymes are known to have divergent

functions. Many of them were proven to participate in the allosteric regulation of conventional enzymes (Lingaraju et al., 2014; Rosenberg et al., 2015), others serve as a scaffold for the assembly of enzyme complexes (Fulcher et al., 2018; Walden et al., 2018). Some pseudoenzymes are involved in positioning the active enzyme in the proximity of its substrate (Schäfer et al., 2014; Murphy et al., 2015; Rosenberg et al., 2015) and regulation of protein localization in a cell (Ng et al., 2013; Schroeder et al., 2014). Despite the growing amount of data, the knowledge about the functions and molecular action mechanisms of the pseudoenzymes remains very elusive, and the role of many of them remains unknown or poorly investigated. One of the pseudoenzymes, whose physiological importance remains poorly understood is the ethylene-dependent gravitropism-deficient and yellow-green-like 3 (EGY3) protein. The EGY3 belongs to the pseudoprotease class and shares homology with the family of site-2-proteases (S2P). These proteases are unusually hydrophobic integral membrane zinc-metalloproteases able to perform the proteolytic cleavage within the cell membrane. They are present, among others, in prokaryotic, mammalian, and plant cells. In general, they are involved in the process called regulated intramembrane proteolysis (RIP) by performing, within the cell membrane, the proteolytic cleavage of membrane-anchored transcription factors (Adamiec et al., 2017). S2P proteases were proven to participate in many different physiological processes. In prokaryotic cells, they are involved in pathogenesis, stress response, and sporulation, and in mammalian cells, they were proven to regulate lipid metabolism (Adamiec et al., 2017). In *Arabidopsis thaliana* five S2P proteolytically active proteases and EGY3 pseudoenzyme have been identified. Only one protease, encoded by the *AT4G20310* gene, was found to be located in the Golgi membrane (for review see Adamiec et al., 2017). Four of the proteases, namely EGY1, EGY2, S2P2, and ARASP, were experimentally confirmed to be located in chloroplasts. Also, the EGY3 pseudoenzyme was experimentally confirmed to be located in the chloroplast thylakoid membrane (Adamiec et al., 2019). The role of S2P in plants is poorly investigated. The lack of EGY1 protease leads in *A. thaliana* to pleiotropic effects, such as yellow-green, early senescence phenotype, deficiency in ethylene-induced gravitropism, or oversensitivity to ammonium stress (Chen et al., 2005; Guo et al., 2008; Yu et al., 2016). Also, the *Arabidopsis* serine protease (ARASP) is crucial for *A. thaliana* development since it lacks leads to emerging small, red cotyledons, underdeveloped roots, no apical meristem, and a life expectancy of fewer than 20 days (Bölter et al., 2006). Even less is known about the only pseudoenzyme homologous to this protease family – the EGY3 protein. This pseudoprotease was identified only in plant cells and remains highly conserved in the plant kingdom. In plants, grown in standard laboratory conditions, the lack of the protease does not lead to any visible phenotype changes; however, in *egy3* mutants, the increased value of the non-photochemical quenching and slower recovery rate after photoinhibitory treatment were observed (Adamiec et al., 2019). It has been also suggested that EGY3 may participate in response to salt stress by promoting the copper/zinc superoxide dismutase 2 (CSD2) stability and H_2O_2-mediated chloroplastic retrograde signaling (Zhuang et al., 2021). The transcriptional data indicate also that expression of the gene encoding EGY3 is significantly increased under the high-temperature treatment. These data suggest that EGY3 protein may be involved in the response to high light or high-temperature stresses; however, the knowledge on this subject remains limited only to a few observations. We decided to investigate this issue.

Materials and methods

EGY3 T-DNA insertion mutants

Two commercially available mutant lines with a T-DNA insertion in the *At1g17870* encoding the EGY3 protein were obtained from NASC (Nottingham Arabidopsis Stock Centre, Nottingham, United Kingdom) and used: SALK_128120 described as *egy3-1* and SALK_042231 described as *egy3-2*. The homozygosity of both lines was previously confirmed with the PCR technique, and the lack of the EGY3 protein was confirmed with the use of an anti-EGY3 antibody (Adamiec et al., 2019).

Growth and stress conditions

Wild-type (WT) and *A. thaliana* (L.) Heynh (ecotype Columbia) as well as *egy3-1* and *egy3-2* mutant lines were grown on sphagnum peat moss and wood pulp in 42-mm Jiffy peat pellets (AgroWit, Przylep, Poland) under photoperiod 16 h of light/8 h of darkness at an irradiance of 110 μmol m^{-2} s^{-1}, relative humidity of 70%, and constant temperature of 22°C for 4 weeks.

The high-temperature stress had been applied by transferring the 4-week plants to 40°C for 1, 3, 6, and 24 h, with the maintained photoperiod.

For the light stress, the plants were exposed to continuous light of intensity 1,000 μmol m^{-2} s^{-1} for 1, 3, 6, and 24 h.

EGY3 gene expression analysis

Total RNA from *A. thaliana* leaves (WT) was isolated using the GeneMATRIX Universal RNA Purification Kit (EURX®, Poland), according to the manufacturer's protocol. Isolated RNA was treated with RNase-free DNase (Thermo Fisher Scientific, Waltham, United States), in accordance with the manufacturer's instruction. Reverse transcription was performed using the RevertAid H Minus First Strand cDNA Synthesis Kit (Thermo Fisher Scientific, Waltham, United States) with random hexamers as primers and 5 μg of total RNA. The quantitative real-time PCR was performed according to Pietrowska-Borek et al. (2020) using the CFX96 Real-Time PCR Detection System (Bio-Rad, Hercules, United States) and iTaq Universal SYBR Green Supermix (Bio-Rad, Hercules, United States). The reaction was carried out in a

total volume of 20 µl with 1 µl of cDNA. For relative *EGY3* gene expression quantification in plants exposed to heat or high light stress, the comparative C_T method was used with the aldehyde dehydrogenase 3 (*ALDH3*, *At4g34240*) (for heat stress variant) and the cyclophilin 5 (*CYP5*, *At2g29960*; for high light stress) as the endogenous control. The amount of target normalized to an endogenous control is given by $2^{-\Delta\Delta CT}$. The primers for the *EGY3, ALDH3*, and *CYP5* genes are as follows:

EGY3:
Forward: 5′-GCCCGTCGTTTCTTGTGCCATC-3′.
Reverse: 5′-AAGCAGAAGCGAGGTCAGGTAC-3′.
ALDH3:
Forward: 5′-GCAGCGTATCTCTTCACAAACAAC-3′.
Reverse: 5′-ATCCCACTCTCCCCAACCCCAC-3′.
CYP5:
Forward: 5′-GAGAAAGGTGTAGGGAAGAGTGG-3′.
Reverse: 5′-CAAACTTCTGACCATAGATTGATTC-3′.

All primers were tested for non-specific amplification and primer-dimer formation by melting curve analysis. For each sample, three biological repetitions were performed, each in three technical repetitions.

Total leaf protein isolation

For single isolation, 100 mg of *A. thaliana* leaf tissue was used. The isolation of total leaf protein was performed with the use of Protein Extraction Buffer (PEB, Vannas, Agrisera), according to the manufacturer's instructions. The concentration of the extracted protein was measured with Lowry et al. (1951) method with the Lowry DC kit (Bio-Rad, Hercules, CA, United States).

SDS-PAGE and immunoblotting

The SDS-PAGE was performed, according to Laemmli (1970), with the use of 12% (w/v) polyacrylamide gels containing 6 M urea (Sigma-Aldrich, St. Louis, United States). After the separation, proteins were transferred to PVDF membranes (Bio-Rad, United States) and a standard western blot procedure was applied (Adamiec et al., 2018). The PVDF membrane was blocked using 4% BSA (BioShop, Burlington, Canada) and incubated with specific, primary antibodies for 90 min. Next incubation with a secondary antibody (Agrisera, Vannas, Sweden) was performed and the relevant bands were digitally registered using the ChemiDoc™MP Imaging System (Bio-Rad, Hercules, CA, United States) after 5 min of incubation with the Clarity Western ECL Substrate (Bio-Rad, Hercules, CA, United States). Quantification of the immunostained bands was performed using GelixOne software (Biostep GmbH, Jahnsdorf, Germany). Only blots with a linear relationship between the strength of the signal and the amount of protein were analyzed. The linearity of the signal was investigated in our previous work (Adamiec et al., 2018).

Antibodies

The highly purified N-terminal region (AA 51–250) of EGY3 from *A. thaliana* was used to produce the specific, polyclonal, rabbit anti-EGY3 antibody. The antibody was custom produced by Agrisera and their specificity has been described by us earlier (Adamiec et al., 2019). Anti-PsaB, anti-GLDP, anti-CSD2, and secondary antibodies were purchased from Agrisera (Vännäs, Sweden).

Chlorophyll fluorescence measurements

Chlorophyll fluorescence measurements were conducted using FMS1 (Photon System Instruments, Brno, Czech Republic) run by Modfluor software. Each measurement was preceded by adaptation in the dark for 30 min. The measurements were performed according to the protocol described by Genty et al. (1989). The minimum fluorescence yield (F_0) was established at the beginning of the measurement. The maximum quantum yield of PSII (F_v/F_m) and quantum efficiency of open centers in the light (F_v'/F_m') were calculated according to Genty et al. (1989). The applied actinic light intensity was equal to the irradiance before dark-adaptation: 110 µmol m^{-2} s^{-1} for control conditions and plants exposed to high-temperature stress and 1,000 µmol m^{-2} s^{-1} for plants exposed to high light. The photochemical quenching (qP), a photochemical yield of photosystem II (ΦPSII) as well as the non-photochemical quenching parameter (NPQ) were calculated according to Maxwell and Johnson (2000). Ten plants from each variant (*WT, egy3-1, and egy3-2*) were measured in each replicate.

2D Electrophoresis and LC–MS/MS analysis

Chloroplast isolation and fractioning

Chloroplasts were isolated according to our previous work (Adamiec et al., 2018) using the Sigma Chloroplast Isolation Kit (Sigma- Aldrich, St. Louis, United States). For single isolation, 20 g of *A. thaliana* leaf tissue was used. The tissue was homogenized in an ice-cold homogenization buffer with the addition of 1% (v/v) Protease Inhibitor Cocktail (PIC; Sigma-Aldrich, St. Louis, United States). The homogenate was filtered through a Mesh 100 filter and centrifuged at 200 *g* for 1 min at 4°C to remove the unbroken cells. Next, the centrifugation at 1,500 *g* for 10 min at 4°C was performed to sediment the chloroplasts and then resuspended in the homogenization buffer with 1% (v/v) PIC. Subsequently, the intact chloroplasts were obtained, as a pellet, by centrifugation of the chloroplast suspension through

40% (w/v) Percoll for 6 min at 1,700 *g*. To separate the stroma and the thylakoid membranes, the intact chloroplasts were resuspended in the lysis buffer with the addition of 1% (v/v) PIC and centrifuged for 10 min at 12,250 *g*. Both the supernatant containing stroma and a green pellet containing the thylakoid membranes were frozen in liquid nitrogen, stored at −80°C, and then used for protein extraction.

Protein extraction from the thylakoids and the stroma

Slightly different procedures were used to extract protein from thylakoids and stroma. For extract protein from thylakoids, the thylakoids membranes were homogenized in 4°C with the EB buffer (Tris–HCl pH 7.5, 25% (w/v) sucrose, 5% glycerol (v/v), 10 mM EDTA, 10 mM EGTA, 5 mM KCl, and 1 mM DTT) with the addition of 0.5% (w/v) PVPP and 1% (v/v) PIC to avoid proteolysis. Subsequently, centrifugation was performed at 600 *g* for 3 min. The supernatant was diluted 2-times with water to reach a 12% concentration of sucrose in the EB buffer and centrifuged for 60 min at 100,000 *g*. The pellet was resuspended in the Tris–HCl buffer (pH 7.5) containing 5 mM EDTA and EGTA and 1% (v/v) PIC. The Bradford method (Bradford, 1976) was used to measure the protein concentration, and then, proteins were solubilized in the presence of 2% (w/v) Brij® 58 (Sigma-Aldrich, St. Louis, United States) for 1 h at 4°C and precipitated with acetone with 10% (w/v) TCA and 0.07% (v/v) β-mercaptoethanol overnight at −20°C. After the precipitation, the proteins were pelleted by centrifugation for 15 min at 20,000 *g*, washed three times with pure acetone, and resuspended in a buffer containing 7 M urea, 3 M thiourea, 2% (w/v) amidosulfobetaine-14 (ASB-14; Sigma-Aldrich, St. Louis, United States), and 65 mM DTT for 2 h at room temperature with constant, gentle shaking and then applied for isoelectrofocusing (Adamiec et al., 2018).

The extraction of stroma proteins consisted of their precipitation with 3 volumes of acetone with the addition of 10% (w/v) TCA and 0.07% (v/v) β-mercaptoethanol overnight at −20°C. The sequential steps of washing the proteins and suspending them in the buffer were identical to those for the thylakoid proteins, except that 2% ASB in the buffer was replaced with 4% CHAPS (Sigma-Aldrich, St. Louis, United States).

Isoelectrofocusing and spot detection

Isoelectrofocusing was carried out using the gel strips forming an immobilized pH gradient from 3 to 10 (Bio-Rad, Hercules, CA, United States). Strips were rehydrated overnight at room temperature and the isoelectrofocusing was performed at 18°C in the Protean i12 IEF Cell (Bio-Rad, Singapore) for 90 min (for thylakoid membrane proteins) or 60 min (for stroma proteins) at 300 V, 90 min at 3,500 V, and 20,000 Vh at 5,500 V. After the IEF strips were equilibrated according to Kubala et al. (2015) and the proteins were separated according to their molecular mass using denatured electrophoresis in 12% (w/v) acrylamide gels with the addition of 6 M urea. After electrophoresis, the gels were stained with Coomassie Brilliant Blue (CBB) G-250 and photographed with a ChemiDoc™MP Imaging System (Bio-Rad, Hercules, CA, United States). Finally, four images, representing two independent biological replicates, were obtained and used for the image analysis.

The spot detection and the image analysis were performed according to our previous work (Adamiec et al., 2018), using the PDQest Advanced 2-D Gel Analysis Software (Bio-Rad, Hercules, United States). Only the differentially accumulated proteins (at $P<0.05$) between WT and *egy3* mutant lines with the ratio of at least 2.0 in the absolute value of protein abundance were taken into consideration and further analyzed. The selected spots were excised manually and analyzed by liquid chromatography coupled to the mass spectrometer in the Laboratory of Mass Spectrometry, Institute of Biochemistry and Biophysics, Polish Academy of Science (Warsaw, Poland), according to the previous description by Kubala et al. (2015). The Mascot Distiller software was used to process the raw data, and then, the obtained protein masses and fragmentation spectra were matched TAIR filter with the use of the Mascot Daemon engine search. The search parameters were set as described previously (Adamiec et al., 2018). Only the peptides with a Mascot score exceeding the threshold value corresponding to < 0.05 false-positive rate have been considered as positively identified.

Detection of hydrogen peroxide

3,3′-diaminobenzidine (DAB) staining was performed according to Daudi and O'Brien (2012). Rosette leaves of the plants treated with abiotic stress and control plants were incubated in the DAB staining solution (10 mM Na_2HPO_4, 0.05% [v/v] Tween, 1 mg/ml DAB, pH: 7.4) overnight. Later, the chlorophyll was cleared by boiling the leaf in a bleaching solution (3 ethanol: 1 acetic acid: 1 glycerol) for 20 min. The samples were photographed using a ChemiDoc™MP Imaging System (Bio-Rad, Hercules, CA, United States).

Quantification of H_2O_2 levels with DAB was performed according to Boyidi et al. (2021) with modifications. The DAB-stained leaves have been weighed, homogenized, extracted in 2 ml on 1 mg of fresh tissue of perchloric acid, and centrifuged at 10,000 *g* for 10 min. Next, the absorbance was measured at 450 nm. The H_2O_2 levels were represented as μmol/g FW.

Spectrophotometric determination of hydrogen peroxide was performed based on the titanium (Ti^{4+}) method according to Becana et al. (1986). *Arabidopsis thaliana* leaves (0.25 g) were homogenized in 3 ml of 100 mM phosphate buffer pH 7.8 with the addition of active charcoal at a proportion of 1:5. The homogenate was centrifuged at 15,000 *g* for 30 min at 4°C. For spectrophotometric measurement, the reactive mixture containing 100 mM phosphate buffer pH 7.8, plant extract, and the titanium reagent consisting of 0.3 mM 4-(2-pyridylazo) resorcinol and 0.3 mM titanium potassium tartrate at the ratio 1:1 was prepared in spectrophotometric cuvettes. The absorbance

was measured at 508 nm against the calibration curve prepared for the standards containing H_2O_2 from 0 to 100 nmol. The accumulation of H_2O_2 was expressed as an amount of H_2O_2 in 1 g of FW.

Results

The changes of *EGY3* expression level in response to high light and high-temperature stresses in wild-type *Arabidopsis thaliana* plants

The real-time PCR experiments revealed that the expression level of the *EGY3* gene is dramatically induced during exposure to the high-temperature stress. The strongest induction of transcription was observed in the initial stages of stress. After 1 h of the exposition of WT plants to 40°C, the relative expression of the *EGY3* gene was induced about 630-fold. The longer exposure to stressful conditions (for 3 h) resulted in a 190-fold change increase in the level of transcription, and after the 6 h of high-temperature stress, the *EGY3* expression was similar to the one in control conditions. After 24 h of plant exposure to high temperature, the increase in *EGY3* expression level was relatively smaller concerning changes observed during the first hours of exposition to stressful conditions and represented 13-fold change concerning the initial level (Figure 1A). Also, during the exposition to high light stress, the increase in the relative expression of the *EGY3* gene was observed, and similarly to high-temperature stress, the most significant increase was detected at the initial stages of exposition to stress. The 1 h of high light stress resulted in 11-fold increase of *EGY3* transcription and 3 h of elevated irradiance caused 23-fold up-regulation. After 6 h of exposition to high light, a 6-fold increase in *EGY3* relative expression level was observed, while after 24 h of high light stress, the abundance of transcript remained at the level similar to control conditions (Figure 1B).

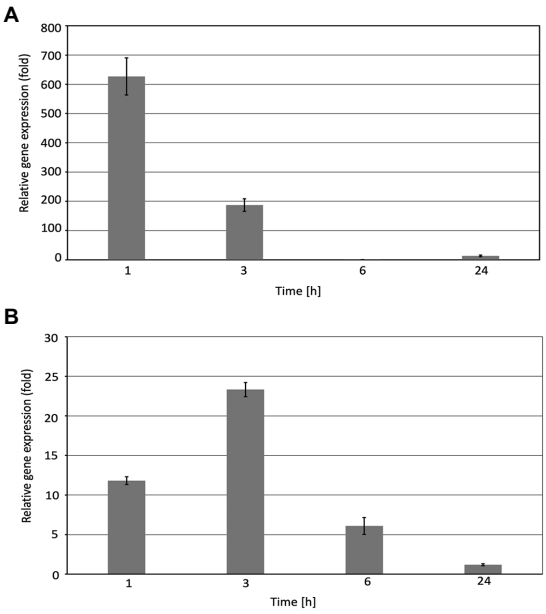

FIGURE 1
Relative *EGY3* gene expression in *Arabidopsis thaliana* leaves exposed to heat stress **(A)** or high light **(B)**. *Arabidopsis thaliana* plants were exposed to 1,000 $\mu molm^{-2}$ s^{-1} or for 40°C for 1 h, 3 h, 6 h, and 24 h, and then, the total RNA was isolated from leaves and transcribed into cDNA used as a template for the quantitative real-time PCR, according to the description in the Material and Methods. *CYP5* and *ALDH3* were used as an endogenous control for the analysis of plants exposed to high light or heat stress, respectively. ± means standard deviation of six replication, an asterisk indicates a statistically significant change compared to the 0 h time base value.

The changes of EGY3 protein abundance in response to high light and high-temperature stresses in wild-type *Arabidopsis thaliana* plants

The changes observed at the gene expression level correlated with changes in protein abundance. During the high-temperature stress, the increase in protein abundance was highest after 1 h and amounted to 250% of the control level. The protein overaccumulated also after 3 and 6 h exposition to a high temperature to 126 and 150% of initial values. The 24 h long exposure to high temperature resulted in a decrease in protein accumulation level to 40% concerning control conditions (Figure 2A).

The 1 h exposition to high light resulted in a 185% increase in protein abundance. A similar level (180%) was observed after 3 h of exposition and the application of stressful conditions for 6 h increased to 150% of the initial value. The 24 h of exposition to increased irradiance did not result in significant changes in EGY3 abundance (Figure 2B).

Comparative analysis of the chloroplast proteome

Based on previous analysis concerning changes in the quantity of *EGY3* transcript and protein, we decided to perform an analysis of changes in the proteome of *egy3* mutants in plants exposed to the elevated irradiance for 3 h. The same exposure time was selected for further research on plants exposed to high temperature. From the WT plants and both *egy3* mutant lines exposed for 3 h to a given stress, the thylakoid membrane fraction and stroma fraction were isolated. Both fractions were subjected to two-dimensional electrophoresis and protein spots whose accumulation level differed at least 2-fold from that observed in wild-type in both *egy3* mutant lines in two separate biological replicates were identified (Figures 3–6). For further analysis by

LC–MS/MS, from the high light stress experimental variant, we choose five protein spots from thylakoid fraction and four from the stroma fraction. From the high-temperature experimental variant, three spots from the thylakoid fraction and five from the stroma fraction were chosen and LC–MS/MS analysis was performed. Based on pH, molecular mass parameters, and score parameters, the most probable proteins whose abundance may be EGY3 dependent were selected (Tables 1 and 2).

Among the protein spots differently accumulating in *egy3* mutants' thylakoid membranes in response to exposition to high light, two were characterized by a decrease in abundance. Within these spots, the Lhcb6 and PsaB proteins were identified. In the remaining three spots, overaccumulation was observed concerning WT plants. Within these spots, subunit NDH-M of NAD(P)H: plastoquinone dehydrogenase complex, PDE334 protein which is part of proton-transporting ATP synthase complex F(o), and ATP synthase epsilon chain (ATPE) were identified (Table 1). The localization of all these proteins in thylakoid membranes was experimentally confirmed (Friso et al., 2004; Peltier et al., 2004; Rumeau et al., 2005). In the stroma, exposition to high light stress leads to overaccumulation protein in *egy3* mutant lines of all four chosen protein spots. Within these spots, ATGSTU20 protein, which is a glutathione transferase, glycine decarboxylase P-protein 1 (AtGLDP1), CPN60A which encodes chaperonin-60 alpha, and heat shock protein CPHSC70 were identified (Table 1). Also, in this case, stromal localization of these proteins was experimentally confirmed (Peltier et al., 2004; Rutschow et al., 2008; Ferro et al., 2010). The only exception is the ATGSTU20 protein, which localization in chloroplasts is described without indication of the compartment (Zybailov et al., 2008). Predictive algorithms indicate, however, no high hydrophobicity regions in the amino acid sequence of this protein, thus its stroma localization seems highly probable (Schwacke et al., 2003).

In the thylakoid fraction from plants exposed to high temperature, three protein spots, which significantly increased abundance in *egy3* mutant, were chosen for LC–MS/MS. Within these spots, PSAD-2 predicted to be photosystem I reaction center subunit II, ferrochelatase 2 (ATFC-II), and ATPase F subunit (ATPF) proteins were identified (Table 2), and localization of these proteins in the thylakoid membrane was experimentally confirmed (Lister et al., 2001; Peltier et al., 2004). Among the protein spots from

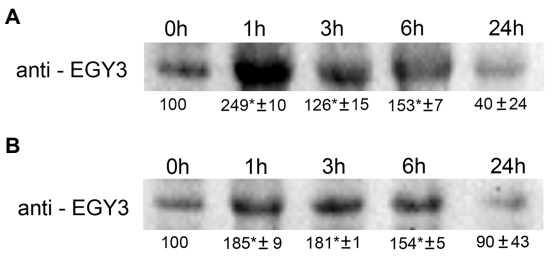

FIGURE 2
Immunoblot quantification of EGY3 protein in wild-type plants (WT) under high-temperature stress **(A)** and during an exposition to high light conditions **(B)**. The plants were exposed for 1 h, 3 h, 6 h, and 24 h for 40°C to cause high-temperature stress and for 1,000 μmolm^{-2} s^{-1} to cause high light stress. "±" means standard deviation, the asterisk means the significant difference in comparison to 0 h time (no stress).

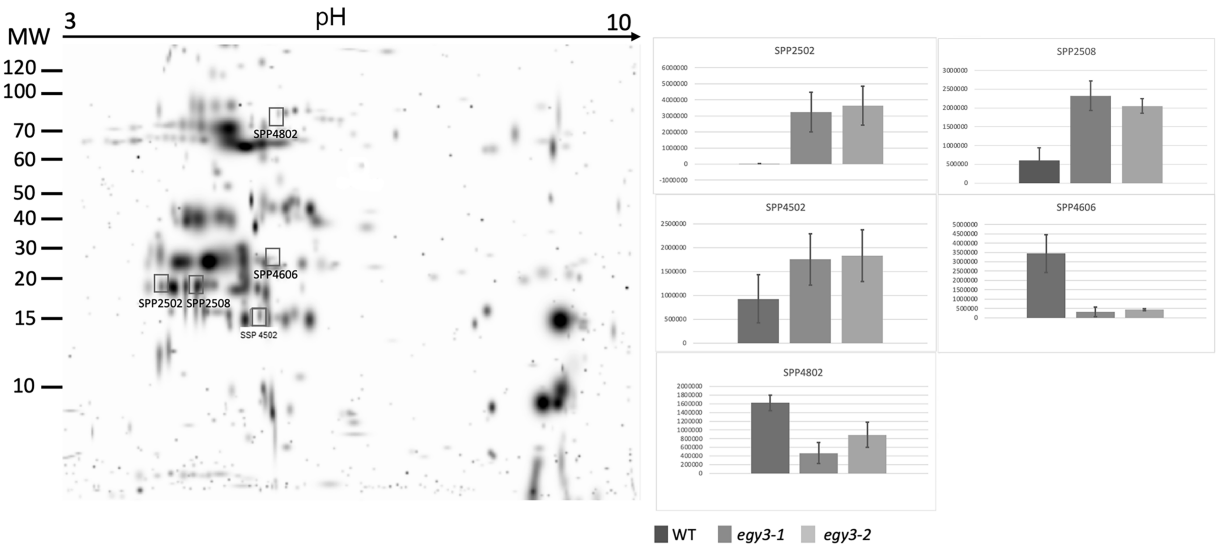

FIGURE 3
Two-dimensional electrophoresis gels of thylakoid membrane proteins isolated from wild-type (WT) and *egy3-1* and *egy3-2* lines, exposed to 3h of high light conditions. Proteins were separated using 2-D gel electrophoresis with IEF (pH 3–10) and detected with Coomassie Brilliant Blue staining. The image is digitally generated using the PDQuest Advanced 2-D Gel Analysis Software, (Bio-Rad, Hercules, United States) master gel, based on four electrophoretic separations made for two independent biological repetitions. The protein accumulation in the bar graphs was expressed in arbitrary units.

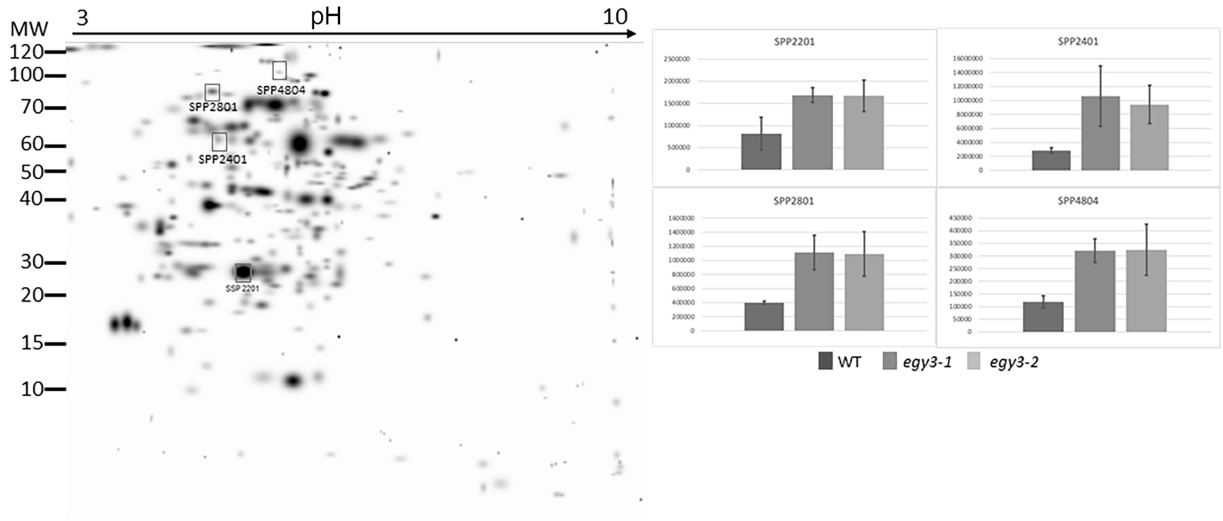

FIGURE 4
Two-dimensional electrophoresis gels of stroma proteins isolated from wild-type (WT) and *egy3-1* and *egy3-2* lines, exposed to 3h of high light conditions. Proteins were separated using 2-D gel electrophoresis with IEF (pH 3–10) and detected with Coomassie Brilliant Blue staining. The image is digitally generated using the PDQuest Advanced 2-D Gel Analysis Software, (Bio-Rad, Hercules, United States) master gel, based on four electrophoretic separations made for two independent biological repetitions. The protein accumulation in the bar graphs was expressed in arbitrary units.

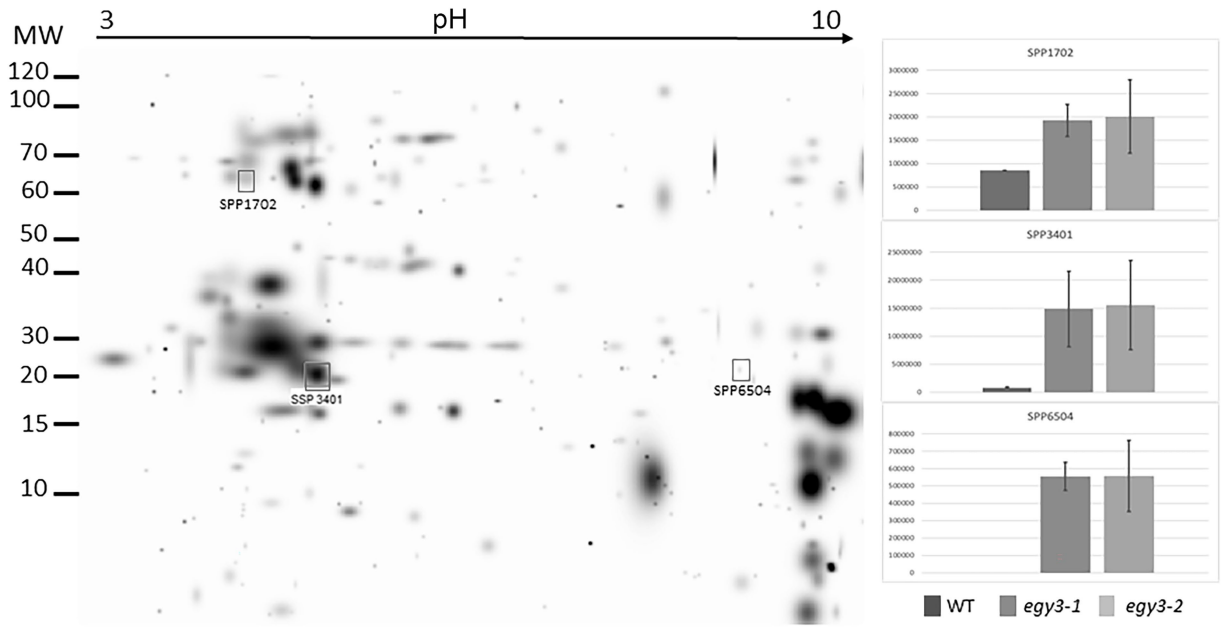

FIGURE 5
Two-dimensional electrophoresis gels of thylakoid membrane proteins isolated from wild-type (WT) and *egy3-1* and *egy3-2* lines, exposed to 3h of 40°C. Proteins were separated using 2-D gel electrophoresis with IEF (pH 3–10) and detected with Coomassie Brilliant Blue staining. The image is digitally generated using the PDQuest Advanced 2-D Gel Analysis Software, (Bio-Rad, Hercules, United States) master gel, based on four electrophoretic separations made for two independent biological repetitions. The protein accumulation in the bar graphs was expressed in arbitrary units.

stroma fraction, two spots were absent in WT plants but present in both *egy3* mutant lines, and three spots with a lower abundance in *egy3* mutants were chosen. In the spots absent in WT plants, ACT domain-containing protein (ACR11) and glycine decarboxylase P-protein 2 (GLDP2) were identified, while in spots with decreased accumulation, RubisCO accumulation factor-like protein, encoded

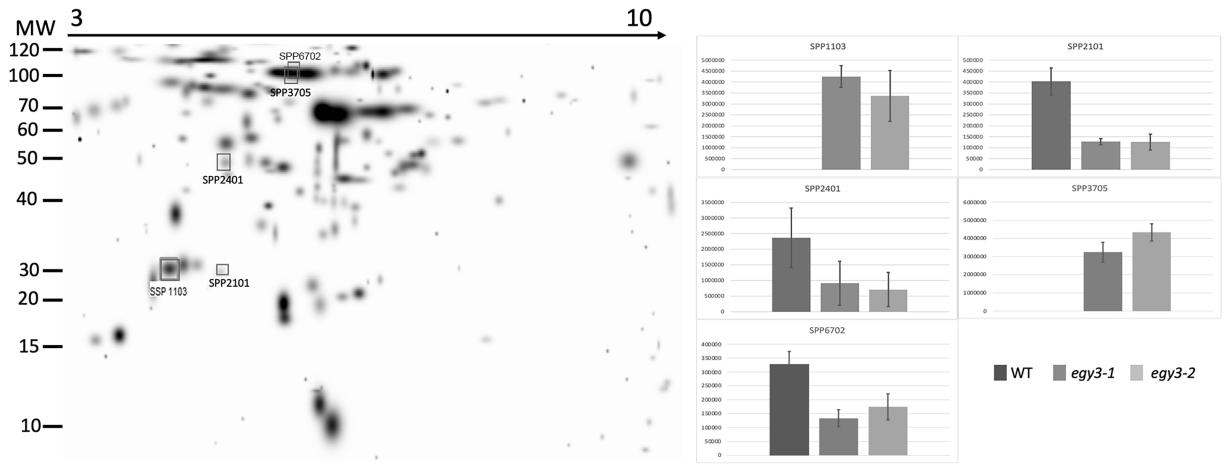

FIGURE 6
Two-dimensional electrophoresis gels of stroma proteins isolated from wild-type (WT) and *egy3-1* and *egy3-2* lines, exposed to 3h of 400°C. Proteins were separated using 2-D gel electrophoresis with IEF (pH 3–10) and detected with Coomassie Brilliant Blue staining. The image is digitally generated using the PDQuest Advanced 2-D Gel Analysis Software, (Bio-Rad, Hercules, United States) master gel, based on four electrophoretic separations made for two independent biological repetitions. The protein accumulation in the bar graphs was expressed in arbitrary units.

by *At5g28500* gene, triosephosphate isomerase (TPI), and glycine decarboxylase P-protein 1 (GLDP1) were present (Table 2). The localization of most of these proteins in chloroplast stroma was experimentally confirmed (Peltier et al., 2004; Rutschow et al., 2008; Ferro et al., 2010), except for GLDP2, which was described as located in chloroplast without indication of a compartment (Zybailov et al., 2008); however, the amino acid sequence of the protein lacks highly hydrophobic regions (Schwacke et al., 2003), thus its localization is stroma seems probable.

The changes in abundance of PsaB and GLDP proteins were confirmed with the immunoblot technique (Figures 7A,B). The accumulation level of PsaB protein after 3 h of exposition to high light in WT plants was 80% of the initial state, while in both *egy3* mutant lines, its abundance was reduced to 15% in the *egy3-1* mutant line and 19% in *egy3-2* mutant line. Significantly greater, in WT plants, loss of PsaB was also observed in both *egy3* mutant lines after 3 h exposition to high temperature. In WT plants, the protein level remained at a level of 88%, while in *egy3* mutant lines, its abundance was decreased to 57% in the *egy3-1* mutant line and 61% in the *egy3-2* mutant line (Figure 7A).

The antibody used for the investigation of changes in abundance of the glycine decarboxylase P-protein was specific for both GLDP1 and GLDP2, so the entire pool of GLDP proteins was investigated. The GLDP1 protein was previously detected in both stroma and thylakoid fraction (Ferro et al., 2010), and GLDP2 is described as located in chloroplast without a more specific indication of the compartment (Zybailov et al., 2008). That is why we used for anti-GLDP hybridization experiments the whole leaf protein fraction. In response to high light stress, in both *egy3* mutant lines, the abundance of GLDP proteins was reduced to 20–30%, while in WT plants, its accumulation level remained similar to control conditions. A similar effect was observed after exposition to high-temperature stress; however, the decrease in GLDP abundance was less dramatic – approximately 50–60% of the initial value (Figure 7B). In the WT plants, exposition to high temperature does not cause changes in GLDP accumulation level.

The changes in abundance of copper/zinc superoxide dismutase 2

Since it was proven that in the salt stress, the EGY3 protein participates in the stabilization of copper/zinc superoxide dismutase 2 (CSD2), which is responsible for the conversion of superoxide anion into hydrogen peroxide and thus is involved in H_2O_2–mediated signaling. We decided to investigate the accumulation changes of CSD2 in *egy3* mutants in response to analyzed stresses. Our results indicate that after 3 h of exposition to high light stress, the abundance of CSD2 in WT plants remains similar, while in both *egy3* mutant lines, its accumulation level is significantly decreased (Figure 8). During the high-temperature stress, however, we did not observe significant differences in the accumulation of the CSD2, between WT plants and *egy3* mutant lines (Figure 8).

The accumulation level of the hydrogen peroxide in *egy3* mutants

The observed changes in the level of the CSD2 accumulation have become a premise for the determination of the changes in the concentration of hydrogen peroxide in *egy3* mutants in response to analyzed stresses. Three different methods of measurement were applied: a method based on the titanium (Ti^{4+}), DAB staining, and spectrophotometric DAB quantification. The results

TABLE 1 The proteins identified as differently accumulating in *egy3* mutants in response for 3h exposition to high light.

Locus	Protein name	Spot number	Direction of change	Fraction	MW	pI	Protein score		Number of peptide matches		Protein coverage (%)	
					Theor/ exper (kDa)	Theor/ exper	I	II	I	II	I	II
AT1G15820	Lhcb6	SPP4606	D	T	28/27.5	7.0/6.7	199	138	2	1	10.9	7
ATCG00340	PsaB	SPP4802	D	T	80/82.5	7.0/6.8	205	114	4	1	6.1	1.6
AT4G32260	PDE334	SPP2508	O	T	24/23.9	6/5.8	401	241	5	5	23.3	19.2
AT4G37925	NDH-M	SPP2502	O	T	24/24.9	5/4.8	956	235	13	3	39.6	18.4
ATCG00470	ATPE	SPP4502	O	T	17/14.5	6.5/5.8	40	32	1	1	11.4	8.1
At1G78370	ATGSTU20	SPP2201	O	S	25/25.1	5.5/5.4	812	767	17	14	33.6	33.6
AT4G33010	AtGLDP1	SPP4804	O	S	115/113.8	6.5/6.5	1,216	840	22	18	12.7	12.6
AT2G28000	CPN60A	SPP2401	O	S	60/62.2	5/5.1	628	710	9	11	16.9	18.9
AT5G49910	CPHSC70-2	SPP2801	O	S	80/77	5/5.2	201	675	5	11	7.8	11.8

Selected spots were cut from two gels representing different *egy3* mutant lines and subjected to a separate LC–MS/MS analysis. Only proteins identified in both replicates were taken for further consideration. Based on pH, molecular mass parameters, and score parameters from proteins identified by the LC–MS/MS method we selected the most probable proteins whose abundance may be EGY3 dependent. D – decrease in *egy3*; O – overaccumulation in *egy3*; T – thylakoid fraction (grey highlighted), S – stroma fraction (non-highlighted). The exact location of individual protein spots on polyacrylamide gels after 2-D electrophoresis is shown in Figure 3 (thylakoid fraction) and Figure 4 (stroma fraction).

obtained with these three methods were consistent. In both *egy3* mutant lines, in the result of the 1 h exposition to the high light, the increase in H_2O_2 concentration was significantly smaller than observed in WT plants (Figures 9A, C). Similarly, exposure to 1 h high-temperature stress leads to a lower, than in WT plants, increase in abundance of hydrogen peroxide (Figures 9B, C).

The functional status of PSII in *egy3* mutants during high light and high-temperature stress

It is well known that both high light and high-temperature stresses cause severe damage to PSII (Yamamoto, 2016). The dramatic changes in EGY3 transcript and protein abundance during both stresses prompt us to investigate the functional status of PSII in *egy3* mutants. The measurements performed with the PAM fluorescence technique included minimum fluorescence yield (F_o), the maximum quantum yield of PSII (F_v/F_m), photochemical quenching (qP), and non-photochemical quenching (NPQ). Unexpectedly, the changes observed in the analyzed parameters were hardly noticeable. The high-temperature stress did not result in any significant differences in values of analyzed parameters between *egy3* mutant lines and WT plants (Figure 10). During the exposition to high light, in *egy3* mutant lines, we did not observe any significant differences in qP parameter values concerning WT plants (Figure 11). The values of minimum fluorescence yield and maximum quantum yield of PSII in *egy3* mutants were similar to those observed in WT plants in most analyzed time variants. The most differentiating parameter was the NPQ since significant differences between both *egy3* mutant lines and wild-type plants were observed in three of the analyzed time points – 0, 1, and 3 h (Figure 10; Table 3).

Discussion

The accumulation of *EGY3* transcript and protein during high-temperature and high light stresses

The performed experiments indicated that the *EGY3* transcript drastically over accumulates after 1 and 3 h of exposition to high-temperature stress. This observation is consistent with previous results, where 16 days old *A. thaliana* plants were exposed to a high temperature which resulted in a significant increase in the abundance of *EGY3* transcript both in roots and shoots (Kilian et al., 2007). In that experiment, however, the temperature stress was applied only for 3 h and then plants were transferred to 25°C for recovery. Our results showed that the longer, 24 h, exposition to high-temperature stress is also accompanied by increased *EGY3* transcript abundance. These results indicate that transcription of *EGY3* increases not only in response to short-term high-temperature stress but is also maintained, however, to a lesser

10.3389/fpls.2022.965143

TABLE 2 The proteins identified as differently accumulating in *egy3* mutants in response for 3h exposition to high temperature.

Locus	Protein name	Spot number	Direction of change	Fraction	MW	pI	Protein score		Number of peptide matches		Protein coverage (%)	
					Theor/exper (kDa)	Theor/exper	I	II	I	II	I	II
At1G03130	PSAD-2	SPP6504	O	T	20/22.3	9.5/9.8	128	56	2	2	10.8	6.9
AT2G30390	ATFC-II	SPP1702	O	T	58/56.8	5.2/5.1	75	72	1	1	2.3	2.3
ATCG00130	ATPF	SPP3401	O	T	19/21	6.0/6,1	151	108	4	3	23.4	13.6
AT1G16880	ACR11	SPP1103	P	S	30/31.4	4.6/4.9	680	684	10	11	16.9	19.7
AT5G28500	RubisCO accumulation factor-like protein	SPP2401	D	S	45/48.3	4.8/5.0	464	348	8	6	14.5	9.7
AT2G26080	GLDP2	SPP3705	P	S	100/114.7	6.2/6.1	366	336	6	5	6.1	4.6
AT4G33010	GLDP1	SPP6702	D	S	100/113.8	6.2/6.5	395	246	8	5	6.8	4.3
AT3G55440	triosephosphate isomerase	SPP2101	D	S	30/27.4	5,2/5.4	318	110	5	2	22	8.8

Selected spots were cut from two gels representing different *egy3* mutant lines and subjected to a separate LC–MS/MS analysis. Only proteins identified in both replicates were taken for further consideration. Based on pH, molecular mass parameters, and score parameters from proteins identified by the LC–MS/MS method, we selected the most probable proteins which abundance may be EGY3 dependent. D – decrease in *egy3*; O – overaccumulation in *egy3*; P – present in *egy3* but not in WT; T – thylakoid fraction (grey highlighted), S – stroma fraction (non-highlighted). The exact location of individual protein spots on polyacrylamide gels after 2-D electrophoresis is shown in Figure 5 (thylakoid fraction) and Figure 6 (stroma fraction).

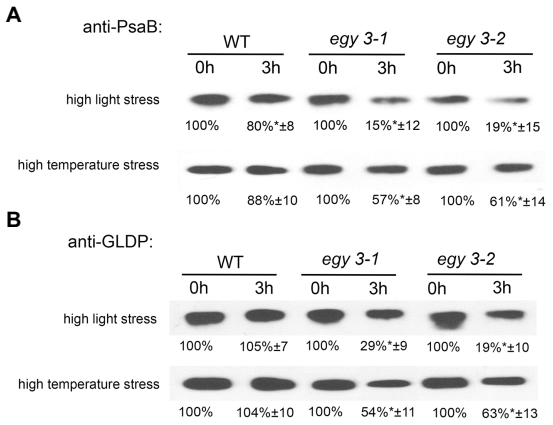

FIGURE 7
Immunoblot quantification of PsaB **(A)** and GLDP **(B)** proteins in wild-type (WT) and *egy3-1* and *egy3-2* mutant plants under high light and high-temperature conditions. Plants were exposed to 1,000 $\mu molm^{-2}$ s^{-1} (high light) or 40°C (high temperature) for 0 and 3 h. Total protein (6 µg) was immunologically analyzed using an anti-PsaB and anti-GLDP antibodies. GelixOne software was used to quantify the protein content. "±" indicates the SD determined in the analysis of samples obtained from three biological replicates, each of which was obtained by isolation of total protein from a minimum of 20 plants.

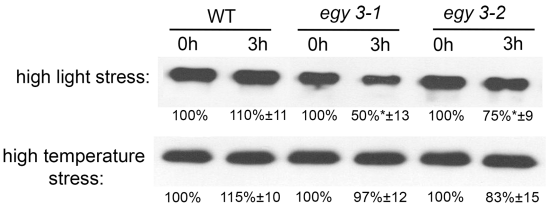

FIGURE 8
Immunoblot quantification of CSD2 protein in wild-type (WT) and *egy3-1* and *egy3-2* mutant plants under high light and high-temperature conditions. Plants were exposed to 1,000 $\mu molm^{-2}$ s^{-1} (high light) or 40°C (high temperature) for 0 and 3 h. Total protein (5 µg) was immunologically analyzed using an anti-CSD2 antibody. GelixOne software was used to quantify the CSD2 content. "±" indicates the SD determined in the analysis of samples obtained from three biological replicates, each of which was obtained by isolation of total protein from a minimum of 20 plants.

degree during long-term exposition to elevated temperature. The transcript levels, however, do not always correlate well with changes in protein abundance. The relationship between the protein accumulation and the level of a transcript was proven to depend on *inter alia* localization and the function of the protein (Baerenfaller et al., 2012; Liu et al., 2016). Our results provide data confirming the abundance of EGY3 protein increases most significantly after 1 h of exposition to high-temperature stress and it remains elevated also after 3 and 6 h of exposition to high temperature, which correlates well with changes observed at the transcriptional level. The 24-h exposition to 40°C leads, however, to a decrease in EGY3 protein level concerning the one observed

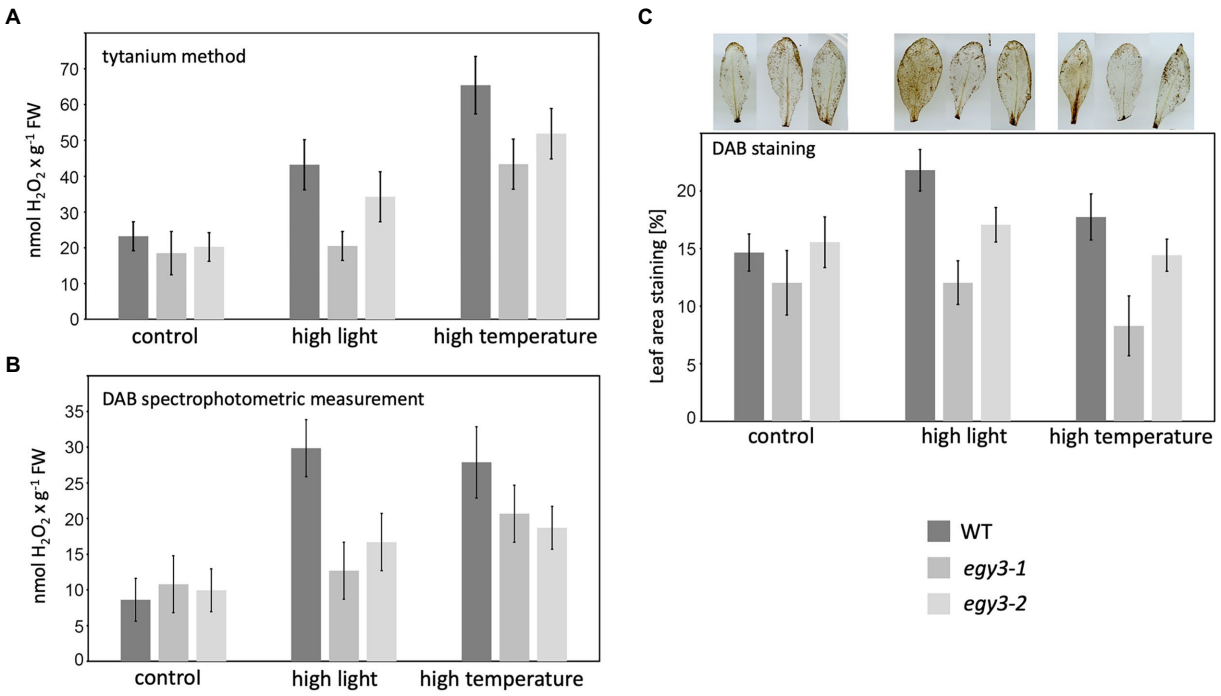

FIGURE 9
Accumulation of hydrogen peroxide in WT plants and *egy3* mutant lines after 1 h exposition to high light and high-temperature stress. **(A)** Titanium (Ti^{4+}) method staining **(B)** DAB staining spectrophotometric measurement **(C)** percentage of leave area staining with DAB. The values presented for Titanium (Ti^{4+}) method staining and DAB staining spectrophotometric measurement are average from two biological replicates (10 plants each). The values presented for the percentage of leave area staining with DAB are average from three biological replicates (10 leaves each).

in control conditions. This is inconsistent with changes in transcript abundance which remains elevated after 24 h of high-temperature stress. Based on these data, it can be assumed that the physiological role of EGY3 is associated with short-term exposure to high-temperature stress.

The changes in the transcription level of *EGY3* in response to high light stress were not investigated so far. Our results indicate that also during this stress after 1 and 3 h of exposition, the increased abundance of *EGY3* transcript is observed. This overaccumulation correlates with protein abundance which was significantly increased after 1, 3 and 6 h of exposition to high irradiance. Thus, EGY3 protein seems also to play an important role in response to short-term exposure to high light stress.

It was shown that the EGY3 pseudoprotease participates in the stabilization of a chloroplastic copper/zinc superoxide dismutase (CSD2) in response to salt stress (Zhuang et al., 2021). Our results indicate that in response to high light stress, the presence of EGY3 pseudoprotease reassures a higher abundance of CSD2. This result correlates with hydrogen peroxide concentrations, which are lower in *egy3* mutant exposed to analyzed stress conditions. These findings agree with the previous findings concerning the EGY3 role in the salt-stress response (Zhuang et al., 2021). The exposition to high-temperature stress, however, did not cause any statistically significant differences in the abundance of CSD2 protein in *egy3* mutants; however, the lower, than in WT plants, the concentration of hydrogen peroxide was observed. This inconsistency may suggest that in the case of temperature stress, there is a different, CDS2-independent mechanism, leading to lower H_2O_2 concentrations and/or a lower activity of CSD2 itself.

The proteins accumulated differently in response to high light stress

Among proteins identified as those whose accumulation level, in response to high light stress, may be dependent on EGY3 were proteins involved in light-dependent photosynthetic reactions. Three of these proteins: ATPE, PDE334, and NDH-M were identified as overaccumulating. The ATPE and PDE334 proteins were predicted to be involved in ATP synthesis (Berardini et al., 2015), while NDH-M is a subunit of the NDH complex involved in cyclic electron transport within PSI (Rumeau et al., 2005) and alleviating of oxidative stress (Peng et al., 2011). In turn, the abundance of PsaB which is the core protein of PSI was decreased. The proteins CPN60A and CPHSC70-2 (*At5g49910*), which were also identified as overaccumulating in *egy3 A. thaliana* mutant lines, were described as participating in protein folding (Berardini et al., 2015). The CPN60A and CPHSC70-2 (*At5g49910*) have, according to the STRING database (Szklarczyk et al., 2018), relatively high coexpression scores (0.588) not only in

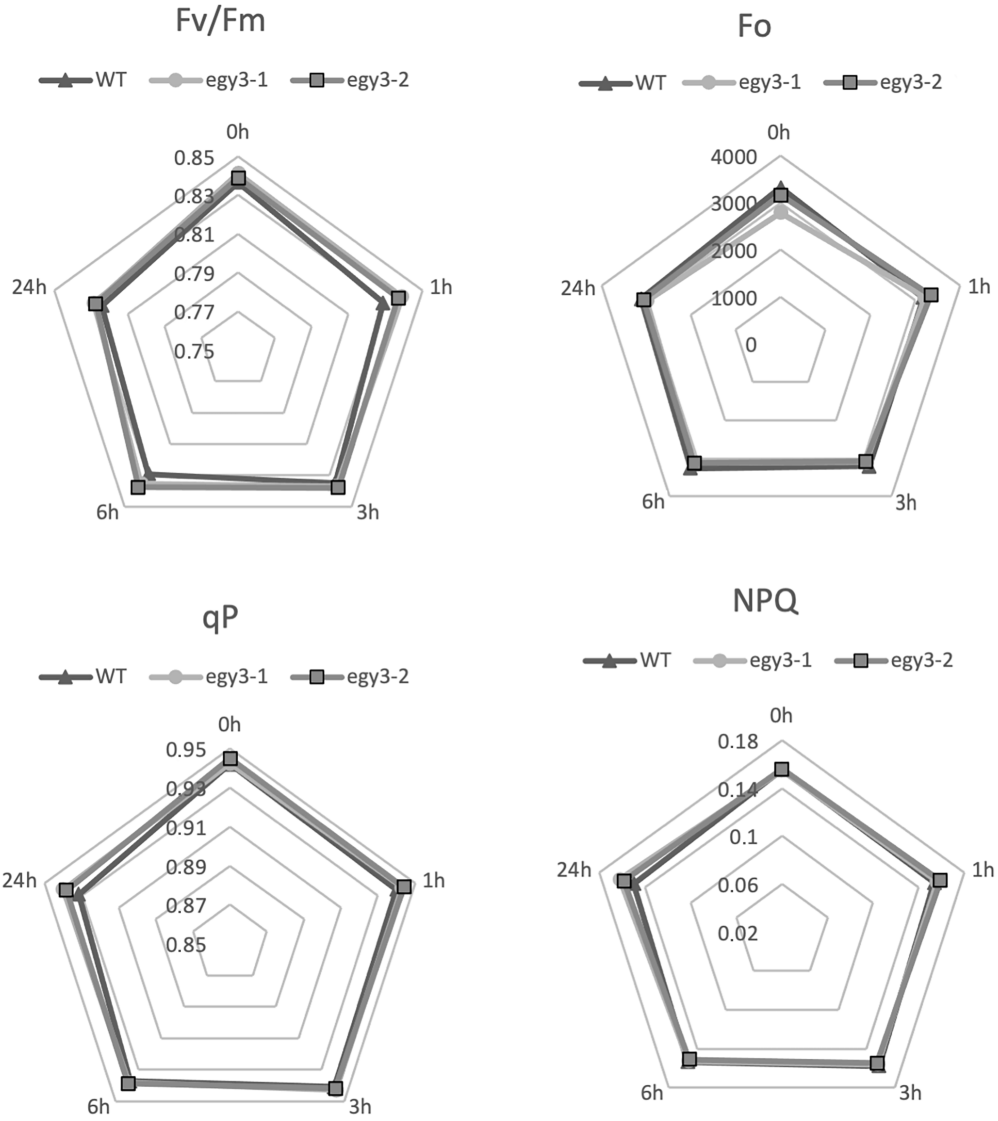

FIGURE 10
Comparison of chlorophyll fluorescence parameters in wild-type (WT) plants and *egy3* mutants during exposition to high-temperature stress. The presented values are average from three biological replicates (10 plants each).

A. thaliana but also in other organisms (0.572). What is more, both proteins were proven to interact with GUN1, a pentatricopeptide-repeat protein that plays a crucial role in the regulation of plastid development and chloroplast-to-nucleus retrograde communication (Colombo et al., 2016). Moreover, CPN60A was proven to participate in RubisCO folding (Gutteridge and Gatenby, 1995). Another overaccumulating protein was glycine decarboxylase P-protein 1 GLDP1. The protein is a subunit of glycine decarboxylase (GDC), which in mitochondria plays a central role in photorespiration (Bauwe et al., 2010), but its presence in chloroplast was also experimentally confirmed (Zybailov et al., 2008; Ferro et al., 2010). However, the function of GLDP1 in chloroplasts remains unknown.

The proteins accumulated differently in response to high-temperature stress

In the protein spots with an abundance increase in response to high temperature, two proteins involved in photosynthesis were identified, namely: PSAD-2, ATPF. The PSAD-2 is associated with PSI protein characterized by very high homology to PSAD-1, which is the core protein of PSI. The ATPF, in turn, is one of the subunits of the chloroplast ATPase complex. Another protein overaccumulating in response to high temperature was ferrochelatase II (ATFC-II), which is thought to be involved in the retrograde regulation of photosynthesis-associated nuclear genes (Woodson et al., 2011). In the spot with a lower accumulation level, the

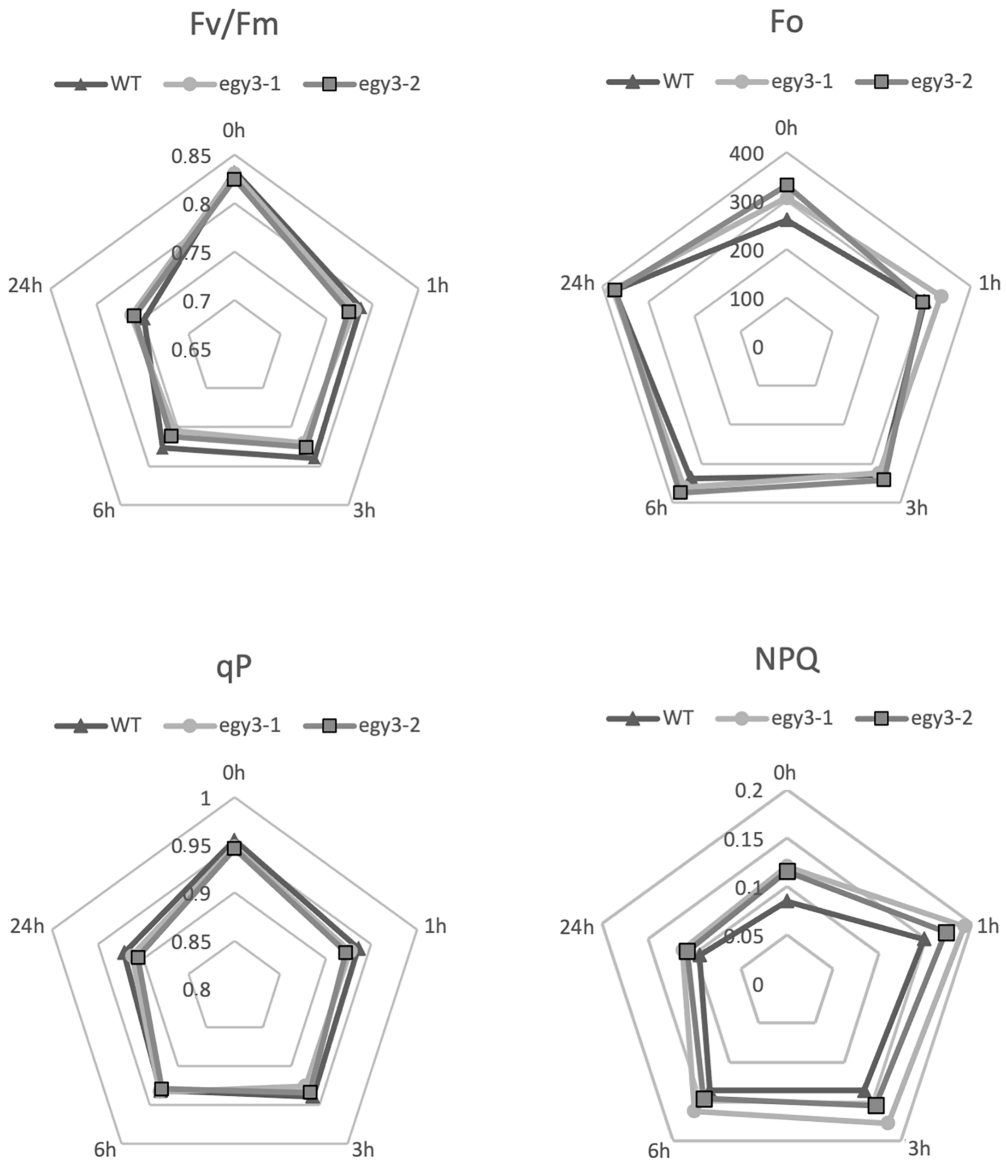

FIGURE 11
Comparison of chlorophyll fluorescence parameters in wild-type (WT) plants and *egy3* mutants during exposition to high light stress. The presented values are average from three biological replicates (10 plants each).

TABLE 3 Statistically significant changes of NPQ parameters during high light stress.

Time-variants	WT	*egy3-1*	*egy3-2*
NPQ			
0 h	0.085 ± 0.010	0.121 ± 0.040*	0.116 ± 0.035*
1 h	0.149 ± 0.041	0.192 ± 0.072*	0.172 ± 0.027*
3 h	0.136 ± 0.030	0.177 ± 0.062*	0.155 ± 0.041*

The asterisks indicate statistically significant differences between the WT and individual mutant lines.

RubisCO accumulation factor was identified. The protein was proven to participate in proper RubisCO assembly (Gruber and Feiz, 2018). Also, triosephosphate isomerase (TPI), one of the enzymes crucial for sugar metabolism, was found to be less abundant in *egy3* mutants, as well as glycine decarboxylase P-protein 1 (GLDP1) protein. In turn, glycine decarboxylase P-protein 2 (GLDP2) was identified in the spot which was absent in WT electropherograms but repeatedly appeared in *egy3* mutants. Similar to GLDP1, GLDP2 is a subunit of the mitochondrial GDC complex, but its presence in chloroplast was previously confirmed experimentally (Ferro et al., 2010). In another spot absent in WT present in *egy3* electropherograms, ACR11 protein was identified. The expression of ACR11 and GLN2 was found to be highly correlated, and the ACR11 was suggested to participate in glutamine metabolism or sensing in *Arabidopsis* (Sung et al., 2011).

Conclusion

The significant accumulation of the *EGY3* transcript as well as the protein itself indicates that EGY3 participates in response to both high-temperature and high light stresses. Since the protein participates in the regulation of hydrogen peroxide content, probably *via* stabilization of CSD2 protein, it can be considered as part of a retrograde chloroplast-nucleus signaling pathway. It remains unclear, however, which chloroplast pathways and processes are regulated in an EGY3-dependent manner. The analysis of the functional status of PSII during high light and high-temperature stresses indicates, however, no significant differences between *egy3* mutants and WT plants. Also, no proteins related to PSII were identified as accumulated differently in *egy3* mutants. This indicates that EGY3 protein does not play a significant function in maintaining the proper functioning of the PSII. The proteins identified as accumulated differently in both analyzed stresses participate in the same processes as RubisCO folding or glycine metabolism. In both stresses, proteins related to PSI were also identified as accumulated differently in *egy3* mutants. This is consistent with previous suggestions that EGY3 may interact with PSI subunits (Zhuang et al., 2021). The results suggest that future experiments aimed to determine the physiological role of EGY3 should be focused rather on PSI and light-independent reactions.

Data availability statement

The original contributions presented in the study are included in the article, further inquiries can be directed to the corresponding author.

Author contributions

MA: developed the article concept, participated in the 2D experiments, fluorescence measurement, data analysis, and drafted the article. JD: performed the RT-PCR experiments and cooperated in hydrogen peroxide detection experiments. ŁW: cooperated in hydrogen peroxide detection experiments. RL: cooperated in developing the concept of paper, participated in the design and realization of experiments, and helped in the data analysis. All authors contributed to the article and approved the submitted version.

Funding

This work was supported by the National Science Center, Poland based on decision number: dec-2019/03/X/NZ3/00303.

Acknowledgments

The equipment used for LC–MS/MS analysis was part-sponsored by the Centre for Preclinical Research and Technology (CePT), a project co-sponsored by the European Regional Development Fund and Innovative Economy, The National Cohesion Strategy of Poland.

Conflict of interest

The authors declare that the research was conducted in the absence of any commercial or financial relationships that could be construed as a potential conflict of interest.

Publisher's note

All claims expressed in this article are solely those of the authors and do not necessarily represent those of their affiliated organizations, or those of the publisher, the editors and the reviewers. Any product that may be evaluated in this article, or claim that may be made by its manufacturer, is not guaranteed or endorsed by the publisher.

References

Adamiec, M., Ciesielska, M., Zalaś, P., and Luciński, R. (2017). *Arabidopsis thaliana* intramembrane proteases. *Acta Physiol. Plant.* 39, 1–7. doi: 10.1007/s11738-017-2445-2

Adamiec, M., Misztal, L., Kasprowicz-Maluśki, A., and Luciński, R. (2019). EGY3: homolog of S2P protease located in chloroplasts. *Plant Biol.* 22, 734–743. doi: 10.1111/plb.13087

Adamiec, M., Misztal, L., Kosicka, E., Paluch-Lubawa, E., and Luciński, R. (2018). *Arabidopsis thaliana egy2* mutants display altered expression level of genes encoding crucial photosystem II proteins. *J. Plant Physiol.* 231, 155–167. doi: 10.1016/j.jplph.2018.09.010

Baerenfaller, K., Massonnet, C., Walsh, S., Baginsky, S., Bühlmann, P., Hennig, L., et al. (2012). Systems-based analysis of Arabidopsis leaf growth reveals adaptation to water deficit. *Mol. Syst. Biol.* 8, 606. doi: 10.1038/msb.2012.39

Bauwe, H., Hagemann, M., and Fernie, A. R. (2010). Photorespiration: players, partners and origin. *Trends Plant Sci.* 15, 330–336. doi: 10.1016/j.tplants.2010.03.006

Becana, M., Aparicio-Tejo, P., Irigoyen, J. J., and Sanchez-Diaz, M. (1986). Some enzymes of hydrogen peroxide metabolism in leaves and root nodules of *Medicago sativa*. *Plant Physiol.* 82, 1169–1171. doi: 10.1104/pp.82.4.1169

Berardini, T. Z., Reiser, L., Li, D., Mezheritsky, Y., Muller, R., Strait, E., et al. (2015). The Arabidopsis information resource: making and mining the "gold standard" annotated reference plant genome. *Genesis* 53, 474–485. doi: 10.1002/dvg.22877

Bölter, B., Nada, A., Fulgosi, H., and Soll, J. (2006). A chloroplastic inner envelope membrane protease is essential for plant development. *FEBS Lett.* 580, 789–794. doi: 10.1016/j.febslet.2005.12.098

Boyidi, P., Trishla, V. S., Botta, H. K., Yadav, D., and Kirti, P. B. (2021). Heterologous expression of rice annexin OsANN5 potentiates abiotic stress tolerance in transgenic tobacco through ROS amelioration. *Plant Stress* 2:100022. doi: 10.1016/j.stress.2021.100022

Bradford, M. M. (1976). A rapid and sensitive method for the quantitation of microgram quantities of protein utilizing the principle of protein-dye binding. *Anal. Biochem.* 72, 248–254. doi: 10.1006/abio.1976.9999

Chen, G., Bi, Y. R., and Li, N. (2005). EGY1 encodes a membrane-associated and ATP-independent metalloprotease that is required for chloroplast development. *Plant J.* 41, 364–375. doi: 10.1111/j.1365-313X.2004.02308.x

Colombo, M., Tadini, L., Peracchio, C., Ferrari, R., and Pesaresi, P. (2016). GUN1, a jack-of-all-trades in chloroplast protein homeostasis and signaling. *Front. Plant Sci.* 7:1427. doi: 10.3389/fpls.2016.01427

Daudi, A., and O'Brien, J. A. (2012). Detection of hydrogen peroxide by DAB staining in Arabidopsis leaves. *Bio-Protocol* 2:e263. doi: 10.21769/BioProtoc.263

Ferro, M., Brugière, S., Salvi, D., Seigneurin-Berny, D., Court, M., Moyet, L., et al. (2010). AT-CHLORO, a comprehensive chloroplast proteome database with subplastidial localization and curated information on envelope proteins. *Mol. Cell. Proteomics* 9, 1063–1084. doi: 10.1074/mcp.M900325-MCP200

Friso, G., Giacomelli, L., Ytterberg, A. J., Peltier, J. B., Rudella, A., Sun, Q., et al. (2004). In-depth analysis of the thylakoid membrane proteome of *Arabidopsis thaliana* chloroplasts: new proteins, new functions, and a plastid proteome database. *Plant Cell* 16, 478–499. doi: 10.1105/tpc.017814

Fulcher, L. J., Bozatzi, P., Tachie-Menson, T., Wu, K. Z. L., Cummins, T. D., Bufton, J. C., et al. (2018). The DUF1669 domain of FAM83 family proteins anchor casein kinase 1 isoforms. *Sci. Signal.* 11, eaao2341. doi: 10.1126/scisignal.aao2341

Genty, B., Briantais, J. M., and Baker, N. R. (1989). The relationship between the quantum yield of photosynthetic electron transport and quenching of chlorophyll fluorescence. *Biochim. Biophys. Acta* 990, 87–92. doi: 10.1016/S0304-4165(89)80016-9

Gruber, A. V., and Feiz, L. (2018). Rubisco assembly in the chloroplast. *Front. Mol. Biosci.* 5:24. doi: 10.3389/fmolb.2018.00024

Guo, D., Gao, X., Li, H., Zhang, T., Chen, G., Huang, P., et al. (2008). EGY1 plays a role in regulation of endodermal plastid size and number that are involved in ethylene-dependent gravitropism of light-grown Arabidopsis hypocotyls. *Plant Mol. Biol.* 66, 345–360. doi: 10.1007/s11103-007-9273-5

Gutteridge, S., and Gatenby, A. A. (1995). Rubisco synthesis, assembly, mechanism, and regulation. *Plant Cell* 7, 809–819. doi: 10.1105/tpc.7.7.809

Kilian, J., Whitehead, D., Horak, J., Wanke, D., Weinl, S., Batistic, O., et al. (2007). The AtGenExpress global stress expression data set: protocols, evaluation and model data analysis of UV-B light, drought and cold stress responses. *Plant J.* 50, 347–363. doi: 10.1111/j.1365-313X.2007.03052.x

Kubala, S., Wojtyla, L., Quinet, M., Lechowska, K., Lutts, S., and Garnczarska, M. (2015). Enhanced expression of the proline synthesis gene P5CSA in relation to seed osmopriming improvement of *Brassica napus* germination under salinity stress. *J. Plant Physiol.* 183, 1–12. doi: 10.1016/J.JPLPH.2015.04.009

Laemmli, U. K. (1970). Cleavage of structural proteins during the assembly of the head of bacteriophage T4. *Nature* 227, 680–685. doi: 10.1038/227680a0

Lingaraju, G. M., Bunker, R. D., Cavadini, S., Hess, D., Hassiepen, U., Renatus, M., et al. (2014). Crystal structure of the human COP9 signalosome. *Nature* 512, 161–165. doi: 10.1038/nature13566

Lister, R., Chew, O., Rudhe, C., Lee, M. N., and Whelan, J. (2001). *Arabidopsis thaliana* ferrochelatase-I and-II are not imported into Arabidopsis mitochondria. *FEBS Lett.* 506, 291–295. doi: 10.1016/S0014-5793(01)02925-8

Liu, Y., Beyer, A., and Aebersold, R. (2016). On the dependency of cellular protein levels on mRNA abundance. *Cell* 165, 535–550. doi: 10.1016/j.cell.2016.03.014

Lowry, O. H., Rosebrough, N. J., Farr, L., and Randall, R. J. (1951). Protein measurement with the Folin phenol reagent. *J. Biol. Chem.* 193, 265–275. doi: 10.1016/S0021-9258(19)52451-6

Maxwell, K., and Johnson, G. N. (2000). Chlorophyll fluorescence—a practical guide. *J. Exp. Bot.* 5, 659–668. doi: 10.1093/jexbot/51.345.659

Murphy, J. M., Farhan, H., and Eyers, P. A. (2017). Bio-zombie: the rise of pseudoenzymes in biology. *Biochem. Soc. Trans.* 45, 537–544. doi: 10.1042/BST20160400

Murphy, J. M., Nakatani, Y., Jamieson, S. A., Dai, W., Lucet, I. S., and Mace, P. D. (2015). Molecular mechanism of CCAAT-enhancer binding protein recruitment by the TRIB1 Pseudokinase. *Structure* 23, 2111–2121. doi: 10.1016/j.str.2015.08.017

Ng, A. A., Logan, A. M., Schmidt, E. J., and Robinson, F. L. (2013). The CMT4B disease-causing phosphatases Mtmr2 and Mtmr13 localize to the Schwann cell cytoplasm and endomembrane compartments, where they depend upon each other to achieve wild-type levels of protein expression. *Hum. Mol. Genet.* 22, 1493–1506. doi: 10.1093/hmg/dds562

Peltier, J. B., Ytterberg, A. J., Sun, Q., and Van Wijk, K. J. (2004). New functions of the thylakoid membrane proteome of *Arabidopsis thaliana* revealed by a simple, fast, and versatile fractionation strategy. *J. Biol. Chem.* 279, 49367–49383. doi: 10.1074/jbc.M406763200

Peng, L., Yamamoto, H., and Shikanai, T. (2011). Structure and biogenesis of the chloroplast NAD(P)H dehydrogenase complex. *Biochim. Biophys. Acta Bioenerg.* 1807, 945–953. doi: 10.1016/J.BBABIO.2010.10.015

Pietrowska-Borek, M., Wojdyła-Mamoń, A., Dobrogojski, J., Młynarska-Cieślak, A., Baranowski, M. R., Dąbrowski, J. M., et al. (2020). Purine and pyrimidine dinucleoside polyphosphates differentially affect the phenylpropanoid pathway in *Vitis vinifera* L. cv. Monastrell suspension cultured cells. *Plant Physiol. B.ioch* 147, 125–132. doi: 10.1016/j.plaphy.2019.12.015

Rosenberg, O. S., Dovala, D., Li, X., Connolly, L., Bendebury, A., Finer-Moore, J., et al. (2015). Substrates control multimerization and activation of the multi-domain ATPase motor of type VII secretion. *Cell* 161, 501–512. doi: 10.1016/j.cell.2015.03.040

Rumeau, D., Bécuwe-Linka, N., Beyly, A., Louwagie, M., Garin, J., Peltier, G. (2005). New subunits NDH-M, -N, and -O, encoded by nuclear genes, are essential for plastid Ndh complex functioning in higher plants. *Plant Cell* 17, 219–232. doi: 10.1105/tpc.104.028282

Rutschow, H., Ytterberg, A. J., Friso, G., Nilsson, R., and van Wijk, K. J. (2008). Quantitative proteomics of a chloroplast SRP54 sorting mutant and its genetic interactions with CLPC1 in arabidopsis. *Plant Physiol.* 148, 156–175. doi: 10.1104/pp.108.124545

Schäfer, I. B., Rode, M., Bonneau, F., Schüssler, S., and Conti, E. (2014). The structure of the Pan2-Pan3 core complex reveals cross-talk between deadenylase and pseudokinase. *Nat. Struct. Mol. Biol.* 21, 591–598. doi: 10.1038/nsmb.2834

Schroeder, C. M., Ostrem, J. M., Hertz, N. T., and Vale, R. D. (2014). A Ras-like domain in the light intermediate chain bridges the dynein motor to a cargo-binding region. *elife* 3, e03351–e03322. doi: 10.7554/eLife.03351

Schwacke, R., Schneider, A., Van Der Graaff, E., Fischer, K., Catoni, E., Desimone, M., et al. (2003). ARAMEMNON, a novel database for Arabidopsis integral membrane proteins. *Plant Physiol.* 131, 16–26. doi: 10.1104/pp.011577

Sung, T. Y., Chung, T. Y., Hsu, C. P., and Hsieh, M. H. (2011). The ACR11 encodes a novel type of chloroplastic ACT domain repeat protein that is coordinately expressed with GLN2 in Arabidopsis. *BMC Plant Biol.* 11, 118. doi: 10.1186/1471-2229-11-118

Szklarczyk, D., Gable, A. L., Lyon, D., Junge, A., Wyder, S., Huerta-Cepas, J., et al. (2018). STRING v11: protein-protein association networks with increased coverage, supporting functional discovery in genome-wide experimental datasets. *Nucleic Acids Res.* 47, D607–D613. doi: 10.1093/nar/gky1131

Walden, M., Masandi, S. K., Pawłowski, K., and Zeqiraj, E. (2018). Pseudo-DUBs as allosteric activators and molecular scaffolds of protein complexes. *Biochem. Soc. Trans.* 46, 453–466. doi: 10.1042/BST20160268

Woodson, J. D., Perez-Ruiz, J. M., and Chory, J. (2011). Heme synthesis by plastid ferrochelatase i regulates nuclear gene expression in plants. *Curr. Biol.* 21, 897–903. doi: 10.1016/j.cub.2011.04.004

Yamamoto, Y. (2016). Quality control of photosystem II: the mechanisms for avoidance and tolerance of light and heat stresses are closely linked to membrane fluidity of the thylakoids. *Front. Plant Sci.* 7:1136. doi: 10.3389/fpls.2016.01136

Yu, F. W., Zhu, X. F., Li, G. J., Kronzucker, H. J., and Shi, W. M. (2016). The chloroplast protease AMOS1/EGY1 affects phosphate homeostasis under phostphate stress. *Plant Physiol.* 172, 1200–1208. doi: 10.1104/pp.16.00786

Zhuang, Y., Wei, M., Ling, C., Liu, Y., Amin, A. K., Li, P., et al. (2021). EGY3 mediates chloroplastic ROS homeostasis and promotes retrograde signaling in response to salt stress in Arabidopsis. *Cell Rep.* 36:109384. doi: 10.1016/j.celrep.2021.109384

Zybailov, B., Rutschow, H., Friso, G., Rudella, A., Emanuelsson, O., Sun, Q., et al. (2008). Sorting signals, N-terminal modifications and abundance of the chloroplast proteome. *PLoS One* 3:e1994. doi: 10.1371/journal.pone.0001994

frontiers | Frontiers in Plant Science

TYPE Mini Review
PUBLISHED 16 August 2022
DOI 10.3389/fpls.2022.974598

OPEN ACCESS

EDITED BY
Zhiping Deng,
Zhejiang Academy of Agricultural Sciences, China

REVIEWED BY
Andreas Bachmair,
University of Vienna, Austria
Lei Wang,
Mississippi State University, United States
Fang Lin,
Lanzhou University, China

*CORRESPONDENCE
Ziwei Li
liziwei1989@126.com

SPECIALTY SECTION
This article was submitted to Plant Abiotic Stress, a section of the journal Frontiers in Plant Science

RECEIVED 21 June 2022
ACCEPTED 28 July 2022
PUBLISHED 16 August 2022

CITATION
Zhang K, Li Y, Huang T and Li Z (2022) Potential application of TurboID-based proximity labeling in studying the protein interaction network in plant response to abiotic stress. *Front. Plant Sci.* 13:974598. doi: 10.3389/fpls.2022.974598

Potential application of TurboID-based proximity labeling in studying the protein interaction network in plant response to abiotic stress

Kaixin Zhang[1,2], Yinyin Li[1], Tengbo Huang[1] and Ziwei Li[1]*

[1]Guangdong Provincial Key Laboratory for Plant Epigenetics, College of Life Sciences and Oceanography, Shenzhen University, Shenzhen, China, [2]Key Laboratory of Optoelectronic Devices and Systems of Ministry of Education and Guangdong, College of Physics and Optoelectronic Engineering, Shenzhen University, Shenzhen, China

Abiotic stresses are major environmental conditions that reduce plant growth, productivity and quality. Protein-protein interaction (PPI) approaches can be used to screen stress-responsive proteins and reveal the mechanisms of protein response to various abiotic stresses. Biotin-based proximity labeling (PL) is a recently developed technique to label proximal proteins of a target protein. TurboID, a biotin ligase produced by directed evolution, has the advantages of non-toxicity, time-saving and high catalytic efficiency compared to other classic protein-labeling enzymes. TurboID-based PL has been successfully applied in animal, microorganism and plant systems, particularly to screen transient or weak protein interactions, and detect spatially or temporally restricted local proteomes in living cells. This review concludes classic PPI approaches in plant response to abiotic stresses and their limitations for identifying complex network of regulatory proteins of plant abiotic stresses, and introduces the working mechanism of TurboID-based PL, as well as its feasibility and advantages in plant abiotic stress research. We hope the information summarized in this article can serve as technical references for further understanding the regulation of plant adaptation to abiotic stress at the protein level.

KEYWORDS

plant, abiotic stress, protein interaction, TurboID, regulation network

Introduction

Plant life needs certain natural factors such as temperature, moisture and nutrition, while plants often suffer from environmental stresses during development including changes of temperature, salinity, water, light, nutrient availability, and toxic chemicals (Vanstraelen and Benkova, 2012; Skalak et al., 2021; Zhou et al., 2021). In response to

these abiotic stresses, various adaptations have evolved in plants at the physiological, molecular, and cellular levels, which are regulated by complex signal transduction pathways (Zhu, 2016). In these important pathways, regulatory proteins play an essential role. Proteins rarely act on their own, while often function as complexes through protein-protein interactions (PPIs) (Struk et al., 2019). Therefore, the study of PPIs can not only infer the protein functions within the cell, but also uncover unidentified proteins from their interactions with known proteins (Zhang et al., 2010). There are two types of PPIs, namely constitutive and regulative, in the cell (Fujikawa et al., 2014). Constitutive PPIs are typically ubiquitous and strong interactions, whereas regulative PPIs occur only in certain cellular or developmental contexts or in response to specific incentives (Morsy et al., 2008). The dynamic changes of regulative PPIs confer cells with the ability to rapidly respond to intracellular and extracellular stimuli (Syafrizayanti et al., 2014). Regulative PPIs have the features of instantaneity, specificity and instability, which make them challenging to be studied (Lalonde et al., 2008).

Many classic PPI approaches, such as Yeast Two-Hybrid (Y2H), Co-Immunoprecipitation (Co-IP), Affinity Purification (AP), Pull-down, Bimolecular Fluorescence Complementation (BiFC), and Split Luciferase (Split-LUC), have been utilized for studying the protein interaction network in plant response to abiotic stresses. These techniques have identified many critical regulatory proteins involved in abiotic stress responses (Urano et al., 2010; Li et al., 2016; Zhang et al., 2016; Han et al., 2020; Qin L. et al., 2021). However, they also have many limitations, which hinder their applications, particularly in the analyses of regulative PPIs. Recently, a new PPI technique named TurboID-based proximity labeling (PL) has been applied in bio-research, which has a number of advantages especially for studying dynamic and transient PPIs (Bohnert et al., 2006; Branon et al., 2018; Zhang et al., 2019; Cho et al., 2020; Li et al., 2021). Although there are only a few cases of its application in plant research, we envision wide usage of this cutting-edge technique in dissecting the protein interaction network that regulates abiotic stress responses in plants.

Classic protein-protein interaction approaches to study plant response to abiotic stresses

Principles of classic protein-protein interaction approaches and their applications in studying plant abiotic stress responses

Classic PPI approaches, including Y2H, Co-IP, AP, Pull-down and BiFC, have been widely utilized in plant studies and introduced in detail in a number of review articles (Drewes and Bouwmeester, 2003; Weinthal and Tzfira, 2009; Zhang et al., 2010; Braun et al., 2013; Ferro and Trabalzini, 2013; Rao et al., 2014). The Y2H system includes bait and prey proteins in frame with DNA-binding domain (BD) or a transactivation domain (AD), respectively. When AD and BD domains are in spatial proximity to each other, expression of the reporter gene is activated to demonstrate the interaction between bait and prey (Causier and Davies, 2002). Co-IP and AP are two *in vivo* PPI approaches under near-physiological conditions. Co-IP and AP have similar principles, which entail overexpression of the bait protein (with or without an affinity tag) in plant protoplast or tissue, and isolation of the bait with its interacting partners (prey) through purification based on antibody-antigen interactions. The isolated bait-prey complex can be analyzed by liquid chromatography tandem-MS (LC-MS/MS) to achieve high throughput analysis (Ransone, 1995; Masters, 2004; Xie et al., 2012; Xing et al., 2016). Pull-down is an *in vitro* method that can be used to detect or validate the direct interaction between bait and prey proteins. In Pull-down approach, bait or prey protein is usually expressed as a fusion protein with tags in bacteria, the immobilizing bait-tag fusion protein on tag specific column is used as affinity support to catch and purify the prey proteins that interact with bait protein, and these prey proteins can be detected by sodium-dodecyl sulfate polyacrylamide gel electrophoresis (SDS-PAGE) and analyzed by western-blotting detection (Louche et al., 2017). BiFC and Split-LUC are based on the principle of fluorescent protein-fragment complementation assay (PCA). The individual N- or C- terminal part of a fluorescent protein normally has no fluorescence signal, but when N- and C- terminal parts are fused with two partner proteins, respectively, interaction of these two proteins will make the N- and C- parts close enough to regain the fluorescent protein structure and activity (Kerppola, 2006, 2008; Azad et al., 2014). The results of BiFC and Split-LUC can both be shown by the emission of the reconstructed fluorescent proteins, and Split-LUC signals can also be quantified by the luciferase activity assay (Kerppola, 2006, 2008; Azad et al., 2014).

Abiotic stresses such as temperature extremes, salinity, drought, reduced nutrient availability, and toxic chemicals are major limiting factors for plant development. Plants have evolved excellent defense mechanisms to protect themselves from abiotic stresses including stress sensing, signal transduction and transcriptional regulation, etc., (Zhang H. et al., 2022). The classic PPI approaches mentioned above are widely used to build up the protein interaction network and identify hub proteins, including transcription factors, signaling molecules and transporter proteins in the regulation of plant response to abiotic stresses (**Supplementary Table 1**). For example, in phosphorus (Pi) deficiency stress, the interaction of the Ubiquitin-Conjugating Enzyme PHO2 and the Pi transporter PHTs had been verified by Y2H and BiFC (Liu et al., 2012), and the feedback inhibition

of SPX-domain proteins on PHOSPHATE STARVATION RESPONSE 1 (PHR1), the central transcriptional regulator of Pi Starvation Responses (PSR), had also been assessed by Y2H, Co-IP and BiFC (Lv et al., 2014). These results greatly contributed to the understanding of the genetic network that controls PSR in plants.

The advantages and disadvantages of the classic protein-protein interaction approaches

Although the classic PPI approaches have been successfully applied in many abiotic stress studies, their shortages cannot be overlooked. For example, Y2H has benefits of high sensitivity, maintaining the natural folding of fusion proteins and convenient operation that bypasses the complicated steps of protein extraction and purification. However, it also has obvious disadvantages, including high technical false positive rates due to the strong spontaneous activation of reporter gene transcription, and toxicity of plant proteins to yeast cells, which can cause false negative results. Also, Y2H often fails to detect protein interactions that rely on post-translational modifications (PTMs). Therefore, Y2H is more suitable for cDNA library screening rather than confirming protein interactions, and the Y2H results often need to be confirmed by other PPI approaches (Hamdi and Colas, 2012; Mehla et al., 2015). Unlike Y2H, Co-IP/AP-MS can be used to pull down protein complexes under native physiological conditions to reflect the *in vivo* binding. But these approaches also suffer from high false positive rates. Also, Co-IP/AP-MS need to overexpress the bait protein which may influence its physiological properties. In addition, the choice of lysis conditions may have strong influence on the result of Co-IP/AP-MS. Lysis conditions may break PPI, and the low solubility of some subcellular structures in normal lysis buffer, e.g., plasmalemma, cytoskeleton and nucleus, may lead to negative results as well. Another shortcoming of Co-IP/AP-MS is that the instantaneous interactions or weak interactions often fail to be detected, and it is unable to distinguish direct and indirect interactions between the examined proteins. Pull-down is an approach used to detect the direct interaction between two proteins *in vitro*, with the outstanding features of being quick, sensitive, and quantifiable. But there are some disadvantages of Pull-down, such as it cannot reflect the protein interactions in plant physiological conditions, and each experiment needs to be optimized to keep characterized interactions from artifacts (Struk et al., 2019). Comparing to Co-IP/AP-MS or Pull-down, BiFC and Split-LUC have the advantage in identifying weak and instantaneous interactions because of the stability of the reconstituted GFP/YFP or LUC complexes. BiFC can also reveal the cellular localization of the PPI complex, which is convenient for further cellular studies. However, BiFC and Split-LUC can only be used to investigate the interaction of two proteins, and the interaction might be influenced by protein conformation, which could be changed after the joining of the N- and C- terminus of fluorescent proteins. These factors all limit the application of BiFC and Split-LUC in high throughput PPI analyses (Kerppola, 2008).

Application of TurboID-based proximity labeling in studying plant abiotic stress responses

Mechanisms and advantages of TurboID-based proximity labeling technique

Due to the above disadvantages of classic PPI approaches and to avoid spurious results from heterologous expression, instantaneous and weak interactions, and indistinguishable cellular localization of the target proteins, enzyme-catalyzed PL techniques have been developed as novel alternative approaches to study PPIs (Qin W. et al., 2021; Xu et al., 2021; Yang et al., 2021; Mair and Bergmann, 2022). TurboID, a biotin ligase, has been exploited as an important PL enzyme with the advantages of non-toxicity and high catalytic efficiency (May et al., 2020).

TurboID is a 35 kDa biotin ligase engineered by yeast display-based directed evolution, which has 15 mutations relative to the wild-type *Escherichia coli* biotin ligase (BirA) (Branon et al., 2018). By fusing TurboID with the target protein of interest and expressing it in cells, when biotin is supplied in the presence of ATP, TurboID catalyzes biotin and forms reactive biotinoyl-5′-AMP (bioAMP) from biotin and ATP. These free bioAMPs are released and diffused to the vicinity of the target protein, which can covalently bind to lysine residues of proteins that are in close proximity to the TurboID enzyme (Roux et al., 2012; Branon et al., 2018). The biotin-labeled proteins are enriched and affinity purified by streptavidin pulldown and subsequently identified by MS, so as to identify the proximal proteins of the target protein (Roux et al., 2012). In contrast to classic methods, TurboID-based PL adds covalently bound tag in living cells, such that spatial relationships and interaction networks are not disrupted. In addition, the TurboID-based PL system simply requires a supply of exogenous non-toxic biotin, which permits it to be applied *in vivo* without causing damage to living cells. Furthermore, TurboID has high catalytic efficiency and biotinylation of proximal proteins can be completed in living cells within 10 min at 25°C, which allows its quick application in plants grown under ambient conditions (Branon et al., 2018; Mair et al., 2019; May et al., 2020; Zhang et al., 2020). Most importantly, TurboID can identify weak and transient

protein interactions in living cells, which frequently fail to be captured by classic Co-IP/AP approaches (Branon et al., 2018; Kim et al., 2019). Moreover, it can also identify rare protein complexes or local organelle proteomes in individual cell types of complex multicellular organisms (Branon et al., 2018; Mair et al., 2019).

Application of TurboID-based proximity labeling in plant research

TurboID-based PL techniques have been applied successfully in a number of biological studies. For example, TurboID-based PL has been used to map local proteomes and screen novel interactors *in vivo* in zebrafish (Xiong et al., 2021). TurboID biotin ligase can also efficiently tag the entire proteome of specific cell types in the mouse brain, and dynamically track and identify tissue-specific or stimulation-specific secretory proteins in living body (Chua et al., 2021; Kim et al., 2021; Sun et al., 2022). TurboID-based PL was also used to identify host proteins interacting with viruses including coronavirus and syndrome coronavirus-2 (SARS-CoV-2), which help to elucidate the mechanism of virus infection and provide resources for the development of antiviral drugs for coronavirus disease 2019 (COVID-19) treatment (V'Kovski et al., 2020; Zhang Y. et al., 2022).

In plant research, TurboID-based PL technology has also been utilized in a variety of systems to study PPIs. For example, TurboID-based PL was used to identify interactors of a plant immune receptor N, which is a Nucleotide-binding Leucine-rich Repeat (NLR) that confers plant resistance to Tobacco Mosaic Virus (TMV) in *Nicotiana benthamiana*. In this work, a new regulator Ubiquitin Protein Ligase E3 Component N-Recognin 7 (UBR7) was found, which directly interacts with N and mediates immunity against plant pathogens (Zhang et al., 2019). TurboID-based PL was also applied to identify partners of the stomatal-specific transcription factor FAMA and help to obtain the nuclear proteome of young guard cells in *Arabidopsis thaliana* seedlings, which demonstrate that TurboID-based PL can be used to detect interactions of low abundant proteins and local proteomes of rare plant cell types (Mair et al., 2019). In addition, TurboID-based PL was also used to characterize neighboring proteins of Brassinosteroid-Insensitive 2 (BIN2), the regulatory kinase of Brassinosteroid (BR) pathways. This study uncovered a suite of previously unidentified BIN2 proximal proteins, which further enriched BIN2-mediated BR signaling networks (Kim et al., 2019). Furthermore, TurboID-based PL was successfully used to identify multiple interacting proteomes in the cell suspension cultures of tomato (*Solanum lycopersicum*), *N. benthamiana* and *Arabidopsis*, which showed that this technology can effectively capture membrane-associated protein interactions in different plant model systems (Arora et al., 2020).

Technical feasibility and advantages of TurboID in the studies of abiotic stresses

Abiotic stresses can be sensed by plants not only at the cell surface, such as by receptors at the cell wall and plasma membrane, but also in intracellular compartments, such as by signaling proteins in the cytoplasm and nucleus. Stress signaling triggers physical or chemical changes of biomolecules in the plant cell, which can lead to a cellular stress response (Zhang H. et al., 2022). Signal transduction in this process involves secondary messengers and regulatory proteins, and the interactions between the components of signaling pathways tend to be transient and dynamic. For example, many kinases in the Mitogen-Activated Protein Kinase (MAPK) signal transduction cascades can be rapidly activated by abiotic stresses. These kinases can affect their own activities by interacting with specific partner proteins and can also modulate the activities of substrates through transient kinase-substrate interactions, thus dynamically acting in various physiological processes and regulating plant tolerance to abiotic stresses (Mishra et al., 2006; Moustafa et al., 2014; Andrasi et al., 2019). In addition, the stress-related PTMs, including phosphorylation, glycosylation, ubiquitination, sumoylation, oxidation, carbonylation and nitrosylation, etc., are also modulated by transient enzyme-substrate interactions because of the rapid turnover of the corresponding enzymes (Wu et al., 2016). Understanding these dynamic and transient PPIs are one of the major challenges in the investigation of the stress signaling network in plants. In this sense, the high efficiency of TurboID-based PL in detecting dynamic and transient protein interactions will make it a particularly useful tool in studying abiotic stress responses in plants. Furthermore, as many regulatory proteins acting in stress signal transduction pathways, such as transcription factors, transmembrane receptors and kinases are in low abundance (Kosova et al., 2011; Abreu et al., 2013), the advantage of TurboID-based PL in capturing low-abundant proteins will also greatly contribute to the identification of stress related factors at the protein level.

Abiotic stress causes multilevel responses, including stress sensing, signal transduction, transcription, transcript processing, translation and PTMs (Zhang H. et al., 2022). These responses can be initiated in various cellular structures including plasma membrane, nucleus, mitochondria, chloroplast, endoplasmic reticulum (ER) and cell wall. The important functions of these cellular structures in stress responses and the involvement of protein interactions in the regulation of their activities suggest that organelle proteome analysis may provide key information of the cellular mechanisms of plant response to stresses (Couee et al., 2006; Nouri and Komatsu, 2010; Pang et al., 2010; Hüner et al., 2012; Komatsu et al., 2012;

10.3389/fpls.2022.974598

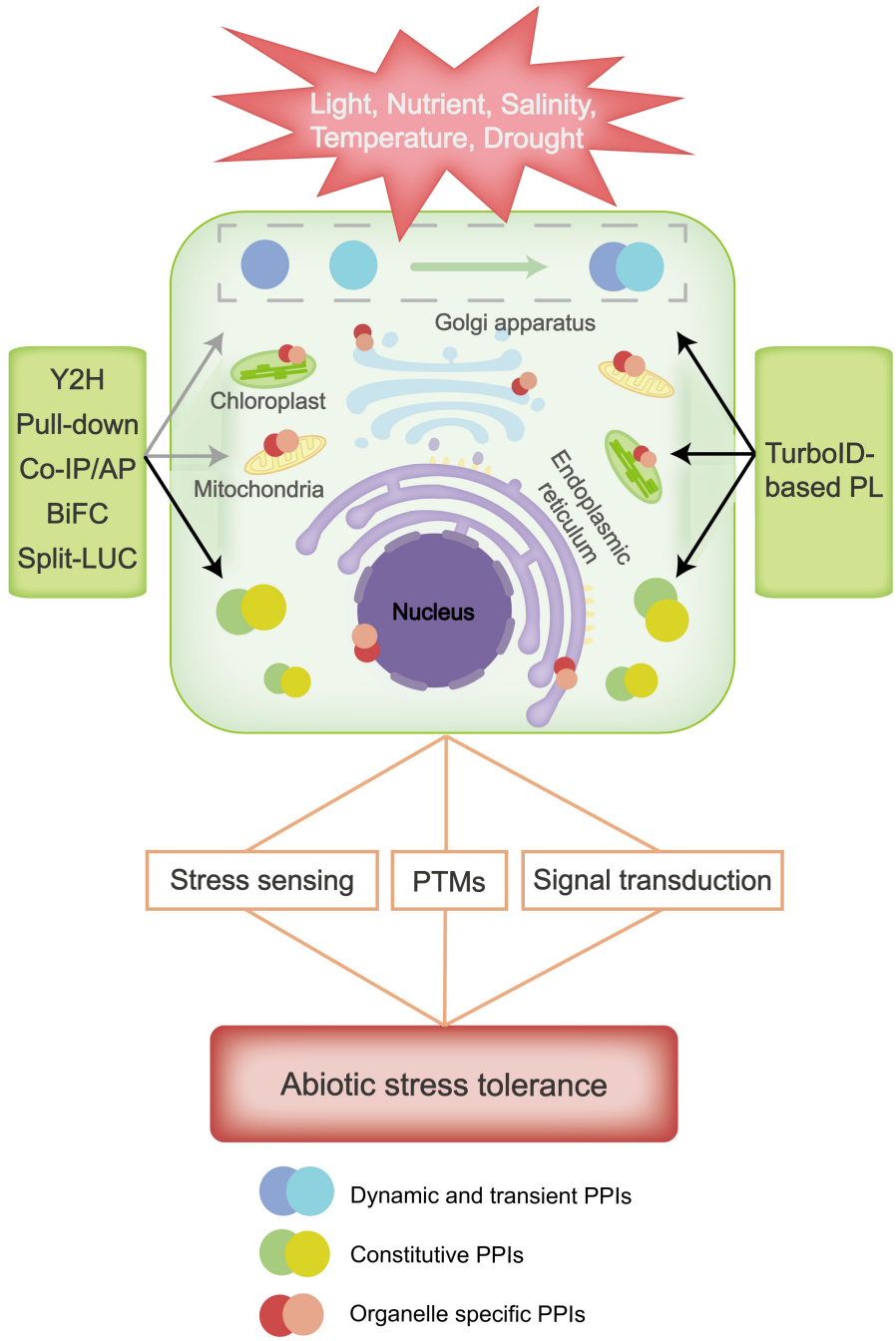

FIGURE 1
Plant resistance to abiotic stresses involves stress sensing, signal transduction and post-translational modifications (PTMs) of proteins, etc., in which many protein-protein interactions (PPIs) are involved. Classic methods such as Yeast Two Hybrid (Y2H), Pull-down, Co-Immunoprecipitation (Co-IP), Affinity Purification (AP), Bimolecular Fluorescence Complementation (BiFC), and Split Luciferase (Split-LUC) can easily detect stable protein interactions, such as constitutive PPIs that are typically macromolecular complex, but they are difficult to detect dynamic and organelle specific interacting proteins in response to abiotic stress. TurboID-based proximity labeling (PL) has great advantages in detecting dynamic, transient and organelle specific interacting proteins, and can be applied to study regulative PPIs under abiotic stress. Black and gray arrows indicate high and low applicability of the classic and TurboID-based technique(s) in detecting the corresponding PPIs.

Yin and Komatsu, 2016). However, due to the dynamic state of organelles and their proteins, clarifying the subcellular distribution and expression of organelle proteins has always been a challenging task (Boisvert et al., 2010). Utilization of TurboID-based PL may open a new avenue for organ and subcellular proteome research. TurboID-based PL has been used

to label proteins located in the cell membrane, mitochondrial matrix, cytoplasm, nucleus, and ER lumen/membrane in mammalian cells (Branon et al., 2018; May et al., 2020). It can also be used to efficiently and specifically detect the proteome of different subcellular components of plants, such as the nuclear proteome of stomatal guard cells in *Arabidopsis* (Mair et al., 2019). Compared with classic tools, TurboID-based PL technology can label the organelle proteome of interest in living cells without isolating tissues and organelles, therefore, it can be used to investigate non-membrane-enclosed organelles that cannot be purified by classic biochemical fractionation methods. Another important application of the TurboID-based PL technology is that it can be used in combination with fluorescent microscopy to assess the cellular compartmentalization information of protein interactions. Because one protein can display diverse functions depending on its subcellular localization (Kosova et al., 2018), this application is helpful for understanding the spatial-specific regulatory process in cells in response to abiotic stress.

Conclusion and perspective

Plants have evolved excellent defense mechanisms to protect themselves from abiotic stresses. Classic PPI approaches like Y2H, Co-IP/AP-MS, Pull-down, BiFC and Split-LUC have contributed to identification of stress-regulatory proteins in plants (**Figure 1**). However, due to their limitations in detecting weak instantaneous interactions, distinguishing cellular localizations and directly assessing protein interactions in subcellular organs, further application of classic PPIs in systematic studies of plant stress responses is largely hindered. As a recently developed PPI approach, TurboID-based PL has been applied in mapping PPIs in a variety of species and has proven especially useful in dissecting signaling pathways (Kim et al., 2019). TurboID-based PL has a number of advantages, such as high flexibility, easy implementation, and great efficiency in detecting protein interactors that are low abundant, transient and specifically expressed in organelles. All of these advantages may greatly help us in our study of the mechanisms of plant stress responses (Kim et al., 2019; Mair et al., 2019; **Figure 1**). However, TurboID-based PL also has its own limitations, which results in their non-applicability in some abiotic stress conditions. For instance, biotin ligase activity is markedly influenced by low temperature, so TurboID-based PL is not suitable for studying cold stress responses. Also, the proximity-dependent labeling method only provide information on which proteins are in proximity to each other, it does not show direct evidence for a physical interaction between these proteins. Therefore, TurboID-based PL may needs to be combined with classic PPI approaches to map protein interactions in plant responses, and new proximity labeling ligases should be developed to overcome these shortcomings of TurboID. Overall, with the continuous renovation of PPI approaches, we believe the future research on protein interactions will provide in-depth knowledge of systematic molecular mechanisms for plant abiotic stress responses.

Author contributions

KZ, YL, TH, and ZL were contributed to the writing of this review. All authors contributed to the article and approved the submitted version.

Funding

This studies on plant organogenesis in Huang lab have been supported by the Guangdong Basic and Applied Basic Research Foundation (2021A1515011035) and Guangdong Special Support Program for Young Talents in Innovation Research of Science and Technology (2019TQ05N940).

Acknowledgments

We thank the Instrumental Analysis Center of Shenzhen University (Lihu Campus) and Central Research Facilities of College of Life Sciences and Oceanography for assistance on our work.

Conflict of interest

The authors declare that the research was conducted in the absence of any commercial or financial relationships that could be construed as a potential conflict of interest.

Publisher's note

Supplementary material

The Supplementary Material for this article can be found online at: https://www.frontiersin.org/articles/10.3389/fpls.2022.974598/full#supplementary-material

References

Abreu, I. A., Farinha, A. P., Negrão, S., Gonçalves, N., Fonseca, C., Rodrigues, M., et al. (2013). Coping with abiotic stress: Proteome changes for crop improvement. *J. Proteom.* 93, 145–168. doi: 10.1016/j.jprot.2013.07.014

Andrasi, N., Rigo, G., Zsigmond, L., Perez-Salamo, I., Papdi, C., Klement, E., et al. (2019). The mitogen-activated protein kinase 4-phosphorylated heat shock factor A4A regulates responses to combined salt and heat stresses. *J. Exp. Bot.* 70, 4903–4918. doi: 10.1093/jxb/erz217

Arora, D., Abel, N. B., Liu, C., Van Damme, P., Yperman, K., Eeckhout, D., et al. (2020). Establishment of proximity-dependent biotinylation approaches in different plant model systems. *Plant Cell* 32, 3388–3407. doi: 10.1105/tpc.20.00235

Azad, T., Tashakor, A., and Hosseinkhani, S. (2014). Split-luciferase complementary assay: Applications, recent developments, and future perspectives. *Anal. Bioanal. Chem.* 406, 5541–5560. doi: 10.1007/s00216-014-7980-8

Bohnert, H. J., Gong, Q., Li, P., and Ma, S. (2006). Unraveling abiotic stress tolerance mechanisms-getting genomics going. *Curr. Opin. Plant Biol.* 9, 180–188. doi: 10.1016/j.pbi.2006.01.003

Boisvert, F. M., Lam, Y. W., Lamont, D., and Lamond, A. I. (2010). A quantitative proteomics analysis of subcellular proteome localization and changes induced by DNA damage. *Mol. Cell Proteom.* 9, 457–470. doi: 10.1074/mcp.M900429-MCP200

Branon, T. C., Bosch, J. A., Sanchez, A. D., Udeshi, N. D., Svinkina, T., Carr, S. A., et al. (2018). Efficient proximity labeling in living cells and organisms with TurboID. *Nat. Biotechnol.* 36, 880–887. doi: 10.1038/nbt.4201

Braun, P., Aubourg, S., Van Leene, J., De Jaeger, G., and Lurin, C. (2013). Plant protein interactomes. *Annu. Rev. Plant Biol.* 64, 161–187. doi: 10.1146/annurev-arplant-050312-120140

Causier, B., and Davies, B. (2002). Analysing protein-protein interactions with the yeast two-hybrid system. *Plant Mol. Biol.* 50, 855–870. doi: 10.1023/a:1021214007897

Cho, K. F., Branon, T. C., Udeshi, N. D., Myers, S. A., Carr, S. A., and Ting, A. Y. (2020). Proximity labeling in mammalian cells with TurboID and split-TurboID. *Nat. Protoc.* 15, 3971–3999. doi: 10.1038/s41596-020-0399-0

Chua, X. Y., Aballo, T., Elnemer, W., Tran, M., and Salomon, A. (2021). Quantitative interactomics of lck-TurboID in living human T cells unveils T cell receptor stimulation-induced proximal lck interactors. *J. Proteome Res.* 20, 715–726. doi: 10.1021/acs.jproteome.0c00616

Couee, I., Sulmon, C., Gouesbet, G., and El Amrani, A. (2006). Involvement of soluble sugars in reactive oxygen species balance and responses to oxidative stress in plants. *J. Exp. Bot.* 57, 449–459. doi: 10.1093/jxb/erj027

Drewes, G., and Bouwmeester, T. (2003). Global approaches to protein-protein interactions. *Curr. Opin. Cell Biol.* 15, 199–205. doi: 10.1016/s0955-0674(03)00005-x

Ferro, E., and Trabalzini, L. (2013). The yeast two-hybrid and related methods as powerful tools to study plant cell signalling. *Plant Mol. Biol.* 83, 287–301. doi: 10.1007/s11103-013-0094-4

Fujikawa, Y., Nakanishi, T., Kawakami, H., Yamasaki, K., Sato, M. H., Tsuji, H., et al. (2014). Split luciferase complementation assay to detect regulated protein-protein interactions in rice protoplasts in a large-scale format. *Rice* 7:11. doi: 10.1186/s12284-014-0011-8

Hamdi, A., and Colas, P. (2012). Yeast two-hybrid methods and their applications in drug discovery. *Trends Pharmacol. Sci.* 33, 109–118. doi: 10.1016/j.tips.2011.10.008

Han, G., Lu, C., Guo, J., Qiao, Z., Sui, N., Qiu, N., et al. (2020). C2H2 zinc finger proteins: Master regulators of abiotic stress responses in plants. *Front. Plant Sci.* 11:115. doi: 10.3389/fpls.2020.00115

Hüner, N. P., Bode, R., Dahal, K., Hollis, L., Rosso, D., Krol, M., et al. (2012). Chloroplast redox imbalance governs phenotypic plasticity: The "grand design of photosynthesis" revisited. *Front. Plant Sci.* 3:255. doi: 10.3389/fpls.2012.00255

Kerppola, T. K. (2006). Design and implementation of bimolecular fluorescence complementation (BiFC) assays for the visualization of protein interactions in living cells. *Nat. Protoc.* 1, 1278–1286. doi: 10.1038/nprot.2006.201

Kerppola, T. K. (2008). Bimolecular fluorescence complementation (BiFC) analysis as a probe of protein interactions in living cells. *Annu. Rev. Biophys.* 37, 465–487. doi: 10.1146/annurev.biophys.37.032807.125842

Kim, K. E., Park, I., Kim, J., Kang, M. G., Choi, W. G., Shin, H., et al. (2021). Dynamic tracking and identification of tissue-specific secretory proteins in the circulation of live mice. *Nat. Commun.* 12:5204. doi: 10.1038/s41467-021-25546-y

Kim, T. W., Chan, H. P., Hsu, C. C., Zhu, J. Y., and Wang, Z. Y. (2019). Application of TurboID-mediated proximity labeling for mapping a GSK3 kinase signaling network in Arabidopsis. *bioRxiv* [Preprint]. doi: 10.1101/636324

Komatsu, S., Kuji, R., Nanjo, Y., Hiraga, S., and Furukawa, K. (2012). Comprehensive analysis of endoplasmic reticulum-enriched fraction in root tips of soybean under flooding stress using proteomics techniques. *J. Proteom.* 77, 531–560. doi: 10.1016/j.jprot.2012.09.032

Kosova, K., Vitamvas, P., Prasil, I. T., and Renaut, J. (2011). Plant proteome changes under abiotic stress-contribution of proteomics studies to understanding plant stress response. *J. Proteom.* 74, 1301–1322. doi: 10.1016/j.jprot.2011.02.006

Kosova, K., Vitamvas, P., Urban, M. O., Prasil, I. T., and Renaut, J. (2018). Plant abiotic stress proteomics: The major factors determining alterations in cellular proteome. *Front. Plant Sci.* 9:122. doi: 10.3389/fpls.2018.00122

Lalonde, S., Ehrhardt, D. W., Loque, D., Chen, J., Rhee, S. Y., and Frommer, W. B. (2008). Molecular and cellular approaches for the detection of protein-protein interactions: Latest techniques and current limitations. *Plant J.* 53, 610–635. doi: 10.1111/j.1365-313X.2007.03332.x

Li, H., Frankenfield, A. M., Houston, R., Sekine, S., and Hao, L. (2021). Thiol-cleavable biotin for chemical and enzymatic biotinylation and its application to mitochondrial TurboID proteomics. *J. Am. Soc. Mass Spectrom.* 32, 2358–2365. doi: 10.1021/jasms.1c00079

Li, J., Ouyang, B., Wang, T., Luo, Z., Yang, C., Li, H., et al. (2016). HyPRP1 gene suppressed by multiple stresses plays a negative role in abiotic stress tolerance in tomato. *Front. Plant Sci.* 7:967. doi: 10.3389/fpls.2016.00967

Liu, T. Y., Huang, T. K., Tseng, C. Y., Lai, Y. S., Lin, S. I., Lin, W. Y., et al. (2012). PHO2-dependent degradation of PHO1 modulates phosphate homeostasis in Arabidopsis. *Plant Cell* 24, 2168–2183. doi: 10.1105/tpc.112.096636

Louche, A., Salcedo, S. P., and Bigot, S. (2017). Protein-protein interactions: Pull-down assays. *Methods Mol. Biol.* 1615, 247–255. doi: 10.1007/978-1-4939-7033-9_20

Lv, Q., Zhong, Y., Wang, Y., Wang, Z., Zhang, L., Shi, J., et al. (2014). SPX4 negatively regulates phosphate signaling and homeostasis through its interaction with PHR2 in rice. *Plant Cell* 26, 1586–1597. doi: 10.1105/tpc.114.123208

Mair, A., and Bergmann, D. C. (2022). Advances in enzyme-mediated proximity labeling and its potential for plant research. *Plant Physiol.* 188, 756–768. doi: 10.1093/plphys/kiab479

Mair, A., Xu, S. L., Branon, T. C., Ting, A. Y., and Bergmann, D. C. (2019). Proximity labeling of protein complexes and cell-type-specific organellar proteomes in Arabidopsis enabled by TurboID. *eLife* 8:e47864. doi: 10.7554/eLife.47864

Masters, S. C. (2004). Co-immunoprecipitation from transfected cells. *Methods Mol. Biol.* 261, 337-350

May, D. G., Scott, K. L., Campos, A. R., and Roux, K. J. (2020). Comparative application of BioID and TurboID for protein-proximity biotinylation. *Cells* 9:1070. doi: 10.3390/cells9051070

Mehla, J., Caufield, J. H., and Uetz, P. (2015). The yeast two-hybrid system: A tool for mapping protein-protein interactions. *Cold Spring Harb. Protoc.* 2015, 425–430. doi: 10.1101/pdb.top083345

Mishra, N. S., Tuteja, R., and Tuteja, N. (2006). Signaling through MAP kinase networks in plants. *Arch. Biochem. Biophys.* 452, 55–68. doi: 10.1016/j.abb.2006.05.001

Morsy, M., Gouthu, S., Orchard, S., Thorneycroft, D., Harper, J. F., Mittler, R., et al. (2008). Charting plant interactomes: Possibilities and challenges. *Trends Plant Sci.* 13, 183–191. doi: 10.1016/j.tplants.2008.01.006

Moustafa, K., AbuQamar, S., Jarrar, M., Al-Rajab, A. J., and Tremouillaux-Guiller, J. (2014). MAPK cascades and major abiotic stresses. *Plant Cell Rep.* 33, 1217–1225. doi: 10.1007/s00299-014-1629-0

Nouri, M. Z., and Komatsu, S. (2010). Comparative analysis of soybean plasma membrane proteins under osmotic stress using gel-based and LC MS/MS-based proteomics approaches. *Proteomics* 10, 1930–1945. doi: 10.1002/pmic.200900632

Pang, Q., Chen, S., Dai, S., Chen, Y., Wang, Y., and Yan, X. (2010). Comparative proteomics of salt tolerance in Arabidopsis thaliana and Thellungiella halophila. *J. Proteome Res.* 9, 2584–2599. doi: 10.1021/pr100034f

Qin, L., Sun, L., Wei, L., Yuan, J., Kong, F., Zhang, Y., et al. (2021). Maize SRO1e represses anthocyanin synthesis through regulating the MBW complex in response to abiotic stress. *Plant J.* 105, 1010–1025. doi: 10.1111/tpj.15083

Qin, W., Cho, K. F., Cavanagh, P. E., and Ting, A. Y. (2021). Deciphering molecular interactions by proximity labeling. *Nat. Methods* 18, 133–143. doi: 10.1038/s41592-020-01010-5

Ransone, L. J. (1995). Detection of protein-protein interactions by coimmunoprecipitation and dimerization. *Methods Enzymol.* 254, 491–497. doi: 10.1016/0076-6879(95)54034-2

Rao, V. S., Srinivas, K., Sujini, G. N., and Kumar, G. N. (2014). Protein-protein interaction detection: Methods and analysis. *Int. J. Proteomics* 2014:147648. doi: 10.1155/2014/147648

Roux, K. J., Kim, D. I., Raida, M., and Burke, B. (2012). A promiscuous biotin ligase fusion protein identifies proximal and interacting proteins in mammalian cells. *J. Cell Biol.* 196, 801–810. doi: 10.1083/jcb.201112098

Skalak, J., Nicolas, K. L., Vankova, R., and Hejatko, J. (2021). Signal integration in plant abiotic stress responses via multistep phosphorelay signaling. *Front. Plant Sci.* 12:644823. doi: 10.3389/fpls.2021.644823

Struk, S., Jacobs, A., Sanchez Martin-Fontecha, E., Gevaert, K., Cubas, P., and Goormachtig, S. (2019). Exploring the protein-protein interaction landscape in plants. *Plant Cell Environ.* 42, 387–409. doi: 10.1111/pce.13433

Sun, X., Sun, H., Han, X., Chen, P. C., Jiao, Y., Wu, Z., et al. (2022). Deep single-cell-type proteome profiling of mousebrain by nonsurgical AAV-mediated proximity labeling. *Anal. Chem.* 94, 5325–5334. doi: 10.1021/acs.analchem.1c05212

Syafrizayanti, Betzen, C., Hoheisel, J. D., and Kastelic, D. (2014). Methods for analyzing and quantifying protein-protein interaction. *Expert. Rev. Proteom.* 11, 107–120. doi: 10.1586/14789450.2014.875857

Urano, K., Kurihara, Y., Seki, M., and Shinozaki, K. (2010). 'Omics' analyses of regulatory networks in plant abiotic stress responses. *Curr. Opin. Plant Biol.* 13, 132–138. doi: 10.1016/j.pbi.2009.12.006

Vanstraelen, M., and Benkova, E. (2012). Hormonal interactions in the regulation of plant development. *Annu. Rev. Cell Dev. Biol.* 28, 463–487. doi: 10.1146/annurev-cellbio-101011-155741

V'Kovski, P., Steiner, S., and Thiel, V. (2020). Proximity labeling for the identification of coronavirus-host protein interactions. *Methods Mol. Biol.* 2203, 187–204. doi: 10.1007/978-1-0716-0900-2_14

Weinthal, D., and Tzfira, T. (2009). Imaging protein-protein interactions in plant cells by bimolecular fluorescence complementation assay. *Trends Plant Sci.* 14, 59–63. doi: 10.1016/j.tplants.2008.11.002

Wu, X., Gong, F., Cao, D., Hu, X., and Wang, W. (2016). Advances in crop proteomics: PTMs of proteins under abiotic stress. *Proteomics* 16, 847–865. doi: 10.1002/pmic.201500301

Xie, G., Kato, H., and Imai, R. (2012). Biochemical identification of the OsMKK6-OsMPK3 signalling pathway for chilling stress tolerance in rice. *Biochem. J.* 443, 95–102. doi: 10.1042/BJ20111792

Xing, S., Wallmeroth, N., Berendzen, K. W., and Grefen, C. (2016). Techniques for the analysis of protein-protein interactions in vivo. *Plant Physiol.* 171, 727–758. doi: 10.1104/pp.16.00470

Xiong, Z., Lo, H. P., McMahon, K. A., Martel, N., Jones, A., Hill, M. M., et al. (2021). In vivo proteomic mapping through GFP-directed proximity-dependent biotin labelling in zebrafish. *eLife* 10:e64631. doi: 10.7554/eLife.64631

Xu, Y., Fan, X., and Hu, Y. (2021). In vivo interactome profiling by enzyme-catalyzed proximity labeling. *Cell Biosci.* 11:27. doi: 10.1186/s13578-021-00542-3

Yang, X., Wen, Z., Zhang, D., Li, Z., Li, D., Nagalakshmi, U., et al. (2021). Proximity labeling: An emerging tool for probing in planta molecular interactions. *Plant Commun.* 2:100137. doi: 10.1016/j.xplc.2020.100137

Yin, X., and Komatsu, S. (2016). Nuclear proteomics reveals the role of protein synthesis and chromatin structure in root tip of soybean during the initial stage of flooding stress. *J. Proteome Res.* 15, 2283–2298. doi: 10.1021/acs.jproteome.6b00330

Zhang, H., Li, W., Mao, X., Jing, R., and Jia, H. (2016). Differential activation of the wheat SnRK2 family by abiotic stresses. *Front. Plant Sci.* 7:420. doi: 10.3389/fpls.2016.00420

Zhang, H., Zhu, J., Gong, Z., and Zhu, J. K. (2022). Abiotic stress responses in plants. *Nat. Rev. Genet.* 23, 104–119. doi: 10.1038/s41576-021-00413-0

Zhang, Y., Shang, L., Zhang, J., Liu, Y., Jin, C., Zhao, Y., et al. (2022). An antibody-based proximity labeling map reveals mechanisms of SARS-CoV-2 inhibition of antiviral immunity. *Cell Chem. Biol.* 29, 5–18. doi: 10.1016/j.chembiol.2021.10.008

Zhang, Y., Li, Y., Yang, X., Wen, Z., Nagalakshmi, U., and Dinesh-Kumar, S. P. (2020). TurboID-based proximity labeling for in planta identification of protein-protein interaction networks. *J. Vis. Exp.* 159:e60728. doi: 10.3791/60728

Zhang, Y., Song, G., Lal, N. K., Nagalakshmi, U., Li, Y., Zheng, W., et al. (2019). TurboID-based proximity labeling reveals that UBR7 is a regulator of N NLR immune receptor-mediated immunity. *Nat. Commun.* 10:3252. doi: 10.1038/s41467-019-11202-z

Zhang, Y. X., Gao, P., and Yuan, J. S. (2010). Plant protein-protein interaction network and interactome. *Curr. Genom.* 11, 40–46. doi: 10.2174/138920210790218016

Zhou, X., Joshi, S., Khare, T., Patil, S., Shang, J., and Kumar, V. (2021). Nitric oxide, crosstalk with stress regulators and plant abiotic stress tolerance. *Plant Cell Rep.* 40, 1395–1414. doi: 10.1007/s00299-021-02705-5

Zhu, J. K. (2016). Abiotic stress signaling and responses in plants. *Cell* 167, 313–324. doi: 10.1016/j.cell.2016.08.029

frontiers | Frontiers in Plant Science

TYPE Original Research
PUBLISHED 18 August 2022
DOI 10.3389/fpls.2022.917652

OPEN ACCESS

EDITED BY
Ling Li,
Mississippi State University,
United States

REVIEWED BY
Zhengrong Hu,
The Chinese Academy of Sciences, China
Monika Chodasiewicz,
King Abdullah University of Science and Technology, Saudi Arabia

*CORRESPONDENCE
Huajun Wang
huajunwang@sina.com

SPECIALTY SECTION
This article was submitted to Plant Abiotic Stress, a section of the journal Frontiers in Plant Science

RECEIVED 11 April 2022
ACCEPTED 26 July 2022
PUBLISHED 18 August 2022

CITATION
Wang J, Li C, Yao L, Ma Z, Ren P, Si E, Li B, Meng Y, Ma X, Yang K, Shang X and Wang H (2022) Global proteome analyses of phosphorylation and succinylation of barley root proteins in response to phosphate starvation and recovery. *Front. Plant Sci.* 13:917652. doi: 10.3389/fpls.2022.917652

Global proteome analyses of phosphorylation and succinylation of barley root proteins in response to phosphate starvation and recovery

Juncheng Wang[1,2], Chengdao Li[3], Lirong Yao[1,2], Zengke Ma[1,2], Panrong Ren[1,2], Erjing Si[1,2], Baochun Li[4], Yaxiong Meng[1,2], Xiaole Ma[1,2], Ke Yang[1,2], Xunwu Shang[2] and Huajun Wang[1,2]*

[1]State Key Lab of Aridland Crop Science/Gansu Key Lab of Crop Improvement and Germplasm Enhancement, Lanzhou, China, [2]Department of Crop Genetics and Breeding, College of Agronomy, Gansu Agricultural University, Lanzhou, China, [3]Western Barley Genetics Alliance, College of Science, Health, Engineering and Education, Murdoch University, Murdoch, WA, Australia, [4]Department of Botany, College of Life Sciences and Technology, Gansu Agricultural University, Lanzhou, China

Phosphate (Pi) stress is an important environmental factor that limits plant growth and development. Of various posttranslational modifications (PTMs), protein phosphorylation and succinylation are the two most important PTMs that regulate multiple biological processes in response to Pi stress. However, these PTMs have been investigated individually but their interactions with proteins in response to Pi stress remain poorly understood. In this study, to elucidate the underlying mechanisms of protein phosphorylation and succinylation in response to Pi stress, we performed a global analysis of the barley root phosphorylome and succinylome in Pi starvation and recovery stages, respectively. A total of 3,634 and 884 unique phosphorylated and succinylated proteins, respectively, corresponding to 11,538 and 2,840 phospho- and succinyl-sites, were identified; of these, 275 proteins were found to be simultaneously phosphorylated and succinylated. Gene Set Enrichment Analysis was performed with a Kyoto Encyclopedia of Genes and Genomes pathway database revealing pathways that significantly enriched in the phosphorylome and succinylome. Such pathways, were dynamically regulated by Pi starvation and recovery treatments, and could be partitioned into distinct metabolic processes. In particular, phosphorylated proteins related to purine, the mitogen-activated protein kinase (MAPK) signaling pathway, pyrimidine, and ATP-binding cassette (ABC) transporters were upregulated in both Pi deprivation and recovery stages. Succinylated proteins, significantly upregulated by both Pi starvation and recovery, were enriched in nitrogen metabolism and phenylpropanoid biosynthesis. Meanwhile, succinylated proteins that were significantly downregulated by both Pi starvation and recovery were enriched in lysine degradation and tryptophan metabolism. This highlighted the importance of these metabolic pathways in regulating

Pi homeostasis. Furthermore, protein–protein interaction network analyses showed that the response of central metabolic pathways to Pi starvation and recovery was significantly modulated by phosphorylation or succinylation, both individually and together. In addition, we discovered relevant proteins involved in MAPK signaling and phenylpropanoid biosynthetic pathways existing in interactions between phosphorylated and succinylated proteins in response to Pi recovery. The current study not only provides a comprehensive analysis of phosphorylated and succinylated proteins in plant responses to Pi starvation and recovery, but also reveals detailed interactions between phosphorylated and succinylated proteins in barley roots.

KEYWORDS

phosphorylation, succinylation, Pi stress, root, corsstalk, barley

Introduction

Proteins play critical roles in essential plant biological processes. Their diversity of functions is regulated by a wide range of posttranslational modifications (PTMs), which are central to the modulation of proteins activity, stability, subcellular localization, and interactions with other functional units (Millar et al., 2019; Willems et al., 2019). In recent decades, based on rapid advances in high-throughput mass spectrometry (MS), more than 461 PTMs have been identified in eukaryotic cells. Thousands of PTM sites can now be comprehensively discovered and quantified in a single proteomics experiment (UniProt Consortium, 2018), including phosphorylation, ubiquitination, sumoylation, glycosylation, acetylation, and succinylation (Willems et al., 2019). Most PTMs of proteins are dynamic, whereby their formation is dependent on the specific targeting of an amino acid residue involving the recognition, addition, or removal of a modification; modular domains are termed a reader, writer, or eraser, respectively (Creixell and Linding, 2012). Furthermore, apart from a single regulatory PTM, multiple PTMs can positively or negatively influence the activities of each other in what is, termed PTM crosstalk (Venne et al., 2014). In plants, such PTMs have been individually investigated in depth among various species; however, studies on PTM crosstalk are only now just emerging.

Phosphorus (P) is an essential mineral macronutrient for plant growth since it is a central component of key molecules such as ATP, nucleic acids, and phospholipids. The roots of plants take up P from soil exclusively in the form of inorganic phosphate (Pi), an ion that is inadequate in sustaining normal plant growth in most agricultural ecosystems due to its low solubility and mobility in soil (Raghothama, 1999; Hinsinger et al., 2011). In fact, the availability of Pi for plants is low, with only about 20% available in applied phosphorus fertilizer. This has aggravated the massive consumption of nonrenewable phosphorus fertilizer resources, causing severe environmental pollution (Pan et al., 2019). To replicate Pi-deficient stress, plants have evolved complex regulatory strategies to improve Pi-acquisition efficiency (i.e., Pi acquisition through the root system), and/or Pi-use efficiency (i.e., Pi remobilization within the plant itself; Vance et al., 2003). In terms of improving Pi-acquisition efficiency, plants modulate their root system architecture by reducing primary roots and increasing lateral root density and root hairs to enlarge the root surface area for Pi uptake in Pi-deficient soils. However, plants also secrete organic acids and enzymes to enhance Pi bioavailability in the rhizosphere soil (Péret et al., 2014).

These well-regulated systems encompass morphological, physiological, biochemical, and molecular adaptations that are controlled by a sophisticated gene regulatory network and are known as the phosphate starvation response (PSR; Chiou and Lin, 2011). In recent years, a growing number of plant studies have revealed that PTM is an important and central regulatory mechanism in the regulation of PSR. Acetylation of histones is essential for the regulation of gene expression for PSRs (Kumar et al., 2021). In Arabidopsis, the histone acetyltransferase, GCN5, positively regulates long non-coding RNA *At4* expression under Pi deficient conditions by modulating its H3K14ac level, resulting in impaired Pi allocation and accumulation in the plant (Wang et al., 2019). Histone deacetylase complex1 (hdc1), involved in the inhibition of primary root growth under Pi deficient conditions, affected the histone H3 acetylation of genes related to the remodeling of root system architecture (Xu et al., 2020). Direct targets of the HDA19 histone deacetylase, complex have not yet been identified. However, several Pi deficiency induced SPX domain containing genes showed decreased expression in HDA19 knock-down *Arabidopsis* lines, including the transcription factors, *SPX3* and *SPX1*. Notably, it is quite possible that HDA19 controls the length of root epidermal cells in response to Pi deficiency by mediating histone PTMs (Chen et al., 2015). Many studies have shown that regulation of ubiquitination is central in the control of PSR in plants, especially in remodeling response of the root system architecture to Pi starvation (Pan et al., 2019). Recently, activation of *Arabidopsis thaliana* plant U box/armadillo repeat-containing E3 ligase9 by receptor kinase2 ubiquitinated the repressor protein of auxin accumulation, and then targeted the autophagy process to improve lateral root development under Pi starvation (Deb et al., 2014). Pi deficiency leads to degradation of the transcription factor, *WRKY6*, mediated by a ubiquitin E3 ligase, PRU1. Ubiquitinated *WRKY6* also significantly

accumulated under Pi-deficient conditions, which reduced the expression of *PHO1* to modulate Pi homeostasis (Ye et al., 2018).

Furthermore, the expression of the SPX-domain containing protein, SPX4, is reduced under Pi-starvation conditions. Its degradation is regulated by two RING-finger ubiquitin E3 ligases, SDEL1 and SDEL2. These ligases directly ubiquitinate the K213 and K299 lysine residues in SPX4 to modulate PHR2 activity, thus coordinately regulating Pi signaling and homeostasis in response to Pi stress in rice (Ruan et al., 2019). SUMOylation has received much attention due to it governing Pi homeostatic responses to Pi deficiency. For example, a small ubiquitin-like modifier (SUMO) E3 ligase, SIZ1, which mediates the SUMOylome, plays a pivotal role in the remodeling of root system architecture (Datta et al., 2018; Fang et al., 2021). In addition, results from the global profiling of phosphorylation during Pi starvation in rice roots revealed decreased phosphorylation of the protein kinases, CK2, mitogen-activated protein kinase (MAPK), and calcium-dependent protein kinase (Yang et al., 2019).

Barley (*Hordeum vulgare* L.) is a major cereal crops that is cultivated worldwide. In spite of barley having a strong tolerance to barren soil, its growth and development are seriously affected by Pi deficiency in many areas across the world (Harlan and Zohary, 1966). Resolving barley PTM regulatory mechanisms in response to a Pi deficit will lead to improvements in phosphate acquisition and utilization efficiency in crops. However, compared with other crops, research on PTMs during the phosphate starvation response in barley is still very limited. We have pioneered research on the identification of phosphorylation and lysine succinylation in barley in response to Pi starvation and the recovery process, respectively (Ma et al., 2021; Wang et al., 2021). Although these studies revealed that phosphorylated and succinylated proteins were involved in a wide variety of biological processes, an understanding of PTM-mediated crosstalk between protein phosphorylation and succinylation is still largely unknown in barley.

Distinct from previous reports, in the present study, we describe a comprehensive map of phosphorylation and succinylation dynamics in barley seedling roots in response to Pi-deficient and Pi-replete processes. In this, a Gene Set Enrichment Analysis (GSEA) strategy was used to analyze the features of phosphorylated and succinylated proteins during Pi starvation and recovery stages, with a focus on the cross talk between protein phosphorylation and succinylation, respectively. We successfully identified 275 proteins that were commonly modified by the two PTMs. Both phosphorylated and succinylated proteins showed a distinct difference in metabolic pathways during Pi starvation and the recovery process. Using these resources, we generated a specific metabolic regulatory network for the responses of phosphorylated and succinylated proteins to changing Pi supply. Our findings provide crucial clues for further understanding the cross talk between phosphorylated and succinylated proteins in response to Pi starvation in plants.

Materials and methods

Plant materials and treatments

The design of this study references the transcriptome analysis of a rice root response to Pi stress starvation and recovery by Secco et al. (2013) and is shown in Figure 1A. In our previous study, a low-Pi tolerant barley (*Hordeum vulgare* L.) genotype GN121 was identified. The roots of this genotype differ in how their architecture changes to respond to Pi starvation compared with low-Pi sensitive GN42 (Ren et al., 2016; Wang et al., 2021). GN121 was used in this present work. Seed germination, growth conditions, and Pi-stress treatment of GN121 plants were as previously described (Ren et al., 2018). Briefly, GN121 seeds without residual endosperm uniformly germinated for 10 days then transferred to modified Hoagland hydroponic nutrient solution with 0.39 mM KH_2PO_4 (high Pi, +Pi) or 0.039 mM KH_2PO_4 (low Pi, –Pi) as the only Pi source. For Pi starvation and re-supply, plants were grown under –Pi for 48 h (Pi-starvation process) and then resupplied with +Pi for 48 h (Pi-recovery process). Roots were harvested under Pi-starvation and Pi-recovery processes after 6 h and 48 h for three biological replicates, respectively. Six roots were randomly collected for each biological replicate. The root samples were frozen in liquid nitrogen and stored at −80°C for protein extraction.

Proteomics analysis

Further details on protein extraction, digestion, phosphopeptide and succinyl-peptide enrichment, liquid chromatography with tandem mass spectrometry (LC–MS/MS) analysis, and database searching are outlined in the our previously articles (Ma et al., 2021; Wang et al., 2021). In summary, for phosphopeptide enrichment, tryptic peptides were dissolved in a 6% (v/v) TFA/50% ACN (v/v) buffer and the supernatant was incubated with an immobilized metal affinity column that bound phosphopeptides. To enrich for succinyl-peptides, tryptic peptides were dissolved in immunoprecipitation buffer and the supernatant was incubated with pre-washed antibody beads (PTM402; PTM Biolabs, Hangzhou, China) that bound succinyl-peptides. Dissolved samples were subsequently injected into an EASY-nLC 1,000 ultraperformance liquid chromatography system (Thermo Fisher Scientific, Waltham, MA, United States) and loaded onto an in-house reversed-phase analytical column (15-cm length, 75 μm i.d.). The electrospray voltage applied was 1.6 kV. Precursors and fragments were detected in a TOF detector, with a m/z scan range from 100 to 1700. Parallel accumulation serial fragmentation (PASEF) mode was used for the primary MS acquisition, and 10 times PASEF-MS/MS scans were acquired 1 cycle with the charge states in the range of 0–5. The dynamic exclusion time was set to 30 s. The resulting MS/MS data were processed using a MaxQuant search engine (v.1.6.6.0). Finally, tandem mass

10.3389/fpls.2022.917652

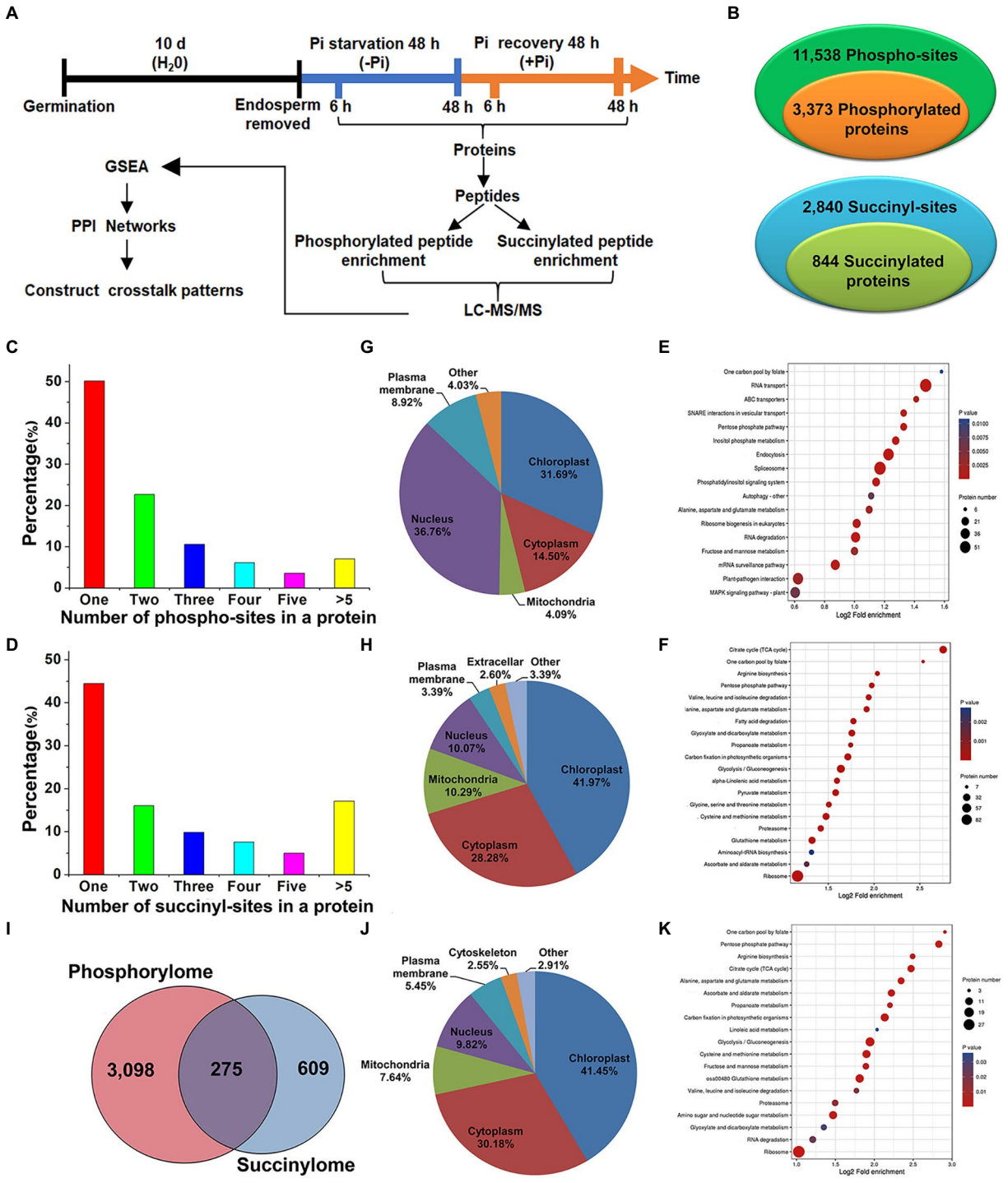

FIGURE 1
Experimental workflow and profiling phosphoproteome and succinylome responses of barley roots to Pi starvation and recovery. The workflow of the integrated analysis of phosphoproteome and succinylome data **(A)**. Detection of phosphorylated and succinylated proteins **(B)**. The number of phospho- and succinyl-sites within phosphorylated **(C)** and succinylated **(D)** proteins, respectively. Subcellular localization and KEGG pathway enrichment analysis of phosphorylated (**G,E**) and succinylated proteins (**H,F**), respectively. Overlap of phosphorylated and succinylated proteins (**I**). Subcellular localization and KEGG pathway enrichment analysis of both phosphorylated and succinylated proteins (**J,K**), respectively. GSEA, Gene Set Enrichment Analysis; KEGG, Kyoto Encyclopedia of Genes and Genomes; LC–MS/MS, liquid chromatography with tandem mass spectrometry; Pi, intracellular phosphate; PPI, protein–protein interaction.

spectra were searched against a *Hordeum vulgare* L. protein database[1] (39,743 protein entries). False discovery rate thresholds for protein, peptide, and modification sites were adjusted to <1% and the minimum score for modified peptides was set to >40. Label-free, intensity-based, absolute quantification values in MaxQuant were used to quantify phosphorylated and succinylated protein abundance (Cox et al., 2014). The mass spectrometry profiles of proteome, phosphoproteome, and succinyl-proteome data are available *via* ProteomeXchange with the identifiers PXD022052, PXD022077 and PXD022053, respectively.

Bioinformatics analysis

The overall aims of this study were to compare different quantified phospho- and succinyl-proteins, and, further, to reveal cross talk patterns between such quantified proteins. First, phospho- and succinyl-proteins were assigned to functional categories using a Kyoto Encyclopedia of Genes and Genomes (KEGG) pathway database. Then, a threshold-free method, Gene Set Enrichment Analysis (GSEA) was used to assess metabolic pathways that were significantly and differentially expressed during Pi-starvation and Pi-recovery processes for individual quantified phospho- and succinyl-proteins, as well as both quantified phospho- and succinyl-proteins, using GSEA software, respectively (Subramanian et al., 2005). Five or more genes were allowed in each set, and the ranked genes were used as inputs to GSEAPreRanked with default options except that gene set permutations were performed 1,000 times. Metabolic pathways with *p*-values less than 0.05 for the permutation test were defined as significant differentially expressed metabolic pathways. The subcellular localization data of proteins was obtained from a Eukaryotes database of Wolfpsort[2] based on annotations (Horton et al., 2007). For the identification of similarly regulated phosphoryl- and succinyl-proteins, expression profile clustering at four different time points was performed using a Mfuzz package (v2.32.0) for R programming language (Kumar and Futschik, 2007). Briefly, the input table of mean normalized protein intensity values was organized into columns with separate rows for each protein. We used a fuzzy c-means (FCM) clustering algorithm; FCM assigns a membership value to each profile in the range [0,1] for each of the c clusters. The final clustering was done with the parameters $c = 6$ and $m = 1.5$. Finally, protein–protein interaction (PPI) networks for identified proteins showing phosphorylation, succinylation and both phosphorylation and succinylation, were obtained from STRING software (v.11.0) and visualized by Cytoscape (3.7.2) software by applying a confidence score of 0.4 (Shannon et al., 2003).

Coimmunoprecipitation and MS/MS analysis

We performed a coimmunoprecipitation (co-IP) assay and MS/MS analysis to further validate protein phosphorylation and succinylation results. Coimmunoprecipitation experiments were performed according to the manufacturer's protocol using phospho-serine (Cat. #3192) and succinylated lysine (Cat. #3089) polyclonal antibodies from Dia-an Biotechnology Incorporation (Wuhan, China). Briefly, roots of GN121 in Pi starvation for 6 h and 48 h, and in Pi recovery for 6 h and 48 h, as described above, were frozen in liquid nitrogen and ground to a fine powder. The powder was lysed for 30 min in ice-cold western blot/immunoprecipitation buffer (Beyotime, Shanghai, China) containing protease and phosphatase inhibitors. Samples were then centrifuged for 10 min at 15,000 × *g* at 4°C, and supernatants transferred to new tubes. Each supernatant was then precleared by incubation with 10 µl of phospho-serine or succinylated lysine polyclonal antibody and 50 µl of protein A/G magnetic beads for 1 h at room temperature, followed by centrifugation and the supernatant discarded. The protein A/G magnetic beads were washed three times with phosphate buffered saline (PBS), and cell lysates (200 µl) were incubated with the corresponding antibody at 4°C overnight. Finally, each pellet was resuspended in 50 µl PBS buffer after washing with PBS three times, and a 20-µl sample was used and subsequently analyzed by western blotting. Western blotting experiments were based on previously described methods by Zeng et al. (2021). The primary antibodies used in the western blot were phospho-serine polyclonal antibody (1,500 in TBST with 5% nonfat milk), and succinylated lysine polyclonal antibody (1,300 in TBST with 5% nonfat milk) incubated overnight at 4°C. A goat anti-rabbit antibody with conjugated horse radish peroxidase was used as a secondary antibody at a 1:5000 dilution in TBST with 3% nonfat milk. The immunoprecipitated proteins eluted from supernatants were used for identification by liquid chromatography (LC)–MS/MS as described above.

Results

Global characterization of protein phosphorylation and succinylation

To compile a comprehensive protein phosphorylation and succinylation profile of barley roots in response to Pi starvation and recovery, we performed a time-course experiment involving Pi deprivation and resupply of Pi-starved plants for up to 48 h. In total, four time points, Pi deprivation at 6 h and 48 h, and Pi resupply at 6 h and 48 h, were selected to assess protein phosphorylation and succinylation changes in roots

1 https://webblast.ipkgatersleben.de/barley_ibsc/downloads (Accessed July 30, 2022).

2 http://www.genscript.com/psort/wolf_psort.html (Accessed July 30, 2022).

(Figure 1A). Our sequential affinity enrichment workflow identified 3,373 and 884 unique phosphorylated and succinylated proteins corresponding to 11,538 and 2,840 phospho- and succinyl-sites, respectively (Figure 1B; Supplementary Table S1). The 3,373 phosphoryl-proteins and 884 succinyl-proteins that were identified accounted for 53.97 and 13.12%, respectively, of the total number of identified barley root proteins.

We next evaluated the distribution of phosphorylation and succinylation sites identified on proteins by counting the number of modification sites. Of the 3,634 detected phosphorylated proteins, those proteins with one, two, three, four, five or more phosphorylation sites comprised 50.13, 22.65, 10.55, 6.11, 3.56, and 7.00% of modified protein sites, respectively (Figure 1C). A pSer modification comprised 73.29%, pThr 24.46%, and pTyr is 2.25% of modified protein sites, respectively (Supplementary Table S1). Of the 884 succinylation proteins detected, about 44.46% contained a single lysine succinylation site. Proteins with two, three, four, five or more succinylated sites comprised 16.06, 9.84, 7.58, 4.98, and 17.08% of modified protein sites, respectively (Figure 1D). Pathway enrichment analysis revealed that proteins modified by phosphorylation and succinylation were involved in distinct metabolic processes although several processes existed in which both PTMs were over-represented. In particular, we found protein phosphorylation predominantly on proteins related to RNA transport, the spliceosome, endocytosis, RNA degradation, and plant pathogen interactions (Figure 1E; Supplementary Table S2), while succinylation occurred on proteins involved in the ribosome, tricarboxylic acid (TCA) cycle, and glycolysis/gluconeogenesis (Figure 1F; Supplementary Table S3). Subcellular location profiles showed that approximately 68.5% of all phosphorylated proteins were located in the nucleus and chloroplasts (Figure 1G). This indicates that the roots may regulate intra-nuclear processes and chloroplast protein functions through the phosphorylation of relevant proteins. Similarly, about 70.25% of all succinylated proteins were located in the cytoplasm and chloroplasts (Figure 1H), which suggests that protein succinylation has a critical role in regulating extensive cytosolic processes. To obtain more detailed information on co-occurring proteins modified by both phosphorylation and succinylation, we compared all identified phosphorylation and succinylation events occurring on proteins. We showed that only 275 proteins were both phosphorylated and succinylated (Figure 1I). Approximately 72.0% of these proteins were located in the cytoplasm and chloroplasts (Figure 1J). Functions related to the ribosome, glycolysis/gluconeogenesis, and glutathione metabolism, especially in ribosome processes, were significantly enriched (Figure 1K; Supplementary Table S4). Taken together, these analyses suggest that protein phosphorylation and succinylation were frequently occurring PTMs that might have essential regulatory roles in the response of barley roots' to Pi stress.

Profiling protein phosphorylation and succinylation involved in responses to Pi stress

To identify differentially expressed metabolic pathways in phosphoryl- and succinyl-proteomes in response to Pi starvation, we employed GSEA to determine the significance of a change in protein expression during Pi deficit and recovery at different time points relative to the control sample. The GSEA of KEGG pathway analysis revealed that both Pi deficit and recovery were enriched in phosphoryl- and succinyl-proteomes in response to Pi stress and could be partitioned into distinct metabolic processes. However, two processes (MAPK signaling, and phenylpropanoid biosynthetic pathways) existed in which both PTMs were over-represented (Figures 2, 3; Supplementary Tables S5–S12). With regard to phosphorylome data, after 6 h of Pi deprivation, proteins related to purine metabolism, the MAPK signaling pathway, pyrimidine metabolism, and another five pathways were significantly upregulated, while proteins belonging to glycerolipid and glycerophospholipid metabolism were significantly downregulated (Figure 2A; Supplementary Table S5). Proteins involved in pyrimidine metabolism, the MAPK signaling pathway, purine metabolism, ABC transporters, and the mRNA surveillance pathway were upregulated, and those involved in oxidative phosphorylation were downregulated after 48 h of Pi deprivation (Figure 2B; Supplementary Table S6). Similarly, during Pi resupply for 6 h, GSEA of KEGG pathway enrichment revealed that proteins that were involved in DNA replication, ABC transporters, the MAPK signaling pathway, and pyrimidine, and purine metabolism were significantly upregulated, while phenylpropanoid biosynthesis was significantly downregulated (Figure 2C; Supplementary Table S7). Proteins belonging to purine and pyrimidine pathway, the MAPK signaling pathway, and ABC transporters were significantly upregulated, and glycolysis of gluconeogenesis, oxidative phosphorylation, and biosynthesis of amino acids were significantly downregulated under Pi resupply for 48 h, respectively (Figure 2D; Supplementary Table S8). In particular, we observed that of these enrichment pathways, only proteins related to purine and pyrimidine metabolism, the MAPK signaling pathway, and ABC transporters were upregulated in either Pi deprivation and/or recovery stages, respectively (Figure 3A).

Furthermore, for succinylome data, in a GSEA analysis of Pi deficiency for 48 h, we found that proteins involved in phenylalanine, nitrogen metabolism, phenylpropaneoide biosynthesis, phenylalanine, tyrosine and tryptophan biosynthesis, alanine, aspartate and glutamate metabolism, and the ribosome metabolic pathway were significantly upregulated, and lysine degradation and tryptophan metabolism were downregulated during Pi starvation, respectively (Figure 4A; Supplementary Table S9). In Pi deficiency for 48 h, proteins related to plant hormone signal transduction, phenylpropanoid biosynthesis, the MAPK signaling pathway, alanine, aspartate and glutamate metabolism, nitrogen metabolism, phenylalanine, tyrosine and tryptophan biosynthesis, and ribosomes were significantly

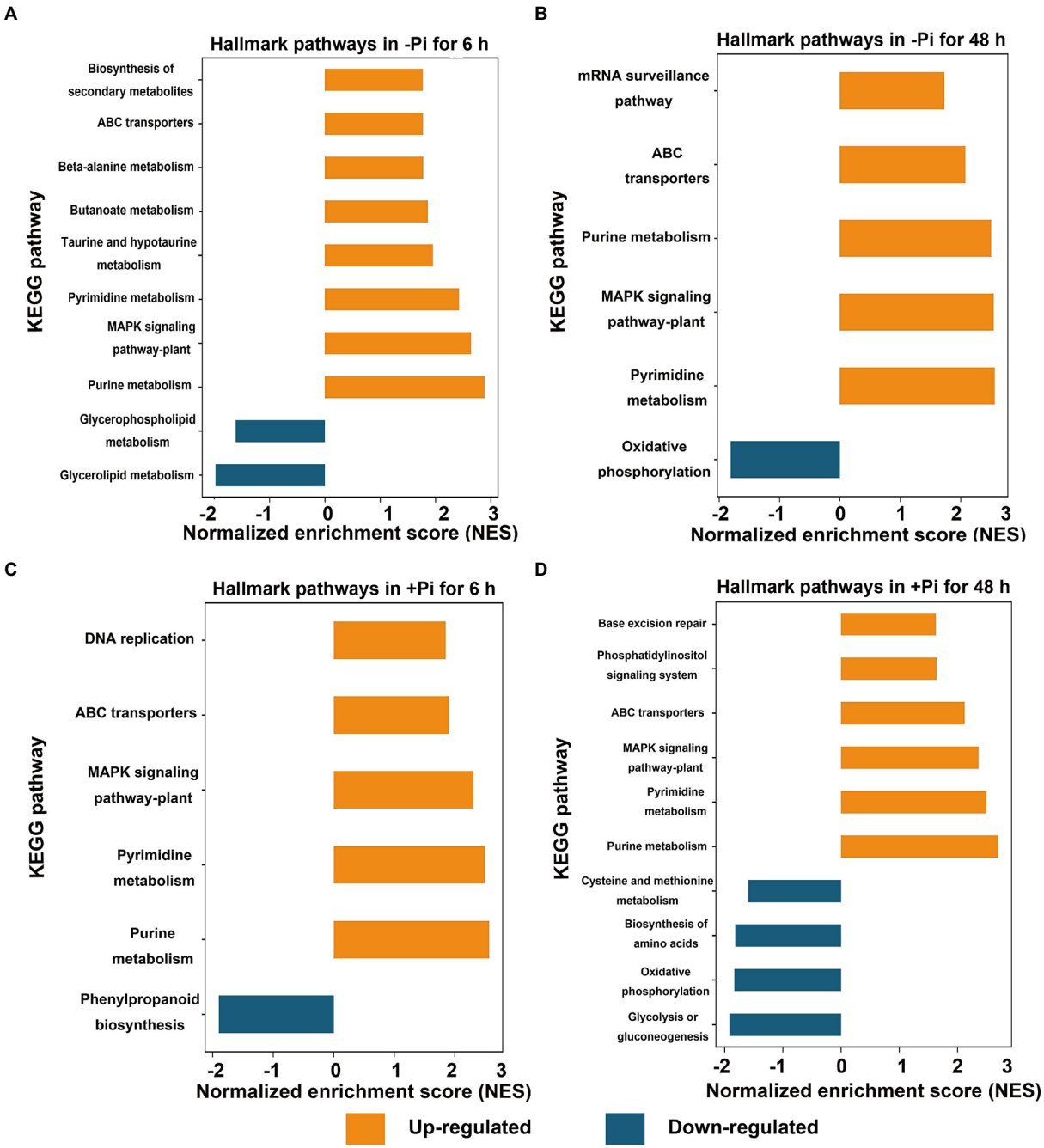

FIGURE 2
GSEA of significantly up (FDR<0.1, NES>1.5; orange) or down (FDR<0.1, NES< −1.5; blue) regulated metabolic pathways in response to Pi starvation (−Pi) for 6 h **(A)** and 48 h **(B)** and Pi recovery (+Pi) for 6 h **(C)** and 48 h **(D)** of phosphorylated proteins, respectively. Gene sets with an FDR < 0.01 are displayed using bar plots. FDR, false discovery rate; GSEA, Gene Set Enrichment Analysis; NES, normalized enrichment score; Pi, intracellular phosphate.

upregulated, while those associated with lysine degradation and tryptophan metabolism were downregulated (Figure 4B; Supplementary Table S10). Under Pi recovery for 6 h, proteins belonging to plant hormone signal transduction, phenylpropanoid biosynthesis, one carbon pool by folate pathway, the MAPK signaling pathway, nitrogen metabolism, and ribosomes were significantly upregulated, while proteins related to lysine degradation and tryptophan metabolism were significantly downregulated, respectively (Figure 4C; Supplementary Table S11). After 48 h of Pi recovery, proteins in nitrogen metabolism, phenylpropanoid biosynthesis, and alanine, aspartate and glutamate metabolism were upregulated, while those related to

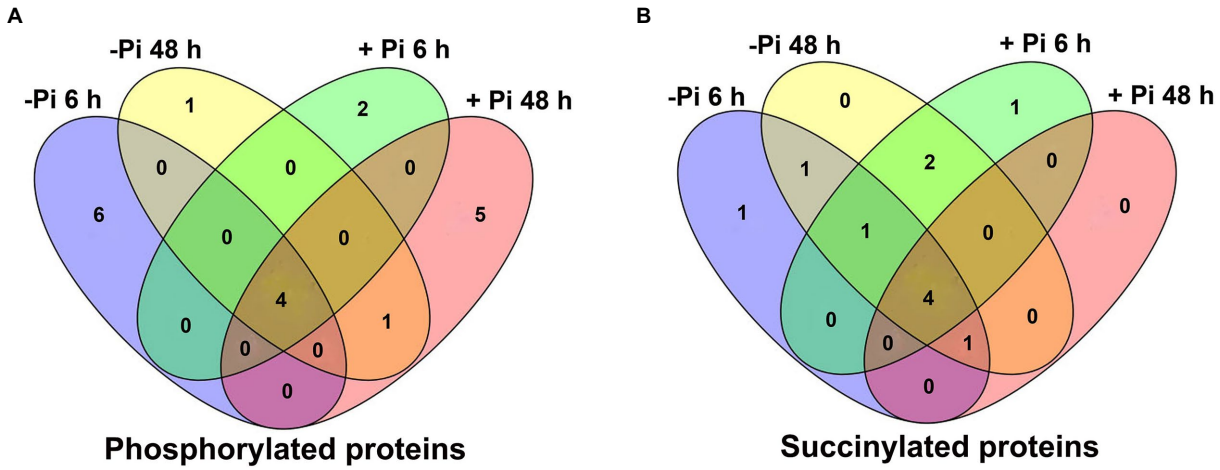

FIGURE 3
Venn diagram representing the overlap of differentially expressed metabolic pathways in Pi starvation (−Pi) for 6 h and 48 h, and Pi recovery (+Pi) for 6 h and 48 h with regard to phosphorylated **(A)** and succinylated **(B)** proteins, respectively. Pi, intracellular phosphate.

lysine degradation and tryptophan metabolism were downregulated significantly (Figure 4D; Supplementary Table S12). Intriguingly, proteins significantly downregulated by both Pi starvation and/or recovery were enriched in lysine degradation and tryptophan metabolism, with both belonging to amino acid metabolism. Meanwhile, proteins that were significantly upregulated by both Pi starvation and/or recovery were enriched for nitrogen metabolism and phenylpropanoid biosynthesis (Figures 3B, 4).

Expression pattern of phosphoryl- and succinyl-proteins in response to Pi stress

To explore the characteristics of phosphoryl- and succinyl-proteins in response to the processes of Pi starvation and then Pi resupply, we classified mainly phosphoryl- and succinyl-proteins into six groups according to their expression patterns in response to Pi treatments (Figures 5A, 6A). From the perspective of protein expression patterns, phosphoryl- and succinyl-proteins showed different response patterns to Pi starvation and recovery. At the same time, it was difficult to determine the protein sets that specifically responded to Pi starvation and recovery. This may have been due to short-term Pi starvation and recovery stages that were insufficient to induce specific Pi stress perception and signal transduction by phosphoryl- and succinyl-proteins. For phosphoryl-proteins, cluster 2 and 4 proteins showed a response to Pi starvation but were not responsive to Pi recovery; these proteins were enriched in starch and sucrose metabolism, urine metabolism, and nitrogen metabolism (Figure 5B; Supplementary Table S13). Cluster 1, 3, 5, and 6 proteins responded to both Pi starvation and resupply; these proteins were mainly enriched in RNA transport, and RNA degradation, among other pathways. This was especially so for proteins belonging to cluster 6 that were continuously upregulated in Pi starvation, and that were enriched in the mRNA surveillance pathway (Figure 5B; Supplementary Table S13).

For succinyl-proteins, cluster 2 proteins responded to Pi starvation and persisted in their response during Pi resupply; proteins belonging to this class were enriched in the TCA cycle, glycolysis/gluconeogenesis, and pyruvate metabolism, among other pathways (Figure 6B; Supplementary Table S14). Cluster 4 and 5 proteins showed a response to Pi recovery but were not responsive to Pi starvation, including those in the response to glycolysis/gluconeogenesis, glyoxylate and dicarboxylate metabolism, TCA cycle, and ribosome pathway. Cluster 1, 3, and 6 proteins responded to both Pi starvation and recovery; such proteins were mainly enriched in the TCA cycle, glyoxylate and dicarboxylate metabolism, ribosome, glycolysis/gluconeogenesis, carbon fixation in photosynthetic organisms, and cysteine and methionine metabolism, among other pathways (Figure 6B; Supplementary Table S14).

Crosstalk of phosphorylome and succinylome in response to Pi stress

To investigate how plant metabolism maybe regulated by phosphorylation and succinylation, we also compared all protein enrichment pathways found to be modified by these PTMs in Pi starvation and recovery processes. Surprisingly, while 275 proteins were shown to undergo both phosphorylation and succinylation events under Pi stress, only two pathways, MAPK signaling and phenylpropanoid biosynthesis pathway, were enriched at the same stress time point of 6 h under Pi resupply (Figures 2, 4). More specifically, for the MAPK signaling pathway, a total of six and two

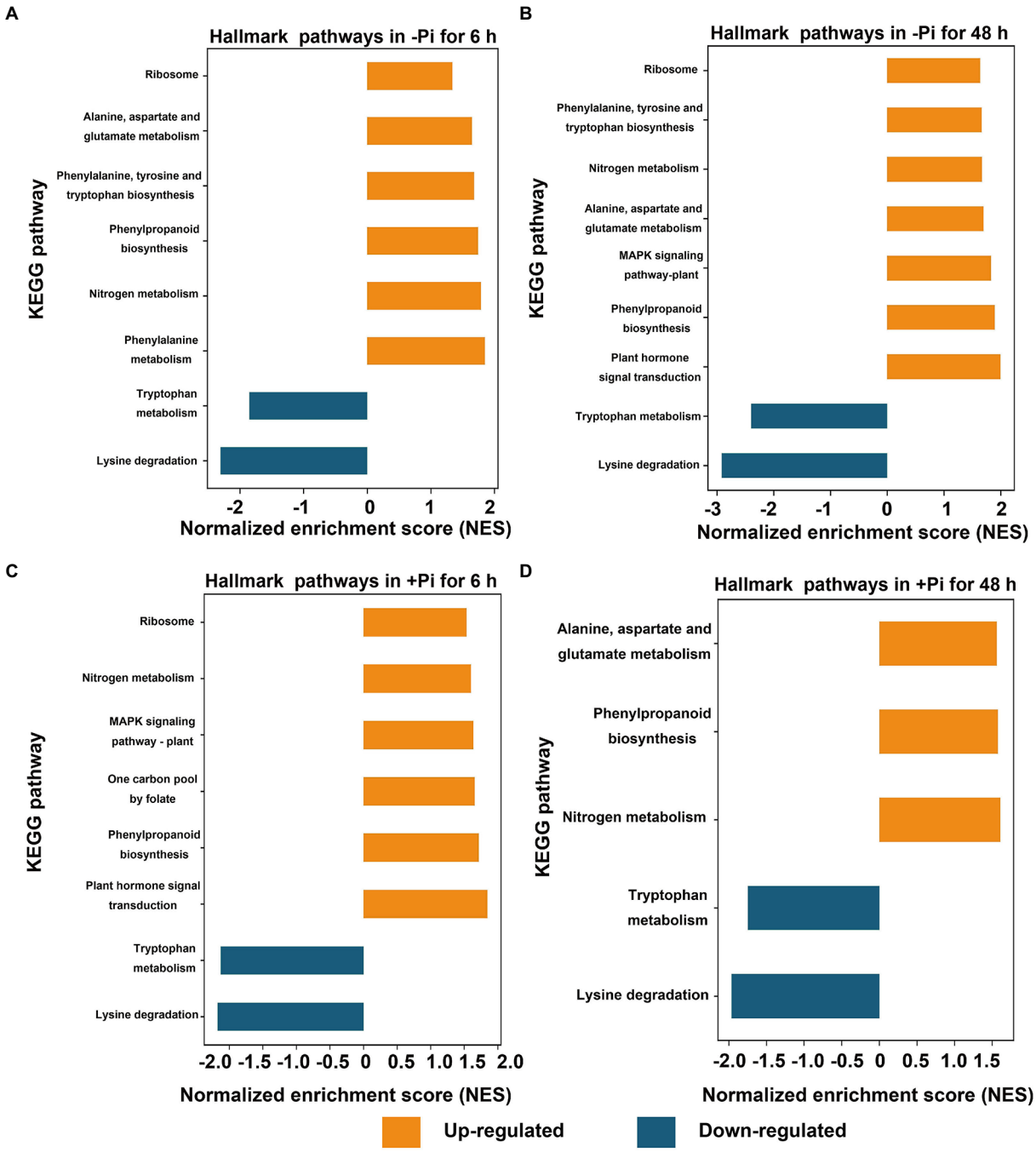

FIGURE 4
GSEA of significantly up- (FDR < 0.1, NES > 1.5; orange) or down- (FDR < 0.1, NES<−1.5; blue) regulated metabolic pathways in response to Pi starvation (−Pi) for 6 h **(A)** and 48 h **(B)**, and Pi recovery (+Pi) for 6 h **(C)** and 48 h **(D)** with regard to succinylated proteins, respectively. Gene sets with an FDR < 0.01 are displayed using bar plots. FDR, false discovery rate; GSEA, Gene Set Enrichment Analysis; NES, normalized enrichment score; Pi, intracellular phosphate.

proteins modified by phosphorylation and succinylation, respectively, were identified as core enrichment proteins. Of these, only one protein, HORVU1Hr1G055440.1 (a nucleoside diphosphate kinase family protein) was modified by both phosphorylation and succinylation (Supplementary Table S15). For the phenylpropanoid biosynthesis pathway, nine and four proteins were identified as core enrichment proteins with modified phosphorylation and succinylation, respectively; none of these were modified by both phosphorylation and succinylation simultaneously (Supplementary Table S15). Thus, this finding indicates that the co-occurrence of phosphorylation and succinylation happens not only on different proteins involved in

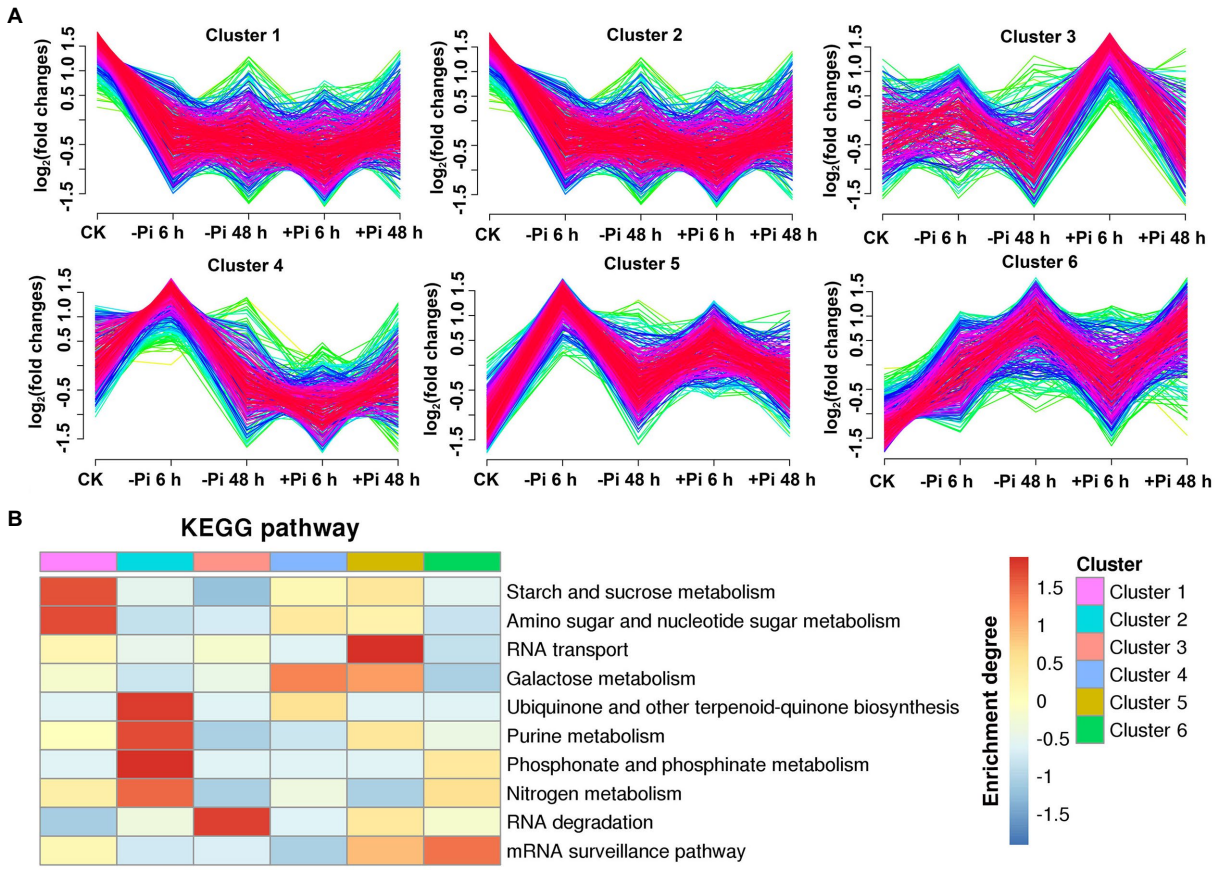

FIGURE 5
Clustering analysis of phosphorylated proteins based on their expression pattern in response to Pi starvation and recovery using a Mfuzz package **(A)**; and KEGG pathways that are overrepresented in each cluster based on the relative phosphorylation intensity relative to control **(B)**. –Pi, Pi starvation; +Pi, Pi recovery. The colored scale bar shows the enrichment degree of pathways in order perform z-score processing on-log (Fisher's exact test *p* value). KEGG, Kyoto Encyclopedia of Genes and Genomes; Pi, intracellular phosphate.

the same pathway, but also on the same proteins at different sites. Finally, to further analyze the crosstalk between both phosphoryl- and succinyl-proteins in Pi starvation and recovery, we constructed PPI networks of both such proteins under Pi starvation and recovery stages, respectively, using Cytoscape software. From these data sets, we found that this crosstalk between phosphoryl- and succinyl-proteins in response to Pi starvation and recovery were highly dynamic and involved in special metabolic processes. During Pi starvation, no metabolic pathways containing both phosphoryl- and succinyl-proteins were enriched. However, Pi resupply resulted in the enrichment of both phosphoryl- and succinyl-proteins associated with amino acid metabolism, such as alanine, aspartate and glutamate metabolism, and cysteine and methionine metabolism (Figure 7; Supplementary Tables S16, S17).

To validate their serine phosphorylated and lysine succinylated status, target proteins were enriched using phospho-serine and succinylated lysine polyclonal primary antibodies and visualized *via* western blotting (Figure 8). Co-immunoprecipitation followed by LC–MS/MS analysis were used to identify serine phosphorylated and lysine succinylated proteins. Finally, a large number of serine phosphorylation and lysine succinylation events were successfully detected in target proteins within the immunoprecipitated samples, respectively (Figures 8A,B). In particular, HORVU1Hr1G055440.1, modified by both phosphorylation and succinylation according to proteomics analysis, exhibited co-modification with phosphorylation and succinylation according to LC–MS/MS analysis. The changes in phosphorylation and succinylation levels were consistent with phosphorylated and lysine succinylated proteomic data (Figures 8C,D), meaning our proteomics analysis of phosphorylation and succinylation results were reliable.

Discussion

Our current understanding of Pi starvation and recovery in plants is largely derived from gene expression, transcriptome, and proteome studies. These have revealed a large number of potential key regulators of Pi homeostasis in plants, especially in *Arabidopsis thaliana* (Thibaud et al., 2010; Woo et al., 2012) and rice (Secco

et al., 2013; Gho et al., 2018). Protein phosphorylation and succinylation are the two most important PTMs for regulating multiple biological processes in plants (Nakagami et al., 2010; Xia et al., 2022). The recent developments of high-resolution mass spectrometry, antibody based affinity enrichment proteomic technology, and powerful bioinformatic tools have substantially contributed to the global analysis of protein phosphorylation and succinylation in barley. In our study in the last year, a large number of phosphoryl- and succinyl-proteins with diverse biological functions were identified to be responsive to Pi stress and recovery in barley roots (Ma et al., 2021; Wang et al., 2021). Although these studies contributed to our understanding of the mechanisms involved in responses to Pi starvation and recovery, they were limited to phosphoryl- and succinyl-proteins that were characterized separately, thus failing to capture any global crosstalk between phosphorylation and succinylation in the regulation of Pi homeostasis. In addition, such studies on phosphoryl- and succinyl-protein pathway enrichment were analyzed by a ranked differential protein list filtered by a particular threshold with a p value < 0.05 and fold-change > 1.5 (Ma et al., 2021; Wang et al., 2021), which is more dependent on differential proteins and has a certain subjectivity (Reimand et al., 2019). Here, in order to overcome the above defects, we used a threshold-free, GSEA approach to explore the underlying mechanisms by which protein phosphorylation and succinylation were involved in responses to Pi starvation and recovery in barley roots. These results provide more comprehensive insights into phosphorylation and succinylation responses to Pi stress.

Phosphorylation plays a prominent role in regulating cellular signaling, whereas succinylation is the primary mechanism for coordinating metabolism and cellular signaling (Swaney et al., 2013; Wu et al., 2019). In this study, a total of 3,373 and 884 unique phosphorylated and succinylated proteins, corresponding to 11,538 and 2,840 phospho- and succinyl-sites, were identified by a thorough investigation conducted on the response of barley roots Pi starvation and recovery, respectively (Figure 1B). We compared the KEGG enrichment of phosphorylated and succinylated proteins. Phosphorylated proteins were mainly localized in the nucleus and chloroplasts. An analysis of KEGG enrichment showed that these phosphorylated proteins were involved in processes such as RNA transport, spliceosome, endocytosis, RNA degradation, and plant pathogen interactions. In contrast, succinylated proteins were principally localized in the cytoplasm and chloroplasts, and enriched pathways were mainly involved with ribosomes, the TCA cycle, and glycolysis/gluconeogenesis (Figure 1). Furthermore, relatively minor overlapping was observed between our phosphorylated and succinylated proteins (Figure 1I). Similar results were obtained for the succinyl and acetyl proteomes of rice leaves (Zhou et al., 2018), and the protein phosphorylation and acetylation of proteins in Arabidopsis organs and seedlings (Uhrig et al., 2019). Such proteins, modified by both phosphorylation and succinylation, were mainly enriched in the cytoplasm and chloroplasts, and predominated in the ribosome pathway (Figure 1J). This suggests that proteins found co-occurring with phosphorylation and succinylation are more likely to be functionally important in protein synthesis in response to Pi stress.

To determine how differences in phosphorylation and succinylation of proteins in roots were represented in response to Pi starvation and recovery, we employed GSEA to identify differentially expressed metabolic pathways. Gene Set Enrichment Analysis revealed the presence of 10, 6, 6, and 10 metabolic pathways differentially expressed under Pi starvation for 6 h and 48 h, and under Pi recovery for 6 h, and 48 h, respectively (Figure 2). Of these pathways, purine, the MAPK signaling pathway, pyrimidine, and ABC transporters were upregulated by enrichment at all time points (Figure 2). It was found that purine metabolism played an important role in the acclimatization of *Arabidopsis* to drought (Watanabe et al., 2010; Itam et al., 2020), and pyrimidine metabolites showed an increasing trend under drought-stress conditions in bread wheat (Itam et al., 2020). The MAPK signaling pathway is a part of the complex signaling network for numerous environmental factors as well as plant growth and development. It is usually activated in response to various abiotic stresses, including nutrient status (Danquah et al., 2014; Kumar et al., 2020). ATP-binding cassette transporters participate in diverse biological processes to copy biotic and abiotic stresses. In Arabidopsis, *ALS3* and its interacting protein, *AtSTAR1*, form an ABC transporter complex, which involves the Pi deficiency induced remodeling of RSA by modulation of Fe homeostasis in roots (Dong et al., 2017). Similarly, eight, nine, eight and five differentially expressed metabolic pathways in succinylation proteins were enriched under Pi starvation for 6 h and 48 h, and Pi recovery for 6 h and 48 h, respectively (Figure 4). We observed that two upregulated, and two downregulated metabolic pathways overlapped between Pi starvation and recovery stages (Figure 4). Downregulated amino acid metabolism, including lysine degradation and tryptophan metabolism, maybe related to a developmental switch to cope with stress and recovery (Batista-Silva et al., 2019). Upregulated nitrogen metabolism and phenylpropanoid biosynthesis contribute to provide basic nutrients and metabolism for plant development, and to copy biotic and abiotic stresses (Limami et al., 2014; Dong and Lin, 2021). These results indicated that barley root phosphorylation and the succinylation protein response to Pi deficiency and recovery were dynamic, with differences at the pathway level.

Furthermore, surprisingly, the number of enriched metabolic pathways found to be overlapping the response of phosphorylation and succinylation proteins to Pi deficiency and recovery was very small. Only two pathways were identified: the MAPK signaling pathway, which was enriched after 48 h of Pi starvation, and the phenylpropanoid biosynthetic and MAPK signaling pathway, which was enriched after 6 h of Pi resupply

10.3389/fpls.2022.917652

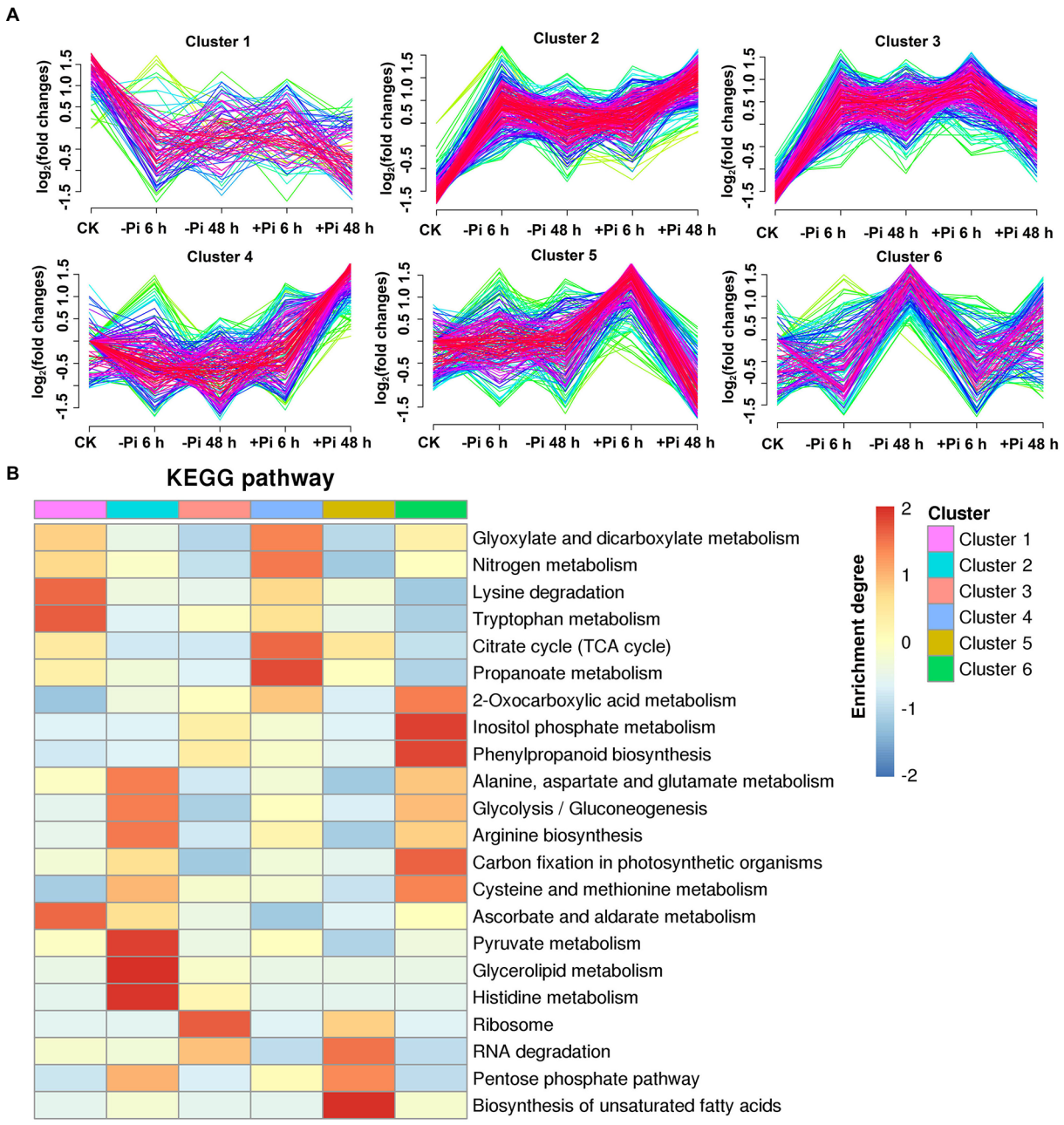

FIGURE 6
Clustering analysis of succinylated proteins based on their expression pattern in response to Pi recovery using a Mfuzz package **(A)** and KEGG pathways that are overrepresented in each cluster based on the succinylation intensity relative to the control **(B)**. –Pi, Pi starvation; +Pi, Pi recovery. The colored scale bar shows the enrichment degree of pathways to perform *z*-score processing on-log (Fisher's exact test *p* value). KEGG, Kyoto Encyclopedia of Genes and Genomes; Pi, intracellular phosphate.

(Figures 2–4). It is worth noting that among all 884 succinylated proteins, 275 were also phosphorylated, accounting for 31% of total succinylated proteins. Thus, we can speculate that MAPK signaling and phenylpropanoid biosynthesis play core roles in response to Pi stress. Consistent with previous transcriptome reports, phenylpropanoid metabolism was enriched in rice roots and shoots in short- and medium-term responses to Pi starvation and recovery (Secco et al., 2013). In this case, a total of eight core proteins belonged to the MAPK signaling pathway (Supplementary Table S15). Of these, the nucleoside diphosphate kinase family of proteins (NDPK; HORVU1Hr1G055440.1) was modified by both phosphorylation and succinylation at one site. The nucleoside diphosphate kinase family of proteins has been found to be involved in a wide range of biological processes including but not limited to signal transduction, and the response to salt

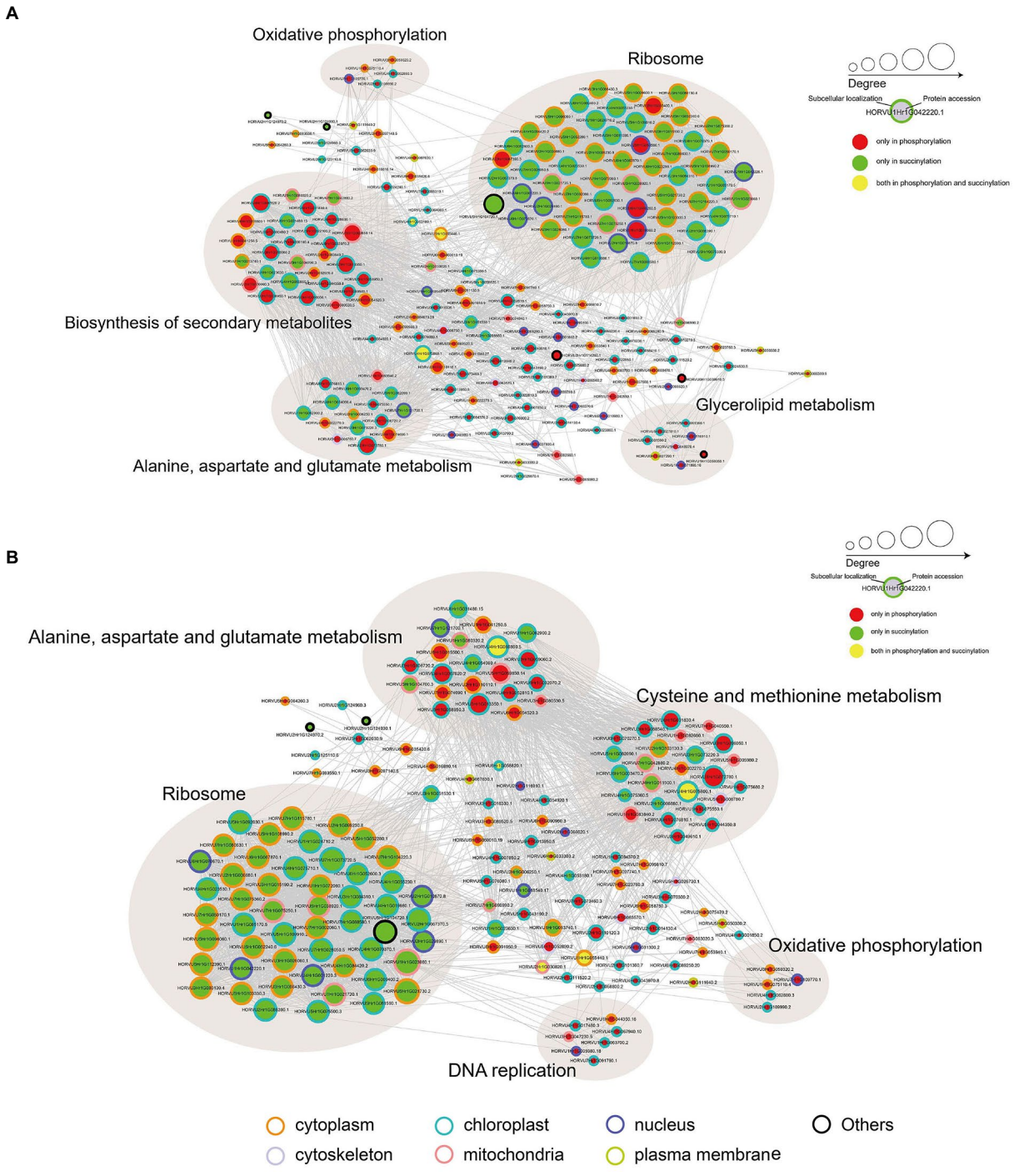

FIGURE 7
Protein–protein interaction (PPI) network analysis of significantly phosphorylated or succinylated, and both phosphorylated and succinylated proteins in response to Pi starvation **(A)** and recovery **(B)**, respectively. Phosphorylated and succinylated proteins belonging to the significantly enriched KEGG pathway in Pi starvation and Pi recovery stages were used for PPI analysis, respectively. PPI network were obtained from STRING software (v.11.0) and visualized by Cytoscape (3.7.2) after applying a confidence score of 0.4. Light brown circles depict clusters of proteins involved in specific metabolic pathways. The circle size represents the number of interaction nodes; the greater the number of interaction nodes, the larger the circle. Node outlines indicate the predicted subcellular localization of proteins. Cytoplasm (orange), cytoskeleton (lavender), mitochondria (pink), nucleus (purple), plasma membrane (green), chloroplast (blue), and others (black). Further details are in Supplementary Tables S16, S17. KEGG, Kyoto Encyclopedia of Genes and Genomes; Pi, intracellular phosphate; PPI, protein–protein interaction.

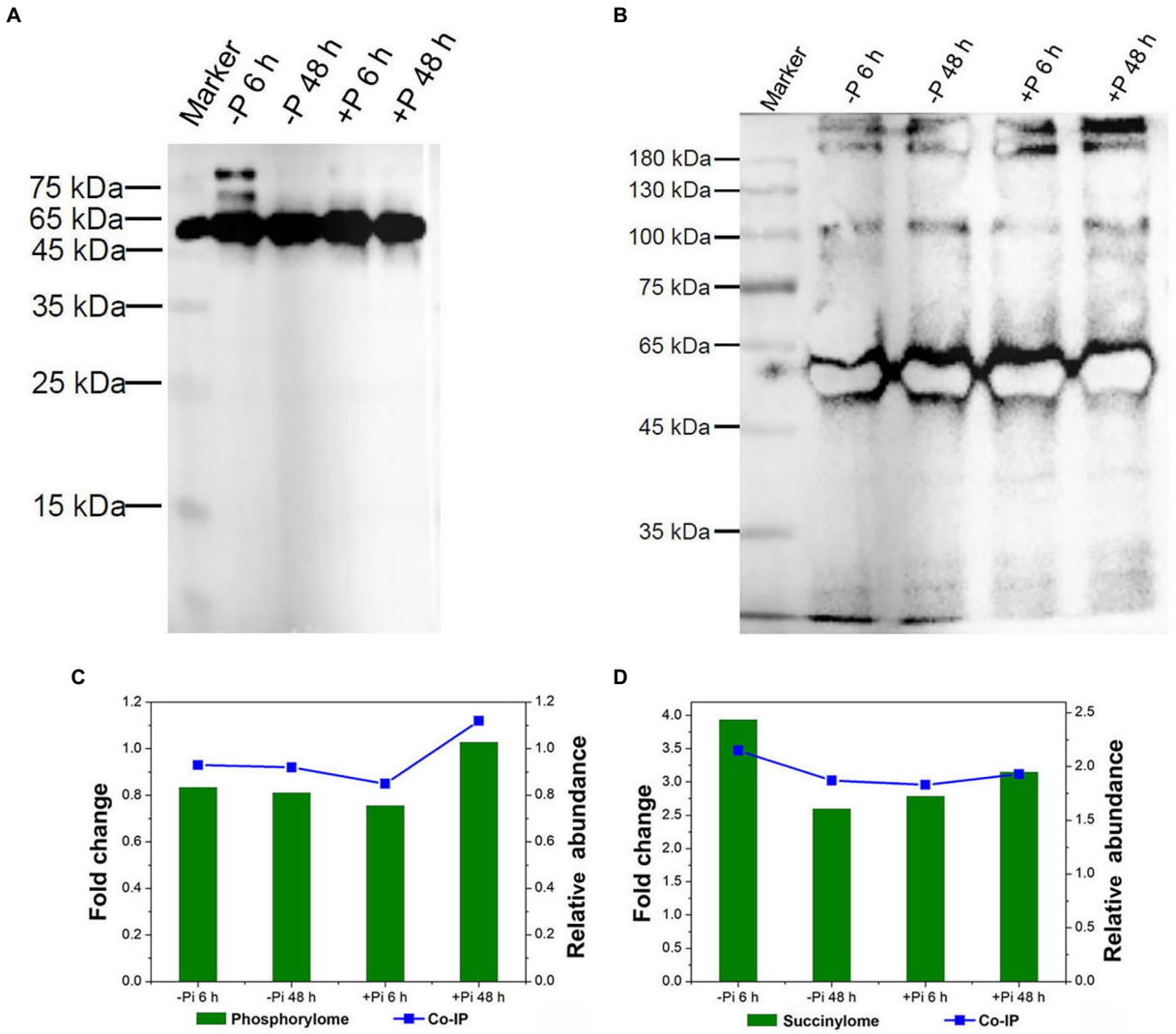

FIGURE 8
Validation of serine phosphorylation and lysine succinylation proteins in Pi starvation (−Pi) for 6 h and 48 h, and Pi recovery (+Pi) for 6 h and 48 h. Serine phosphorylation **(A)** and lysine succinylation **(B)** proteins were enriched by co-IP with phospho-serine and succinylated lysine polyclonal antibodies, respectively, followed by western blotting. Comparison of the phosphorylation **(C)** and succinylation **(D)** level of HORVU1Hr1G055440.1 in proteomic data (left Y-axis) and co-IP experiments (right Y-axis). Co-IP, co-immunoprecipitation; Pi, intracellular phosphate.

stress (Luzarowski et al., 2017). Proteins modified only by phosphorylation include protein kinase superfamily proteins (HORVU4Hr1G001850.2 and HORVU2Hr1G075470.2; one site), respiratory burst oxidase homologue D (HORVU4Hr1G081670.1; one site), ethylene-insensitive protein 2 (HORVU5Hr1G050330.2; three sites), and respiratory burst oxidase homolog B (HORVU4Hr1G086500.9; three sites). In comparison, 40S ribosomal protein S6a (HORVU2Hr1G010870.8) was modified by only succinylation at five sites. Additionally, 15 core enrichment proteins belonging to the phenylpropanoid biosynthesis pathway were modified by phosphorylation and succinylation (Supplementary Table S15). Of these, four proteins were all identified as alcohol dehydrogenase, with from one to three phosphorylation sites. Alcohol dehydrogenase play a role in growth, development, and abiotic and biotic stresses in plants, such as cold stress regulation (Su et al., 2020), wounding (Kim et al., 2010), and lignin biosynthesis (Cheng et al., 2013). Similarly, only four proteins with succinylation one site were identified as peroxidase superfamily proteins, which are involved in plant development and the stress response (Bela et al., 2015). In addition, it is noteworthy that phenylalanine ammonia-lyase 2 (HORVU6Hr1G058820.1), which was related to the stress response with two succinylation sites, was enriched in core succinylation proteins. Finally, our global proteome analyses of phosphorylation and succinylation of barley root proteins

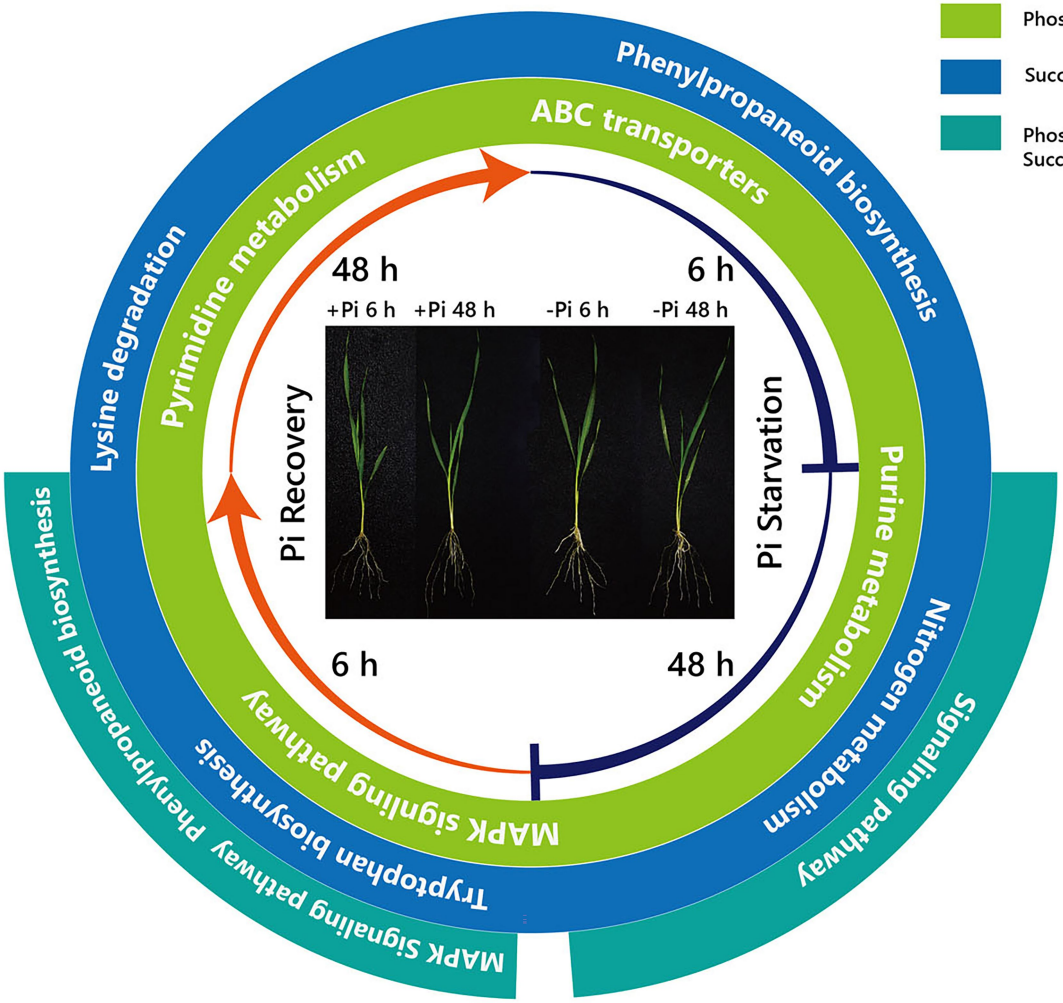

FIGURE 9
Summary of KEGG pathways of phosphorylated and succinylated proteins in response to Pi starvation and recovery. From the inside, the first and second circles show pathways overlapping the response of phosphorylation and succinylation proteins to Pi deficiency and recovery, respectively. The third circle shows pathways overlapping between the response of phosphorylation and succinylation proteins to deficiency and recovery. −Pi, Pi starvation; +Pi, Pi recovery. KEGG, Kyoto Encyclopedia of Genes and Genomes; Pi, intracellular phosphate.

covering the 48 h Pi starvation and 48 h Pi recovery stages, generated a comprehensive overview of the dynamic responses to Pi homeostasis for barley root proteins involved in different metabolic pathways (Figure 9) Phosphorylation and succinylation proteins related to MAPK signaling and phenylpropanoid biosynthetic pathways were relatively active in response to Pi stress.

Conclusion

This study aimed to elucidate the underlying mechanisms of protein phosphorylation, and succinylation in response to Pi stress. Our data indicate that in a proportion of barley roots, phosphorylation and succinylation are dynamically regulated by Pi starvation and recovery treatments, which may be important for plants to cope with Pi stress conditions. Marked differences exist between phosphorylation and succinylation proteins in significantly enriched metabolic pathways during Pi starvation and recovery at the same time point. Furthermore, overlapping proteins modified by both phosphorylation and succinylation were primarily enriched in MAPK signaling, and phenylpropanoid biosynthetic pathways. Protein–protein interaction network analyses indicated that the response of central metabolic pathways to Pi starvation and recovery was significantly modulated by phosphorylation or, succinylation, or both. Our study provides new evidence for protein phosphorylation and succinylation regulating the activities of key proteins involved in plant responses to Pi starvation and recovery.

Data availability statement

The mass spectrometry data from the succinylome and proteome have been deposited in ProteomeXchange with the dataset identifiers, PXD022052 and PXD022053, respectively.

Author contributions

JW, CL, and PR carried out the proteomic analysis and drafted the manuscript. ZM, LY, BL, YM, and XM participated in material culture and performed the statistical analysis. HW and XS conceived of the study, and participated in its design. HW, ES, and KY helped to draft the manuscript. All authors have read and approved the final manuscript.

Funding

This work was supported by the China Agriculture Research System (Grant CARS-05-04B-2); Industrial Support Project of Colleges and Universities in Gansu Province (2021CYZC-12); National Natural Science Foundation of China (31960426, 32160460, 32160496); Fuxi Talent Project of Gansu Agricultural University (Ganfx-03Y06); Key Projects of Natural Science Foundation of Gansu Province (20JR10RA507; 21JR7RA801).

Acknowledgments

We thank the professionals of BioMed Proofreading LLC for copyediting this manuscript.

Conflict of interest

The authors declare that the research was conducted in the absence of any commercial or financial relationships that could be construed as a potential conflict of interest.

Publisher's note

Supplementary material

The Supplementary material for this article can be found online at: https://www.frontiersin.org/articles/10.3389/fpls.2022.917652/full#supplementary-material

References

Batista-Silva, W., Heinemann, B., Rugen, N., Nunes-Nesi, A., Araújo, W. L., Braun, H. P., et al. (2019). The role of amino acid metabolism during abiotic stress release. *Plant Cell Environ.* 42, 1630–1644. doi: 10.1111/pce.13518

Bela, K., Horváth, E., Gallé, Á., Szabados, L., Tari, I., and Csiszár, J. (2015). Plant glutathione peroxidases: emerging role of the antioxidant enzymes in plant development and stress responses. *J. Plant Physiol.* 176, 192–201. doi: 10.1016/j.jplph.2014.12.014

Chen, C., Wu, K., and Schmidt, W. (2015). The histone deacetylase HDA19 controls root cell elongation and modulates a subset of phosphate starvation responses in Arabidopsis. *Sci. Rep.* 5, 1–11. doi: 10.1038/srep15708

Cheng, H., Li, L., Xu, F., Cheng, S., Cao, F., Wang, Y., et al. (2013). Expression patterns of a cinnamyl alcohol dehydrogenase gene involved in lignin biosynthesis and environmental stress in Ginkgo biloba. *Mol. Biol. Rep.* 40, 707–721. doi: 10.1007/s11033-012-2111-0

Chiou, T., and Lin, S. (2011). Signaling network in sensing phosphate availability in plants. *Annu. Rev. Plant Biol.* 62, 185–206. doi: 10.1146/annurev-arplant-042110-103849

Cox, J., Hein, M. Y., Luber, C. A., Paron, I., and Nagaraj, N. (2014). Accurate proteome-wide label-free quantification by delayed normalization and maximal peptide ratio extraction, termed MaxLFQ. *Mol. Cell. Proteom.* 13, 2513–2526. doi: 10.1074/mcp.M113.031591

Creixell, P., and Linding, R. (2012). Cells, shared memory and breaking the PTM code. *Mol. Syst. Biol.* 8:598. doi: 10.1038/msb.2012.33

Danquah, A., de Zelicourt, A., Colcombet, J., and Hirt, H. (2014). The role of ABA and MAPK signaling pathways in plant abiotic stress responses. *Biotechnol. Adv.* 32, 40–52. doi: 10.1016/j.biotechadv.2013.09.006

Datta, M., Kaushik, S., Jyoti, A., Mathur, N., Kothari, S. L., and Jain, A. (2018). SIZ1-mediated SUMOylation during phosphate homeostasis in plants: looking beyond the tip of the iceberg. *Semin. Cell Dev. Biol.* 74, 123–132. doi: 10.1016/j.semcdb.2017.09.016

Deb, S., Sankaranarayanan, S., Wewala, G., Widdup, E., and Samuel, M. A. (2014). The S-domain receptor kinase arabidopsis receptor kinase2 and the u box/armadillo repeat-containing e3 ubiquitin ligase9 module mediates lateral root development under phosphate starvation in arabidopsis. *Plant Physiol.* 165, 1647–1656. doi: 10.1104/pp.114.244376

Dong, N., and Lin, H. (2021). Contribution of phenylpropanoid metabolism to plant development and plant–environment interactions. *J. Integr. Plant Biol.* 63, 180–209. doi: 10.1111/jipb.13054

Dong, J., Piñeros, M. A., Li, X., Yang, H., Liu, Y., Murphy, A. S., et al. (2017). An arabidopsis ABC transporter mediates phosphate deficiency-induced remodeling of root architecture by modulating iron homeostasis in roots. *Mol. Plant* 10, 244–259. doi: 10.1016/j.molp.2016.11.001

Fang, Q., Zhang, J., Yang, D., and Huang, C. (2021). The SUMO E3 ligase SIZ1 partially regulates STOP1 SUMOylation and stability in Arabidopsis thaliana. *Plant Signal. Behav.* 16:1899487. doi: 10.1080/15592324.2021.1899487

Gho, Y., An, G., Park, H., and Jung, K. (2018). A systemic view of phosphate starvation-responsive genes in rice roots to enhance phosphate use efficiency in rice. *Plant Biotechno. Rep.* 12, 249–264. doi: 10.1007/s11816-018-0490-y

Harlan, J. R., and Zohary, D. (1966). Distribution of wild wheats and barley. *Science* 153, 1074–1080. doi: 10.1126/science.153.3740.1074

Hinsinger, P., Betencourt, E., Bernard, L., Brauman, A., Plassard, C., Shen, J., et al. (2011). P for two, sharing a scarce resource: soil phosphorus acquisition in the rhizosphere of intercropped species. *Plant Physiol.* 156, 1078–1086. doi: 10.1104/pp.111.175331

Horton, P., Park, K., Obayashi, T., Fujita, N., Harada, H., et al. (2007). WoLF PSORT: protein localization predictor. *Nucleic Acids Res.* 35, W585–W587. doi: 10.1093/nar/gkm259

Itam, M., Mega, R., Tadano, S., Abdelrahman, M., Matsunaga, S., Yamasaki, Y., et al. (2020). Metabolic and physiological responses to progressive drought stress in bread wheat. *Sci. Rep.* 10:17189. doi: 10.1038/s41598-020-74303-6

Kim, Y., Bae, J. M., and Huh, G. (2010). Transcriptional regulation of the cinnamyl alcohol dehydrogenase gene from sweetpotato in response to plant developmental stage and environmental stress. *Plant Cell Rep.* 29, 779–791. doi: 10.1007/s00299-010-0864-2

Kumar, L., and Futschik, M. E. (2007). Mfuzz: a software package for soft clustering of microarray data. *Bioinformation* 2, 5–7. doi: 10.6026/97320630002005

Kumar, K., Raina, S. K., and Sultan, S. M. (2020). Arabidopsis MAPK signaling pathways and their cross talks in abiotic stress response. *J. Plant Biochem. Biotechnol.* 29, 700–714. doi: 10.1007/s13562-020-00596-3

Kumar, V., Thakur, J. K., and Prasad, M. (2021). Histone acetylation dynamics regulating plant development and stress responses. *Cell. Mol. Life Sci.* 78, 4467–4486. doi: 10.1007/s00018-021-03794-x

Limami, A. M., Diab, H., and Lothier, J. (2014). Nitrogen metabolism in plants under low oxygen stress. *Planta* 239, 531–541. doi: 10.1007/s00425-013-2015-9

Luzarowski, M., Kosmacz, M., Sokolowska, E., Jasińska, W., Willmitzer, L., Veyel, D., et al. (2017). Affinity purification with metabolomic and proteomic analysis unravels diverse roles of nucleoside diphosphate kinases. *J. Exp. Bot.* 68, 3487–3499. doi: 10.1093/jxb/erx183

Ma, Z., Wang, J., Li, C., Ren, P., Yao, L., Li, B., et al. (2021). Global profiling of phosphorylation reveals the barley roots response to phosphorus starvation and resupply. *Front. Plant Sci.* 12:676432. doi: 10.3389/fpls.2021.676432

Millar, A. H., Heazlewood, J. L., Giglione, C., Holdsworth, M. J., Bachmair, A., and Schulze, W. X. (2019). The scope, functions, and dynamics of posttranslational protein modifications. *Annu. Rev. Plant Biol.* 70, 119–151. doi: 10.1146/annurev-arplant-050718-100211

Nakagami, H., Sugiyama, N., Mochida, K., Daudi, A., Yoshida, Y., Toyoda, T., et al. (2010). Large-scale comparative phosphoproteomics identifies conserved phosphorylation sites in plants. *Plant Physiol.* 153, 1161–1174. doi: 10.1104/pp.110.157347

Pan, W., Wu, Y., and Xie, Q. (2019). Regulation of ubiquitination is central to the phosphate starvation response. *Trends Plant Sci.* 24, 755–769. doi: 10.1016/j.tplants.2019.05.002

Péret, B., Desnos, T., Jost, R., Kanno, S., Berkowitz, O., and Nussaume, L. (2014). Root architecture responses: in search of phosphate. *Plant Physiol.* 166, 1713–1723. doi: 10.1104/pp.114.244541

Raghothama, K. G. (1999). Phosphate acquisition. *Annu. Rev. Plant Biol.* 50, 665–693. doi: 10.1146/annurev.arplant.50.1.665

Reimand, J., Isserlin, R., Voisin, V., Kucera, M., Tannus-Lopes, C., Rostamianfar, A., et al. (2019). Pathway enrichment analysis and visualization of omics data using g:profiler, GSEA, Cytoscape and EnrichmentMap. *Nat. Protoc.* 14, 482–517. doi: 10.1038/s41596-018-0103-9

Ren, P., Ma, X., Li, B., Meng, Y., Lai, Y., Si, E., et al. (2016). Identification and selection of low-phosphate-tolerant germplasm in barley (Hordeum vulgare L.). *Soil Sci. Plant Nutr.* 62, 471–480. doi: 10.1080/00380768.2016.1223521

Ren, P., Meng, Y., Li, B., Ma, X., Si, E., Lai, Y., et al. (2018). Molecular mechanisms of acclimatization to phosphorus starvation and recovery underlying full-length transcriptome profiling in barley (Hordeum vulgare L.). *Front. Plant Sci.* 9:500. doi: 10.3389/fpls.2018.00500

Ruan, W., Guo, M., Wang, X., Guo, Z., Xu, Z., Xu, L., et al. (2019). Two RING-finger ubiquitin e3 ligases regulate the degradation of SPX4, an internal phosphate sensor, for phosphate homeostasis and signaling in rice. *Mol. Plant* 12, 1060–1074. doi: 10.1016/j.molp.2019.04.003

Secco, D., Jabnoune, M., Walker, H., Shou, H., Wu, P., Poirier, Y., et al. (2013). Spatio-temporal transcript profiling of rice roots and shoots in response to phosphate starvation and recovery. *Plant Cell* 25, 4285–4304. doi: 10.1105/tpc.113.117325

Shannon, P., Markiel, A., Ozier, O., Baliga, N. S., Wang, J. T., Ramage, D., et al. (2003). Cytoscape: a software environment for integrated models of biomolecular interaction networks. *Genome Res.* 13, 2498–2504. doi: 10.1101/gr.1239303

Su, W., Ren, Y., Wang, D., Su, Y., Feng, J., Zhang, C., et al. (2020). The alcohol dehydrogenase gene family in sugarcane and its involvement in cold stress regulation. *BMC Genomics* 21:521. doi: 10.1186/s12864-020-06929-9

Subramanian, A., Tamayo, P., Mootha, V. K., Mukherjee, S., Ebert, B. L., Gillette, M. A., et al. (2005). Gene set enrichment analysis: a knowledge-based approach for interpreting genome-wide expression profiles. *Proc. Natl. Acad. Sci.* 102, 15545–15550. doi: 10.1073/pnas.0506580102

Swaney, D. L., Beltrao, P., Starita, L., Guo, A., Rush, J., Fields, S., et al. (2013). Global analysis of phosphorylation and ubiquitylation cross-talk in protein degradation. *Nat. Methods* 10, 676–682. doi: 10.1038/nmeth.2519

Thibaud, M., Arrighi, J., Bayle, V., Chiarenza, S., Creff, A., et al. (2010). Dissection of local and systemic transcriptional responses to phosphate starvation in Arabidopsis. *Plant J.* 64, 775–789. doi: 10.1111/j.1365-313X.2010.04375.x

Uhrig, R. G., Schläpfer, P., Roschitzki, B., Hirsch-Hoffmann, M., and Gruissem, W. (2019). Diurnal changes in concerted plant protein phosphorylation and acetylation in Arabidopsis organs and seedlings. *Plant J.* 99, 176–194. doi: 10.1111/tpj.14315

UniProt Consortium (2018). UniProt: the universal protein knowledgebase. *Nucleic Acids Res.* 46, 2699. doi: 10.1093/nar/gky092

Vance, C. P., Uhde Stone, C., and Allan, D. L. (2003). Phosphorus acquisition and use: critical adaptations by plants for securing a nonrenewable resource. *New Phytol.* 157, 423–447. doi: 10.1101/gr.1239303

Venne, A. S., Kollipara, L., and Zahedi, R. P. (2014). The next level of complexity: crosstalk of posttranslational modifications. *Proteomics* 14, 513–524. doi: 10.1002/pmic.201300344

Wang, J., Ma, Z., Li, C., Ren, P., Yao, L., Li, B., et al. (2021). Dynamic responses of barley root succinyl-proteome to short-term phosphate starvation and recovery. *Front. Plant Sci.* 12:649147. doi: 10.3389/fpls.2021.649147

Wang, T., Xing, J., Liu, Z., Zheng, M., Yao, Y., Hu, Z., et al. (2019). Histone acetyltransferase GCN5-mediated regulation of long non-coding RNA At4 contributes to phosphate starvation response in Arabidopsis. *J. Exp. Bot.* 70, 6337–6348. doi: 10.1093/jxb/erz359

Watanabe, S., Nakagawa, A., Izumi, S., Shimada, H., and Sakamoto, A. (2010). RNA interference-mediated suppression of xanthine dehydrogenase reveals the role of purine metabolism in drought tolerance in Arabidopsis. *FEBS Lett.* 584, 1181–1186. doi: 10.1016/j.febslet.2010.02.023

Willems, P., Horne, A., Van Parys, T., Goormachtig, S., De Smet, I., et al. (2019). The plant PTM viewer, a central resource for exploring plant protein modifications. *Plant J.* 99, 752–762. doi: 10.1111/tpj.14345

Woo, J., MacPherson, C. R., Liu, J., Wang, H., Kiba, T., Hannah, M. A., et al. (2012). The response and recovery of the Arabidopsis thalianatranscriptome to phosphate starvation. *BMC Plant Biol.* 12, 62. doi: 10.1186/1471-2229-12-62

Wu, Z., Huang, R., and Yuan, L. (2019). Crosstalk of intracellular post-translational modifications in cancer. *Arch. Biochem. Biophys.* 676:108138. doi: 10.1016/j.abb.2019.108138

Xia, L., Kong, X., Song, H., Han, Q., and Zhang, S. (2022). Advances in proteome-wide analysis of plant lysine acetylation. *Plant Commun.* 3:100266. doi: 10.1016/j.xplc.2021.100266

Xu, J. M., Wang, Z. Q., Wang, J. Y., Li, P. F., Jin, J. F., Chen, W. W., et al. (2020). Low phosphate represses histone deacetylase complex1 to regulate root system architecture remodeling in Arabidopsis. *New Phytol.* 225, 1732–1745. doi: 10.1111/nph.16264

Yang, J., Xie, M., Yang, X., Liu, B., and Lin, H. (2019). Phosphoproteomic profiling reveals the importance of CK2, MAPKs and CDPKs in response to phosphate starvation in rice. *Plant Cell Physiol.* 60, 2785–2796. doi: 10.1093/pcp/pcz167

Ye, Q., Wang, H., Su, T., Wu, W., and Chen, Y. (2018). The ubiquitin e3 ligase PRU1 regulates WRKY6 degradation to modulate phosphate homeostasis in response to low-Pi stress in arabidopsis. *Plant Cell* 30, 1062–1076. doi: 10.1105/tpc.17.00845

Zeng, F., Pang, H., Chen, Y., Zheng, H., Li, W., Ramanathan, S., et al. (2021, 2021). First succinylome profiling of vibrio alginolyticus reveals key role of lysine succinylation in cellular metabolism and virulence. *Front. Cell. Infect. Microbiol.* 10:626574. doi: 10.3389/fcimb.2020.626574

Zhou, H., Finkemeier, I., Guan, W., Tossounian, M., Wei, B., et al. (2018). Oxidative stress-triggered interactions between the succinyl- and acetyl-proteomes of rice leaves. *Plant Cell Environ.* 41, 1139–1153. doi: 10.1111/pce.13100

frontiers | Frontiers in Plant Science

TYPE Review
PUBLISHED 02 September 2022
DOI 10.3389/fpls.2022.994710

OPEN ACCESS

EDITED BY
Mateusz Labudda,
Warsaw University of Life Sciences-SGGW, Poland

REVIEWED BY
Wojciech Makowski,
University of Agriculture in Krakow, Poland
Fardous Mohammad Safiul Azam,
Neijiang Normal University, China

*CORRESPONDENCE
Phetole Mangena
phetole.mangena@ul.ac.za;
mangena.phetole@gmail.com

SPECIALTY SECTION
This article was submitted to Plant Proteomics and Protein Structural Biology, a section of the journal Frontiers in Plant Science

RECEIVED 15 July 2022
ACCEPTED 10 August 2022
PUBLISHED 02 September 2022

CITATION
Mangena P (2022) Pleiotropic effects of recombinant protease inhibitors in plants. *Front. Plant Sci.* 13:994710. doi: 10.3389/fpls.2022.994710

Pleiotropic effects of recombinant protease inhibitors in plants

Phetole Mangena*

Department of Biodiversity, Faculty of Science and Agriculture, School of Molecular and Life Sciences, University of Limpopo, Polokwane, Limpopo, South Africa

Recombinant gene encoded protease inhibitors have been identified as some of the most effective antidigestive molecules to guard against proteolysis of essential proteins and plant attacking proteases from herbivorous pests and pathogenic microorganisms. Protease inhibitors (PIs) can be over expressed in transgenic plants to complement internal host defense systems, *Bt* toxins in genetically modified pest resistance and abiotic stress tolerance achieved through cystatins expression. Although the understanding of the role of proteolytic enzymes and their inhibitors encoded by both endogenous and transgenes expressed in crop plants has significantly advanced, their implication in biological systems still requires further elucidations. This paper, therefore, succinctly reviewed most recently published literature on recombinant proteases inhibitors (RPIs), focusing mainly on their unintended consequences in plants, other living organisms, and the environment. The review discusses major negative and unintended effects of RPIs involving the inhibitors' non-specificity on protease enzymes, non-target organisms and ubiquitous versatility in their mechanism of inhibition. The paper also discusses some direct and indirect effects of RPIs such as degradation by distinct classes of proteases, reduced functionality due to plant exposure to severe environmental stress and any other potential negative influences exerted on both the host plant as well as the environment. These pleiotropic effects must be decisively monitored to eliminate and prevent any potential adverse effects that transgenic plants carrying recombinant inhibitor genes may have on non-target organisms and biodiversity.

KEYWORDS

abiotic stress, biotic stress, genetic engineering, proteolysis, protease enzymes, recombinant protease inhibitors, transgenic lines

Introduction

Abiotic stresses such as drought and extreme temperatures, including biotic stress factors like phytopathogenic microorganisms trigger the production of extracellular and intracellular protease enzymes. Proteases, also known as proteolytic enzymes, are a group of digestive enzymes that break down long polypeptide chains into smaller amino acid chains and eventually into single individual amino acids (Ravee et al., 2018). Several studies

have indicated that endogenous and exogenous secretion of protease enzymes in plant cell's cytoplasms is associated with their exposure to biotic and abiotic stress (Morrell and Sadanandom, 2019; Stael et al., 2019; Ali and Baek, 2020; van der Hoorn and Klemencic, 2021). Proteolytic enzymes are responsible for a striking variety of biological processes that include signal initiation, transmission, and termination of many cellular processes (van der Hoorn and Klemencic, 2021). Proteases also play a key regulatory role in plant metabolism by maintaining effective protein quality controls, eliminating nonfunctional proteins, and are used in systemic defense responses. Among these important biological roles, biochemical degradation of cell proteins through hydrolysis of peptide bonds serves as the main primary function of proteolytic enzymes (Morrell and Sadanandom, 2019). However, these enzymes were also found to be associated with the occurrence of cell death (necrosis, excessive chlorosis, and programmed cell death) during senescence of tissues and organs, cell differentiation (Santos and Figueredo, 2021), and additionally acting as critical regulators during embryogenesis, cuticle formation, chloroplast biogenesis and stomatal development (van der Hoorn and Klemencic, 2021). According to D'Ippolito et al. (2021), plant proteases were also found to be involved in signal transductions among phytohormones and the adjustment of stomatal apertures during the exposure of plants to drought stress.

Nevertheless, protease enzymes also induce the formation of reactive oxygen species (ROS) detected during plant exposure and response to abiotic stresses, especially water deficit stress (Liu et al., 2019; Ali and Baek, 2020). Low and feverish temperatures were also reported to induce proteases that diminish plant productivity by causing a rapid burst of ROS in the chloroplasts (Luo and Kim, 2021). The dynamic changes in environmental conditions involving pathogen invasion also caused the expression of distinct digestive enzymes produced either by host plant or invading pathogen and herbivorous insect pests. Al-Ani et al. (2022) demonstrated a trypsin-serine like protease activity of fungi and nematodes during plant parasitism and antibiosis. Most fungal and nematode species inject secretions into plant cells with trypsin-like or serine proteinase activity. For instance, two serine protease enzymes were demonstrated in soybean cyst nematode (*Heterodera* spp. and *Globodera* spp.), and saprophytic fungi used to digest plant tissue proteins to favor the invading pathogenic metabolism and spreading of the infections (Silva et al., 2018; Rodríguez-Sifuentes et al., 2020). Interestingly, plants can produce many different molecules in response to attacks by pathogenic microorganisms and insect pests, or in dealing with the effects of abiotic stresses.

Moreover, the art of recognizing the role of proteolytic enzymes and their inhibitors in plant metabolic systems have led to the development and expression of recombinant protease inhibitors (RPIs). Recombinant protease inhibitors are enhanced protein molecules produced by transgenic plants that are used to inhibit the harmful effects of proteolysis during the exposure of plants to several environmental stress factors. Although, PIs can be naturally expressed by the plants to inhibit the activity of proteases, the RPIs are rather overexpressed by transgenes that are artificially incorporated into host plant genomes using recombinant DNA technology. Several transgenic plants expressing RPIs have been developed and used for resistance against biotic and abiotic stresses, especially for drought tolerance and resistance to plant disease causing pathogens. Some of the major crop species that are genetically engineered to express such recombinant protease inhibitors to reduce proteolytic activities are exemplified in Table 1.

Among them, species such as corn, cotton, rice, wheat, and soybean form part of the major crops that are genetically engineered using *Agrobacterium tumefaciens*-mediated genetic transformation to express recombinant genes like *Oryzacystatin I* (*OC-I*), *Oryzacystatin II* (*OC-II*) and cowpea trypsin inhibitor (*Cry1Ac*) for elevated levels of proteinases inhibiting proteins. A handful of studies continue to report the functional significance and efficiency of these partly stable proteins for an increasing number of applications particularly, for the protection of crops against phytopathogens and their potential role as biopesticides (Kim et al., 2009; Grosse-Holz and van der Hoorn, 2016; Clemente et al., 2019). A number of non-target organisms can also be exposed to these RPIs, especially the animals and humans who feed from the RPI containing crops (Im et al., 2021). Recently, the potential risk of *Bt* crops on non-target organisms such as insect pollinators, decomposers, prying insect predators, and the alteration of nutritional value of the crop have drawn a lot of public concerns. The nutritional value of most transgenic plant materials gets limited by the high presence of naturally occurring and induced compounds which interfere with the amounts and quality of nutrients, including nutrient digestion, absorption and assimilation in animals that consume them. Although, in legume crops for instance, postharvest operations such as storage treatments and processing are employed widely for removal of antinutritive factors, potential overexpression of RPIs inherently lowered the quality of food products by enhancing the production of phytic acid (Clarke and Wiseman, 2000). These negative effects necessitated research into breeding for low Bowman-Birk and Kunitz trypsin recombinant protease inhibitors in soybean and other cereal grain crops such as maize, rice and wheat (Rodríguez-Sifuentes et al., 2020). Thus, these and other studies showed that overexpression of RPI genes such as *OC-I*, *OC-II* and *Cry1Ac* exerts a strong influence on crop performance and grain quality.

However, many of these concerns were due to the cultivation of *Bt* crops as reported by Rukarwa et al. (2014) indicating that *Cry* proteins expressed in transgenic sweetpotato had some adverse effects on non-target *Coleopterans* such as ground, rove, and ladybird beetles. In contrast, Yang et al. (2021) reported evidence showing that some protease inhibitors hindered various enzymatic activities in the larval midgut of *Cry* protein resistant

Abbreviations: *Bt*, *Bacillus thuringiensis*; Cry, Crystal; *OC-I*, *Oryzacystatin I*; *OC-II*, *Oryzacystatin-II*; PI, Protease inhibitor; ROS, Reactive oxygen species; RPI, Recombinant protease inhibitor.

TABLE 1 Recombinant protease inhibitors expressed in transgenic plants and their targeted proteinase enzymes.

Plant species	Common name	Recombinant protease inhibitor	Targeted proteinases	References
Citrullus lanatus	Watermelon	Trypsin inhibitor 1	Serine-type endopeptidases	Srikanth and Chen 2016
Elaeis guineensis	Oil palm	Mustard trypsin inhibitor	Serine	De Leo et al., 2001
Glycine max (L.) Merr.	Soybean	Oryzacystatin I, Oryzacystatin II	Cysteine	Mangena 2020
Gossypium hirsutum	Cotton	Potato type I,	Serine	Dunse et al., 2010
Hordeum vulgare	Barley			
Oryza sativa L.	Rice	Barley trypsin inhibitor, soybean trypsin inhibitors, potato carboxypeptidase inhibitors	Serine	Quilis et al., 2007
Medicago sativa	Alfalfa	Oryzacystatin II	Cysteine	Ninkovic et al., 2007
Saccharum officinarum L.	Sugarcane	Cysteine protease inhibitor	Cysteine	Soares-Costa et al., 2002
Solanum lycopersicum	Tomato	Barley serine protease inhibitor, barley cysteine protease inhibitor	Serine, cysteine	Hamza et al., 2018
Solanum tuberosum	Potato	Cowpea trypsin inhibitor, chicken egg white cystatin	Serine, cysteine	Bell et al., 2003), Cowgill et al., 2002
Triticum aestivum	Wheat	Potato serine protease inhibitor, potato cysteine protease inhibitor	Serine, cysteine	Gupta et al., 2010, Solomon et al., 1999
Zea mays L.	Corn	Barley HvCPI 1-13	Cysteine	Carrillo et al., 2011

Cnaphalocrocis medinalis, thereby reducing the insect's ability to degrade *Bt* toxins. These findings, including many other reports on the pleiotropic effects of transgenic proteins like *Cry* proteins and RPIs are contradictory warranting further research and analysis in the role of these recombinant proteins in the agricultural system. In the current review, potential unintended consequences of recombinant protease inhibitors are discussed, and the gist of postulated direct and indirect impacts of these protease inhibitors on plant health and the environment are also interrogated. A literature survey was limited to biochemical, physiological, and partly morphological pleiotropic effects of RPI overexpression in transgenic plants. But most importantly, the paper deliberates on some of the intrinsic negative characteristics such as ubiquity, non-specificity, and proteolytic degradation of protease inhibitors intended for protection during plant response to biotic and abiotic stresses.

Stress induced proteolysis in plants

Plants, including many other eukaryotic and prokaryotic organisms comprise a variety of proteins functioning as catalysts, storage, structural, transport and regulatory molecules. Regulatory proteins are those that regulate DNA and RNA expressions as well as cell to cell recognition and signal transductions (Rasheed et al., 2020). Storage proteins, especially those contained within the seeds' cotyledon comprise essential and/or semi-essential protein molecules serving as building blocks in which their structures and aggregations are key to their functionality in living organisms. Plant seeds contain larger amounts of abundant and usable stored proteins than any other part of the plant, especially when compared to roots and shoots. In leguminous crops 7S and 11S globulins are the most predominant storage proteins, followed by 2S, 9S and 11S globulins (Mouzo et al., 2018). These proteins are synthesized during plant growth and development, accumulating more during seed development within membrane-bound protein bodies and serving as reservoirs of amino acids, reduced sulfur, nitrogen, and carbon molecules required for plant establishment post germination (Dimina et al., 2022).

Other groups of proteins are synthesized based on plants enduring biotic and abiotic stress. Hence, plants exhibiting high sensitivity to environmental stresses such as drought and salinity have also demonstrated higher expressions of protease enzymes under stressful conditions. These proteolytic enzymes are responsible for the catalysis of hydrolytic cleavage of numerous specific peptide bonds, together with the assembly of 2S and 11S globulin storage proteins mostly found in dicot plants (Mangena, 2020). The classification and cleavage of peptide bonds by proteolytic enzymes is based mainly on the catalytic amino acid residue found in the enzyme's active site (serine protease, cysteine protease, aspartic protease, and metalloprotease). Some molecular and catalytic information of the structure and applications of these protease enzymes are summarized in Table 2. When plants are exposed to stressful conditions, activation of genes that biochemically promote the expression and activity of proteolytic enzymes take place. Even though, proteolysis serves as one of the key catabolic processes in living organisms, protein induction and all metabolic activities that are regulated by these enzymes need to be controlled in order to avoid occurrence of any hazardous actions.

Total control is necessary because the overexpression of proteolytic enzyme may negatively affect cellular metabolism by hydrolytic degradation of essential proteins. This may take place while plants express proteases for purposes of metabolically counteracting the detriments of stress through dismantling of misfolded and damaged proteins, as well as maintaining sufficient

TABLE 2 Classification, general features, and examples of plant-based proteases with their industrial application.

Protease type	Catalytic residue group	Molecular weight (kDa)	Protein	Application
Aspartic protease	Aspartate	30 80	Arctiumisin Cardosin	Alcohol, bioactive peptide production and dairy industry
Cysteine proteases	Cysteine	24.5 28–32.5 23.8 23.4	Actinidin Bromelain Ficin Papain	Fish, animal feed, baking, and textile industry, including bioethanol production.
metalloprotease	Zn^{2+}, Ca^{2+} or Mn^{2+}	92	MMP-like proteases	Bioactive peptide production and biomedicine
Serine protease	Serine, histidine	55	Carnein Milin	Brewing and dairy industry

Marino and Funk (2011) and, Troncoso et al. (2022).

turnover of cellular proteins (Gregersen et al., 2008, 2013; Mahajan and Badgujar, 2010; Diaz-Mendoza et al., 2016). Furthermore, Toderich et al. (2020) also reported a differential composition of essential total proteins and free amino acid content due to salinity stress in seeds of new quinoa genotypes (*Chenopodium quinoa* W.). However, as environmental stresses continue to be the most challenging stress constraints globally, many researchers are thus, prompted to develop transgenic and non-transgenic lines that have been genetically enhanced to increase seed protein yield and oil while circumventing negative effects caused by these growth limiting factors (Taunk et al., 2019; Kumar et al., 2020; Selamat and Nadarajah, 2021).

Role of protease inhibitors in plants

A major impediment for successful germination, seedling development and overall growth of the plant is the exposure and susceptibility to environmental stress. For years many researchers have been studying the biosynthesis and regulation of specific chemicals associated with defense mechanisms in plants against various stress factors. Some of these chemicals remain unclear while others are considered to be secondary plant metabolites which play key selective regulatory roles during growth, development, and reproduction in plants, and they occur in all other living organisms such as bacteria, fungi, and animals (Demain and Fang, 2000; Isah, 2019). However, the type and concentration of specific chemicals produced by the plant during exposure to stress is determined by various intrinsic and extrinsic factors. These include the plant species/genotype, developmental stage, physiological status, and the environment (Isah, 2019). These factors likewise suggest the adaptive response of plants to stress, defense mechanism and the type of defensive stimuli required.

The specific chemicals used in defense are either constitutive in various plant tissues or are synthesized in response to the exposure to the specific type of stress. On the other hand, complex molecules such as proteins (lectins, enzymes, or enzyme inhibitors), alkaloids and terpenes are inducible constitutive compounds (Moreira et al., 2018). In various plants, proteins that include proteolytic enzymes and protease enzyme inhibitors can be synthesized in response to biotic and abiotic stress. The occurrence of proteases in turn may activate genes that naturally code for the production of protease inhibitors. This system has been widely studied by plant breeding scientists to mostly complement the development of disease and insect pest resistance in transgenic plants. Protease inhibitors constitute approximately 50% of the total amount of proteins found in various crop plants. These proteins include inhibitors of endopeptidases and exopeptidases found under the classification shown in Table 2. Protease inhibitors, therefore, form complexes with these protease enzymes and then inhibit their proteolytic activity, in addition to protecting certain cellular constituents, tissues and fluids (Dunse et al., 2010; Carrillo et al., 2011; Clemente et al., 2019).

Furthermore, some of the protease inhibitors such as potato protease inhibitors (PPI) have a broad spectrum of inhibitory activity. The Kunitz-type serine protease inhibitor serves as the most abundant inhibitor in the Solanaceae and Fabaceae family, representing approximately 44% of the total amount of protease inhibitors in potatoes (*Solanum tuberosum*) with additional 50 and 80% of chymotrypsin and trypsin, respectively (Dunse et al., 2010; Gupta et al., 2010; Herwade et al., 2021). In plant genetic improvement, cysteine and serine protease inhibitors have been widely reported for antidigestive and protection of crops against herbivores (Herwade et al., 2021). Senthilkumar et al. (2009) earlier reported varied inhibiting activity against trypsin and papain proteins, further showing resistance to both insects and phytopathogens. For instance, the report indicated that larvae of *Helicoverpa armigera* that ingested tobacco leaves either died or showed delayed growth and development. Tohidfar and Khosravi (2015) also highlighted the role of cowpea trypsin inhibitor (*CpTI*) which was successfully engineered in several crops (rice, cotton, wheat, rape seed, and eggplant) for protection against attacks by beetles and aphids. *CpTI*, *Bacillus thuringiensis* (*Bt*) and *Bt*-Xtra containing three *CryIAc* from *B. thuringiensis*, *bar* gene from *Streptomyces hygroscopicus* and *pinII* gene from potato coding potato protease inhibitor have also been developed in transgenic plants for abiotic stress resistance (Tohidfar and Khosravi, 2015; Losvik et al., 2018; Lang et al., 2021).

Pleiotropic effects of recombinant protease inhibitors

Although, numerous studies demonstrated efficient use of RPIs as effective anti-hydrolytic degradation of essential compounds, tissues and for protection of crops against pests and pathogenic organisms. The pleiotropic effects of RPIs in plant protection still need to be clarified. Many scientific and unscientific concerns have been raised in the past, and many more are still emerging due to the fact that the insertion of a transgene into a plant may result to unforeseen and potentially undesirable effects. Roundup Ready (RR) crops serve as excellent example, showing such negative and discouraging pleiotropic effects. Various reports stated that RR crops are responsible for the increasing development of superweeds and other plant types showing resistance to the Roundup (Glyphosate) herbicide. According to Green and Siehl (2021), the sole reliance on glyphosate [N-(phosphonomethyl)glycine, CAS No. 1071-83-6] for weed control potentially led to evolved resistance against this herbicide. In soybean, growth and yield of RR-soy lines were significantly influenced by both the herbicide (Cuvaca et al., 2021) and hot weather conditions causing the splitting of stems due to high lignin content produced (Martens et al., 2018). These unintended effects, however, suggest that increased expression of enzymes or proteins from the transgene may affect the balance of the relevant metabolic pathways. Table 3 summarizes some of the recombinant genes of prokaryotic and eukaryotic origin that are used in the expression of recombinant inhibitors to confer resistance to biotic and abiotic stress in plants. Among them, is the cowpea *CpTI* gene constructed by insertion into a pBIN19 derivative plasmid vector and expressed in plants using *Agrobacterium tumefaciens* through CaMV35S promotor and 3′ NOS terminator (Zhou et al., 2017). These recombinant inhibitors mostly act by either tightly binding to the active site of the protease enzyme as pseudo-substrates or would use trapping, which is a rapid conformational change that traps the cognate protease in a covalent complex fashion (Sabotic and Kos, 2012).

Non-enzyme specificity of protease inhibitors

Stress-induced proteolysis also leads to the degradation of proteins into component amino acids residues which ultimately denatures and affect the function of the proteins. It is, however, reported that stress, particularly, abiotic stress causes approximately more than 60% of crop yield losses due to severe changes in protein and secondary metabolite accumulation (Rodziewicz et al., 2019). The composition of cellular proteins is usually altered by environmental conditions, reflecting the true physiological and biochemical outcome of stress on the plant and its genetic capabilities. Depending on the level of stress, plants accumulate or enhance the expression of particular proteins to protect themselves against environmental stress. Classes of proteolytic proteins expressed during stress in plants include endo- and exo-peptidases found within enzyme families of serine proteases, cysteine proteases, aspartic proteases and metalloprotease which were discussed in detail above. Accordingly, these peptidases are able to function individually or as a complex, serving as an active proteolytic machinery (Mangena, 2020). A major problem involving protease is that the proteolytic activity of these enzymes is not limited to the cleavage of a number of bonds or hydrolysis of individual amino acid constituents used as building blocks for the synthesis of new catalytic and structural proteins (Solomon et al., 1999; Gupta et al., 2010; Clemente et al., 2019). However, their activity is also inherently associated with the activation or expression of protein enzymes inhibitors as mentioned in the previous section. These enzyme inhibitors are purposefully expressed to balance and interact in some way with the protease enzyme concentrations to prevent it from causing severe metabolic disruptions leading to tissue senescence. Furthermore, these protease inhibitors also serve a critical role in preventing the progression of pathogenesis resulting from pathogen-induced proteases (Wang et al., 2020). Such enzyme inhibitions could be non-specific within a family of peptidases, affecting the function of proteases in a class having similar mechanisms of action. These inhibitors may cause physical or

TABLE 3 Recombinant protease inhibitor genes used to engineer plants for biotic and abiotic stress resistance originating from plants, bacteria, and fungi.

Recombinant protease inhibitor gene	Target protein	Inhibitory mechanism	Engineered crop	References
Alpha-1-antitrypsin	Trypsin	Tight binding	Tomato	Agarwal et al., 2008
Serpin	Cysteine/ papain	Trapping	Rice	Singh et al., 2016
Aprotinin	Chymotrypsin	Tight binging	Corn	Sabotic and Kos 2012
Carboxypeptidase Y inhibitor	Serine carboxypeptidase Y	Phospholipid binding	Tomato	Abdeen et al., 2005
CpTI	Trypsin	Tight binding	Soybean	Clemente et al., 2019
Pot PI-I	Proteinase	Tight binding	Cotton	Dunse et al., 2010
Pot PI-II	Proteinase	Tight binding	Cotton	Dunse et al., 2010
Kunitz trypsin-inhibitor-3	Trypsin	Tight binding	Tobacco	do Amaral et al., 2022
OC-1	Cysteine	Tight binding	Soybean	Mangena 2020
CMe	Trypsin	Tight binding	Rice	Alfonso-Rubi et al., 2003

chemical interactions with enzymes, ultimately and reversibly or irreversibly denaturing the protein portion of the enzyme. Other inhibitors such as the cysteine protease inhibitors inhibit catalytic activity of cysteine proteases by binding to the enzyme's active site to create a distortion as pseudo-substrate (Table 3). Binding to the active site of the enzyme as indicated in Figure 1 enables the inhibitors to block access of the targeted specific protein substrates for catalysis (Kopitar-Jerala, 2012).

Although, various reports show that increased levels and activity of protease inhibitors were correlated with the plant's resistance to biotic and abiotic stress, the non-specificity of these protease inhibitors has, however, potently prohibited the growth of plants by significantly altering metabolic processes and interfering with the overall growth and development of plants. Natural protease inhibitors, together with recombinant inhibitors whose concentrations in the cell may be difficult to control can interact with several enzymes in high affinity and even not be easily removed. However, the difficulties expressed by many scientists in developing new and effective RPIs for agricultural or medicinal purposes include problems associated with identifying a specific inhibitor that efficiently blocks the active sites of specific proteolytic enzymes (Figure 1), and the generation of new inhibitors for evolving new targets of proteases. Moreover, other stress types can also be caused or facilitated by multiple protease-mediated processes. Therefore, to continue with the successfully application of RPIs in agriculture, new protease inhibitors need to be discovered and their recombinant genes successfully cloned into bacterial vectors for efficient plant transformation, which remains a challenge and a daunting task. Genetic manipulation of plants also remains highly inefficient, without a routinely successful, genotype independent transformation protocol, and further insights onto the hurdles facing direct or indirect recombinant DNA technology, as well as its genetic, molecular, and regulatory element requirements are thoroughly discussed in a review by Basso et al. (2020). For purposes of efficiently establishing new beneficial and widely functional protease inhibitors such as recombinant serine protease inhibitors (*rBbKI*), serine and cysteine inhibitors (*rBbCI*) derived from native inhibitors discovered from *Bauhinia bauhinioides* seeds, as well as serine and metalloprotease inhibitors from *Enterolobium contortisiliquum* seeds, more knowledge of their structure, selectivity and specificity to the different peptidase enzymes, including their target enzyme activity, must be gathered (Ferreira et al., 2019; Bonturi et al., 2022).

Ubiquity associated problems

Protease inhibitors are essential tools for maintaining protein balance in the cells to minimize the detrimental effects of biotic and abiotic stress. Evidence of variations in inhibitor levels in response to stress that causes incidences of diverse types of metabolic dysfunctions have also surfaced. Shams and Bano (2017) reported that protease inhibitors like cystatins do not mainly serve as just inhibitors blocking the activity of thiol peptidases, but they also take part in a variety of metabolic and growth processes. In general, protease inhibitors are highly diverse and ubiquitous, inhibiting proteases and other enzymes that are inconstitutive of their natural substrates. Nevertheless, the rejection of transgenic crops by the public and these potential negative effects envisaged from functional diversity of recombinant inhibitors continue to discourage their application

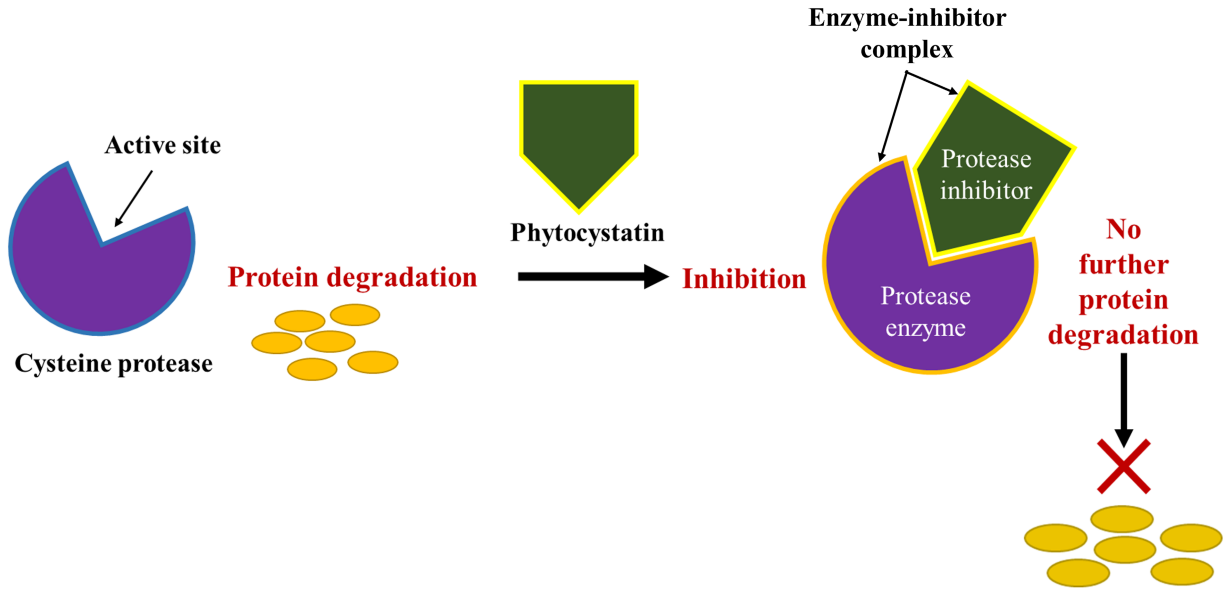

FIGURE 1
A typical inhibitory action of protease inhibitor (cysteine) on protein degradation through the formation of enzyme-inhibitor complex.

in biotechnology. Recombinant PIs' activity and specificity have been widely emphasized with the purpose of obtaining stress-induced proteins specific inhibitors that are important for accurate and rapid deterrence of particular stress causing factors.

Nonetheless, various reports showed that one of the main limitations to the application of recombinant protease inhibitors containing uniform functionality against more complex stress factors (microbial pathogens and drought) is the fact that environmental stresses can affect the different metabolic pathways at the same time with varied intensity. Furthermore, biotic stresses such as herbivorous pests rapidly evolve and get adapted to the use of a specific RPIs against them, especially, by maintaining diverse digestive enzymes and overexpression of enzymes that are highly insensitive to the recombinant protease inhibitors (Fischer et al., 2015). Meanwhile, overall stability and yield of recombinant protease inhibitors could be achieved by targeting specific enzymes and with protein expression and sequestration taking place in specific cellular compartments.

Proteolytic degradation of recombinant protease inhibitors

Despite the abundance and diversity of recombinant protease inhibitors found in prokaryotic and eukaryotic cells, significant gene expression barriers in heterologous systems still remains a challenge. Generally, the expression of transgenes encoding RPIs and the transfer, for higher expression of these recombinant protease inhibitor genes in subsequent generations through direct and indirect gene transfer methods such as particle bombardment and *Agrobacterium*-mediated genetic transformation are still problematic. Among the challenges facing gene expression, high level accumulation of recombinant protease inhibitors, improper regulation, and inhibitor proteolysis also presents the most significant barriers to the wider applications of RPIs to confer stress resistance in plants. Some peptidases found in bacteria (*Escherichia coli*) and yeast (*Saccharomyces cerevisiae*) demonstrated a rapid cleavage of recombinant protease inhibitors for purpose of impeding their activity (Gomes et al., 2018; Ma et al., 2020). Similarly, the accumulation of protease inhibitors from transgenic plants' cytoplasm may lead to the formation of inclusion bodies or be degraded by endogenous proteases. Such effects were also reported by Peng et al. (2019) during the production and recovery of recombinant proteins using biological systems such as bacteria and yeasts for pharmaceutical and medicinal purposes.

In simpler terms, the expression or accumulation of recombinant protease inhibitors in transgenic plants may be recognized as "foreign or abnormal" protein bodies triggering their rapid degradation through various well-characterized ubiquitin-mediated proteolytic pathways. Although not many reports present the mechanism of interaction between intracellular proteases and recombinant proteases in plants, the degradation pathways appear to be similar to those in bacterial and fungal cells. Viegas et al. (2017) presented evidence indicating that some leaf vacuolar proteases active under mildly acidic pH significantly altered the efficiency and integrity of recombinant protease inhibitor proteins. This study also emphasized the fact that, specific mechanisms underlying the action of these plant proteins against recombinant proteins remains unknown. However, in contrast with microbial production of recombinant protease inhibitors for pharmaceutical purposes and other industrial applications, plant proteases taking part in proteolysis of recombinant proteins, and mutant plants that lack proteases potentially damaging to RPIs are not available for crop improvement purposes. Therefore, according to Viegas et al. (2017), Jutras et al. (2019), and others, future research should focus on devising specific strategies for counteracting the effects of vacuolar proteases by identifying and characterizing their specific proteolytic activities in plants. However, for purposes of recombinant protein extraction in plant tissue for industrial uses instead of conferring stress tolerance, these proteins can be accumulated in extracellular compartments and in the endoplasmic reticulum (ER) *via* secretory pathways to prevent and control proteolysis in transgenic plant cells (Viegas et al., 2017; Gomes et al., 2018; Jutras et al., 2019; Peng et al., 2019).

Phenotype overexpression

Interestingly, several recombinant protease inhibitor genes are regulated in stressed plants. Gene products like RPIs have been widely identified and characterized in detail for their antinsecticidal, antimicrobial and antiviral properties, especially with artificial feeding experiments involving different transgenic lines. Dang and van Damme (2015) reported transgenic plants encoding pokeweed antiviral protein (*PAP*), curcin 2 and dianthin from *Phytolacca americana*, *Jatropha curcas* and *Dianthus caryophyllus*, respectively. The transgenic lines exhibited increased resistance to *Rhizoctonia solani* Kuhn, a soil-inhibiting parasitic fungi that causes collar rot, root rot, damping off and wire stem disease in cultivated crop plants (Butler, 2018). The *PAP* gene was introduced into plant species such as tobacco and potato plants by genetic transformation using *A. tumefaciens*. All transgenic plant expressing *PAP* or mutant derivative of the *PAP* gene showed enhanced resistance to different viral infections. However, overexpression of recombinant proteins remains a complex biological process that is not well understood, may lead to herbicide/pesticide resistance and disruption of the overall growth processes in plants (Losvik et al., 2018; Clemente et al., 2019). In most cases, overexpression of RPIs have led to improved stress resistant phenotypes. Losvik et al. (2018) reported upregulation and overexpression of a recombinant protease inhibitor, *C12c* controlling resistance against aphids in barley (*Hordeum vulgare* L.).

Overexpression of *Brassica oleracea* cysteine protease inhibitor (*BoCP1*) was also reported to reduced total protease activity while retaining cellular soluble protein content and delaying postharvest

senescence by down-regulating different senescence-regulating cysteine protease genes (Tan et al., 2017). *Malus prunifolia* cystatin 4 (*MpCYS4*) localized in the nucleus, cytoplasm and plasma membrane of onion epidermal cells (Tan et al., 2017) resulted in ABA-hypersensitivity. Nevertheless, it should be noted that, although such enhanced ABA-induced stomatal closures and altered expression of ABA-induced stress responsive genes improved drought stress tolerance, prolonged closure of stomata may negatively influence plant growth, development and recovering of plants to stress. Under normal circumstance, ABA sensitivity facilitate shoot growth and root development, enhancing salt and drought stress tolerance in transgenic plants (Sun et al., 2020). Limited effects on plant stress avoidance were also reported by Plessis et al. (2011) and Bi et al. (2019) due to the expression of ABA-hypersensitivity in mutant plants.

Biochemical and physiological effects

As briefly described on the previous section, the overexpression of recombinant protease inhibitors triggers ABA-hypersensitivity which signaled prolonged closure of stomata in *Arabidopsis* (Bi et al., 2019). Inevitably, the closure of stomata was brought about by the reduction in turgor pressure following a massive efflux of potassium ions (K^+) and anions from guard cells, inhibiting the activity of plasma membrane H^+-ATPase and CO_2 uptake for photosynthesis. Reduction in the negative impacts of drought and other abiotic stresses is associated with increased water use efficiency (WEU) occurring under lower physiological control of stomatal conductance (Haworth et al., 2016). Most protease inhibitors in plants are proteinaceous competitive inhibitors that tightly bind to the active sites of proteases to cause detrimental disruption of processes catalyzed by these enzymatic proteins. However, the overexpression of RPIs can potentially inhibit the role of small ubiquitin-like modifier (SUMO) proteins regulating the normal functioning of metabolism during exposure to biotic and abiotic stress. In plants, SUMO mediated cellular processes are induced by heat, drought, and oxidative stress whereby these proteins are involved in maintaining genome stability, chromatin regulation, transcription, translational RNA splicing, ribosome biogenesis and other cell cycle-related processes (Morrell and Sadanandom, 2019).

Many SUMOylation proteins (15–20%) playing critical roles ranging from proteasomal degradation, biosynthesis of complex macromoles and regulation of individual protein activities during stress could be inhibited by RPIs overexpressed in transgenic plants. Furthermore, Hou et al. (2018) indicated that all SUMO proteases are cysteine proteolytic enzymes which can be easily and rapidly inhibited by cysteine protease inhibitors. Cysteine proteases are specialized proteases found widely in all eukaryotic organisms, including transgenic and non-transgenic plants, and play a key role in many growth processes ranging from germination to plant tissue senescence (Morrell and Sadanandom, 2019). Above reports generally indicate the metabolic or physio-biochemical interference effects caused by protease inhibitors which will be better explained by the unintended environmental effects noted for *Bt* toxins and other non-target organisms discussed in the next topic. Additionally, protease inhibitors also exhibit direct interfering effects on endogenous proteases altering the physiological or compositional characteristics of the transgenic host plant. In this case, RPIs could rapidly interfere with the regulation of several metabolic processes such as the elimination of misfolded proteins, polypeptide pre- and pros-region processing during protein maturation and turnover of certain essential proteins (Solomon et al., 1999; Buono et al., 2019; Bonturi et al., 2022).

Environmental effects

In humans for instance, the occurrence of several inherited disease such as epilepsy and emphysema have been attributed to the pleiotropic effects of some specific protease inhibitors (Clemente et al., 2019). Various reports suggested significant effects of RPIs on negligible phenotypic changes, metabolic changes, insensitivity to protease inhibitors and inhibition of non-targeted organisms and proteins. Clemente et al. (2019) also discussed the potential role of serine protease inhibitors for herbivorous insect control which indiscriminately affect insect larvae of non-target organism. Serine protease inhibitors expressed in transgenic plant tissues were mobilized into the insect digestive tract along with the food and then blocked protein digestion leading to insect malnutrition and eventually its growth and development retardation. Serine protease inhibitors such as soybean Kunitz and Bowman-Birk inhibitors have been characterized for their potential control of herbivores. But major limitation arose when the use of these overexpressed recombinant proteins prohibited the utilization of transgenic plants for food and feed manufacturing as they also serve as antinutritional factors (Mittal et al., 2021).

Furthermore, serine-type inhibitors bovine aprotinin and tomato Kunitz-type cathepsin D inhibitor expressed in potato caused altered leaf protein contents expressed ectopically in transgenic crop plants (Munger et al., 2012). Several latest studies still describe the use of recombinant protease inhibitors as potent pesticides (Shams and Bano, 2017; Bonturi et al., 2022); however, these herbivorous insects also developed various strategies to cope with the dietary protease inhibitors. These evolutionary strategies render the use of recombinant protease inhibitors ineffective as evolving pests also demonstrate the ability to overexpress proteolytic enzymes to outcompete inhibitory proteins, and likewise use alternative classes of proteases to improve their insensitivity against the inhibitors. The inhibitory potency of RPIs against insect pests and pathogenic infection continues to be investigated since many researchers believe that the benefits outweigh their disadvantages. Other unintended effects of RPIs include their

inhibitory role against proteases in non-targeted organisms which recently also caused a serious public uproar. Arpaia et al. (2021) reported a decline in bee pollinator populations in Europe as a result of both natural and entropic environmental factors. Nevertheless, traits such as *Cry* gene-based toxins and double strand RNA (dsRNA) are implicated on having lethal and sublethal effects on non-target species such as the insect pollinators. According to literature, recombinant protease inhibitors may directly or indirectly affect non-target organisms through the establishment of formal ecological interactions and through intermediary herbivorous/carnivorous feeding among organisms with the one that primarily fed on the recombinant material (Abbas, 2018; Lang et al., 2019; Dang et al., 2021).

Final considerations and conclusion

A survey of current scientific literature indicates that proteolytic enzymes and their inhibitors play a crucial role in various biological processes involving the degradation of essential metabolic proteins, regulation of cellular protein catabolism and the inhibition of proteases induced during the exposure of plants to environmental stress. Most living organisms, including plants mainly contain serine proteases, cysteine proteases, aspartic proteases and some metalloproteases that are primarily involved in protein digestion and detoxification (Yang et al., 2021). When combined with environmental stress, proteolytic enzymes could be very debilitating to crops and plant life in general. Recombinant protease inhibitors have been expressed in various crop species to specifically confer resistance and protection against such various types of stress factors. RPIs play the most important function of keeping endogenous proteases' digestive activities under control, while preventing invasion and attacks by pathogenic microorganisms and insect pests.

Recombinant genes overexpressing these RPIs were then introgressed in many horticultural crops for the aforesaid reasons. Nevertheless, these RPIs have been implicated in harming a number of non-target organisms (Rukarwa et al., 2014). The most obvious were pollinators interacting with flowers of transgenic plants, and predators that feed on targeted insect pests that has consumed plant materials containing RPIs. All non-target organisms will be severely affected, especially if they fail to express enzymes that could digest the inhibitors to detoxify the protein. So far, reports show that these organisms are mainly affected by PIs found in transgenic materials either directly or indirectly. Inadvertently, potential phenotypic changes in the transgenic plants as a result of transgene expression may directly affect pollinators or pollination patterns. Other pleiotropic effects arising from altered biochemical pathways with changes in essential metabolic products, abundance of unwanted byproducts (ROS), expression of new types of proteases and several phenotypic consequences may also occur.

Consequently, both proteases and their inhibitors may be harmful to pests, despite being essential for the maintenance and survival of plants during their acclimation to stressful habitat conditions, causing phenotypic and cellular disruptions when present in the cells in higher concentrations (Sharma and Gayen, 2021). However, unlike many other studies in genetically modified crops, the application of RPIs for plant improvement did not cause a spike in studies evaluating their negative impacts on living organisms and environment. Thus, pleiotropic effects of RPIs are not easy to assess once transgenic lines are not associated with major apparent environmental risks but are related more with cost reductions of adopting the technology for improved crop performance and productivity, both in the field and during postharvest processing. But, going beyond these effects, application of RPIs is still encouraged without limitations since they contribute to cost and risk reductions, especially in the pharmaceutical industry, and further contribute to reduced risk associated with the use of chemical pesticides. A major impediment to increasing crop yield is that the exposure of plants to environmental stress is frequently coupled with the expression of proteolytic enzymes. Nonetheless, the overexpression of proteases in plant cells may differ according to the type and level of stress, and the plant genotype-dependent resistance. In the initial stage during metabolism, protease enzyme expression often serves as mediators of signal initiation during the onset of stress, escalations occur leading to the termination of certain cellular processes and then followed by hormonal inductions as the stress progresses (Ali and Baek, 2020; D'Ippolito et al., 2021). All of these effects emphasize the need for scientists to continue research in recombinant protease inhibitor expression for regulating protease activity, but modulation should be accompanied by very minimal pleiotropic effects on crop's life cycle, animal and human health, and the environment.

Author contributions

The author confirms being the sole contributor of this work and has approved it for publication.

Acknowledgments

The author would like to acknowledge APC financial support of the Department of Research Administration and Development at the University of Limpopo.

Conflict of interest

The author declares that the paper was prepared in the absence of any commercial or financial relationships that could be construed as a potential conflict of interest.

Publisher's note

References

Abbas, M. S. T. (2018). Genetically engineered (modified) crops (*bacillus thuringiensis* crops) and the world controversy on their safety. *Egypt J. Biol. Pest. Control* 28:52. doi: 10.1186/s41938-018-0051-2

Abdeen, A., Virgos, A., Olivella, E., Villanueva, J., Alviles, X., Gabarra, R., et al. (2005). Multiple insect resistance in transgenic tomato plants over-expressing two families of plant proteinase inhibitor. *Plant Mol. Biol.* 57, 189–202. doi: 10.1007/s11103-004-6959-9

Agarwal, S., Singh, R., Sanyal, I., and Amla, D. V. (2008). Expression of modified gene encoding functional human α-1-antitrypsin protein in transgenic tomato plants. *Transgenic Res.* 17, 881–896. doi: 10.1007/s11248-008-9173-8

Al-Ani, L. K. T., Soares, F. E. F., Sharma, A., de los Santos-Villalobos, S., Valdivia-Padilla, A. V., and Aguilar-Marcelino, L. (2022). Strategy of nematophagous fungi in determining the activity of plant parasitic nematodes and their prospective role in sustainable agriculture. *Front. Fungal Biol.* 3:863198. doi: 10.3389/ffunb.2022.863198

Alfonso-Rubi, J., Ortego, F., Costanera, P., Carbonero, P., and Diaz, I. (2003). Transgenic expression of trypsin inhibitor CMe from barley in *Indica* and *Japonica* rice, confers resistance to the rice weevil *Sitophilus oryzae*. *Transgenic Res.* 12, 23–31. doi: 10.1023/A.1022176207180

Ali, M. S., and Baek, K.-H. (2020). Protective roles of cytosolic and plastidal proteosomes on abiotic stress and pathogen invasion. *Plan. Theory* 9:832. doi: 10.3390/plants9070832

Arpaia, S., Smagghe, G., and Sweet, J. B. (2021). Biosafety of bee pollinators in genetically modified agro-ecosystems. Current approach and further development in the EU. *Pest Manag. Sci.* 77, 2659–2666. doi: 10.1002/ps.6287

Basso, M. F., Arraes, F. B. M., de-Sa, M. G., VJZ, M., Alves-Ferreira, M. A., and MFG, d.-S. (2020). Insight into genetic and molecular elements for transgenic crop development. *Front. Plant Sci.* 11:509. doi: 10.3389/fpls.2020.00509

Bell, H. A., Down, R. E., Fitches, E. C., Edwards, J. P., and Gatehouse, A. M. R. (2003). Impact of genetically modified potato expressing plant-derived insect resistance genes on the predatory bug *Podisus maculiventris* (Heteroptera: Pentatomide). *Biocontrol Sci. Tech.* 13, 729–741. doi: 10.1080/09583150310001606543

Bi, C., Ma, Y., Wang, X.-F., and Zhang, D.-P. (2019). Overexpression of the transcription factor NF-YCP confers abscisic acid hypersensitivity in *Arabidopsis*. *Plant Mol. Biol.* 95, 425–439. doi: 10.1007/s11103-017-0661-1

Bonturi, C. R., Teixeira, A. B. S., Rocha, V. M., Valente, P. F., Oliveira, J. R., Filho, C. M. B., et al. (2022). Plant kunitz inhibitors and their interaction with protease: current and potential pharmacological targets. *Int. J. Mol. Sci.* 23:4742. doi: 10.3390/ijms23094742

Buono, R. A., Hudecek, R., and Nowack, M. K. (2019). Plant proteases during developmental programmed cell death. *J. Exp. Bot.* 70, 2097–2112. doi: 10.1093/jxb/erz072

Butler, E. E. (2018). *Rhizoctonia solani* as a parasite of fungi. *Mycologia* 49, 354–373. doi: 10.1080/00275514.1957.12024650

Carrillo, L., Martinez, M., Ramessar, C. I., Castanera, P., Ortego, F., and Diaz, I. (2011). Expression of a barley cystatin gene in maize enhances resistance against phytophagous mites by altering their cysteine-proteases. *Plant Cell Rep.* 30, 101–112. doi: 10.1007/s00299-010-0948-z

Clarke, E. J., and Wiseman, J. (2000). Developments in plant breeding for improved nutritional quality of soya beans II. Anti-nutritional factors. *J. Agric. Sci.* 134, 125–136. doi: 10.1017/S0021859699007443

Clemente, M., Corigliano, M. G., Pariani, S. A., Sanchez-Lopez, E. F., Sander, V. A., and Ramos-Duarte, V. A. (2019). Plant serine protease inhibitors: biotechnological application in agriculture and molecular farming. *Int. J. Mol. Sci.* 20:1345. doi: 10.3390/ijms20061345

Cowgill, S. E., Wright, C., and Atkinson, H. J. (2002). Transgenic potatoes with enhanced levels of nematode resistance do not have altered susceptibility to non-target aphids. *Mol. Ecol.* 11, 821–827. doi: 10.1046/j.1365-294x.2002.01482.x

Cuvaca, I., Kuezevic, S., Scott, J., and Osipitan, A. O. (2021). Growth and yield losses of roundup ready soybean as influenced by micro-rates of 2,4-D. *Sus. Agric. Res.* 10, 27–32. doi: 10.5539/sar.v10n4p27

D'Ippolito, S., Rey-Burusco, M. F., Feingold, S. E., and Guevara, M. G. (2021). Role of proteases in the response of plants to drought. *Plant Physiol. Biochem.* 168, 1–9. doi: 10.1016/j.plaphy.2021.09.038

Dang, L., and van Damme, E. J. M. (2015). Toxic proteins in plants. *Phytochemistry* 117, 51–64. doi: 10.1016/j.phytochem.2015.05.020

Dang, C., Zhou, X., Sun, C., Wang, F., Peng, Y., and Ye, G. (2021). Impacts of *Bt* rice on non-target organisms assessed by the harzard quotient (HQ). *Ecotoxicol. Environ. Saf.* 207:111214. doi: 10.1016/j.ecoenv.2020.111214

De Leo, F., Bonade-Bottino, M., Ceci, L. R., Gallerani, R., and Jouanin, L. (2001). Effects of a mustard trypsin inhibitor expressed in different plants on three lepidopteran pests. *Insect Biochem. Mol. Biol.* 31, 593–602. doi: 10.1016/s0965-1748(00)00164-8

Demain, A. L., and Fang, A. (2000). The natural functions of secondary metabolites. *Adv. Biochem. Engineer/Biotechnol.* 69, 1–39. doi: 10.1007/s-540-44964-7_1

Diaz-Mendoza, M., Velasco-Arroyo, B., Santamaria, E., Gonzalez-Melendi, P., Martinez, M., and Diaz, I. (2016). Plant senescence and proteolysis: two processes with one destiny. *Genet. Mol. Biol.* 39, 329–338. doi: 10.1590/1678-4685-GMB-2016-0015

Dimina, L., Rémond, D., Huneau, J.-F., and Mariotti, F. (2022). Combining plant proteins to achieve amino acid profiles adapted to various nutritional objectives-an exploratory analysis using linear programming. *Front. Nutr.* 8:809685. doi: 10.3389/fnut.2021.809685

do Amaral, M., ACO, F., Santos, A. S., dos Santos, E. C., Ferreira, M. M., Gesteira, A. S., et al. (2022). TcTI, a Kunitz-type trypsin inhibitor from cocoa associated with defense against pathogens. *Sci. Rep.* 12:698. doi: 10.1038/s41598-021-04700-y

Dunse, K. M., Stevens, J. A., Lay, F. T., and Anderson, M. A. (2010). Coexpression of potato type I and II proteinase inhibitors gives cotton plants protection against insect damage in the field. *PNAS* 107, 15011–15015. doi: 10.1073/pnas.1009241107

Ferreira, R. S., Napoleao, T. H., Silva-Lucca, R. A., Silva, M. C. C., Paira, P. M. G., and Oliva, M. L. V. (2019). The effects of Enterolobium contortisiliquum serine protease inhibitor on the survival o the termite *Nasutitermes corniger*, and its use as affinity adsorbent to purity termite protease. *Pest Manag. Sci.* 75, 632–638. doi: 10.1002/ps.5154

Fischer, M., Kuckenberg, M., Kastilan, R., Muth, J., and Gebhardt, C. (2015). Novel in vitro inhibitory functions of potato tuber proteinaceous inhibitors. *Mol. Gen. Genomics.* 290, 387–398. doi: 10.1007/s00438-014-0906-5

Gomes, A. M. V., Carmo, T. S., Carvalho, L. S., Bahia, F. M., and Parachin, N. S. (2018). Comparison of yeasts as hosts for recombinant protein production. *Microorganisms* 6:38. doi: 10.3390/microorganisms6020038

Green, J. M., and Siehl, D. L. (2021). History and outlook for glyphosate-resistant crops. *Rev. Envron. Contam. Toxicol.* 255, 67–91. doi: 10.1007/398_2020_54

Gregersen, P. L., Culetic, A., Boschian, L., and Krupinska, K. (2013). Plant senescence and crop productivity. *Plant Mol. Biol.* 82, 603–622. doi: 10.1007/s11103-013-0013-8

Gregersen, P. L., Holm, P. B., and Krupinska, K. (2008). Leaf senescence and nutrient remobilization in barley and wheat. *Plant Biol.* 10, 37–49. doi: 10.1111/j.1438-8677.2008.00114.x

Grosse-Holz, F. M., and van der Hoorn, R. A. L. (2016). Juggling jobs: roles and mechanisms of multifunctional protease inhibitors in plants. *New Physiol.* 210, 794–807. doi: 10.1111/nph.13839

Gupta, V. C., Jaiswal, J. P., Sharma, I., and Kumar, A. (2010). Investigating the role of cystatin in conferring stage dependent resistance against karmal bunt of wheat. *Food Agric. Immunol.* 21, 65–79. doi: 10.1080/09540100903427314

Hamza, R., Perez-Hedo, M., Urbaneja, A., Ramba, J. L., Granell, A., Geddour, K., et al. (2018). Expression of two barley proteinase inhibitors in tomato promotes endogenous defensive response and enhances resistance to *Tuta absoluta*. *BMC Plant Biol.* 18, 24–14. doi: 10.1186/s12870-018-1240-6

Haworth, M., Kill, D., Materassi, A., Raschi, A., and Centritto, M. (2016). Impaired stomatal control is associated with reduced photosynthetic physiology in crop species grown at elevated [CO2]. *Front. Plant Sci.* 7:1568. doi: 10.3389/fpls.2016.01568

Herwade, A. P., Kasar, S. S., Rane, N. R., Ahmed, S., Maras, J. S., and Pawar, P. J. K. (2021). Characterisation of a bowman-birk type trypsin inhibitor purified from seeds of *Solanum surattense*. *Sci. Rep.* 11, 1–10. doi: 10.1038/s41598-021-87980-8

Hou, S., Jamieson, P., and He, P. (2018). The cloak, dagger and shield: proteases in plant-pathogen interaction. *Biochem. J.* 475, 2491–2509. doi: 10.1042/BCJ20170781

Im, S. Y., Bonturi, C. R., Nakahata, A. M., Nakaie, C. R., Pott, A., Pott, V. J., et al. (2021). Differences in the inhibitory specificity distinguish the efficiency of plant protease inhibitors on mouse fibrosarcoma. *Plan. Theory* 10:602. doi: 10.3390/plants10030602

Isah, T. (2019). Stress and defense responses in plant secondary metabolite production. *Biol. Res.* 52, 39–25. doi: 10.1186/s40659-019-0246-3

Jutras, P. V., Grosse-Holz, F., Kaschani, F., Kaiser, M., Michaud, D., and van der Hoorn, A. L. (2019). Activity-based proteomics reveals nine target proteases for the recombinant protein-stabilising inhibitor SI CYS8 in *Nicotiana benthamiana*. *Plant Biotechnol. J.* 17, 1670–1678. doi: 10.1111/pbi.13092

Kim, J.-K., Park, S.-C., Hwang, I., Cheong, H., Nah, J.-W., and Hahm, K.-S. (2009). Protease inhibitors from plants with antimicrobial activity. *Int. J. Mol. Sci.* 10, 2860–2872. doi: 10.3390/ijms10062860

Kopitar-Jerala, N. (2012). The role of cysteine proteinase and their inhibitors in the host-pathogen cross talk. *Curr. Protein Pept. Sci.* 13, 767–775. doi: 10.2174/138920312804871102

Kumar, A., Singh, S., Gaurav, A. K., Srivastava, S., and Verma, J. P. (2020). Plant growth-promoting bacteria: biological tools for the mitigation of salinity stress in plants. *Front. Microbiol.* 11:1216. doi: 10.3389/fmicb.2020.01216

Lang, A., Lee, M., Dolek, M., Berchtold, J., and Otto, M. (2019). Laboratory tests with Lepidoptera to assess non-target effects of *Bt* maize pollen: analysis of current studies and recommendations for a standardised design. *Environ. Sci. Euro.* 31:39. doi: 10.1186/s12302-019-02202-2

Lang, J.-g., Zhang, D.-d., Dy, L., Zhao, S.-y., Wang, C.-y., Xiao, Y.-t., et al. (2021). Expression profiles of CryIAb protein and its insecticidal efficacy against the invasive fall armyworm for Chinese domestic GM maize DBN9736. *J. Integr. Agric.* 20, 792–803. doi: 10.1016/S2095-3119(20)63475-X

Liu, H., Able, A. J., and Able, J. A. (2019). Genotypic performance of Australian durum under single and combined water-deficit and heat stress during reproduction. *Sci. Rep.* 9:14986. doi: 10.1038/s41598-019-49871-x

Losvik, A., Beste, L., Stephens, J., and Jonsson, L. (2018). Overexpression of the aphid-induced serine protease inhibitor C12c gene in barley affects the generalist green peach aphid, not the specialist bird cherry-oat aphid. *PLoS One* 13:e0193816. doi: 10.1371/journal.pone.0193816

Luo, S., and Kim, C. (2021). Current understanding of temperature stress-responsive chloroplast FtsH metalloproteases. *Int. J. Mol. Sci.* 22:12106. doi: 10.3390/ijms222212106

Ma, Y., Lee, C.-J., and Park, J.-S. (2020). Strategies for optimising the production of proteins and peptides with multiple disulfide bonds. *Antibiotics* 9:541. doi: 10.3390/antibiotics9090541

Mahajan, R., and Badgujar, S. B. (2010). Biological aspects of proteolytic enzymes: a review. *J. Pharm. Res.* 3, 2048–2068.

Mangena, P. (2020). Phytocystatins and their potential application in the development of drought tolerance plants in soybean (*Glycine max* L.). *Protein Pept. Lett.* 27, 135–144. doi: 10.2174/0928665266661910141254 53

Marino, G., and Funk, C. (2011). Matrix metalloproteinases in plants: a brief overview. *Physiol. Plant.* 145, 196–202. doi: 10.1111/j.1399-3054.2011.01544.x

Martens, M., Hoss, S., Neumann, G., Afzal, J., and Reichenbecher, W. (2018). Glyphosate, a chelating agent-relevant for ecological risk assessment? *Environ. Sci. Pollut. Res. Int.* 25, 5298–5317. doi: 10.1007/s11356-017-1080-1

Mittal, P., Kumar, V., Rani, A., and Golchale, S. M. (2021). Bowman-Birk inhibitor in soybean: genetic variability in relation to total trypsin inhibitor activity and elimination of Kunitz trypsin inhibitor. *Notula Scientia Biologicae* 13:10836. doi: 10.15835/nsb13110836

Moreira, X., Abdala-Roberts, L., Gols, R., and Rancisco, M. (2018). Plant domestication decreases both constitutive and induced chemical defenses by direct selection against defensive traits. *Sci. Rep.* 8:12678. doi: 10.1038/s41598-018-31041-0

Morrell, R., and Sadanandom, A. (2019). Dealing with stress: a review of plant SUMO proteases. *Front. Plant Sci.* 10, 1122. doi: 10.3389/fpls.2019.01122

Mouzo, D., Bernal, J., Lopez-Pedrouso, M., Franco, D., and Zapata, C. (2018). Advances in the biology of seed and vegetative storage proteins based on two-dimensional electrophoresis coupled to mass spectrometry. *Molecules* 23:2462. doi: 10.3390/molecules23102462

Munger, A., Coenen, K., Cantin, L., Goulet, C., Vaillancourt, L.-P., Goulet, M.-C., et al. (2012). Beneficial unintended effects of a cereal cystatin in transgenic lines of potato, *Solanum tuberosum*. *BMC Plant Biol.* 12, 1–12. doi: 10.1186/1471-2229-12-198

Ninkovic, S., Miljus-Dukic, J., Radovic, S., Maksimovic, V., Lazarevic, J., Vinterhalter, B., et al. (2007). *Phytodecta fornicate* Bruggermann resistance mediated by oryzacystatin II proteinase inhibitor transgene. *Plant Cell Tissue Organ Cult.* 91, 289–294. doi: 10.1007/s11240-007-9296-2

Peng, C., Shi, C., Cao, X., Li, Y., Liu, F., and Lu, F. (2019). Factors affecting recombinant protein secretion efficiency in gram-positive bacteria: signal peptide and beyond. *Front. Bioeng. Biotechnol.* 7:139. doi: 10.3389/fbioe.2019.00139

Plessis, A., Cournol, R., Effroy, D., Perez, V. S., Botran, L., Kraepiel, Y., et al. (2011). New ABA-hypersensitive *Arabidopsis* mutants are affected in loci mediating responses to water deficit and *Dickeya dadantii* infection. *PLoS One* 6:e20243. doi: 10.1371/journal.pone.0020243

Quilis, J., Meynard, D., Vila, L., Aviles, F. X., Quiderdoni, E., and San Segundo, B. (2007). A potato carboxypeptidase inhibitor gene provides pathogen resistance in transgenic rice. *Plant Biotechnol. J.* 5, 537–553. doi: 10.1111/j.1467-7652.2007.00264.x

Rasheed, A., Mahmood, A., Maqbool, R., Albaqami, M., Sher, A., Sattar, A., et al. (2020). Key insights to develop drought-resilient soybean: a review. *J. King Saud. Univ. Sci.* 34:102089. doi: 10.1016/j.jksus.2022.102089

Ravee, A., Baharin, A., Cho, W.-T., Ting, T.-K., and Goh, H. H. (2018). Protease activity is maintained in *Nepenthes ampullaria* digestive fluids depleted of endogenous proteins with compositional changes. *Physiol. Plant.* 173, 1967–1978. doi: 10.1111/ppl.13540

Rodríguez-Sifuentes, L., Marszalek, J. E., Chuck-Hernández, E., and Serna-Saldívar, S. O. (2020). Legumes protease inhibitors as biopesticides and their defense mechanisms against biotic factors. *Int. Mol. Sci.* 21, 3322. doi: 10.3390/ijms21093322

Rodziewicz, P., Chmielewska, K., Sawikowska, A., Marczak, L., Luczak, M., Bednarek, P., et al. (2019). Identification of drought responsive proteins and related proteomic QTLs in barley. *J. Exp. Bot.* 70, 2823–2837. doi: 10.1093/jxb/erz075

Rukarwa, R. J., Mukasa, S. B., Odongo, B., Ssemakula, G., and Ghislain, M. (2014). Identification of relevant non-target organisms exposed to weevil-resistant Bt sweetpotato in Uganda. 3. *Biotech* 4, 217–226. doi: 10.1007/s13205-013-0153-1

Sabotic, J., and Kos, J. (2012). Microbial and fungal protease inhibitors-current and potential applications. *Appl. Microbiol. Biotechnol.* 93, 1351–1375. doi: 10.1007/s00253-011-3834-x

Santos, R. B., and Figueredo, A. (2021). Two sides of the same story in grapevine pathogen interactions. *J. Exp. Bot.* 72, 3367–3380. doi: 10.1093/jxb/erab091

Selamat, N., and Nadarajah, K. K. (2021). Meta-analysis of quantitative traits loci (QTL) identified in drought response in rice (*Oryza sativa* L.). *Plant* 10, 716. doi: 10.3390/plants10040716

Senthilkumar, R., Cheng, C.-P., and Yeh, K.-W. (2009). Genetically pyramiding protease-inhibitor genes for dual broad-spectrum resistance against insect and phytopathogens in transgenic tobacco. *Plant Biotechnol.* 8, 65–75. doi: 10.1111/j.1467-7652.2009.00466.x

Shams, A., and Bano, B. (2017). Journey of cystatins from being mere thiol protease inhibitors to at heart of many pathological conditions. *Int. J. Biol. Macromol.* 102, 674–693. doi: 10.1016/j.ijbiomac.2017.04.071

Sharma, P., and Gayen, D. (2021). Plant protease as regulator and signaling molecule for enhancing environmental stress-tolerance. *Plant Cell Rep.* 40, 2081–2095. doi: 10.1007/s00299-021-02739-9

Silva, K. J. P., Mahna, N., Mou, Z., and Folta, K. M. (2018). NPR1 as a transgenic crop protection strategy in horticultural species. *Hortic. Res.* 5, 15. doi: 10.1038/s41438-018-0026-1

Singh, S., Singh, A., and Nandi, A. K. (2016). The rice OsSAG12-2 gene codes for a functional protease that negatively regulates stress-induced cell death. *J. Biosci.* 41, 445–453. doi: 10.1007/s12038-016-96-9626-9

Soares-Costa, A., Beltramini, L. M., Thiemann, O. H., and Henrique-Silve, F. (2002). A sugarcane cystatin: recombinant expression, purification and antifungal activity. *Biochem. Biophys. Res. Commun.* 296, 1194–1199. doi: 10.1016/s0006-291x(02)02046-6

Solomon, M., Belenghi, B., Delledonne, M., and Levine, M. (1999). The involvement of cysteine proteases and protease inhibitor genes in the regulation of programmed cell death in plants. *Plant Cell* 11, 431–443. doi: 10.1105/tpc.11.3.431

Srikanth, S., and Chen, Z. (2016). Plant protease inhibitors in therapeutics-focus on cancer therapy. *Front. Pharmacol.* 7, 470. doi: 10.3389/fphar.2016.00470

Stael, S., van Breusegem, F., Gevaert, K., and Nowack, M. K. (2019). Plant proteases and programmed cell death. *J. Exp. Bot.* 70, 1991–1995. doi: 10.1093/jxb/erz126

Sun, F., Yu, H., Qu, J., Cao, Y., Ding, L., Feng, W., et al. (2020). Maize ZmBES1/BZR1-5 decrease ABA sensitivity and confers tolerance to osmotic stress in transgenic *Arabidopsis*. *Int. J. Mol. Sci.* 21, 996. doi: 10.3390/ijms21030996

Tan, Y., Li, M., Yan, Y., Sun, X., Wang, N., Liang, B., et al. (2017). Overexpression of MpCYS4, a phytocystatin gene from *Malus prunifolia* (wild.) Borkh, enhances stomatal closure to confer drought tolerance in transgenic *Arabidopsis* and apple. *Front. Plant Sci.* 8, 1–15. doi: 10.3389/fpls.2017.00033

Taunk, J., Rani, A., Singh, R., Yadav, N. R., and Yadav, R. C. (2019). "Genomic strategies for improving abiotic stress tolerance in crop plants," in *Genetic Enhancement of Crops for Tolerance to Abiotic Stress: Mechanisms and Approaches-*

Sustainable Development and Biodiversity. eds. V. Rajpal, D. Sehgal, A. Kumar and S. Raina (Cham: Springer), 205–230. doi: 10.1007/978-3-319-91956-0_9

Toderich, K. N., Mamadrahimov, A. A., Khaitov, B. B., Karimov, A. A., Soliev, A. A., Nanduri, K. R., et al. (2020). Differential impact of salinity stress on seeds minerals, storage proteins, fatty acids, and squalene composition of new quinoa genotype, grown in hyper-arid desert environments. *Front. Plant Sci.* 11:607102. doi: 10.3389/fpls.2020.607102

Tohidfar, M., and Khosravi, S. (2015). Transgenic crops with an improved resistance to biotic stresses. A review. *Biotechnol. Agron. Soc. Environ.* 19, 62–70.

Troncoso, F. D., Sanchez, D. L., and Ferreira, M. L. (2022). Production of plant proteases and new biotechnological applications: an updated review. *Chem. Open* 11:e202200017. doi: 10.1002/open.202200017

van der Hoorn, R. A. L., and Klemencic, M. (2021). Plant proteases from molecular mechanisms to functions in development and immunity. *J. Exp. Bot.* 72, 3337–3339. doi: 10.1093/jxb/erab129

Viegas, V. S. M., Ocampo, C. G., and Petrucelli, S. (2017). Vacuolar deposition of recombinant proteins in plant vegetative organs as a strategy to increase yields. *Bioengineering* 8, 203–211. doi: 10.1080/21655979.2016.1222994

Wang, Y., Wang, Y., and Wang, Y. (2020). Apoplastic proteases: powerful weapons against pathogen infection in plants. *Plant Commun.* 1, 1–10. doi: 10.1016/j.xplc.2020.100085

Yang, Y.-j., Xu, H.-x., Z-h, W., and Lu, Z.-x. (2021). Effects of inhibitors on the protease profiles and degradation of activated cry toxins in larval midgut juices of *Cnaphalocrocis medinalis* (Lepidoptera: Pyralidae). *J. Integrative Agric.* 20, 2195–2203. doi: 10.1016/S2095-3119(20)63316-0

Zhou, Z., Li, Y., Yuan, C., Zhang, Y., and Qu, L. (2017). Transgenic tobacco expressing the TAT-Helicokinin-1-CpTI fusion protein show increased resistance and toxicity to *Helicoverpa armigera* (Lepidoptera: Noctuidae). *Genes* 8, 28. doi: 10.3390/gene8010028

frontiers | Frontiers in Plant Science

TYPE Original Research
PUBLISHED 29 September 2022
DOI 10.3389/fpls.2022.994056

OPEN ACCESS

EDITED BY
Shaojun Dai,
Shanghai Normal University, China

REVIEWED BY
SHAILENDRA PRATAP SINGH,
Institute of Science, Banaras Hindu University, India
Wu Xu,
University of Louisiana at Lafayette, United States

*CORRESPONDENCE
Feng Ge
gefeng@ihb.ac.cn
Mingkun Yang
yangmingkun@ihb.ac.cn

SPECIALTY SECTION
This article was submitted to Plant Proteomics and Protein Structural Biology, a section of the journal Frontiers in Plant Science

RECEIVED 14 July 2022
ACCEPTED 12 September 2022
PUBLISHED 29 September 2022

CITATION
Zhang Y, Wang Y, Wei W, Wang M, Jia S, Yang M and Ge F (2022) Proteomic analysis of the regulatory networks of ClpX in a model cyanobacterium *Synechocystis* sp. PCC 6803.
Front. Plant Sci. 13:994056.
doi: 10.3389/fpls.2022.994056

Proteomic analysis of the regulatory networks of ClpX in a model cyanobacterium *Synechocystis* sp. PCC 6803

Yumeng Zhang[1,2,3], Yaqi Wang[1,2,3], Wei Wei[1,2,3], Min Wang[4], Shuzhao Jia[4], Mingkun Yang[1,2,3]* and Feng Ge[1,2,3]*

[1]State Key Laboratory of Freshwater Ecology and Biotechnology, Institute of Hydrobiology, Chinese Academy of Sciences, Wuhan, China, [2]Key Laboratory of Algal Biology, Institute of Hydrobiology, Chinese Academy of Sciences, Wuhan, China, [3]College of Advanced Agricultural Sciences, University of Chinese Academy of Sciences, Beijing, China, [4]The Analysis and Testing Center, Institute of Hydrobiology, Chinese Academy of Sciences, Wuhan, China

Protein homeostasis is tightly regulated by protein quality control systems such as chaperones and proteases. In cyanobacteria, the ClpXP proteolytic complex is regarded as a representative proteolytic system and consists of a hexameric ATPase ClpX and a tetradecameric peptidase ClpP. However, the functions and molecular mechanisms of ClpX in cyanobacteria remain unclear. This study aimed to decipher the unique contributions and regulatory networks of ClpX in the model cyanobacterium *Synechocystis* sp. PCC 6803 (hereafter *Synechocystis*). We showed that the interruption of *clpX* led to slower growth, decreased high light tolerance, and impaired photosynthetic cyclic electron transfer. A quantitative proteomic strategy was employed to globally identify ClpX-regulated proteins in *Synechocystis* cells. In total, we identified 172 differentially expressed proteins (DEPs) upon the interruption of *clpX*. Functional analysis revealed that these DEPs are involved in diverse biological processes, including glycolysis, nitrogen assimilation, photosynthetic electron transport, ATP-binding cassette (ABC) transporters, and two-component signal transduction. The expression of 24 DEPs was confirmed by parallel reaction monitoring (PRM) analysis. In particular, many hypothetical or unknown proteins were found to be regulated by ClpX, providing new candidates for future functional studies on ClpX. Together, our study provides a comprehensive ClpX-regulated protein network, and the results serve as an important resource for understanding protein quality control systems in cyanobacteria.

KEYWORDS

cyanobacteria, proteases, proteostasis, quantitative proteomics, ClpX

Introduction

Cyanobacteria are a large group of prokaryotic photoautotrophic microorganisms that play crucial roles in the global carbon and nitrogen cycles (Khalifa et al., 2021). As one of the oldest forms of life on Earth, cyanobacteria are present in almost every habitat, including various extreme environments and adverse physiological growth conditions (Schirrmeister et al., 2011). Extreme environments often disturb cellular protein homeostasis (proteostasis), resulting in protein denaturation and oxidative damage, which leads to cell death. To cope with harsh and changing environmental conditions, cyanobacteria have evolved versatile protein quality control (PQC) mechanisms to sense environmental signals and implement adaptive changes (Franklin, 2021; Cui et al., 2021).

In cyanobacteria, unlike the ubiquitin-proteasome system found in eukaryotic systems, proteostasis is regulated by the PQC system, mainly depending on AAA+ (ATPases associated with a variety of cellular activities) proteolytic machines, which are composed of two distinct parts: molecular chaperones and proteases (He and Mi, 2016). Among the diverse proteolytic machines, including ClpXP, ClpCP, and HslUV, the ClpXP proteolytic complex is the representative AAA+ proteolytic machine (Olivares et al., 2016) and is regarded as the most characterized and conserved (Baker and Sauer, 2012; Stahlhut et al., 2017). It consists of a ring hexamer of the ClpX subunit (Glynn et al., 2009) and the self-compartmentalized serine protease ClpP, in which two stacked heptameric rings enclose a barrel-shaped chamber (Stanne et al., 2007; Alexopoulos et al., 2012).

ClpX is a hexameric ATPase with diverse functions, including substrate binding, adaptor functions, protein unfolding, and polypeptide translocation. Unfolding and translocation require ATP binding and hydrolysis to power changes in enzyme conformation that drive these mechanical processes (Kim et al., 2000; Joshi et al., 2004). At the same time, ClpP needs to bind to ClpX to cleave polypeptides that are translocated into its proteolytic chamber. The resulting peptide fragments must be small enough to exit the chamber and subsequently be degraded by exopeptidases to free amino acids (Baker and Sauer, 2012).

The ClpXP proteolytic complex has been revealed to participate in the modulation of several cellular activities, including cell division (Camberg et al., 2011), cell cycle regulation (Lau et al., 2015), and bacterial virulence (Li et al., 2010), by precisely degrading multiple regulatory proteins. Nevertheless, independent of ClpP, ClpX is known to prevent protein aggregation (Burton and Baker, 2005), disassemble preformed aggregates (Burton and Baker, 2005), and unfold proteins without degradation (Baker and Sauer, 2012). Interestingly, some organisms such as yeast do not contain ClpP but only ClpX (Whitman et al., 2018). ClpX influences the transcription of genes involved in peptidoglycan synthesis, cell division, and the type seven secretion system in *Staphylococcus aureus* (Jensen et al., 2019). Furthermore, ClpX has been reported to be an important factor in subverting host immune clearance mechanisms in *Bacillus anthracis* (McGillivray et al., 2009) and is engaged in McpA proteolysis, which is modulated by the cell cycle in *Caulobacter crescentus* (Tsai and Alley, 2001).

As the molecular chaperone, ClpX is required for substrate recognition and delivery of target proteins to the ClpP peptidase chamber, suggesting that ClpX functions in a manner that contributes to the degradation of the ClpXP proteolytic complex, and thus precisely regulates multiple cellular processes. In cyanobacteria, a study revealed that ClpX is required to regulate the circadian gating of cell division (Cohen et al., 2018). In addition, *clpX* can affect the circadian period by regulating the transcription of ribosomal protein genes in cyanobacteria (Imai et al., 2013). However, our understanding of the functions and molecular mechanisms of ClpX in cyanobacteria is still unknown.

Hence, we aimed to investigate the unique contributions and regulatory network of ClpX in a model cyanobacterium *Synechocystis* sp. PCC 6803 (hereafter *Synechocystis*). *Synechocystis* is one of the most widely used model organisms for photosynthesis and carbon metabolism studies (Knoop et al., 2010), and is amenable to genetic modification (Yu et al., 2013). In this study, we constructed a *clpX* insertion mutant of *Synechocystis* and found that depletion of *clpX* results in slower growth, decreased high light tolerance, and impaired cyclic photosynthetic electron transfer. We then used a quantitative proteomic strategy to identify the ClpX-regulated proteins in *Synechocystis*. Based on the results of the proteomic and functional studies, we constructed a ClpX regulatory network in *Synechocystis* and provided novel insights into the functions and molecular mechanisms of the PQC system in cyanobacteria.

Materials and methods

Cyanobacteria strains and culture conditions

Synechocystis cells were photoautotrophically cultured in liquid BG11 medium under constant illumination of 40 μmol photons m^{-2} s^{-1}, aerated with filtered air at 30°C. To determine growth rates, the OD_{730} was measured every 12 h using a spectrophotometer (MAPADA, Shanghai, China). The growth curve under high light was measured under constant illumination of 250 μmol photons m^{-2} s^{-1} for a total of 96h. For high light treatments, logarithmic growth phase cells (OD_{730} = 0.7 to 0.8) were immediately illuminated at 250 μmol photons m^{-2} s^{-1} for 1.5 h.

10.3389/fpls.2022.994056

Mutant construction

The *clpX* mutant strain was constructed by homologous recombination. Briefly, an approximately 500 bp sequence flanking the *clpX* gene derived from *Synechocystis* genomic DNA was amplified by PCR using the following primers: *clpX*-AF/*clpX*-AR and *clpX*-BF/*clpX*-BR. The kanamycin resistance cassette (derived from the PRL446 plasmid) was amplified using a pair of primers, *kana*-F, and *kana*-R. The PCR products were then fused by fusion PCR. The fused fragment was then inserted into the TA cloning vector PMD19-T (Takara, Japan), and subsequently transformed into *Synechocystis* strain as previously described (Carpentier, 2004). In a word, the *clpX* gene was inactivated by insertion of a kanamycin resistance cassette, and Δ*clpX* was regarded as *clpX* insertion mutant. The transformants were selected on BG11 medium supplemented with kanamycin (50μg/ml) and further confirmed by PCR using the primers *clpX*-F and *clpX*-R. All the primers and conditions for the PCR amplification are listed in Table S1.

Photosynthetic oxygen evolution

For photosynthetic oxygen evolution rate assay, cells in the exponential growth phase were harvested and adjusted to a final concentration of 1.0 (OD_{730}) with fresh BG11 liquid media. *Synechocystis* strains were determined under cell culture conditions using an oxygen electrode system (Hansatech Instruments Ltd, Norfolk, UK) while maintaining a 30°C circulating water bath and stirring the cell suspension, as previously described (Nomura et al., 2006). The saturating light intensity was measured at 800 μE m^{-2} s^{-1}, and 10 mM $NaHCO_3$ was added as the electron acceptor.

Chlorophyll fluorescence

For chlorophyll fluorescence measurement, cells in the exponential growth phase were harvested and adjusted to a final concentration of 0.8 (OD_{730}) with fresh BG11 liquid media. After dark adaptation for 15 min, cell viability was determined using a Dual-PAM-100 fluorescence photosynthesis analyzer (Heinz Walz Gmbh, Effeltrich, Germany) at room temperature. The minimum fluorescence (F_0) and maximum fluorescence (F_m) levels were detected using the Dual-PAM software, and the maximal photochemical efficiency of photosystem II (PSII) in the dark-adapted state was calculated using the following formula: $F_v/F_m = (F_m–F_o)/F_m$ as previously described (Campbell et al., 1998). Transient increases in chlorophyll fluorescence after turning off actinic light (AL) were monitored as previously described (Shikanai et al., 1998).

$P700^+$ oxidation-reduction kinetics analysis

For $P700^+$ oxidation-reduction kinetics, cells in the exponential growth phase were harvested and adjusted to a final concentration of 3.0 (OD_{730}). After dark adaptation for 15 min, the redox state of $P700^+$ was measured using Dual-PAM-100 under an absorbance signal from 820 nm to 860 nm in the absence of 10 mM dichlorophenyl dimethylurea (DCMU), and the reduction kinetics were fitted and calculated using GraphPad Prism software (version 8.4) (https://www.graphpad.com/updates) (Swift and Sciences, 1997), as previously described (Zhao et al., 1998).

Bright-field and fluorescence microscopy

Synechocystis cells were collected by centrifugation at 5,000 g for 5 min at 30°C and washed three times with phosphate-buffered saline (PBS). Then visualized using a fluorescent microscope (Olympus, BX53, Japan) in the bright-field and RFP channel at a magnification of 100×.

Transmission electron microscopy

Samples were prepared as previously described (Golecki, 1988). Briefly, *Synechocystis* cells were collected by centrifugation at 5,000 g for 5 min at 30°C, fixed overnight with 2.5% (v/v) glutardialdehyde, incubated in 1% (v/v) osmium tetroxide at 4°C for 16h and dehydrated through a graded ethanol series (Mohr et al., 2010). Then the samples were embedded in 1% Seakem agarose and cut into ultrathin sections. Ultrathin sections were mounted on pioloform-coated copper grids and poststained with 2% uranyl acetate and lead citrate (Reynolds, 1963). Micrographs were recorded using a transmission electron microscope system (Hitachi, HT-7700, Japan) at 80 kV.

Whole-cell absorption spectra

Synechocystis cells were harvested at the mid-exponential growth phase and concentrated to the same optical density at 750 nm. Absorbance was detected using a SpectraMax M5 platform (Molecular Devices, America). Excitation was at 488 nm, and emission was collected from 400 to 750 nm with a sampling interval of 2 nm. Each spectrum is the average of three measurements.

Measurement of intracellular ROS

The intracellular ROS production was assessed by using ROS assay kit ((Beyotime, China) according to the user's manual protocols. Briefly, *Synechocystis* cells were collected and incubated with PBS buffer containing 10μM 6-carboxy-2',7'-dichlorodihydrofluorescein diacetate (DCFH-DA) and 10μg/mL Rosup for 30 min (Zhu et al., 2020). The fluorescence signal of ROS was detected by the SpectraMax M5 platform (Molecular Devices, America) at the emission wavelength of 525 nm and excitation wavelength of 488 nm.

Lipid peroxidation assay

The Lipid peroxidation was assessed by using MDA assay kit (Beyotime, China) according to the user's manual protocols. *Synechocystis* cells were harvested and lysed by sonication (Scientz Biotechnology, China) for 20 min at 135 W, on ice. Supernatants were collected by centrifugation at 5,000 g for 20 min at 4°C and quantified using the BCA Protein Assay Kit (Beyotime, China). Supernatants were then mixed with the same volume of 20% (w/v) trichloroacetic acid (TCA) containing 0.65% (w/v) thiobarbituric acid (TBA). After incubation at 100°C for 15 min, the mixed samples were centrifuged at 1,000×g for 10 min, and the absorbance of the supernatant at 532 nm was measured by the SpectraMax M5 platform (Molecular Devices, America). For quantification, the range of the MDA standard curve was from 1 to 25 μmol.

Protein extraction and trypsin digestion

Samples for proteomic analysis were harvested at the mid-exponential growth phase by centrifuging at 5,000 g for 5 min at 4°C and washed three times with phosphate-buffered saline (PBS). WT and Δ*clpX* samples were from three independent cell cultures. The samples were further resuspended in pre-cooled lysis buffer (PBS supplemented with 1 mM phenylmethylsulfonyl fluoride) and lysed by sonication (Scientz Biotechnology, Ningbo, China) for 20 min at 135 W, on ice. Undissolved cellular debris was removed by centrifugation at 5,000 g for 20 min at 4°C, and the supernatant was collected and quantified using the BCA Protein Assay Kit (Beyotime, Jiangsu, China). 100 μg of each sample was reduced by 25 mM dithiothreitol (DTT) at 37°C for 1 h and alkylated using 50 mM iodoacetamide (IAM) for 1 h in the dark to block reduced cysteine residues. The samples were digested with trypsin (1:100 w/w) for 6 h, and then additional trypsin (1:100 w/w) was added for a total of 24h digestion at 37°C. Following this, 0.1% (v/v) trifluoroacetic acid (TFA) was added to the resulting peptide mixtures to terminate the reaction. Samples were desalted using self-packed C18 SPE columns (C18, SBEQ-CA0801, Anple, shanghai) and dried using a vacuum centrifuge.

Tandem mass tag labeling and high-performance liquid chromatography fractionation

Peptide samples were labeled using the TMT reagent 6-Plex kit (Thermo Fisher Scientific), according to the manufacturer's instructions. The samples were labeled as follows: WT1:127N; WT2:128C; WT1:130N; ClpX-1:127C; ClpX-2:129N; ClpX-3:130C. The labeled peptides were mixed in equal amounts, resuspended in 5 mM NH_4OH, and fractionated using an LC20AD high-pressure pump (Shimadzu Corporation, Kyoto, Japan). In detail, peptides were loaded onto a Waters XBridge Shield C18 RP column (4.6 mm * 250 mm, 3.5 μm particle size) and washed with a gradient of buffer B (5 mM NH_4OH in 80% acetonitrile) 5% to 80% at a rate of 1 mL/min for 90 min. Finally, the eluted peptides were combined into 12 fractions and dried using vacuum centrifugation.

LC-MS/MS analysis

Peptides were dissolved in 1% formic acid and loaded onto an analytical column (C18, 75 μm × 50 cm, 2 μm, Thermo Fisher Scientific) using an EASY-nLC 1200 System (Thermo Fisher Scientific). The peptides were eluted using solvent B (0.1% formic acid in 80% ACN, v/v) at a constant flow rate of 250 nl/min with a linear solvent gradient: 0–6 min, 2–10% B; 6–51 min, 10–20% B; 51–58 min, 20–80% B; 58–62 min, 80% B; 62–63 min, 80–2% B; 63–70 min, 2% B. Subsequently, 2μg of each sample was injected into a nano electrospray ion source, ionized and sprayed into a Q Exactive HF-X mass spectrometer (Thermo Fisher Scientific). MS data collection was performed using Xcalibur 3.0, in data-dependent acquisition mode with automatic alteration (1MS scan followed by 20MS/MS scans). A full MS scan with an m/z range of 350–1800 was acquired at a 60,000 resolution with a minimum signal intensity of 10,000. The top 15 precursor ions with charge states of 2–6 were selected for MS/MS fragmentation by high-energy collision dissociation (HCD) with a normalized collision energy of 25%. The electrospray voltage was set at 2.2 kV. The dynamic exclusion duration of the precursor ion was set to 30 s, and the isolation width of the precursor ion was set to 1.4 m/z. The maximum injection times were 20 ms and 200 ms for MS and MS/MS, respectively.

Protein identification and quantification

All MS/MS spectra were searched against the *Synechocystis* protein database from the CyanoBase online website (http://genome.kazusa.or.jp/cyanobase, released in 2015) (Fujisawa et al., 2017) combined with the reverse decoy database and common contaminants using MaxQuant software (version 1.6.15.0) (https://www.maxquant.org/) (Cox and Mann, 2008). The parameters were set as follows: two maximum missed cleavage sites were permitted for trypsin; carbamidomethylation (Cys) was set as a fixed modification; oxidation (Met), deamidation (Asn/Gln), and acetylation (protein N-terminal) were set as variable modifications. 6-PlexTMT was set as a reporter ion. The mass deviations of precursor ions and fragment ions were set to 20 ppm and 0.02 Da, respectively, and the false discovery rate (FDR) thresholds for peptide and protein identification were specified at a maximum of 1%. Peptide sequences with less than six amino acids were excluded, and proteins that exceeded one unique peptide were identified. Quantification was performed using the Perseus software (version 1.5.6.0) (https://maxquant.net/perseus/) and Microsoft Excel (version Home & Student 2021). Only the proteins identified and quantified in three biological replicates were used for relative quantification. A two-sample Student's t-test was used for the statistical evaluation. Differentially expressed proteins were defined as fold-change ≥ 1.2, ≤ 0.83, and $p < 0.05$.

Bioinformatics analysis

To analyze the biological functions of the identified differentially expressed proteins (DEPs), they were grouped into biological process, molecular function, and cellular component classes based on the gene ontology (GO) terms using Blast2GO software (https://www.blast2go.com/) (Conesa and Gotz, 2008). Enrichment analyses of GO terms were performed using the DAVID bioinformatics resource (https://david.ncifcrf.gov/) (Huang et al., 2009). For our data, the corresponding *p*-value < 0.05 was considered statistically significant. The subcellular localization of the bacterial proteins was predicted using PSORTb (version3.0) (https://www.psort.org/psortb/) (Yu et al., 2010). To further explore the function of the DEPs, they were mapped to metabolic pathways using the KEGG database (https://www.kegg.jp/). The interaction network of DEPs was predicted by the STRING database (https://cn.string-db.org/) (Mering et al., 2003), further classified using the Markov Cluster Algorithm (MCL) clustering option, and visualized using Cytoscape (version3.8.0) (https://cytoscape.org/) (Shannon et al., 2003). Protein homologies were analyzed using BLASTP in the NCBI database. The domains of the Clp protease family in *Synechocystis* were annotated using the SMART online website (http://smart.embl-heidelberg.de/) (Schultz et al., 2000) and visualized using the IBS software (version1.0.3). The conserved motifs of ClpX proteins were predicted using the MEME online suite (http://meme-suite.org/tools/meme) with default settings (Bailey et al., 2009). To investigate the evolutionary conservation of the ClpX protein, a phylogenetic tree was constructed using MEGA software (version 11) (https://megasoftware.net/) with the neighbor-joining algorithm (NJ) method (Kumar et al., 2018). To visualize the distribution of the Clp protease family, a genomic map was created by using the DNA plotter tool (https://www.sanger.ac.uk/tool/dnaplotter/) (Carver et al., 2009). The complete genome of *Synechocystis* was obtained from the NCBI for Biotechnology Information website (https://www.ncbi.nlm.nih.gov/).

Data dependent acquisitionand parallel reaction monitoring

PRM experiments were performed to confirm the expression levels of proteins obtained from quantitative proteomics. According to the results of the quantitative proteomic analysis, a list containing the mass-to-charge ratio of the unique precursor peptides of the proteins of interest was chosen for PRM analysis. A list of these peptides is shown in Table S2. For DDA-based experiments, peptides were analyzed in DDA acquisition mode using an online nano-flow EASY-nLC 1200 system with an analytical column (0.3 mm × 150 mm, 3 μm particle size, ChromXP, C18). Samples were eluted using solvent B (0.1% FA dissolved in 100% ACN) at a constant flow rate of 300 nl/min for 100 min with the following gradient: 2–6%, 0–1 min; 6–17%, 1–61 min; 17–23%, 61–74 min; 23–32%, 74–87 min, 32–38%, 87–90 min; 39–90%, 90–91 min; 90%, 91–100 min. A full-scan MS event was acquired between 300 and 1,800 m/z at a 60,000 resolution, and the top 20 precursor ions (200–2,000 m/z) were selected for subsequent MS/MS scans. The isolation window was set to 2.0 m/z. Fragmentation was performed using HCD with an NCE of 28% and analyzed with a resolution of 15,000 in Orbitrap. The dynamic exclusion was set at 30 s. The maximum injection times for both full MS and MS/MS were 30 ms and 50 ms, respectively. The AGC targets for both MS and MS/MS were set to 3E6 and 2E5, respectively. For the PRM experiments, the peptides were analyzed in PRM acquisition mode. MS/MS was analyzed at a resolution of 60,000 with an isolation window of 1.2 m/z. The maximum injection times for both full MS and MS/MS were 50 and 110 ms, respectively. The remaining parameters were the same as those used in the DDA-based experiments.

Data analysis of PRM

Protein identification was performed using ProteomeDiscovery v2.3 software (Thermo Fisher Scientific). The DDA datasets were

searched in the *Synechocystis* protein database using CyanoBase (http://genome.kazusa.or.jp/cyanobase) (Fujisawa et al., 2017). The parameters were set as follows: two maximum missed cleavage sites were permitted for trypsin; carbamidomethylation (Cys) was set as a fixed modification; oxidation (Met), deamidation (Asn/Gln), and acetylation (protein N-terminal) were set as variable modifications. The mass deviations of the precursor and fragment ions were set to 10 ppm and 0.02 Da, respectively. The FDR was set to <1%. For the acquired PRM data, raw and msf files were imported into Skyline (v.3.5.1.9942) (MacLean et al., 2010) to analyze peptide transitions. Peptides with low signal-to-noise ratios and/or evidence of any interference were given no further consideration and the 3–5 transitions and 3–10 most intense fragment ions were used. Peaks were manually checked for correct integration, and the transition peak areas under the curve (AUC) of the targeted peptides were obtained from the summed AUCs of each transition. The abundance of each peptide was normalized to the average abundance of each protein. The mean value of the targeted peptide abundance was used to calculate the fold change among the same protein.

Results

Evolutionary conservation of Clp protease family and ClpX protein

The Clp protease family is found in almost all bacterial species. The Clp protease system consists of two main components: Clp proteases and Clp molecular chaperones. In *Synechocystis*, the Clp protease family contains five proteolytic-like proteins (ClpP1, ClpP2, ClpP3, ClpR, and ClpP4) and four Clp molecular chaperones (ClpX, ClpB1, ClpB2, and ClpC). First, we performed a conservation analysis of *Synechocystis* Clp proteases with other species, including *Synechococcus* 7002, *Nostoc* 7120, *Synechococcus* 7942, *Synechococcus* 9311, *Nostoc* 73102, *Bacillus subtilis*, and *Escherichia coli*, using BLASTP, the similarities in percentage were shown in Table S3. The Clp proteases and molecular chaperones of *Synechocystis* are highly conserved across all species. The protease ClpP subunits shared 71% to 87% identity with their cyanobacterial counterparts, sharing 67.37% identity with *B. subtilis*, and 67.02% with *E. coli*. The chaperone ClpX of *Synechocystis* was found to be conserved in all other species, showing 75–82% identity with other cyanobacteria, 62.53% with *B. subtilis*, and 60.66% with *E. coli*. The results indicated that Clp proteins are highly conserved across different species. We speculate that the functions of these proteins may be conserved and essential in these species, especially in cyanobacteria. The number of homologous proteins in each species is shown in Figure 1A. To further characterize the structure of these Clp proteins in *Synechocystis*, we performed structural domain analysis of the Clp proteins using the SMART online website. Among these Clp proteins, the typical domain architecture of the Clp molecular chaperone consists of a specific N-terminal domain (colored red or orange) that serves as a binding site for adaptor proteins and substrates, followed by one or two characteristic conserved modules, namely AAA modules, each of which is required for ATP binding and hydrolysis (Figure 1B). To show the global distribution of Clp proteins in the genome of *Synechocystis*, we constructed a circular map to visualize these proteins (Figure 1C). Further phylogenetic analysis revealed that the ClpX protein is highly conserved among different species, especially in cyanobacteria (Figure 1D). To analyze the structural features of ClpX, we explored the conserved motifs of this protein using the MEME tool (http://meme-suite.org/tools/meme). As shown in Figure 1D and Figure S1, almost all prokaryotes included eight conserved motifs among different species. However, only one specific motif has been identified in cyanobacteria. We speculated that it might play an important role in fulfilling a specific regulatory function.

Functional effects of *ClpX* in *Synechocystis*

To explore the function of ClpX, we constructed a *clpX* insertion mutant (Δ*clpX*) using a homologous recombination strategy (Figure S2). We measured the ability of the Δ*clpX* strain to grow photoautotrophically. As expected, the growth rate of the Δ*clpX* strain was slower than that of the wild-type (WT) strain under normal light conditions (constant illumination of 40 μmol photons m^{-2} s^{-1}) (Figure 2A). Besides, we observed the cell morphology and cell membrane morphology of WT and Δ*clpX* strain. No significant difference in morphology was detected between WT and Δ*clpX* strain (Figures S3, S4). Because *Synechocystis* is a model cyanobacterium capable of oxygenic photosynthesis, we examined the photosynthetic phenotype in both the WT and Δ*clpX* strains. We found that the maximal photochemical quantum yield of PSII (*Fv*/*Fm*) and oxygen evolution rates of the Δ*clpX* strain were similar to those of the WT (Figures 2B-C). Interestingly, the Δ*clpX* strain exhibited a slight difference in the post-illumination chlorophyll fluorescence increase (Figure 2D). Considering that post-illumination increases in chlorophyll fluorescence are thought to be involved in the cyclic electron flow around photosystem I (PSI), this suggests that ClpX may affect PSI cyclic electron transport. Furthermore, $P700^+$ oxidation-reduction kinetics showed that the $P700^+$ oxidation-reduction rate decreased overall, and the half-life ($t_{1/2}$) of the Δ*clpX* strain was significantly longer than that of the WT strain (Figure 2E). Therefore, our findings demonstrate that ClpX may play a regulatory role in PSI cyclic electron flow. As mentioned above, *clpX* interruption under normal light conditions affects growth and cyclic electron transport. We further found that the

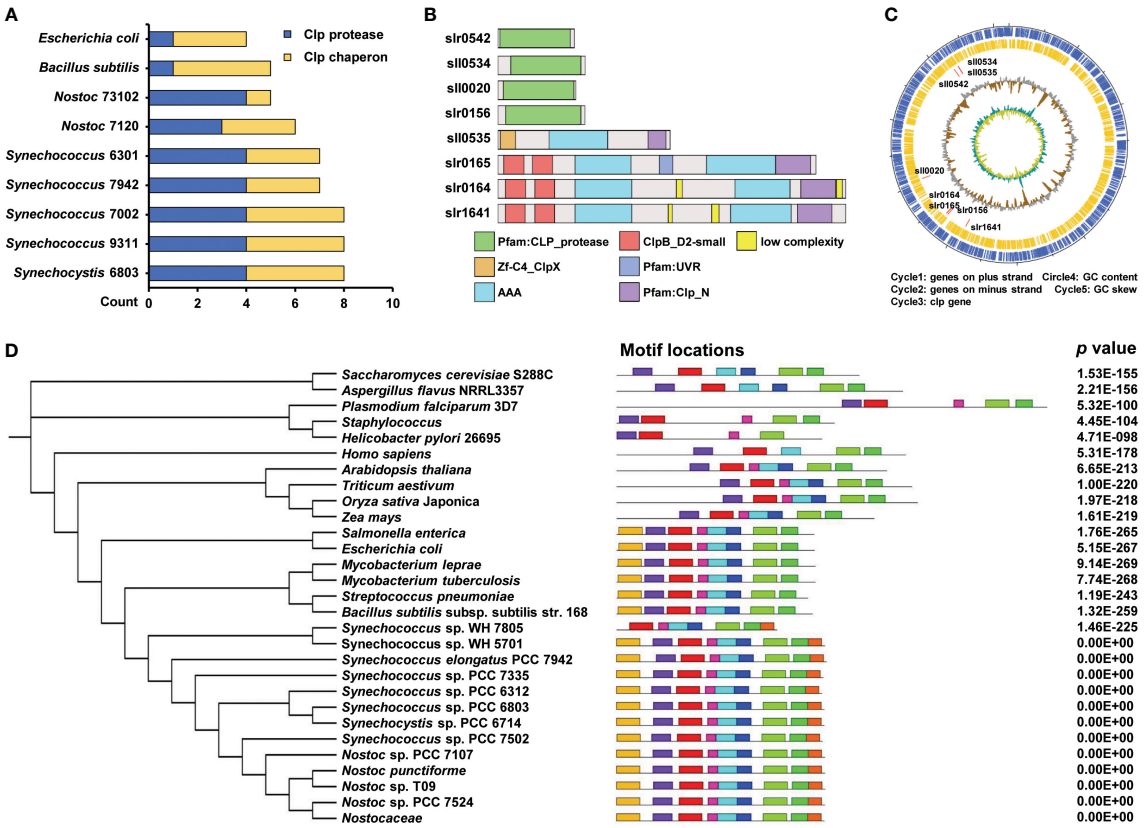

FIGURE 1
Conservativeness analysis of Clp family. **(A)** Comparing the number of *Synechocystis* sp. PCC 6803 Clp protease family homologs in different species. The blue and yellow columns indicate the count of Clp protease and Clp chaperon, respectively. **(B)** Schematic diagram of protein domains of Clp protease family from *Synechocystis* sp. PCC 6803. **(C)** The circos diagram indicates the whole *Synechocystis* sp. PCC 6803 genome. The outermost layer and inner layer denote the genes on the plus strand and minus strand in the genome, respectively. The third, fourth, and innermost layers denote the genomic position of the 8 Clp protease family members, % GC content, and GC skew, respectively. **(D)** Phylogenetic tree and motifs of ClpX protein. The tree was generated using a neighbor-joining algorithm. The conserved motif was analyzed using the MEME tool and nine different motifs were identified. Different motifs are denoted by different borders and colors, and the same color in different ClpX proteins refers to the same motif. Their combined p values are on the right side of the figure.

growth rate of the Δ*clpX* strain was significantly lower than that of the WT strain when cultured under high-light conditions (Figure 2F). Consistently, the *Fv*/*Fm*, oxygen evolution rate, post-illumination increase in chlorophyll fluorescence, and $P700^+$ oxidation-reduction rate were significantly lower in the Δ*clpX* strain, compared to that of the WT (Figure 2G-J). To examine pigment content, the whole cell absorption spectra of WT and Δ*clpX* strain were detected, and their absorbances of all kinds of pigments were similar (Figure S5). Besides, we detected the relative proportion of intracellular ROS between WT and Δ*clpX* and their lipid peroxidation levels. Obvious differences were observed between WT and Δ*clpX* strain in these experiments, suggesting the Δ*clpX* strain could be under oxidative stress (Figure S6). Collectively, these observations demonstrate that ClpX plays an important role in cell growth and photosynthesis in *Synechocystis*.

Identification of ClpX-regulated proteins in *Synechocystis*

To explore the potential regulatory mechanism of the ClpX protein in *Synechocystis*, a tandem mass tag (TMT)-labeled quantitative proteomic strategy was used to identify dysregulated proteins upon the interruption of *clpX* (Figure 3A). Pearson's correlation coefficients were calculated based on the $\log_2$-transformed protein intensities among the three biological replicates of the WT and *ΔclpX* groups to assess the reproducibility of the TMT-based quantitative proteomic data. The strong correlations with corresponding coefficients $r >$ 0.99 indicated high repeatability among the three replicates (Figure 3B). The high-quality proteomic data obtained enabled us to identify 2,629 proteins (Table S4), accounting for approximately 75% of the predicted *Synechocystis* proteins.

10.3389/fpls.2022.994056

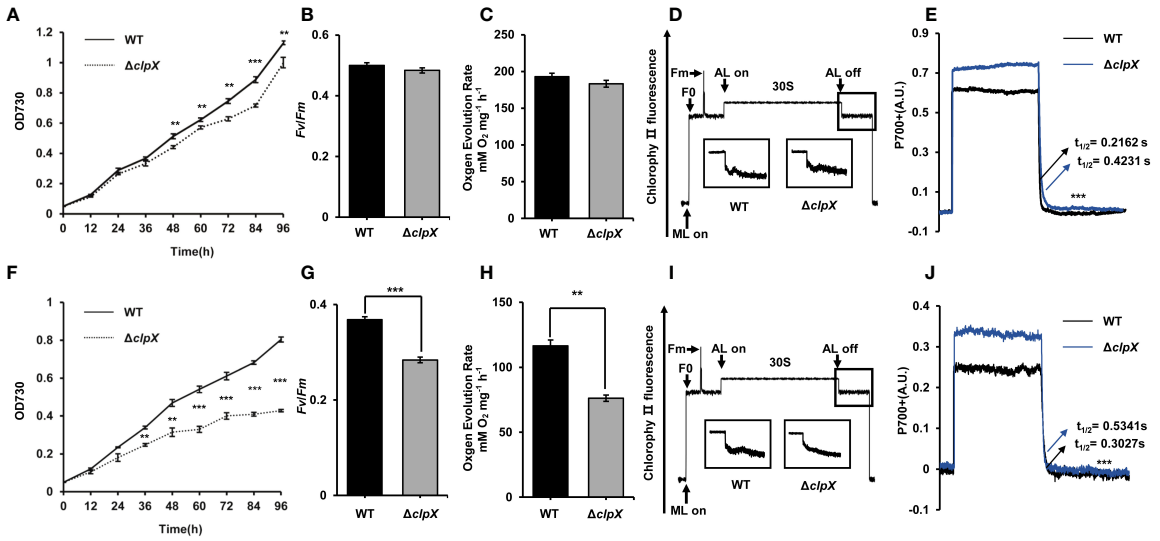

FIGURE 2
Functional effects of *clpX* in *Synechocystis*. **(A)** Growth curves of the wild type (WT) and Δ*clpX* strains under normal light (NL). **(B)** Measurement of maximum photochemistry efficiency (*Fv*/*Fm*) of the WT and Δ*clpX* strains under NL. **(C)** Measurement of oxygen evolution rates of the WT and Δ*clpX* strains under NL. **(D)** Analysis of the transient increase in chlorophyll fluorescence after the termination of AL illumination of the WT and Δ*clpX* strains under NL. **(E)** $P700^+$ reduction kinetics of the WT and Δ*clpX* strains in the presence of DCMU under NL. **(F)** Growth curves of the WT and Δ*clpX* strain under high light (HL). **(G)** Measurement of maximum photochemistry efficiency (*Fv*/*Fm*) of the WT and Δ*clpX* strains under HL. **(H)** Measurement of oxygen evolution rates of the WT and Δ*clpX* strains under HL. **(I)** Analysis of the transient increase in chlorophyll fluorescence after the termination of AL illumination of the WT and Δ*clpX* strains under HL. **(J)** $P700^+$ reduction kinetics of the WT and Δ*clpX* strains in the presence of DCMU under HL. ML, measuring light; AL, actinic light. Data are presented as the mean ± SD from three independent experiments. Statistical significance was determined by two-sample Student's *t*-test (**, $p < 0.01$; ***, $p < 0.001$).

Among these, 2,618 proteins were quantifiable using the stringent filtering criteria described in the Materials and Methods section. A total of 172 proteins were differentially expressed between the WT and ΔclpX strains according to the standard of p-value<0.05 and |log2FC|≥1.20 (Figure 3C and Table S5). Among these DEPs, 94 proteins showed a fold change ≥ 1.20 and 72 proteins showed a fold change ≤ 0.83. Volcano plots, in which the fold change (log_2) of DEPs is plotted against the corresponding *p*-value, are shown in Figure 3D. These DEPs will provide novel candidates for future studies that will allow assessment of their physiological roles and significance in ClpX-regulated processes.

Functional characterization of ClpX-regulated proteins

To better understand the biological function of ClpX-regulated proteins, all identified DEPs were annotated according to the gene ontology (GO) system using Blast2GO software (Table S6). The annotation results obtained from the biological processes demonstrated that most of the DEPs were involved in metabolic and cellular processes, localization, biological regulation, and response to a stimulus. Moreover, a group of down-regulated proteins was found to be involved in signaling and obsolete electron transport. From this perspective, our observations support the previous conclusion that ClpX-regulated proteins may play an important role in metabolism regulatory functions and stress responses (Figures 4A-B) (Sokolenko et al., 2002). Regarding molecular functions, DEPs were widely distributed in transcription regulator, transducer, and catalytic activity, as well as binding. Some downregulated proteins were annotated as having antioxidant activity, indicating the importance of ClpX in the stress response (Figures 4A-B). Although the subcellular localization of proteins will provide novel insight into their biological function, the localization of the majority of the DEPs was not predicted (unknown), according to the subcellular localization analyzed by PSORTb (Table S7). In addition, a large number of DEPs were assigned to the cytoplasm, where a series of biological processes such as carbon, nitrogen, and amino acid metabolism, and protein degradation occur. These results were in line with the results of the biological process annotation that considerable DEPs were classified as being involved in metabolic and cellular processes, and biological regulation. In addition, some DEPs were located in the outer and cytoplasmic membrane, suggesting

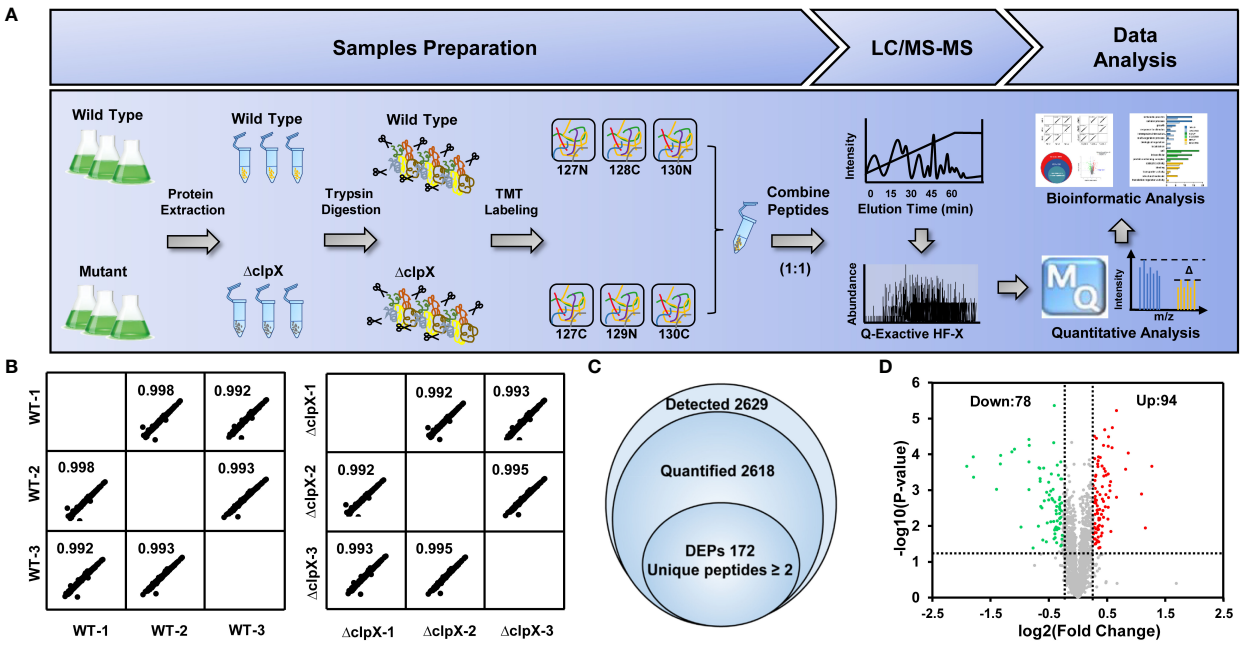

FIGURE 3
Workflow and quantitative proteomics data. **(A)** Workflow for TMT labeling quantitative proteomic strategy. **(B)** Pairwise correlation of peak area of identified proteins between three biological replicates. **(C)** Venn diagram showing the overlap of the number of detected proteins quantified proteins, and differentially expressed proteins (DEPs). **(D)** Volcano plots showing *p*-values ($-\log_{10}$) versus the fold change ($\log_2$) of DEPs. Proteins with $p < 0.05$ and fold change > 1.2 or < 0.83 are considered to be differentially expressed. Upregulated and downregulated proteins are marked as red and green dots, respectively.

that these DEPs may be related to stimuli, signal transducer activity, transporter activity, and obsolete electron transport (Figures 4A-B).

GO enrichment analysis was performed to elucidate the biological functions of the ClpX-regulated proteins (Table S8). As depicted in Figures 4C, our data showed that ClpX-regulated proteins were significantly enriched in the peptide biosynthetic process and peptide and cellular protein metabolic processes, based on biological process enrichment. According to the results of the molecular function enrichment analysis, we found that the

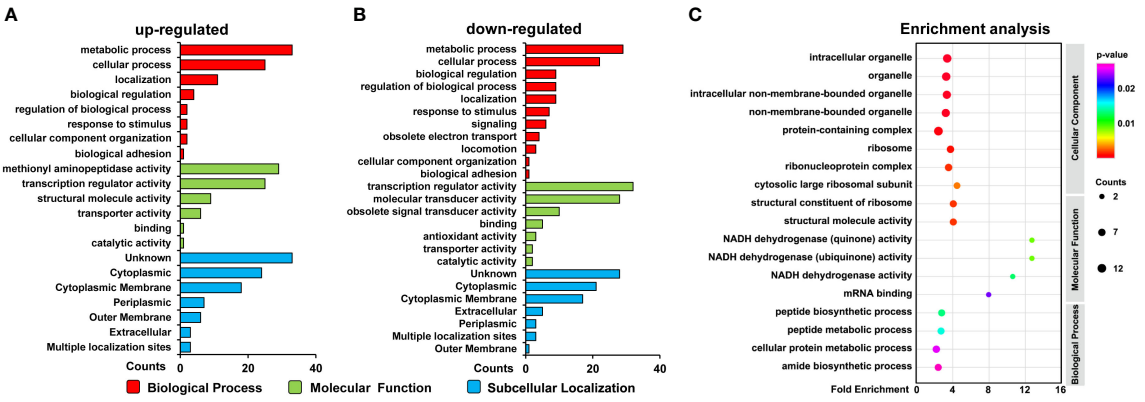

FIGURE 4
Functional analysis of differentially expressed proteins (DEPs). **(A)** GO classification of the upregulated proteins and **(B)** downregulated proteins. **(C)** GO enrichment of the DEPs. Circle size indicates the number of enriched proteins. Color saturation represents the significance level.

DEPs were mostly enriched for binding and enzymatic activities, such as mRNA binding and NADH dehydrogenase activity. Within the GO cellular component categories, a large proportion of DEPs were associated with ribosomes, ribonucleoprotein complexes, cytosolic large ribosomal subunits, and structural constituents of ribosomes. Our functional annotation analysis indicated widespread roles of ClpX in fulfilling the delicate regulatory function in *Synechocystis*, similar to that in other organisms (Claunch et al., 2018; Lo et al., 2020; Kirsch et al., 2020).

Functional interaction networks of ClpX-regulated proteins

To further explore the biological roles of the identified DEPs, an overall protein-protein interaction network (PPI) was constructed using the STRING database. The network incorporated 94 nodes and 197 edges and was visualized using Cytoscape (Figure S7 and Table S9). Each edge was examined using a score as the edge weight to quantify interaction confidence. Usually, the average node degree is used to represent the average number of edges per node in a PPI network, and a higher value for the degree indicates a highly connected network and is likely to be more robust. The average node degree of 3.12 implicated more edges connecting to nodes in our data. Moreover, a small *p*-value (3.85×10^{-08}) of PPI enrichment was obtained in our network, suggesting that the observed degree of edges was significant, and the identified DEPs were functionally connected. Based on this network, we characterized protein complexes of DEPs, and six highly interconnected clusters were observed according to the Markov cluster algorithm (MCL). In line with our GO annotation results, the top cluster (cluster I), clusters III, IV, and VI consisted of DEPs related to transport-related, signal transduction mechanism, anti-sigma factor antagonist domain, and phosphate transport, implying that these DEPs may play functional roles in transporter activity and stress response. Cluster V consisted of metabolism-associated proteins, such as Nodb homology and xylose isomerase-like domain complex. These findings suggest that ClpX-regulated proteins are involved in diverse cellular processes in *Synechocystis*.

ClpX-regulated proteins involved in metabolism

Accumulating evidence has revealed that ClpX can recognize the amino acid sequences of substrates, serving as tethering or degradation tags, for further protease-mediated protein degradation (Zhang and Zuber, 2007). Based on a previous study (Kirsch et al., 2020) and the results of our functional annotation, we anticipated that *clpX* interruption would disturb cellular metabolic processes in *Synechocystis*. Consistent with this notion, DEPs were found to be involved in metabolic pathways, ATP-binding cassette (ABC) transporters, signal transduction, and defense mechanisms (Table S10A). As shown in Figure S8, S9A, *clpX* interruption led to the downregulation of key enzymes involved in carbon metabolism, including hydrolysis of glycogen (glgX, encoded by slr1857) and the glycolytic pathway (pfkA2, encoded by sll0745; and yibo, encoded by slr1945). In addition, *clpX* interruption led to significantly decreased expression of proteins involved in nitrogen metabolisms, such as the cytochrome b subunit of nitric oxide reductase norB (sll0450) and glutamate–ammonia ligase glnN (slr0288). Interestingly, the proteins involved in purine and pyrimidine metabolism, such as '*de novo*' UMP biosynthetic process protein (sll0744), were also downregulated, which was in line with a previous study (Kirsch et al., 2021). The interruption of *clpX* affects the two-component signal transduction system and ABC transporters of phosphate, iron, manganese, phospholipid, and sulfate. Consistently, all phosphate transporter-associated proteins, including sphX (sll0679), pstS (sll0680), pstB1 (sll0683), pstB2 (sll0684), pstC (sll0681), pstC (slr1248), pstS (slr1247), and ziaA (slr0798) were significantly downregulated, whereas the iron(III) transporter hitB (slr0327), manganese transporter mntC (sll1598), phospholipid transporter ycf22 (sll1002), and sulfate transporter bicA (sll0834) exhibited significant upregulation, indicating the presence of different regulatory roles of ClpX, similar to the results from other organisms. Moreover, two-component system proteins, such as two-component sensor histidine kinase (sll1590), two-component hybrid sensor and regulator (sll1296), and two-component system response regulator (sll1330), were also significantly upregulated, suggesting that ClpX may play an important role in stress response. Notably, because the Clp protease complex can degrade most ribosomal proteins (Kuroda et al., 2001; Kuroda, 2006), the interruption of *clpX* may consequently give rise to the upregulation of ribosomal constituent proteins (mainly the 50S large subunit), including rplB (sll1802), rplX (sll1807), rpsK (sll1817), rplT (sll0767), rpsL (sll1096), and rpmI (ssl1426). Furthermore, many proteases, such as hhoA (sll1679), ymxG (slr1331), htrA (slr1204), methionine aminopeptidase (sll0555), and putative carboxypeptidase (sll0777), were significantly upregulated. As mentioned above, ClpX functions as a chaperone for proteases, assisting in the protein degradation process. Therefore, the interruption of *clpX* may affect the proteolytic function of proteases, and some compensatory effects may be stimulated.

Among the 172 DEPs, 89 were annotated as hypothetical or unknown proteins in the *Synechocystis* database. Next, we performed functional annotation for these hypothetical or unknown proteins using BLASTP homology searches and CD-search for conserved domain annotations (Table S10B). Notably,

more than half of these proteins can be annotated and assigned to metabolic pathways, ABC transporters, two-component signal transduction, regulation of gene expression, protein degradation, and defense mechanisms (Figures S8, S9B). These findings provide new candidates for future functional studies of ClpX.

Validation of the DEPs by parallel reaction monitoring (PRM) analysis

To independently verify the changes in the abundance of DEPs measured in our TMT-labeled quantitative proteomics experiments, PRM analysis was performed to further confirm twenty-four of the identified DEPs (Table S11). These validation experiments were performed on the same batch of extracted peptide samples used for quantitative proteomics experiments. All data were imported into Skyline software to further check the peak shape and retention time of each peptide segment. To evaluate the correlation between PRM-based protein expression and TMT-labeled quantitative proteomics data, we performed a Pearson correlation analysis based on the $\log_2$-transformed abundance of transitions for the 24 selected proteins among the biological replicates. According to the scatter plot, the strong linear correlation observed indicates a high level of reproducibility among the replicates (Figure 5A). We then constructed a heatmap based on the 24 selected proteins to analyze the consistency of expression levels between PRM-based proteins and TMT-labeled quantitative proteins. As shown in Figure 5B, the quantified results obtained from PRM were mostly in agreement with those of TMT-labeled quantitative proteomics. The identified DEPs were grouped into five categories according to their specific functions. ClpX-regulated proteins involved in the regulation of gene expression and protein degradation, as well as defense mechanisms, were significantly upregulated. The selected proteins in metabolic pathways were downregulated, except for dihydrodipicolinate synthase (slr0550). The remaining proteins, including ABC transporter-binding protein and cation efflux system protein involved in nickel and cobalt tolerance, were upregulated in the *ΔclpX* strain, whereas the other proteins in ABC transporters and signal transduction were mostly down-regulated. The high consistency indicated that our PRM validation assay was reliable for measuring relative protein expression levels. The extracted transitions of the representative peptides from 50S ribosomal protein L2 (sll1802), 50S ribosomal protein L24 (sll1807), 50S ribosomal protein L35 (ssl1426), and 30S ribosomal protein S11 (sll1817) are shown in Figure 5C.

Discussion

ClpX functions as a chaperone of the ATP-dependent protease ClpP, forming ClpXP proteolytic complexes, which are essential for maintaining proteostasis by disposing of damaged or unneeded proteins, as well as for the conditional degradation of functional proteins in response to external or internal signals (Sauer et al., 2004). However, the molecular details of this process remain poorly understood.

To globally search for ClpX-regulated proteins in *Synechocystis*, we compared the protein profiles of the WT and Δ*clpX* strains using a quantitative proteomic strategy. A total of 172 DEPs were identified, and the differential expression levels of 24 proteins were confirmed by PRM analysis. Bioinformatics analysis suggested that these DEPs were enriched in a variety of biological regulatory pathways, including glycolysis, amino acid biosynthesis, nitrogen assimilation, photosynthetic electron transport, ABC transporters, and two-component signal transduction. Therefore, we provided a proteome-wide view of the regulatory networks of ClpX in this model cyanobacterium.

In this study, we demonstrated that ClpX plays an essential role in growth. It is reported that ClpXP proteolytic complex plays a role in cell division by modulating the level of FtsZ through degradation, and may degrade multiple cell division proteins, thereby modulating the balance of the components required for division (Camberg et al., 2011). Moreover, ClpX is required to relieve a clock-induced cell division checkpoint (Cohen et al., 2018). Furthermore, NOA1, which is essential for mitochondrial protein synthesis, oxidative phosphorylation, and ATP production, is one of the substrates of the ClpXP proteolytic complex (Al-Furoukh et al., 2014). Overall, these reports were consistent with our experimental results, and ClpX may influence the growth of cyanobacteria by affecting cell division and metabolism.

Based on previous reports (Rowland et al., 2011) and our results, we mapped ClpX-regulated proteins to KEGG pathways and constructed a hypothetical model to depict the potential regulatory mechanisms of ClpX in *Synechocystis* (Figure 6). Cyanobacteria have an intricate light-harvesting apparatus that captures light and synthesizes ATP and NADPH by driving photosynthetic electron transport pathways (Mullineaux, 2014). As it's an essential step for the degradation of photodamaged proteins in photosynthetic organisms (Stanne et al., 2009), several dysregulated proteins associated with the electron transport chain, including photosystem II PsbH protein (ssl2598), cytochrome b6f complex petC (sll1182), and ferredoxin (ssl2559), were identified in the Δ*clpX* strain, owing to the existence of reduced photosynthetic performance. In addition, our experimental results demonstrated that the interruption of *clpX* decreased the $P700^+$ oxidation-reduction rate in the presence of DCMU and that cyclic electron transport was dominant at the same time. The interruption of *clpX* also influenced the increase in transient chlorophyll fluorescence, which is involved in PSI cyclic electron transport. Thus, our data suggest that ClpX may influence cyclic electron transport by regulating the expression of these photosynthesis-related proteins.

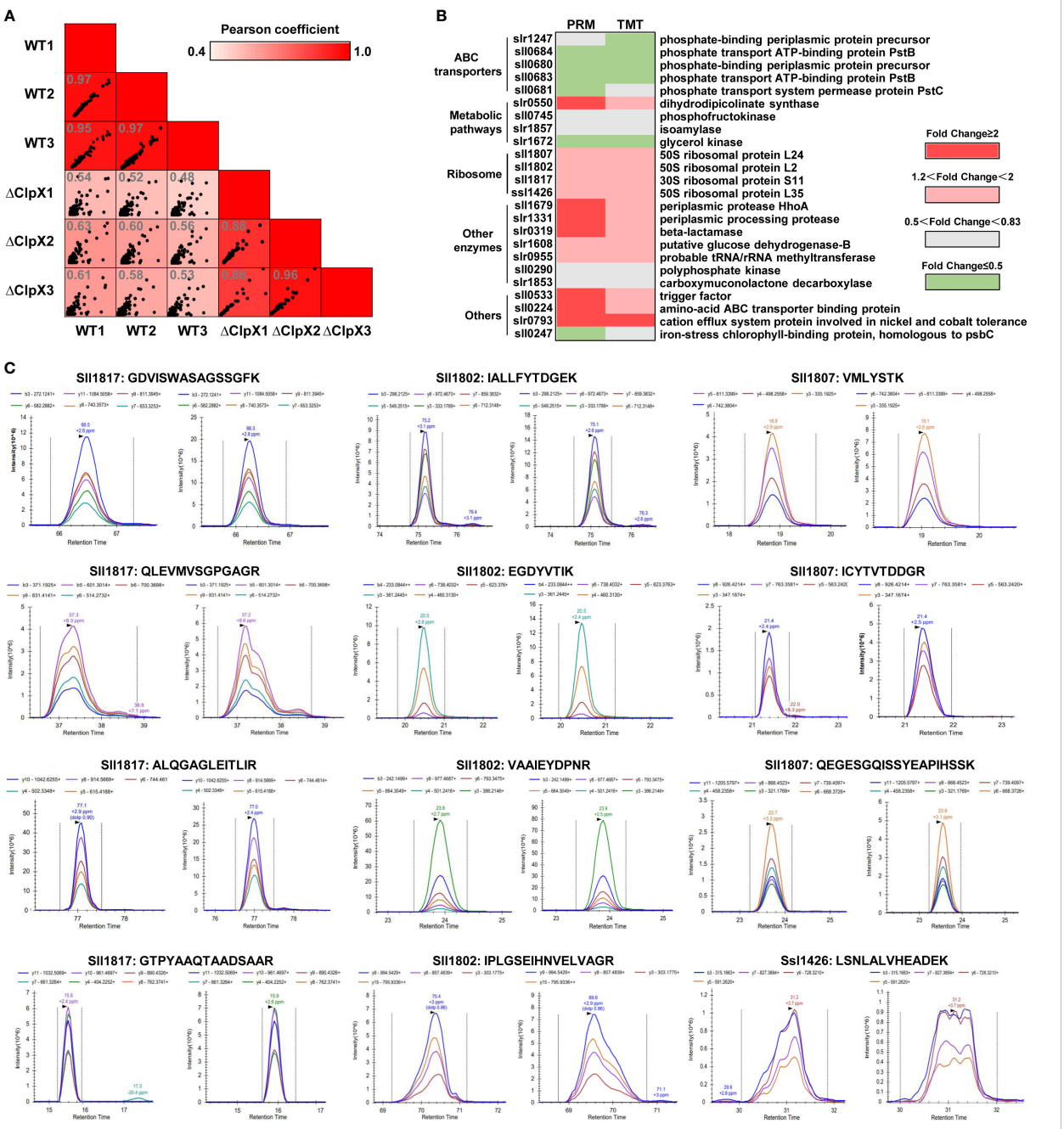

FIGURE 5
Validation of DEPs using Parallel Reaction Monitoring (PRM) analysis. **(A)** Pairwise correlation of peak area of transitions for the selected DEPs between three biological replicates. **(B)** Heatmap showing the expression levels of the DEPs selected for validation by PRM. **(C)** Chromatograms represent the fragment ion extracted-ion chromatograms (XICs) for the representative peptides from the WT and *ΔClpX* strains.

Given the important roles of ClpX in stress responses, such as temperature (LaBreck et al., 2017; Roy et al., 2019), pH (Roy et al., 2019), and Fe^{2+} stresses (Bennett et al., 2018), we anticipated that ClpX may also have functions in the high light response in cyanobacteria. As expected, the Δ*clpX* strain exhibited slow growth and photosynthetic electron transport rates under high light conditions (Figure 2). It is noteworthy that many proteins associated with ABC transporters and two-component signal transduction systems were dysregulated after *clpX* interruption, such as phosphate assimilation, nitrogen availability, and manganese starvation (Figure 6). The two-component signal transduction system represents a crucial means of sensing and

responding to environmental changes both intra- and extracellularly in bacteria (Koretke et al., 2000). The sensor histidine kinase can respond to intra- or extracellular signals by catalyzing the phosphorylation of related response regulators, which are then capable of adjusting gene expression or cellular physiology to cope with the changes that occur in its environment (Storz and Hengge, 2010). ABC transporters are membrane proteins that couple the transport of diverse substrates across cellular membranes to ATP hydrolysis (Hollenstein et al., 2007), which plays an important role in environmental adaptation. Increasing evidence suggests that ABC transporters and signal transduction systems often work together to respond to environmental change (Dintner et al., 2011; Dintner et al., 2014). In this study, we identified several DEPs involved in the Pst system, which is an ATP-dependent ABC transporter-type system that includes phosphate-binding proteins and transmembrane protein units (Rao and Torriani, 1990). For instance, several Pst system members were downregulated after *clpX* interruption, including sll0680 (pstS), sll0681 (pstC), sll0683 (pstB1), slr1248 (pstC), and slr1247 (pstS). PstS is a phosphate-binding periplasmic protein commonly found in cyanobacteria, PstA and PstC are transmembrane subunits that form a channel in the inner membrane, and PstB is a membrane protein that contains an ATP-binding domain (Su et al., 2007; Jin et al., 2021). PstA, PstB, and PstC constitute the ABC-type Pst transporter system. PstS can bind to Pi and transport it through the Pst transporter system by hydrolysis of ATP and interacts with the Pst transporter system to transmit the signal to the sensor kinase SphS (Rao and Torriani, 1990; Tiwari et al., 2015). Likewise, phosphate availability sensing is regulated by a two-component regulatory system, SphS-SphR, in cyanobacteria, which is orthologous to PhoB-PhoR in *E. coli* (Hirani et al., 2001; Suzuki et al., 2004). In this system, specific environmental signals are sensed by membrane-bound histidine kinases, activating response regulators to regulate the expression of target genes and finally mediate specific cellular responses against the stimulus (Mascher et al., 2006). Based on these data, we suggest that ClpX may affect the high-light adaptation of *Synechocystis* through the regulation of a two-component signal transduction system and ABC transporters.

In this study, many ribosomal proteins were found to be dysregulated in the Δ*clpX* strain, suggesting that ClpX may affect

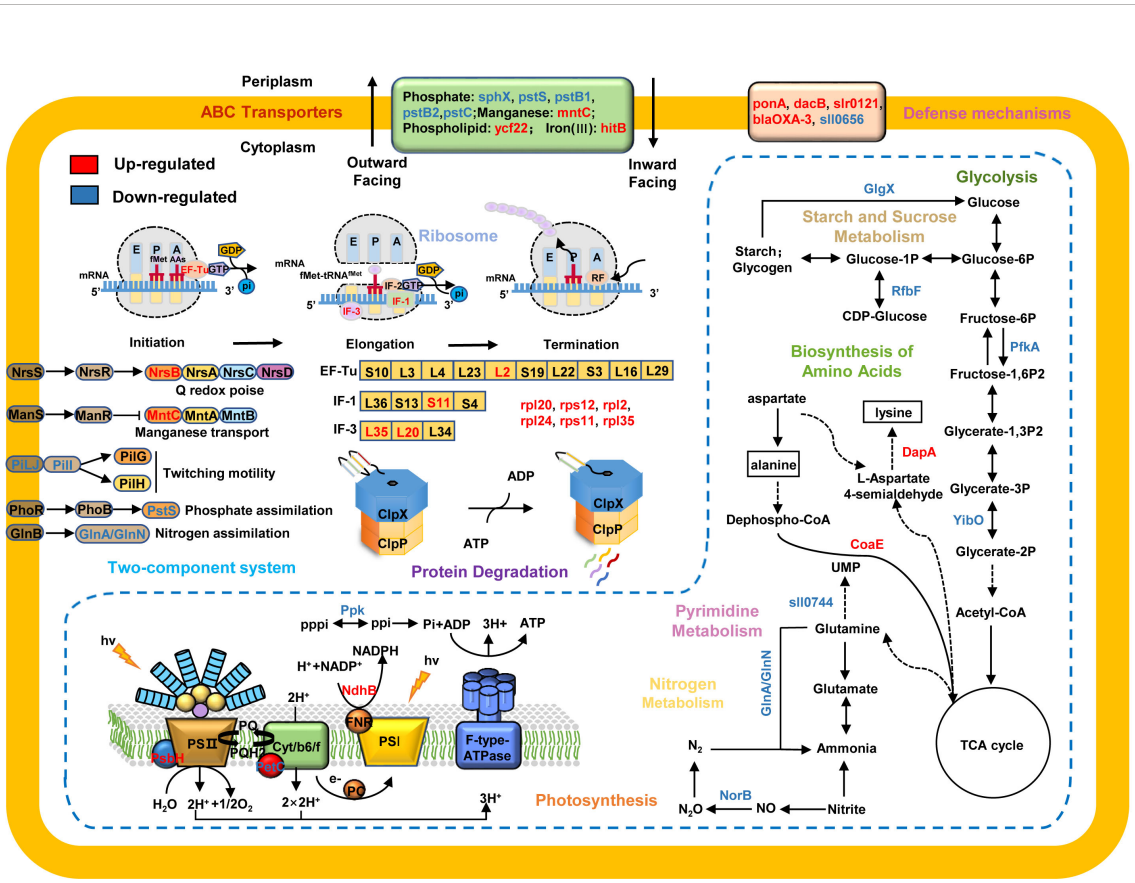

FIGURE 6
A proposed model showing the regulatory networks of ClpX in *Synechocystis* sp. PCC 6803. The upregulated proteins are highlighted in red and downregulated proteins are in blue. Arrows represent state transitions or metabolite fluxes.

global protein abundance by regulating the expression of ribosome-associated proteins (Figure 6). Ribosomes are macromolecular machines responsible for the process of translation, and encode mRNAs into polypeptide chains with high speed and accuracy (Green and Noller, 1997). Ribosomes fold polypeptides during their synthesis to decrease the risk of protein misfolding and aggregation, contributing to the maintenance of proteostasis (Cassaignau et al., 2020). Although several intricate mechanisms ensure efficient and precise protein synthesis, some mistakes inevitably occur during protein synthesis (Frischmeyer et al., 2002; Haebel et al., 2004). Misfolded or partially folded proteins often aggregate and/or interact inappropriately with other components, leading to the impairment of cell viability and eventually cell death (Mishra and Grover, 2016). Specific proteases, including ClpAP and ClpXP, which can target specific degradation signals, are recruited to degrade these aberrant proteins (Gottesman et al., 1998; Song and Eck, 2003). Several ribosomal proteins can be captured by the ClpXP complex in *E. coli* (Flynn et al., 2003). The isolated ribosomal complex also contains the ClpXP complex in *E. coli*, HepG2, and human cell lines (Fux et al., 2019). Thus, our data suggest that ClpX may play a biological role by targeting ribosome-associated proteins in *Synechocystis*.

A large number of hypothetical or unknown proteins have been identified as dysregulated proteins in response to *clpX* interruption. Based on our re-annotation results, many hypothetical proteins were classified as clustered regularly interspaced short palindromic repeat (CRISPR)-associated proteins (Table S7). It has been reported that *clpP* deficiency increases the expression of CRISPR-associated genes in *Streptococcus* mutants (Chattoraj et al., 2010). An increasing number of studies have pointed to the direct links between CRISPR-associated proteins and the regulation of a range of stress-related phenomena (Louwen et al., 2014). For the first time, we found that *clpX* interruption may lead to the dysregulation of CRISPR-associated proteins in *Synechocystis*. This study provides new candidates for future functional studies of ClpX and novel insights into the mechanisms of protein homeostasis in cyanobacteria.

In conclusion, we established a ClpX regulatory network in *Synechocystis* based on the results of proteomic and functional studies. The identified comprehensive catalog of proteins provides a valuable resource for further mechanistic investigations of protein quality control systems in cyanobacteria.

Data availability statement

The original contributions presented in the study are publicly available. This data can be found here: iProX, IPX0004691000.

Author contributions

MY and FG: conceptualization. YZ, YW, WW, MW, and SJ: methodology. YZ, YW, and MY: investigation and writing-original draft preparation. WW, MW, and SJ: data curation. MY, FG: writing-review and editing. WW, MW, SJ: visualization. WW and FG: funding acquisition. All authors have read and agreed to the published version of the manuscript.

Funding

This work was supported by the National Key Research and Development Program of China (2020YFA0907400), the National Natural Science Foundation of China (grant no. 31870756), the Chinese Academy of Sciences Grant QYZDY-SSW-SMC004, the China Postdoctoral Science Foundation to W.W. (2021M703432), and the State Key Laboratory of Freshwater Ecology and Biotechnology to W.W. (2022FB03).

Acknowledgments

We thank the Analysis and Testing Center of Institute of Hydrobiology and Micrometer Biotech Company (Hangzhou, China) for their helps in proteomic experiments.

Conflict of interest

The authors declare that the research was conducted in the absence of any commercial or financial relationships that could be construed as a potential conflict of interest.

Publisher's note

Supplementary material

The Supplementary Material for this article can be found online at: https://www.frontiersin.org/articles/10.3389/fpls.2022.994056/full#supplementary-material

References

Alexopoulos, J. A., Guarne, A., and Ortega, J. (2012). ClpP: a structurally dynamic protease regulated by AAA+ proteins. *J. Struct. Biol.* 179, 202–210. doi: 10.1016/j.jsb.2012.05.003

Al-Furoukh, N., Kardon, J. R., Krüger, M., Szibor, M., Baker, T. A., and Braun, T. (2014). NOA1, a novel ClpXP substrate, takes an unexpected nuclear detour prior to mitochondrial import. *PLoS One* 9. doi: 10.1371/journal.pone.0103141

Bailey, T. L., Boden, M., Buske, F. A., Frith, M., Grant, C. E., Clementi, L., et al. (2009). MEME SUITE: tools for motif discovery and searching. *Nucleic Acids Res.* 37, W202–W208. doi: 10.1093/nar/gkp335

Baker, T. A., and Sauer, R. T. (2012). ClpXP, an ATP-powered unfolding and protein-degradation machine. *Biochim. Biophys. Acta* 1823, 15–28. doi: 10.1016/j.bbamcr.2011.06.007

Bennett, B. D., Redford, K. E., and Gralnick, J. A. (2018). Survival of anaerobic Fe (2+) stress requires the ClpXP protease. *J. Bacteriol.* 200:e00671–17. doi: 10.1128/JB.00671-17

Burton, B. M., and Baker, T. A. (2005). Remodeling protein complexes: Insights from the AAA+ unfoldase ClpX and mu transposase. *Protein Sci.* 14, 1945–1954. doi: 10.1110/ps.051417505

Camberg, J. L., Hoskins, J. R., and Wickner, S. (2011). The interplay of ClpXP with the cell division machinery in escherichia coli. *J. Bacteriol.* 193, 1911–1918. doi: 10.1128/JB.01317-10

Campbell, D., Hurry, V., Clarke, A. K., Gustafsson, P., OüQuist, G. J. M., and Reviews, M. B. (1998). Chlorophyll fluorescence analysis of cyanobacterial photosynthesis and acclimation. *Microbiology and molecular biology reviews* 62, 667–683. doi: 10.1128/MMBR.62.3.667-683.1998

Carpentier, R. (2004). *Photosynthesis research protocols* (Springer, New York, USA).

Carver, T., Thomson, N., Bleasby, A., Berriman, M., and Parkhill, J. (2009). DNAPlotter: circular and linear interactive genome visualization. *Bioinformatics* 25, 119–120. doi: 10.1093/bioinformatics/btn578

Cassaignau, A. M., Cabrita, L. D., and Christodoulou, J. J. A. R. O. B. (2020). How does the ribosome fold the proteome? *Annual review of biochemistry* 89, 389–415. doi: 10.1146/annurev-biochem-062917-012226

Chattoraj, P., Banerjee, A., Biswas, S., and Biswas, I. (2010). ClpP of streptococcus mutans differentially regulates expression of genomic islands, mutacin production, and antibiotic tolerance. *J. Bacteriol.* 192, 1312–1323. doi: 10.1128/JB.01350-09

Claunch, K. M., Bush, M., Evans, C. R., Malmquist, J. A., and Mcgillivray, S. M. (2018). Transcriptional profiling of the clpX mutant in bacillus anthracis reveals regulatory connection with the lrgAB operon. *Microbiology* 164, 659–669. doi: 10.1099/mic.0.000628

Cohen, S. E., Mcknight, B. M., and Golden, S. S. (2018). Roles for ClpXP in regulating the circadian clock in synechococcus elongatus. *Proc. Natl. Acad. Sci. U.S.A.* 115, E7805–E7813. doi: 10.1073/pnas.1800828115

Conesa, A., and Gotz, S. (2008). Blast2GO: A comprehensive suite for functional analysis in plant genomics. *Int. J. Plant Genomics* 2008, 619832. doi: 10.1155/2008/619832

Cox, J., and Mann, M. (2008). MaxQuant enables high peptide identification rates, individualized p.p.b.-range mass accuracies and proteome-wide protein quantification. *Nat. Biotechnol.* 26, 1367–1372. doi: 10.1038/nbt.1511

Cui, J., Xie, Y., Sun, T., Chen, L., and Zhang, W. (2021). Deciphering and engineering photosynthetic cyanobacteria for heavy metal bioremediation. *Sci. Total Environ.* 761, 144111. doi: 10.1016/j.scitotenv.2020.144111

Dintner, S., Heermann, R., Fang, C., Jung, K., and Gebhard, S. (2014). A sensory complex consisting of an ATP-binding cassette transporter and a two-component regulatory system controls bacitracin resistance in bacillus subtilis. *J. Biol. Chem.* 289, 27899–27910. doi: 10.1074/jbc.M114.596221

Dintner, S., Staron, A., Berchtold, E., Petri, T., Mascher, T., and Gebhard, S. (2011). Coevolution of ABC transporters and two-component regulatory systems as resistance modules against antimicrobial peptides in firmicutes bacteria. *J. Bacteriol.* 193, 3851–3862. doi: 10.1128/JB.05175-11

Flynn, J. M., Neher, S. B., Kim, Y.-I., Sauer, R. T., and Baker, T. A. (2003). Proteomic discovery of cellular substrates of the ClpXP protease reveals five classes of ClpX-recognition signals. *Mol. Cell* 11, 671–683. doi: 10.1016/S1097-2765(03)00060-1

Franklin, D. J. (2021). Examining the evidence for regulated and programmed cell death in cyanobacteria. how significant are different forms of cell death in cyanobacteria population dynamics? *Front. Microbiol.* 12, 633954. doi: 10.3389/fmicb.2021.633954

Frischmeyer, P. A., Hoof, V. A. N., O'donnell, K., Guerrerio, A. L., Parker, R., and Dietz, H. C. J. S. (2002). An mRNA surveillance mechanism that eliminates transcripts lacking termination codons. *Science* 295, 2258–2261. doi: 10.1126/science.1067338

Fujisawa, T., Narikawa, R., Maeda, S.-I., Watanabe, S., Kanesaki, Y., Kobayashi, K., et al. (2017). CyanoBase: a large-scale update on its 20th anniversary. *Nucleic acids research* 45, D551–D554. doi: 10.1093/nar/gkw1131

Fux, A., Korotkov, V. S., Schneider, M., Antes, I., and Sieber, S. A. (2019). Chemical cross-linking enables drafting ClpXP proximity maps and taking snapshots of *In situ* interaction networks. *Cell Chem. Biol.* 26, 48–590.e7. doi: 10.1016/j.chembiol.2018.10.007

Glynn, S. E., Martin, A., Nager, A. R., Baker, T. A., and Sauer, R. T. (2009). Structures of asymmetric ClpX hexamers reveal nucleotide-dependent motions in a AAA+ protein-unfolding machine. *Cell* 139, 744–756. doi: 10.1016/j.cell.2009.09.034

Golecki, J. R. (1988). 3 Analysis of the Structure and Development Bacterial Membranes (Outer, Cytoplasmic and Intracytoplasmic Membranes). Methods in microbiology. Elsevier. 20, 61–77.

Gottesman, S., Roche, E., Zhou, Y., Sauer, R. T.DEVELOPMENT (1998). The ClpXP and ClpAP proteases degrade proteins with carboxy-terminal peptide tails added by the SsrA-tagging system. *Genes & development* 12, 1338–1347. doi: 10.1101/gad.12.9.1338

Green, R., and Noller, H. F. (1997). Ribosomes and translation. *Annual review of biochemistry* 66, 679–716. doi: 10.1146/annurev.biochem.66.1.679

Haebel, P. W., Gutmann, S., and Ban, N. (2004). Dial tm for rescue: tmRNA engages ribosomes stalled on defective mRNAs. *Current opinion in structural biology* 14, 58–65. doi: 10.1016/j.sbi.2004.01.010

He, Z., and Mi, H. (2016). Functional characterization of the subunits n, h, J, and O of the NAD(P)H dehydrogenase complexes in synechocystis sp. strain PCC 6803. *Plant Physiol.* 171, 1320–1332. doi: 10.1104/pp.16.00458

Hirani, T. A., Suzuki, I., Murata, N., Hayashi, H., and Eaton-Rye, J. J. (2001). Characterization of a two-component signal transduction system involved in the induction of alkaline phosphatase under phosphate-limiting conditions in synechocystis sp PCC. *Plant molecular biology* 6803. 45, 133–144. doi: 10.1023/A:1006425214168

Hollenstein, K., Dawson, R. J., and Locher, K. (2007). Structure and mechanism of ABC transporter proteins. *Current opinion in structural biology* 17, 412–418. doi: 10.1016/j.sbi.2007.07.003

Huang, D. A., Sherman, W., and Lempicki, R. A. (2009). Systematic and integrative analysis of large gene lists using DAVID bioinformatics resources. *Nat. Protoc.* 4, 44–57. doi: 10.1038/nprot.2008.211

Imai, K., Kitayama, Y., and Kondo, T. (2013). Elucidation of the role of clp protease components in circadian rhythm by genetic deletion and overexpression in cyanobacteria. *J. Bacteriol.* 195, 4517–4526. doi: 10.1128/JB.00300-13

Jensen, C., Fosberg, M. J., Thalso-Madsen, I., Baek, K. T., and Frees, D. (2019). Staphylococcus aureus ClpX localizes at the division septum and impacts transcription of genes involved in cell division, T7-secretion, and SaPI5-excision. *Sci. Rep.* 9, 16456. doi: 10.1038/s41598-019-52823-0

Jin, H., Wang, Y., Fu, Y., and Bhaya, D. J. E. M. (2021). The role of three-tandem pho boxes in the control of the c-p lyase operon in a thermophilic cyanobacterium. *Environmental Microbiology* 23, 6433–6449. doi: 10.1111/1462-2920.15750

Joshi, S. A., Hersch, G. L., Baker, T. A., Sauer, R. T., and Biology, M. (2004). Communication between ClpX and ClpP during substrate processing and degradation. *Nature structural & molecular biology* 11, 404–411. doi: 10.1038/nsmb752

Khalifa, S. A. M., Shedid, E. S., Saied, E. M., Jassbi, A. R., Jamebozorgi, F. H., Rateb, M. E., et al. (2021). Cyanobacteria-from the oceans to the potential biotechnological and biomedical applications. *Mar. Drugs* 19, 867–879. doi: 10.3390/md19050241

Kim, Y.-I., Burton, R. E., Burton, B. M., Sauer, R. T., and Baker, T. A. (2000). Dynamics of substrate denaturation and translocation by the ClpXP degradation machine. *Molecular Cell* 5, 639–648. doi: 10.1016/S1097-2765(00)80243-9

Kirsch, V. C., Fetzer, C., and Sieber, S. A. (2020). Global inventory of ClpP- and ClpX-regulated proteins in staphylococcus aureus. *J. Proteome Res.* 20, 867–879. doi: 10.1021acs.jproteome.0c00668

Kirsch, V. C., Fetzer, C., and Sieber, S. A. (2021). Global inventory of ClpP- and ClpX-regulated proteins in staphylococcus aureus. *J. Proteome Res.* 20, 867–879. doi: 10.1021/acs.jproteome.0c00668

Knoop, H., Zilliges, Y., Lockau, W., and Steuer, R. J. P. P. (2010). The metabolic network of synechocystis sp. *PCC 6803: systemic prop. autotrophic. growth.* 154, 410–422. doi: /10.1104/pp.110.157198

Koretke, K. K., Lupas, A. N., Warren, P. V., Rosenberg, M., Brown, J. R.EVOLUTION (2000). Evolution of two-component signal transduction. *Molecular Biol Evo.* 17, 1956–1970. doi: 10.1093/oxfordjournals.molbev.a026297

Kumar, S., Stecher, G., Li, M., Knyaz, C., and Tamura, K. (2018). MEGA X: Molecular evolutionary genetics analysis across computing platforms. *Mol. Biol. Evol.* 35, 1547–1549. doi: 10.1093/molbev/msy096

Kuroda, A. (2006). A polyphosphate-lon protease complex in the adaptation of escherichia coli to amino acid starvation. *Biosci. Biotechnol. Biochem.* 70, 325–331. doi: 10.1271/bbb.70.325

Kuroda, A., Nomura, K., Ohtomo, R., Kato, J., Ikeda, T., Takiguchi, N., et al. (2001). Role of inorganic polyphosphate in promoting ribosomal protein degradation by the lon protease in e. coli. *Science* 293, 705–708. doi: 10.1126/science.1061315

LaBreck, C. J., May, S., Viola, M. G., Conti, J., and Camberg, J. L. (2017). The protein chaperone ClpX targets native and non-native aggregated substrates for remodeling, disassembly, and degradation with ClpP. *Front. Mol. Biosci.* 4, 26. doi: 10.3389/fmolb.2017.00026

Lau, J., Hernandez-Alicea, L., Vass, R. H., and Chien, P. (2015). A phosphosignaling adaptor primes the AAA+ protease ClpXP to drive cell cycle-regulated proteolysis. *Mol. Cell* 59, 104–116. doi: 10.1016/j.molcel.2015.05.014

Li, Y., Yamazaki, A., Zou, L., Biddle, E., Zeng, Q., Wang, Y., et al. (2010). ClpXP protease regulates the type III secretion system of dickeya dadantii 3937 and is essential for the bacterial virulence. *Molecular plant-microbe interactions* 23, 871–878. doi: 10.1094/MPMI-23-7-0871

Lo, H. H., Liao, C. T., Li, C. E., Chiang, Y. C., and Hsiao, Y. M. (2020). The clpX gene plays an important role in bacterial attachment, stress tolerance, and virulence in xanthomonas campestri s pv. campestris. *Arch. Microbiol.* 202, 597–607. doi: 10.1007/s00203-019-01772-3

Louwen, R., Staals, R. H., Endtz, H. P., Van Baarlen, P., and van der Oost, J. (2014). The role of CRISPR-cas systems in virulence of pathogenic bacteria. *Microbiol. Mol. Biol. Rev.* 78, 74–88. doi: 10.1128/MMBR.00039-13

MacLean, B., Tomazela, D. M., Shulman, N., Chambers, M., Finney, G. L., Frewen, B., et al. (2010). Skyline: an open source document editor for creating and analyzing targeted proteomics experiments. *Bioinformatics* 26, 966–968. doi: 10.1093/bioinformatics/btq054

Mascher, T., HELMANN, J. D., UNDEN, G. J. M., and REVIEWS, M. B. (2006). Stimulus perception in bacterial signal-transducing histidine kinases. *Microbiol. Mol. Biol. Rev.* 70, 910–938. doi: 10.1128/MMBR.00020-06

McGillivray, S. M., Ebrahimi, C. M., Fisher, N., Sabet, M., Zhang, D. X., Chen, Y., et al. (2009). ClpX contributes to innate defense peptide resistance and virulence phenotypes of bacillus anthracis. *J. Innate Immun.* 1, 494–506. doi: 10.1159/000225955

Mering, C. V., Huynen, M., Jaeggi, D., Schmidt, S., Bork, P., and Snel, B. (2003). STRING: a database of predicted functional associations between proteins. *Nucleic Acids Res.* 31, 258–261. doi: 10.1093/nar/gkg034

Mishra, R. C., and Grover, A. (2016). ClpB/Hsp100 proteins and heat stress tolerance in plants. *Critical Reviews in Biotechnology* 36, 862–874. doi: 10.3109/07388551.2015.1051942

Mohr, R., VOß, B., SCHLIEP, M., KURZ, T., MALDENER, I., ADAMS, D. G., LARKUM, A. D., CHEN, M., and HESS, W. R. J. T. I. J. (2010). A new chlorophyll d-containing cyanobacterium:evidence for niche adaptation in the genus Acaryochloris. *The ISME Journal* 4, 1456–1469.

Mullineaux, C. W. (2014). Electron transport and light-harvesting switches in cyanobacteria. *Front. Plant Sci.* 5, 7. doi: 10.3389/fpls.2014.00007

Nomura, C. T., Sakamoto, T., and Bryant, D. A. (2006). Roles for heme-copper oxidases in extreme high-light and oxidative stress response in the cyanobacterium synechococcus sp. PCC 7002. *Arch. Microbiol.* 185, 471–479. doi: 10.1007/s00203-006-0107-7

Olivares, A. O., Baker, T. A., and Sauer, R. T. (2016). Mechanistic insights into bacterial AAA+ proteases and protein-remodelling machines. *Nat. Rev. Microbiol.* 14, 33–44. doi: 10.1038/nrmicro.2015.4

Rao, N., and Torriani, A. (1990). Molecular aspects of phosphate transport in escherichia coli. *Molecular Microbiol.* 4, 1083–1090. doi: 10.1111/j.1365-2958.1990.tb00682.x

REYNOLDS, E. S. J. T. J. O. C. B. (1963). The use of lead citrate at high pH as an electron-opaque stain in electron microscopy. *J. Cell. Biol.* 17, 208.

Rowland, J. G., Simon, W. J., Prakash, J. S. S., and Slabas, A. R. (2011). Proteomics reveals a role for the RNA helicase crhR in the modulation of multiple metabolic pathways during cold acclimation of synechocystis sp. PCC6803. *J. Proteome Res.* 10, 3674–3689. doi: 10.1021/pr200299t

Roy, S., Zhu, Y., Ma, J., Roy, A. C., Zhang, Y., Zhong, X., et al. (2019). Role of ClpX and ClpP in streptococcus suis serotype 2 stress tolerance and virulence. *Microbiol. Res.*, 223–225. doi: 10.1016/j.micres.2019.04.003

Sauer, R. T., Bolon, D. N., Burton, B. M., Burton, R. E., Flynn, J. M., Grant, R. A., et al. (2004). Sculpting the proteome with AAA(+) proteases and disassembly machines. *Cell* 119, 9–18. doi: 10.1016/j.cell.2004.09.020

Schirrmeister, B. E., Antonelli, A., and Bagheri, H. C. (2011). The origin of multicellularity in cyanobacteria. *BMC Evolutionary Biol* 11, 1–21. doi: 10.1186/1471-2148-11-45

Schultz, J., Copley, R. R., Doerks, T., Ponting, C. P., and Bork, P. (2000). SMART: a web-based tool for the study of genetically mobile domains. *Nucleic Acids Res.* 28, 231–234. doi: 10.1093/nar/28.1.231

Shannon, P., Markiel, A., Ozier, O., Baliga, N. S., Wang, J. T., Ramage, D., et al. (2003). Cytoscape: a software environment for integrated models of biomolecular interaction networks. *Genome Res.* 13, 2498–2504. doi: 10.1101/gr.1239303

Shikanai, T., Endo, T., Hashimoto, T., Yamada, Y., Asada, K., and Yokota, A. (1998). Directed disruption of the tobacco ndhB gene impairs cyclic electron flow around photosystem I. *Proceedings of the National Academy of Sciences* 95, 9705–9709. doi: 10.1073/pnas.95.16.9705

Sokolenko, A., Pojidaeva, E., Zinchenko, V., Panichkin, V., Glaser, V. M., Herrmann, R. G., et al. (2002). The gene complement for proteolysis in the cyanobacterium synechocystis sp. PCC 6803 and arabidopsis thaliana chloroplasts. *Curr. Genet.* 41, 291–310. doi: 10.1007/s00294-002-0309-8

Song, H. K., and Eck, M. (2003). Structural basis of degradation signal recognition by SspB, a specificity-enhancing factor for the ClpXP proteolytic machine. *Molecular Cell* 12, 75–86. doi: 10.1016/S1097-2765(03)00271-5

Stahlhut, S. G., Alqarzaee, A. A., Jensen, C., Fisker, N. S., Pereira, A. R., Pinho, M. G., et al. (2017). The ClpXP protease is dispensable for degradation of unfolded proteins in staphylococcus aureus. *Sci. Rep.* 7, 11739. doi: 10.1038/s41598-017-12122-y

Stanne, T. M., Pojidaeva, E., Andersson, F. I., and Clarke, A. K. (2007). Distinctive types of ATP-dependent clp proteases in cyanobacteria. *J. Biol. Chem.* 282, 14394–14402. doi: 10.1074/jbc.M700275200

Stanne, T. M., Sjogren, L. L. E., Koussevitzky, S., and Clarke, A. K. (2009). Identification of new protein substrates for the chloroplast ATP-dependent clp protease supports its constitutive role in arabidopsis. *Biochem. J.* 417, 257–268. doi: 10.1042/BJ20081146

Storz, G., and Hengge, R. (2010). *Bacterial stress responses* (Washington, USA: American Society for Microbiology Press).

Su, Z., Olman, V., and Xu, Y. (2007). Computational prediction of pho regulons in cyanobacteria. *Bmc Genomics* 8, 1–12. doi: 10.1186/1471-2164-8-156

Suzuki, S., Ferjani, A., Suzuki, I., and Murata, N. (2004). The SphS-SphR two component system is the exclusive sensor for the induction of gene expression in response to phosphate limitation in synechocystis. *J. Biologic. Chem.* 279, 13234–13240. doi: 10.1074/jbc.M313358200

Swift, M. L., and Sciences, C. (1997). GraphPad prism, data analysis, and scientific graphing. *J. Biologic. Chem.* 37, 411–412. doi: 10.1021/ci960402j

Tiwari, B., Singh, S., Kaushik, M. S., and Mishra, A. K. (2015). Regulation of organophosphate metabolism in cyanobacteria. *A review.* 84, 291–302. doi: 10.1134/S0026261715030200

Tsai, J. W., and Alley, M. R. (2001). Proteolysis of the caulobacter McpA chemoreceptor is cell cycle regulated by a ClpX-dependent pathway. *J. Bacteriol.* 183, 5001–5007. doi: 10.1128/JB.183.17.5001-5007.2001

Whitman, J. C., Paw, B. H., and Chung, J. (2018). The role of ClpX in erythropoietic protoporphyria. *Hematol. Transfus Cell Ther.* 40, 182–188. doi: 10.1016/j.htct.2018.03.001

Yu, N. Y., Wagner, J. R., Laird, M. R., Melli, G., Rey, S., Lo, R., et al. (2010). PSORTb 3.0: improved protein subcellular localization prediction with refined localization subcategories and predictive capabilities for all prokaryotes. *Bioinformatics* 26, 1608–1615. doi: 10.1093/bioinformatics/btq249

Yu, Y., You, L., Liu, D., Hollinshead, W., Tang, Y. J., and Zhang, F. (2013). Development of synechocystis sp. PCC 6803 as a phototrophic cell factory. *Mar. Drugs* 11, 2894–2916. doi: 10.3390/md11082894

Zhang, Y., and Zuber, P. J. J. O. B. (2007). Requirement of the zinc-binding domain of ClpX for spx proteolysis in bacillus subtilis and effects of disulfide stress on ClpXP activity. *J. Bacteriol.* 189, 7669–7680. doi: 10.1128/JB.00745-07

Zhao, J., Li, R., and Bryant, D. A. (1998). Measurement of photosystem I activity with photoreduction of recombinant flavodoxin. *Analytical biochemistry* 264, 263–270. doi: 10.1006/abio.1998.2845

Zhu, Z., Yang, M., Bai, Y., GE, F., and Wang, S. J. E. M. (2020). Antioxidant-related catalase CTA1 regulates development, aflatoxin biosynthesis, and virulence in pathogenic fungusAspergillus flavus. *Environmental Microbiol.* 22, 2792–2810. doi: 10.1006/abio.1998.2845

frontiers | Frontiers in Plant Science

TYPE Original Research
PUBLISHED 02 November 2022
DOI 10.3389/fpls.2022.1023388

OPEN ACCESS

EDITED BY
Mateusz Labudda,
Warsaw University of Life Sciences-SGGW, Poland

REVIEWED BY
Justyna Fidler,
Warsaw University of Life Sciences, Poland
Catherine Rayon,
University of Picardie Jules Verne, France

*CORRESPONDENCE
Yanye Ruan
yanyeruan@syau.edu.cn
Quan Sun
2001500029@syau.edu.cn

SPECIALTY SECTION
This article was submitted to Plant Proteomics and Protein Structural Biology, a section of the journal Frontiers in Plant Science

RECEIVED 19 August 2022
ACCEPTED 10 October 2022
PUBLISHED 02 November 2022

CITATION
Chen S, Shi F, Li C, Sun Q and Ruan Y (2022) Quantitative proteomics analysis of tomato root cell wall proteins in response to salt stress. *Front. Plant Sci.* 13:1023388. doi: 10.3389/fpls.2022.1023388

Quantitative proteomics analysis of tomato root cell wall proteins in response to salt stress

Shuisen Chen, Fei Shi, Cong Li, Quan Sun* and Yanye Ruan*

College of Bioscience and Biotechnology, Shenyang Agricultural University, Shenyang, China

Cell wall proteins perform diverse cellular functions in response to abiotic and biotic stresses. To elucidate the possible mechanisms of salt-stress tolerance in tomato. The 30 d seedlings of two tomato genotypes with contrasting salt tolerances were transplanted to salt stress (200 mM NaCl) for three days, and then, the cell wall proteins of seedling roots were analyzed by isobaric tags for relative and absolute quantification (iTRAQ). There were 82 and 81 cell wall proteins that changed significantly in the salt-tolerant tomato IL8-3 and the salt-sensitive tomato M82, respectively. The proteins associated with signal transduction and alterations to cell wall polysaccharides were increased in both IL8-3 and M82 cells wall in response to salt stress. In addition, many different or even opposite metabolic changes occurred between IL8-3 and M82 in response to salt stress. The salt-tolerant tomato IL8-3 experienced not only significantly decreased in Na^+ accumulation but also an obviously enhanced in regulating redox balance and cell wall lignification in response to salt stress. Taken together, these results provide novel insight for further understanding the molecular mechanism of salt tolerance in tomato.

KEYWORDS

tomato, cell wall, root, salt stress, iTRAQ

1 Introduction

Salinity is one of the most important environmental stresses affecting a wide variety of physiological and biochemical changes in crops. Salinity inhibits the growth and development of crops and disrupts metabolism, such as reducing photosynthesis, respiration and protein synthesis (Liang et al., 2018; Zörb et al., 2019). Plant roots are the primary site of salinity perception and injury, and roots sense and pass the salinity signal to the shoot for appropriate changes (Munns and Tester, 2008). The root system also plays a vital role in improving crop salt tolerance through its potential for improving access to water and limiting salt acquisition (Jung and McCouch, 2013). Therefore, the stress sensitivity of a plant's roots limits the productivity of the entire plants. Fortunately,

plants enact some mechanisms to mitigate salt stress, such as exclusion of Na^+ from plant cells and compartmentalization of Na^+ into vacuoles (Deinlein et al., 2014), alterations to the ultrastructure of the cell wall and subcellular organelles, and alterations to *de novo* protein biosynthesis and enzymatic activity (Ma et al., 2006).

Tomato (*Solanum lycopersicum*) is a vital vegetable with economic significance worldwide, and it has become a model species in plant research (Quinet et al., 2019). Nevertheless, most cultivated tomato species are sensitive to salt stress throughout growth and development, which restricts the production area, the quality and yield of tomato (Zaki and Yokoi, 2016; Pailles et al., 2020). The response of tomato to salt stress varies depending on the cultivar. The majority of tomato cultivars have the genetic potential of tolerance to moderate salt stress (Singh et al., 2012). To enhance the salt tolerance of tomato, the physiological responses of tomato under salt stress conditions have been extensively studied (Rivero et al., 2014; Bai et al., 2018). Transcriptomic and proteomics analyses have been performed to illuminate the responses of tomato to salt stress over the past decade (Nveawiah-Yoho et al., 2013; Gong et al., 2014; Albaladejo et al., 2018), and many genes that participate in salt tolerance have been well studied (Kou et al., 2019). However, the explicit molecular mechanisms of tomato tolerance to salt stress are still not clear.

Plant cell walls are complex and dynamic structures that are essential for the modulation of some stress signals (Komatsu and Yanagawa, 2013; Houston et al., 2016). Although cell wall proteins account for only 5~10% of the extracellular matrix mass, they perform diverse cellular functions in response to abiotic and biotic stresses (Le Gall et al., 2015; Rui and Dinneny, 2020). Among the three types of cell wall proteins, soluble proteins, weakly bound cell wall proteins and strongly bound cell wall proteins, the isolation of the strongly bound cell wall proteins was hampered by a number of technical difficulties (Jamet et al., 2006). Although the characterization of plant cell wall proteins remains challenging and requires a combination of various analytical approaches, there have been rapid advances in cell wall protein research combined with proteomics approaches (Komatsu and Yanagawa, 2013; Adelaide et al., 2018). To gain information about protein changes in cell walls, many types of stress-associated cell wall proteins have been identified in crops, and these researches have shown that cell wall proteins play an important role in stress signal transduction, cell defense and rescue, cell wall modification, etc (Wolf, 2017; Du et al., 2022; Wolf, 2022). The top leaflets showed less stress signs by salinity have an increased expression of cell wall-related genes in tomato (Hoffmann et al., 2021). Therefore, comparative proteomic analyses of the tomato cell wall could provide novel information on the underlying mechanisms of tomato responses to environmental stresses.

2 Materials and methods

2.1 Plants growth

IL8-3 (tolerant to salt stress) and M82 (sensitive to salt stress), were used in the present study. Seeds of both tomato genotypes were sterilized by a 0.2% (v/v) sodium hypochlorite solution for 10 min. Then, the seeds were rinsed extensively with deionized water. The surface sterilized seeds were germinated on moistened filter paper in the dark at 28°C for three days. The germinated seedlings were transferred onto the moistened gauze in a plastic basin (17 cm × 25 cm) for five days. The plastic basin was placed in an illuminated culture room (300 - 320 μmol m^{-2} s^{-1}, 24°C day/22°C night, 16 h photoperiod). Following germination, the seedlings were grown hydroponically in a plastic container filled with Hoagland nutrient solution. Considering the nutrient requirements of tomato seedlings, the initial solution was 1/4 of the full-strength for the first 5 days, and then, the nutrient solution was replaced with 1/2 of the full-strength for another 5 days. Next, the full strength nutrient solution was used and refreshed every 5 days. When the seedlings had grown for 30 days, half of the seedlings were shifted to a nutrient solution containing 200 mM NaCl. The remaining half of the seedlings under the NaCl-free nutrient solution were used as controls. The roots and leaves were harvested on the 3rd day after NaCl was added. For the cell wall proteomic analysis, the roots from each treatment were washed with distilled water and then immediately chilled in liquid nitrogen. The sample was stored at -80°C for further use. Each treatment was replicated four times.

2.2 Measurements of biomass, Na^+ and K^+ concentrations

Roots and shoots were harvested separately on the 3rd day after NaCl was added. The seedlings were baked at 105°C for 15 min and then dried at 70°C to constant weight. The dry weight was weighted, and then, the seedlings (ca. 0.1000 g) were digested in concentrated HNO_3-$HClO_4$ (5:1 v/v) using a digestion block system. The Na^+ and K^+ concentrations were assayed using a flame photometer (FP640, Precision and Scientific Instrument, Shanghai, China).

2.3 Reactive oxygen species metabolism assay

The content of hydrogen peroxide (H_2O_2) and superoxide anion (O_2^-), and the activity of superoxide dismutase (SOD) and peroxidase (POD) that from cell wall protein extraction were

determined by each specific assay kit according to the the corresponding kit specification (Comin Botechnology, Suzhou, China).

2.4 Cell wall protein extraction

Cell wall proteins isolation was performed as previously described with modifications (Feiz et al., 2006; Francin-Allami et al., 2015). Briefly, 0.5 g (fresh weight) of roots and 0.1 g of PVPP were ground into powder using a mortar and pestle under liquid nitrogen, the powder was transferred into a 2-mL tube and filled with extracted buffer (0.6 M sucrose, 2.0 mM EDTA, 1.0 mM PMSF and 5.0 mM acetate buffer, pH 4.6). After shaking at 4°C for 30 min, the solution was centrifuged at 12,000 g for 30 min (4°C). The pellet was washed with 5 mM acetate buffer (pH 4.6). Then, the pellet was incubated with successive salt solutions as follows: twice in a 0.2 M $CaCl_2$ solution (5 mM acetate buffer, 0.2 M $CaCl_2$ and 10 µL protease inhibitor cocktail (Sigma-Aldrich, St. Louis, MO, USA)) for 2 h, followed by two washes in a 2 M LiCl solution (5 mM acetate buffer, 2 M LiCl and 10 µL protease inhibitor cocktail (Sigma-Aldrich, St. Louis, MO, USA)) for 2 h. Finally, $CaCl_2$ and LiCl fractions were combined as cell wall fractions for further proteins precipitation. Four biological replicates were performed.

2.5 iTRAQ analysis

Cell wall proteins (ca. 100 µg) were reduced with 10 mM DTT for 2 h at 56°C. Then, the proteins were alkylated with 55 mM iodoacetamide at 24°C in the dark for 45 min. Then, the proteins were digested with trypsin at a 20:1 mass ratio for 12 h at 37°C. The peptide mixtures were labeled using the iTRAQ reagents 8-plex kit according to the manufacturer's instructions (AB Sciex Inc., MA, USA). Four independent biological replicates were performed. The mixed labeled peptides were fractionated using a 4.6 × 250 mm Kindtex-C18 column (Phenomenex, Torrance, CA, USA) in a RIGOL L-3120 infinity high-performance liquid chromatography (HPLC) system (Beijing RIGOL Technology Co., Ltd., Beijing, China). LC-MS/MS analysis and mass spectrometry analysis were carried out at the National Center for Protein Science in Beijing using a TripleTOF® 6600 system. ProteinPilot™ 5.0 (AB Sciex, MA, USA) software was used to analyze the raw mass spectrum data. Tandem mass spectra were extracted and searched using MS/MS data interpretation algorithms within ProteinPilot™ software 5.0 (Paragon Algorithm). The NCBI nonredundant protein database for *Solanum lycopersicum* (39020 sequences, 2020) was used for the database searching, and the mass tolerance was set to 0.05 Da. A unused confidence score of > 1.3 was used. The identified proteins with at least two matched peptides, confidence higher than 95%, and an FDR (false discovery rate)< 1% were used to perform protein quantification. Subsequently, proteins with a 2.0-fold change ($p< 0.05$) with good reproducibility that were detected in at least three replicates of the four biological replicates were termed differentially abundant proteins (DAPs).

2.6 Bioinformatics analysis

STRING (version 11.0) (https://string-db.org/) was employed to perform a protein-protein interaction analysis and statistical enrichment tests were executed for KEGG pathway annotations (Szklarczyk et al., 2015). The signal peptide sequence was predicted by SignalP (version 5.0) (Nielsen, 2017), and nonclassical secretory proteins were predicted by SecretomeP server 2.0 with an NN score above 0.6 (Bendtsen et al., 2004). The presence of functional domains and functional classification of DAPs using the *ProtAnnDB* (http://www.polebio.lrsv.ups-tlse.fr/WallProtDB/) in-house tool (San and Jamet, 2015)

2.7 Statistical analysis

Experimental data are presented as the means and standard deviations (SD). Each physiological parameter was examined with four biological replicates. SAS 9.2 (SAS Institute, Cary, NC, USA) with the SAS PROC ANOVA LSD model was used to perform the analysis of variance for the physiological data. A value of $p<0.05$ was considered to be statistically significant.

3 Results

3.1 Comparison of different salt-tolerant tomatoes in response to salt stress

The physiological responses of tomato to salt stress were investigated in the present study. Compared with the NaCl-free condition, the obvious signs of dehydration in leaves were exhibited in both tomato genotypes under short-term salt stress (200 mM NaCl for 3 days), especially the salt-sensitive M82 (Figure 1A). Short-term salt stress did not affect the root and shoot dry weights of either tomato (Figures 1B, C). However, the shoot dry weight of IL8-3 (tolerant to salt stress) was significantly higher than that of M82 (sensitive to salt stress) (Figure 1C). Moreover, salt stress noticeably increased the Na^+ content in the roots and shoots of both tomato genotypes (Figures 1D, E). The Na^+ content of the shoots in M82 was significantly higher than that in IL8-3 under salt stress (Figure 1E). In addition, the salt-sensitive tomato M82 trended

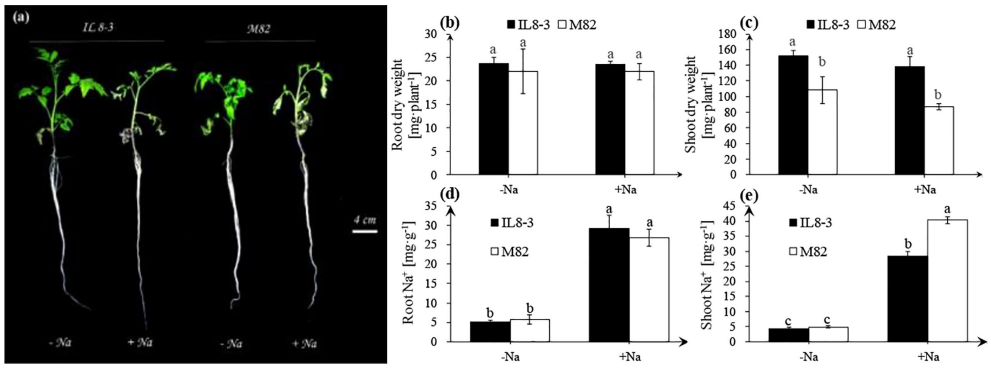

FIGURE 1
Tomato growth and physiological indices **(A)**, the alterations of root dry weight **(B)**, shoot dry weight **(C)**, root Na^+ content **(D)**, shoot Na^+ content **(E)** under NaCl-free condition (-Na) and 200 mM NaCl stress (+Na). The seedlings of two tomato genotypes, IL8-3 (tolerant to salt stress) and M82 (sensitive to salt stress), were grown under nutrient solution without NaCl for 30 days, then the seedlings shift to nutrient solution with or without 200 mM NaCl for 3 days. Values represent the mean ± SD of four independent replicates, bars with different letters show significant differences (ANOVA, LSD, $P<0.05$).

to accumulate more Na^+ in shoots under salt stress, with up to 40 $mg{\cdot}g^{-1}$ Na^+ in shoots and 27 $mg{\cdot}g^{-1}$ Na^+ in roots. Both the Na^+ contents in the roots and shoots of IL8-3 were 29 $mg{\cdot}g^{-1}$ Na^+ under salt stress (Figures 1D, E). These results demonstrated that the two tomato genotypes with different salt tolerances had the different absorption and distribution of Na^+ in response to short-term salt stress.

Salt stress significantly increased O_2^-content and H_2O_2 content in roots of both tomato genotypes, but there was no significant difference between IL8-3 and M82 (Figures 2A, B). Antioxidant enzyme activities were significantly increased in roots of both tomato genotypes, and the salt-tolerant tomato, IL8-3, showed a higher SOD and POD activities under salt stress (Figures 2C, D).

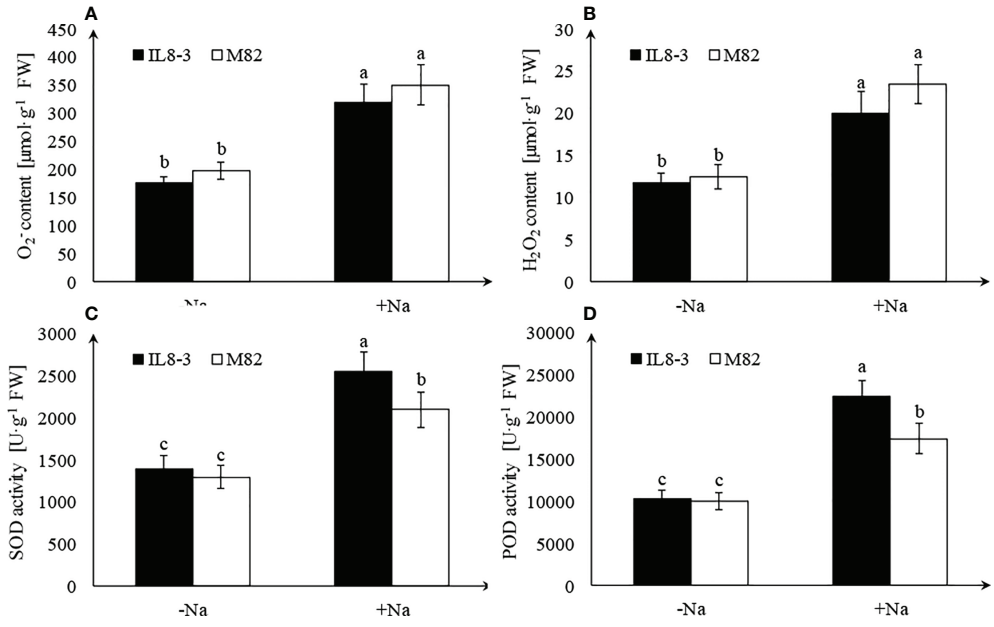

FIGURE 2
Effect of salt stress on reactive oxygen species (ROS) accumulation and antioxidant enzyme activities. O_2^-content **(A)**, H_2O_2 content **(B)**, SOD activity **(C)**, POD activity **(D)**, under NaCl-free condition (-Na) and 200 mM NaCl stress (+Na). Values represent the mean ± SD of four independent replicates, bars with different letters show significant differences (ANOVA, LSD, $P<0.05$).

3.2 Identified differential proteins of root cell wall in response to salt stress

To reveal the salt-tolerant mechanisms of tomato at the protein level, a comparative proteomics analysis combining isobaric tags for relative and absolute quantification (iTRAQ) and mass spectrometry was carried out on the root cell wall of the salt-tolerant tomato IL8-3 and salt-sensitive tomato M82. Finally, 82 DAPs (in the area with the white line) and 81 DAPs (in the area with the white line) in IL8-3 (Figure S1A) and M82 (Figure S1B) were selected for further analysis. There were 38 DAPs increased in protein abundance and 44 DAPs decreased in protein abundance in IL8-3 in response to salt stress. Moreover, 43 of the 82 DAPs were predicted to have signal peptides and 11 of the 82 DAPs were nonclassical secretory proteins (Table S1). There were 33 DAPs increased in protein abundance and 8 DAPs decreased in protein abundance of IL8-3 have the functional categories in *WallProDB* (Figure 3). In M82, 28 DAPs increased in protein abundance and 53 DAPs decreased in protein abundance under salt stress. Forty-five of the 81 DAPs were predicted to have signal peptides and 8 of the 81 DAPs were nonclassical secretory proteins (Table S2). There were 11 DAPs increased in protein abundance and 28 DAPs decreased in protein abundance of M82 have the functional categories in *WallProDB* (Figrue 3). More cell wall proteins were classified into proteins acting on carbohydrates, oxido-reductases, and proteases both in IL8-3 or M82. Cell wall proteins with interaction domains of M82 was more than that of IL8-3 (Figrue 3). In addition, 25 DAPs were identified in both IL8-3 and M82 in response to salt stress (Table 1). Sixteen DAPs (6 increased and 10 decreased) showed same trend in both tomato genotypes in response to salt stress (Table 1). Interestingly, 5 DAPs increased in IL8-3 and decreased in M82. In contrast, 4 DAPs decreased in

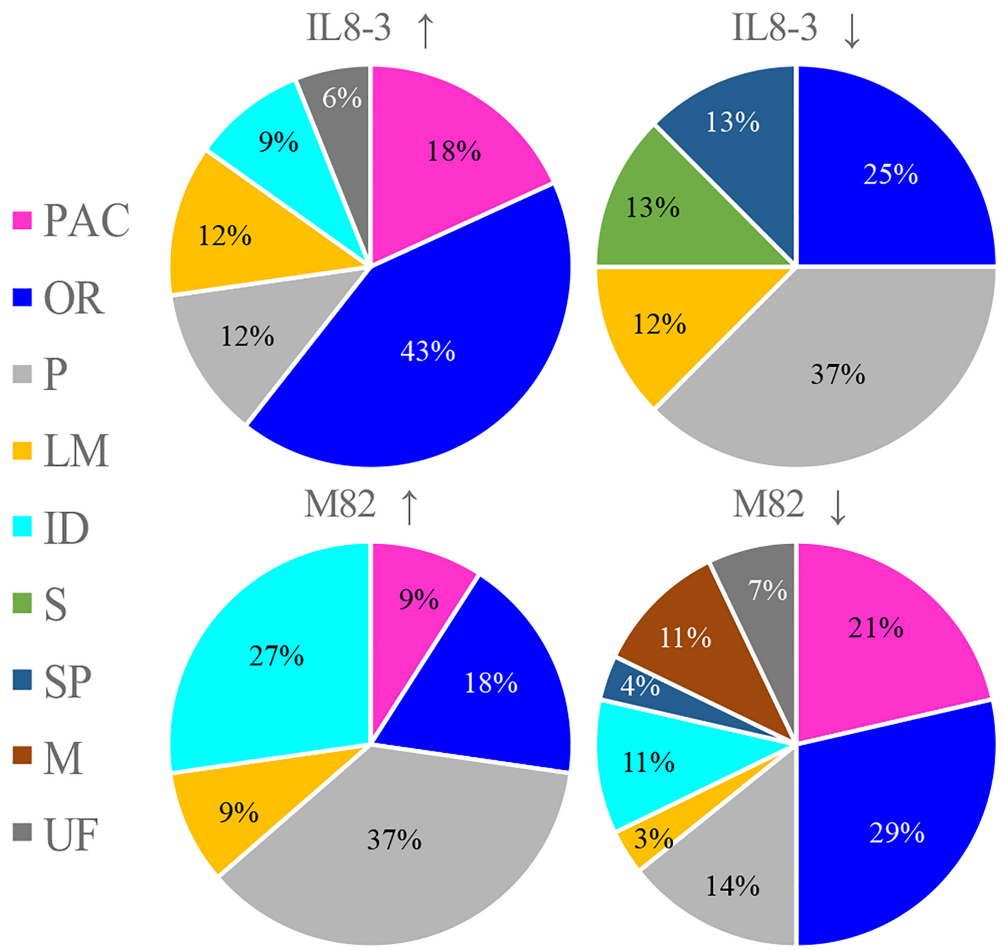

FIGURE 3
Overview showing the distribution in functional classes of the cell wall protein (http://www.polebio.lrsv.ups-tlse.fr/WallProtDB/). Cultivars with up arrow and with down arrow represent the increased and decreased in protein abundance in response to salt stress, respectively. PAC stands for proteins acting on carbohydrates, OR for oxido-reductases, P for proteases, LM for proteins related to lipid metabolism, ID for proteins with interaction domains, S for signaling, SP for structural proteins, M for miscellaneous and UF for unknown function.

TABLE 1 DAPs (differential abundant proteins) showed the same or opposite trend between salt-tolerant IL8-3 and salt-sensitive M82 under salt stress.

[※]No.	Accession #	Protein name	Fold		SP orNSP
			IL8-3	M82	
DAPs with the same trend under salt stress					
CW1	NP_001234249.1	xyloglucan-specific fungal endoglucanase inhibitor protein precursor	9.58 ± 0.02↑	4.35 ± 0.10↑	SP
CW2	NP_001299819.1	glucan endo-1,3-beta-glucosidase B precursor	8.05 ± 0.02↑	3.13 ± 0.11↑	SP
CW3	NP_001307321.1	miraculin precursor	6.37 ± 0.02↑	11.73 ± 0.03↑	SP
CW4	XP_004235260.1	PLAT domain-containing protein 3	3.59 ± 0.02↑	2.84 ± 0.08↑	SP
5	NP_001234099.1	alcohol dehydrogenase 2	3.54 ± 0.07↑	5.41 ± 0.03↑	-
6	NP_001234615.1	ethylene-responsive proteinase inhibitor 1 precursor	5.42 ± 0.06↑	4.13 ± 0.02↑	SP
CW7	XP_004245302.1	peroxidase 45-like	3.06 ± 0.96↓	16.13 ± 0.79↓	SP
CW8	XP_004240143.1	peroxidase 27-like	3.57 ± 0.68↓	13.72 ± 0.66↓	SP
CW9	XP_004247590.1	leucine-rich repeat extensin-like protein 6	3.75 ± 0.94↓	12.32 ± 1.77↓	SP
10	XP_004228473.1	60S ribosomal protein L30	3.97 ± 0.72↓	3.71 ± 0.23↓	-
11	XP_010312055.1	40S ribosomal protein S28	4.63 ± 0.84↓	20.40 ± 1.39↓	-
12	XP_010323242.1	dihydrolipoyllysine-residue acetyltransferase component 2 of pyruvate dehydrogenase complex, mitochondrial-like isoform X2	7.19 ± 0.68↓	5.30 ± 0.67↓	-
13	NP_001352840.1	peptidyl-prolyl cis-trans isomerase FKBP15-2 precursor	3.01 ± 1.43↓	6.35 ± 2.64↓	SP
14	XP_004244016.1	enhancer of mRNA-decapping protein 4-like	8.10 ± 0.96↓	3.66 ± 0.39↓	-
15	XP_004251613.1	peroxisomal fatty acid beta-oxidation multifunctional protein AIM1	3.90 ± 1.13↓	4.20 ± 1.13↓	-
16	XP_004239837.1	uncharacterized protein LOC101252396	2.86 ± 0.67↓	3.59 ± 0.38↓	SP
DAPs with the opposite trend under salt stress					
CW17	XP_004232441.1	peroxidase 72	4.26 ± 0.11↑	7.33 ± 0.48↓	SP
CW18	NP_001333832.1	multicopper oxidase-like protein precursor	3.27 ± 0.09↑	3.18 ± 0.33↓	SP
CW19	XP_004234931.1	monocopper oxidase-like protein SKS1	2.94 ± 0.06↑	3.28 ± 1.37↓	SP
CW20	XP_004230031.1	aspartyl protease AED3	2.68 ± 0.03↑	7.84 ± 1.24↓	SP
21	XP_004247036.1	auxin-induced in root cultures protein 12	3.97 ± 0.09↑	2.88 ± 0.73↓	SP
22	XP_004244803.1	proteasome subunit alpha type-5	2.69 ± 0.41↓	8.34 ± 0.03↑	-
23	XP_010327686.1	glutamate dehydrogenase isoform X1	3.40 ± 0.39↓	11.22 ± 0.02↑	-
24	XP_010312196.1	5-methyltetrahydropteroyltriglutamate–homocysteine methyltransferase isoform X1	2.77 ± 0.72↓	6.46 ± 0.05↑	-
25	XP_019067358.1	12S seed storage protein CRD	3.76 ± 0.83↓	3.00 ± 0.13↑	NSP

[※] Cell wall related protein labeled CW before the No. Fold changes with up arrow ("↑") behind and with down arrow ("↓") behind represent the increased and decreased in protein abundance in response to salt stress, respectively. SP refers to the presence of a signal peptide sequence predicted by SignalP (version 4.0). NSP indicates nonclassical secretory proteins predicted by SecretomeP server 2.0 with an NN score > 0.600.

IL8-3 and increased in M82 (Figure S2 and Table 1). Based on the proteins identified, it is clear that 80% of the DAPs varied widely between IL8-3 and M82. These results indicated that IL8-3 and M82 might have different adaptive strategies in response to salt stress, at least at protein level.

The DAPs showed opposite trend between salt-tolerant IL8-3 and salt-sensitive M82 were used to compare the difference of salt tolerance between the two tomato genotypes. There proteins only identified in IL8-3 or M82, respectively. There were 18 proteins related to cell metabolism, which 11 proteins increased in protein abundance in IL8-3 and 7 proteins decreased in protein abundance in M82 in response to salt stress (Table 2). For the 13 peroxidases proteins, 8 proteins increased in protein abundance in IL8-3 and 5 proteins decreased in protein abundance in M82 in response to salt stress (Table 3). These results indicated that the cell wall metabolism and peroxidases endowed IL8-3 with higher salt tolerance.

3.3 Enriched pathways in which the differentially abundant proteins participated

STRING software was used to enrich the Kyoto Encyclopedia of Genes and Genomes (KEGG) pathways. In the present study, 5 pathways and 18 pathways were enriched based on the 38 DAPs that increased and 44 DAPs that decreased in IL 8-3, respectively. Fourteen pathways and 5 pathways were enriched based on the 28 DAPs that increased and 53 DAPs that decreased in M82, respectively (Table S3). Ten KEGG pathways were enriched in both tomato genotypes. The most significant KEGG pathways for the identified proteins were metabolic pathways (65 DAPs) and biosynthesis of secondary metabolites (43 DAPs) (Table 4). In addition, some of the pathways had contradictory alterations between IL8-3 and M82. The DAPs involved in the phenylpropanoid biosynthesis pathway were increased in IL8-3

TABLE 2 Differentially abundant proteins (DAPs) related to cell wall metabolism that identified from IL8-3 and M82 under salt stress.

No.	Protscore	%Cov (95)	Peptide (95%)	Accession No.	Name	Fold change		
						IL8-3	M82	
1	42.89	35.0	52	XP_004232833.3	polyphenol oxidase, chloroplastic-like	6.72 ± 0.03↑	-	
2	28.45	62.1	50	XP_004250402.1	lignin-forming anionic peroxidase	5.69 ± 0.07↑	-	SP
3	146.07	53.5	565	XP_004232737.1	pectinesterase	4.01 ± 0.10↑	-	NSP
4	63.43	44.1	63	NP_001234303.1	beta-galactosidase precursor	3.52 ± 0.06↑	-	SP
5	39.35	31.3	48	XP_010324292.1	glycerophosphodiester phosphodiesterase GDPDL4	2.89 ± 0.09↑	-	SP
6	21.59	26.0	25	XP_004247400.1	pectinesterase-like	2.86 ± 0.10↑	-	NSP
7	17.84	30.6	21	NP_001234798.1	glucan endo-1,3-beta-glucosidase A precursor	2.79 ± 0.06↑	-	SP
8	46.30	42.2	39	NP_001234842.2	beta-galactosidase 4 precursor	2.46 ± 0.08↑	-	SP
9	37.39	32.3	31	XP_004245738.1	monocopper oxidase-like protein SKU5	2.70 ± 0.09↑	-	SP
10	78.72	54.5	137	XP_019070934.1	subtilisin-like protease SBT1.7	5.12 ± 0.03↑	-	SP
11	74.53	54.0	198	NP_001234774.1	subtilisin-like protease precursor	3.39 ± 0.07↑	-	SP
12	37.38	56.5	35	XP_010322133.1	alpha-galactosidase 3	-	2.86 ± 0.28↓	SP
13	20.91	27.0	18	NP_001234416.1	beta-glucosidase 08 precursor	-	4.23 ± 1.89↓	SP
14	61.04	45.0	143	NP_001233857.1	pectinesterase/pectinesterase inhibitor U1 precursor	-	7.35 ± 1.35↓	
15	14.45	56.0	19	XP_004248663.1	dirigent protein 22	-	15.19 ± 1.50↓	SP
16	35.69	31.3	26	NP_001300811.1	beta-galactosidase 5	-	3.49 ± 1.40↓	SP
17	78.39	60.4	220	XP_004232982.1	subtilisin-like protease SBT5.6	-	2.82 ± 0.76↓	SP
18	35.47	29.1	28	XP_004231026.1	subtilisin-like protease SBT1.6	-	4.15 ± 0.22↓	SP

Fold changes with up arrow ("↑") and with down arrow ("↓") represent the increased and decreased in protein abundance in response to salt stress, respectively. '-' represent not identified. SP refers to the presence of a signal peptide sequence predicted by SignalP (version 4.0). NSP indicates nonclassical secretory proteins predicted by SecretomeP server 2.0 with an NN score > 0.600.

but decreased in M82. While the DAPs involved in carbon metabolism, pyruvate metabolism, glycolysis/gluconeogenesis, biosynthesis of amino acids, alanine, aspartate and glutamate metabolism pathways were decreased in IL8-3, they increased in M82 (Table 4). These results indicated that the salt-tolerant tomato IL8-3 and salt-sensitive tomato M82 might acclimatize to salt stress through different metabolism alterations.

3.4 Protein-protein interactions

To determine how tomato roots cells transmit salt signals, further analysis of the 25 DAPs identified in both tomato genotypes was performed using the STRING software with a confidence score higher than 0.5. Two groups of proteins interacting with each other were identified in the two tomato

TABLE 3 Differentially abundant proteins (DAPs) belong to peroxidase family that identified from IL8-3 and M82 under salt stress.

No.	Protscore	%Cov(95)	Peptide(95%)	Accession No.	Name	Fold change		
						IL8-3	M82	
1	67.72	60.8	174	NP_001334412.1	peroxidase 12 precursor	15.26 ± 0.01↑	-	SP
2	93.10	82.7	464	NP_001334411.1	peroxidase 12 precursor	12.62 ± 0.00↑	-	SP
3	35.95	50.5	62	XP_004234138.1	suberization-associated anionic peroxidase 2-like	7.22 ± 0.04↑	-	SP
4	25.99	55.2	35	XP_004247506.1	peroxidase 44-like	5.38 ± 0.09↑	-	SP
5	24.78	41.1	24	NP_001296734.1	peroxidase 51 precursor	3.98 ± 0.03↑	-	SP
6	77.97	81.7	226	XP_004253400.1	peroxidase 70	3.85 ± 0.01↑	-	SP
7	34.48	50.2	46	XP_004231908.1	peroxidase 51	2.79 ± 0.06↑	-	SP
8	25.84	52.4	26	XP_004240883.1	peroxidase P7	2.79 ± 0.13↑	-	SP
9	67.98	66.0	203	NP_001334930.1	peroxidase superfamily protein precursor	-	3.55 ± 1.07↓	SP
10	49.69	74.4	110	XP_004245974.1	peroxidase 27-like	-	5.41 ± 0.62↓	SP
11	53.89	71.1	83	XP_004249055.1	cationic peroxidase 1	-	5.71 ± 1.03↓	SP
12	39.18	62.7	67	XP_004233538.1	peroxidase 72-like	-	12.94 ± 7.43↓	SP
13	44.14	74.1	96	XP_004251512.1	peroxidase 27	-	42.50 ± 2.41↓	SP

Fold changes with up arrow ("↑") and with down arrow ("↓") represent the increased and decreased in protein abundance in response to salt stress, respectively. '-' represent not identified. SP refers to the presence of a signal peptide sequence predicted by SignalP (version 4.0). NSP indicates nonclassical secretory proteins predicted by SecretomeP server 2.0 with an NN score > 0.600.

10.3389/fpls.2022.1023388

TABLE 4 KEGG pathway enriched based on the differentially abundant proteins (DAPs) both in IL8-3 and M82.

No.	Pathway ID	Term Description	Number of DAPs				
			IL8-3↑	IL8-3↓	M82↑	M82↓	Total
1	sly01100	Metabolic pathways	15	18	11	21	65
2	sly01110	Biosynthesis of secondary metabolites	12	10	6	15	43
3	sly00940	Phenylpropanoid biosynthesis	10	0	0	11	21
4	sly01200	Carbon metabolism	0	7	3	0	10
5	sly00620	Pyruvate metabolism	0	3	2	0	5
6	sly00010	Glycolysis/Gluconeogenesis	0	3	2	0	5
7	sly01230	Biosynthesis of amino acids	0	3	2	0	5
8	sly00250	Alanine, aspartate and glutamate metabolism	0	2	2	0	4
9	sly00190	Oxidative phosphorylation	0	3	0	3	6
10	sly00350	Tyrosine metabolism	2	0	3	0	5

The up and down arrow behind the cultivars represent increased and decreased protein abundance under salt stress, respectively.

genotypes (Figure 4). The first group included: auxin-induced in root cultures protein 12 (AIR12), 40S ribosomal protein S28 (RPS28) and 60S ribosomal protein L30 (RPL30). AIR12 was associated with signaling, and RPS28 and RPL30 were associated with secondary metabolite biosynthesis. The second group included multicopper oxidase-like protein precursor (MCOP) and xyloglucan-specific fungal endoglucanase inhibitor protein precursor (XEGIP). MCOP was characterized as a defense-related protein, and XEGIP was characterized as a cell wall modification. In the protein interaction groups, only the AIR12 and MCOP showed the opposite changes in IL8-3 and M82 in response to salt stress.

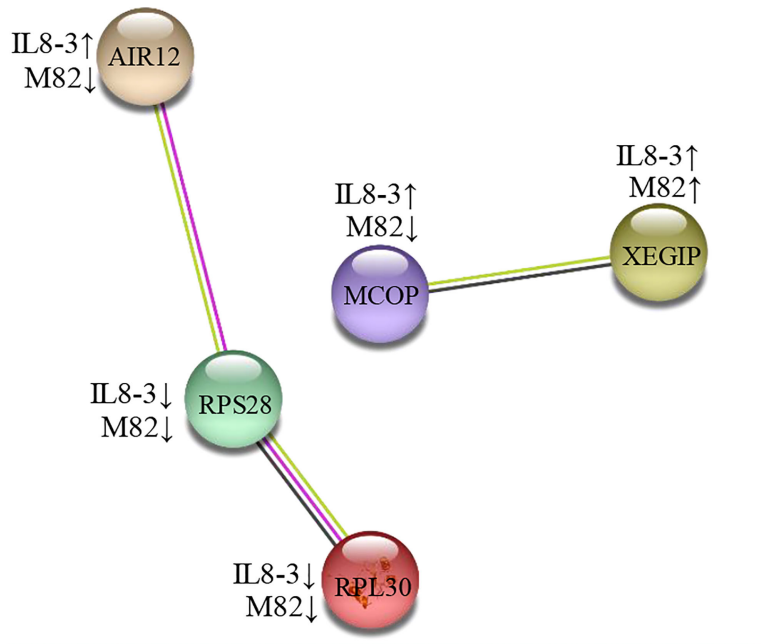

FIGURE 4
A protein interaction network of differentially abundant proteins (DAPs) under salt stress both of IL8-3 and M82. The network was built using a STRING software (https://string-db.org/) with medium confidence. The nodes represent the DAP, and the line color indicates the type of interaction evidence. The up and down arrow behind the cultivars represent increased and decreased in protein abundance under salt stress, respectively. AIR12, auxin-induced in root cultures protein 12; RPS28, 40S ribosomal protein S28; RPL30, 60S ribosomal protein L30, MCOP, multicopper oxidase-like protein precursor; XEGIP, xyloglucan-specific fungal endoglucanase inhibitor protein precursor.

4 Discussion

4.1 Common changes to the metabolic mechanism of IL8-3 and M82 under salt stress

Sixteen DAPs (approximately 20% of the identified DAPs) showed the same change trends under salt stress across both tomato genotypes (Table 1), which reflected the commonality of metabolic alterations in resistance to salt stress. Among these DAPs, ten were predicted to contain a signal peptide (Table 1). The DAPs that participate in cell wall modification, such as glucan endo-1,3-beta-glucosidase B precursor, which belongs to the glycoside hydrolases (GHs) family, increased in both tomato genotypes under salt stress. GHs play a key role in the degradation and reorganization of cell wall polysaccharides (Minic and Jouanin, 2006), and the alteration of cell wall polysaccharides may increase tolerance to salt stress in *Artemisia annua* (Corrêa-Ferreira et al., 2019). Xyloglucan-specific fungal endoglucanase inhibitor protein precursor (XEGIP) is involved in cell wall growth and play a vital role in plant defense. In addition, XEGIP-related proteins play a general role in protecting plants against biotic and abiotic stresses (Qin, 2003; Jones and Perez, 2014). The ethylene-responsive proteinase inhibitor 1 precursor and PLAT domain-containing protein (PLAT) 3, which are involved in signaling, also increased in both tomato genotypes under salt stress (Table 1). PLAT is a positive regulator of abiotic stress tolerance involved in the regulation of plant growth, and it might be a downstream target of the abscisic acid (ABA) signaling pathway (Hyun et al., 2014). In addition, the peptidyl-prolyl isomerases FKBP15-2, which negatively modulates lateral root development in *Arabidopsis* (Wang et al., 2020), also decreased in both tomato genotypes under salt stress in the present study. Taken together, these results indicated that both tomato genotypes have some common metabolic changes to resist salt stress.

4.2 Contrasting changes to the metabolic mechanisms of IL8-3 and M82 under salt stress

Nine DAPs (10% of the identified DAPs) showed contrasting changes between IL8-3 and M82 under salt stress. Interestingly, all 5 DAPs that predicted to have signal peptides increased in the salt-tolerant IL8-3 but decreased in the salt-sensitive M82 in response to salt stress (Table 1).

Cell wall localized peroxidase 72 plays an important role in lignification in *Arabidopsis* (Herrero et al., 2013). Salt stress induced the biosynthesis and deposition of lignin in the cell wall has been well reviewed (Oliveira et al., 2020). The aspartyl protease AED1 was induced locally and systemically during systemic acquired resistance signaling (Breitenbach et al., 2014). We speculated that the increase in peroxidase 72 and aspartyl protease AED3 might enhance the salt resistance of IL8-3.

Auxin-induced in root cultures protein 12 (AIR12) was interacted with RPS28 and RPL30 in the present study (Figure 4). AIR12 was predicted to function outside the cell, and the isolated AIRs from *Arabidopsis* were related to cell wall modification functions (Neuteboom et al., 1999). In addition, AIR12 is potentially involved in redox signaling and interacts directly with multicopper oxidase on the apoplastic side of the membrane for the directional growth of *Arabidopsis* roots (Sedbrook et al., 2002). These results indicated that in comparison to M82, the salt-tolerant tomato IL8-3 has a more positive metabolic resistance response to salt stress.

4.3 Differences in the mechanisms of responses to salt stress between the two tomato genotypes

Approximately 70% of the DAPs were only detected in IL8-3 or M82 respectively in response to salt stress. These results reflected that the two tomato ***genotype***s adapt to the salt stress by different metabolic changes.

4.3.1 Cell wall modification positively regulates salt tolerance in tomato

Since the alteration of cell wall components and structures is an important adaption to saline environments, the DAPs that participate in the cell wall metabolism were compared in the two tomato genotypes with contrasting salt tolerant. Most of the proteins related to cell wall metabolism were increased in the salt-tolerant tomato IL8-3 but decreased in the salt-sensitive tomato M82, in response to salt stress (Table 2). These proteins resulted in alterations to cell wall polysaccharides and lignification. Pectins play a vital role in determining cell wall properties. Pectin methylesterase was positively modulates the salt tolerance of *Arabidopsis* (Yan et al., 2018). In the present study, pectinesterases was increased in IL8-3 but decreased in M82 in response to salt stress (Table 2). Under salt stress, the primary and secondary cell walls expanded (Le Gall et al., 2015), and the cell walls of salt-tolerant plants usually became more rigid under salt stress (Muszyńska et al., 2014). Salt stress affects the secondary cell wall formation by altering lignin biosynthesis, which increases root lignification (Oliveira et al., 2020; Kong et al., 2021). The proteins related to lignification, such as lignin-forming anionic peroxidase and monocopper oxidase-like protein SKU5 were increased in IL8-3, while the dirigent protein 22 decreased in M82 (Table 2). These results indicated that the higher salt tolerance of IL8-3 than that of M82 was positively related to cell wall modification.

4.3.2 Peroxidases enhance the salt tolerance of tomato

Peroxidase is involved in ROS signaling and redox reactions. Plasma membrane NDPH-oxidase is activated when the plants are subjected to stress, and then, superoxide is released into the cell wall and spontaneously converted to H_2O_2. Peroxidase can remove H_2O_2 and result in the cross-linking of cell wall components (Wolf et al., 2012). In the present study, 8 peroxidases increased in IL8-3 and 5 peroxidases decreased in M82 in response to salt stress (Table 3). The peroxidase (POD) activity of IL8-3 was significantly higher than that of M82 in response to salt stress (Figure 2D). Overexpression of peroxidase also enhances the salt tolerance of soybean (Jin et al., 2019). Therefore, in comparison to M82, the salt-tolerant tomato IL8-3 has a better capacity for ROS scavenging than M82 in response to salt stress.

The peroxidase superfamily has three distantly related structural classes. Class III peroxidases containing N-terminal signal peptides secreted to the cell wall or surrounding medium and vacuoles are found in terrestrial plants (Duroux and Welinder, 2003). This class III peroxidase is mainly considered as cell wall-localized protein that plays a vital role in physiological functions and developmental processes, including cell wall hardening, pathogen penetration resistance, wounding and other abiotic stresses (Cosio and Dunand, 2009). Cell wall stiffening by peroxidases occurs mostly through lignin polymerization in cell walls (Francoz et al., 2015). Salt stress induces the gene expression of peroxidase, which has a putative role in cell wall lignification in *Ginkgo biloba* (Novo-Uzal et al., 2014). In the present study, all of the 13 peroxidases were predicted to have N-terminal signal peptides (Table 3). Therefore, these proteins might be different members of the class III peroxidases family, which could participate in the cell wall lignification. These results reflected that the peroxidase may facilitate tomato tolerance to salt stress and that the salt-tolerant tomato IL8-3 could better maintain the stability of the cell wall by increasing root cell wall lignification in response to salt stress.

4.4 Proposed molecular model of tomato salt stress

Based on the comparative analysis of cell wall proteomics and physiological differences between two tomato genotypes with contrasting tolerance to salt stress, a salt tolerance model of tomato was proposed (Figure 5). The two tomato genotypes with contrasting salt tolerances showed some common mechanisms under salt stress: the proteins involved in signaling and the cell wall polysaccharides increased in response to salt stress. In addition, the salt-tolerant tomato IL8-3 can efficiently modulate the metabolic pathways to resist salt stress. Cell wall lignification increased in IL8-3 because the proteins related to lignin metabolism increased under salt stress. Peroxidases with a signal peptide not only participates in regulating redox balance but also are involved in cell wall modification. These proteins increased under salt stress and caused IL8-3 to better regulate metabolic changes to resist salt stress.

5 Conclusions

Overall, a quantitative proteomic approach was performed to comprehensively study differential proteins in the cell walls of two tomato genotypes with contrasting salt tolerances. Enrichment of 82 and 81 proteins changed significantly in IL8-3 and M82, respectively. Fifty proteins were predicted to have signal peptides or nonclassical secretory proteins in both IL8-3 and M82. However, most of the proteins (70%) were only identified in IL8-3 or M82. Some common mechanisms that enable salt stress resistance, such as increasing signal

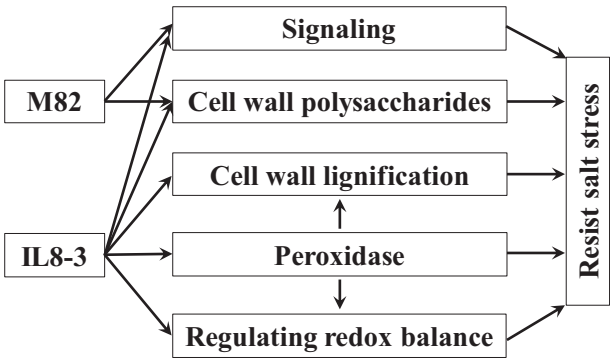

FIGURE 5
A proposed model of salt tolerance in tomato based on the cell wall proteomics of seedling roots. Arrows denote positive effects.

transduction and altering cell wall polysaccharides, were observed in the two tomato genotypes. However, the salt-tolerant tomato IL8-3, significantly decreased Na^+ accumulation and enhanced the regulation of the redox balance and cell wall metabolism in response to salt stress. Interestingly, these metabolic changes in the salt-sensitive M82 showed different or even opposite changes under salt stress. Compared to M82, IL8-3 better maintained plant growth, signal transduction, peroxidases activities and cell wall lignification in response to salt stress. The present study may provide novel insights for further understanding the molecular mechanisms of salt tolerance in tomato.

Data availability statement

The original contributions presented in the study are included in the article/Supplementary Material. Further inquiries can be directed to the corresponding authors.

Author contributions

SC: Methodology, Investigation, Writing-Original draft preparation. FS: Investigation, Data curation. CL: Visualization, software. QS and YR: Reviewing and Editing. All authors contributed to the article and approved the submitted version.

Funding

This study was supported by the Science and Technology Planning Project of Shenyang Municipality (Grant No. 21-110-3-06).

Conflict of interest

The authors declare that the research was conducted in the absence of any commercial or financial relationships that could be construed as a potential conflict of interest.

Publisher's note

All claims expressed in this article are solely those of the authors and do not necessarily represent those of their affiliated organizations, or those of the publisher, the editors and the reviewers. Any product that may be evaluated in this article, or claim that may be made by its manufacturer, is not guaranteed or endorsed by the publisher.

Supplementary material

The Supplementary Material for this article can be found online at: https://www.frontiersin.org/articles/10.3389/fpls.2022.1023388/full#supplementary-material

References

Adelaide, J., Vincent, B., and Elisabeth, J. (2018). Plant cell wall proteomics as a strategy to reveal candidate proteins involved in extracellular lipid metabolism. *Curr. Protein Pept. Sci.* 19, 190–199. doi: 10.2174/1389203718666170918152859

Albaladejo, I., Egea, I., Morales, B., Flores, F. B., Capel, C., Lozano, R., et al. (2018). Identification of key genes involved in the phenotypic alterations of *res* (*restored cell structure by salinity*) tomato mutant and its recovery induced by salt stress through transcriptomic analysis. *BMC Plant Biol.* 18, 213. doi: 10.1186/s12870-018-1436-9

Bai, Y., Kissoudis, C., Yan, Z., Visser, R. G. F., and Gerard, V. D. L. (2018). Plant behaviour under combined stress: tomato responses to combined salinity and pathogen stress. *Plant J.* 93 (4), 781–793. doi: 10.1111/tpj.13800

Bendtsen, J. D., Jensen, L. J., Blom, N., von Heijne, G., and Brunak, S. (2004). Feature-based prediction of non-classical and leaderless protein secretion. *Protein Eng. Des. Sel.* 17, 349–356. doi: 10.1093/protein/gzh037

Breitenbach, H. H., Wenig, M., Wittek, F., Jordá, L., Maldonado-Alconada, A. M., Sarioglu, H., et al. (2014). Contrasting roles of the apoplastic aspartyl protease APOPLASTIC, ENHANCED DISEASE SUSCEPTIBILITY1-DEPENDENT1 and LEGUME LECTIN-LIKE PROTEIN1 in *Arabidopsis* systemic acquired resistance. *Plant Physiol.* 165, 791–809. doi: 10.1104/pp.114.239665

Corrêa-Ferreira, M. L., Viudes, E. B., de Magalhães, P. M., Paixão de Santana Filho, A., Sassaki, G. L., Pacheco, A. C., et al. (2019). Changes in the composition and structure of cell wall polysaccharides from *Artemisia annua* in response to salt stress. *Carbohydr Res.* 483, 107753. doi: 10.1016/j.carres.2019.107753

Cosio, C., and Dunand, C. (2009). Specific functions of individual class III peroxidase genes. *J. Exp. Bot.* 60, 391–408. doi: 10.1093/jxb/ern318

Deinlein, U., Stephan, A. B., Horie, T., Luo, W., Xu, G., and Schroeder, J. I. (2014). Plant salt-tolerance mechanisms. *Trends Plant Sci.* 19, 371–379. doi: 10.1016/j.tplants.2014.02.001

Duroux, L., and Welinder, K. G. (2003). The peroxidase gene family in plants: a phylogenetic overview. *J. Mol. Evol.* 57, 397–407. doi: 10.1007/s00239-003-2489-3

Du, K., Zhao, W., Mao, Y., Lv, Z., Khattak, W. A., Ali, S., et al. (2022). Maize ear growth is stimulated at the fourth day after pollination by cell wall remodeling and changes in lipid and hormone signaling. *J. Sci. Food Agric.* 102 (12), 5429–5439. doi: 10.1002/jsfa.11896

Feiz, L., Irshad, M., Pont-Lezica, R. F., Canut, H., and Jamet, E. (2006). Evaluation of cell wall preparations for proteomics: a new procedure for purifying cell walls from *Arabidopsis* hypocotyls. *Plant Methods* 2, 10. doi: 10.1186/1746-4811-2-10

Francin-Allami, M., Merah, K., Albenne, C., Rogniaux, H., Pavlovic, M., Lollier, V., et al. (2015). Cell wall proteomic of *Brachypodium distachyon* grains: A focus on cell wall remodeling proteins. *Proteomics* 15, 2296–2306. doi: 10.1002/pmic.201400485

Francoz, E., Ranocha, P., Nguyen-Kim, H., Jamet, E., Burlat, V., and Dunand, C. (2015). Roles of cell wall peroxidases in plant development. *Phytochemistry* 112, 15–21. doi: 10.1016/j.phytochem.2014.07.020

Gong, B., Zhang, C., Li, X., Wen, D., Wang, S., Shi, Q., et al. (2014). Identification of NaCl and $NaHCO_3$ stress responsive proteins in tomato roots using iTRAQ-based analysis. *Biochem. Bioph. Res. Co.* 446, 417–422. doi: 10.1016/j.bbrc.2014.03.005

Herrero, J., Fernández-Pérez, F., Yebra, T., Novo-Uzal, E., Pomar, F., Pedreño, M.Á., et al. (2013). Bioinformatic and functional characterization of the basic

peroxidase 72 from *Arabidopsis thaliana* involved in lignin biosynthesis. *Planta* 237, 1599–1612. doi: 10.1007/s00425-013-1865-5

Hoffmann, J., Berni, R., Sutera, F. M., Gutsch, A., Hausman, J. F., Saffie-Siebert, S., et al. (2021). The effects of salinity on the anatomy and gene expression patterns in leaflets of tomato cv. micro-tom. *Genes (Basel)* 29, 12(8):1165. doi: 10.3390/genes12081165

Houston, K., Tucker, M. R., Chowdhury, J., Shirley, N., and Little, A. (2016). The plant cell wall: A complex and dynamic structure as revealed by the responses of genes under stress conditions. *Front. Plant Sci.* 7. doi: 10.3389/fpls.2016.00984

Hyun, T. K., Graaff, E., van der, Albacete, A., Eom, S. H., Großkinsky, D. K., Böhm, H., et al. (2014). The *Arabidopsis* PLAT domain protein1 is critically involved in abiotic stress tolerance. *PloS One* 9, e112946. doi: 10.1371/journal.pone.0112946

Jamet, E., Canut, H., Boudart, G., and Pont-Lezica, R. F. (2006). Cell wall proteins: a new insight through proteomics. *Trends Plant Sci.* 11, 33–39. doi: 10.1016/j.tplants.2005.11.006

Jin, T., Sun, Y., Zhao, R., Shan, Z., Gai, J., and Li, Y. (2019). Overexpression of peroxidase gene *GsPRX9* confers salt tolerance in soybean. *Int. J. Mol. Sci.* 20(15), 3745. doi: 10.3390/ijms20153745

Jones, R. W., and Perez, F. G. (2014). Constitutive expression of a XEGIP in potato results in phenotypic changes suggesting endogenous inhibition of cell wall growth. *Potato Res.* 57, 133–144. doi: 10.1007/s11540-014-9260-6

Jung, J. K. H., and McCouch, S. (2013). Getting to the roots of it: Genetic and hormonal control of root architecture. *Front. Plant Sci.* 4. doi: 10.3389/fpls.2013.00186

Komatsu, S., and Yanagawa, Y. (2013). Cell wall proteomics of crops. *Front. Plant Sci.* 4. doi: 10.3389/fpls.2013.00017

Kong, Q., Mostafa, H. H. A., Yang, W., Wang, J., Nuerawuti, M., Wang, Y., et al. (2021). Comparative transcriptome profiling reveals that brassinosteroid-mediated lignification plays an important role in garlic adaption to salt stress. *Plant Physiol. Biochem.* 158, 34–42. doi: 10.1016/j.plaphy.2020.11.033

Kou, X., Chen, X., Mao, C., He, Y., Feng, Y., Wu, C., et al. (2019). Selection and mechanism exploration for salt-tolerant genes in tomato. *J. Hortic. Sci. Biotechnol.* 94, 171–183. doi: 10.1080/14620316.2018.1486739

Le Gall, H., Philippe, F., Domon, J. M., Gillet, F., Pelloux, J., and Rayon, C. (2015). Cell wall metabolism in response to abiotic stress. *Plants (Basel)* 4, 112–166. doi: 10.3390/plants4010112

Liang, W., Ma, X., Wan, P., and Liu, L. (2018). Plant salt-tolerance mechanism: A review. *Biochem. Bioph. Res. Co.* 495, 286–291. doi: 10.1016/j.bbrc.2017.11.043

Ma, S., Gong, Q., and Bohnert, H. J. (2006). Dissecting salt stress pathways. *J. Exp. Bot.* 57, 1097–1107. doi: 10.1093/jxb/erj098

Minic, Z., and Jouanin, L. (2006). Plant glycoside hydrolases involved in cell wall polysaccharide degradation. *Plant Physiol. Biochem.* 44, 435–449. doi: 10.1016/j.plaphy.2006.08.001

Munns, R., and Tester, M. (2008). Mechanisms of salinity tolerance. *Annu. Rev. Plant Biol.* 59, 651–681. doi: 10.1146/annurev.arplant.59.032607.092911

Muszyńska, A., Jarocka, K., and Kurczynska, E. U. (2014). Plasma membrane and cell wall properties of an aspen hybrid (*Populus tremula* × *tremuloides*) parenchyma cells under the influence of salt stress. *Acta Physiol. Plant* 36, 1155–1165. doi: 10.1007/s11738-014-1490-3

Neuteboom, L. W., Ng, J. M., Kuyper, M., Clijdesdale, O. R., Hooykaas, P. J., and van der Zaal, B. J. (1999). Isolation and characterization of cDNA clones corresponding with mRNAs that accumulate during auxin-induced lateral root formation. *Plant Mol. Biol.* 39, 273–287. doi: 10.1023/a:1006104205959

Nielsen, H. (2017). "Predicting secretory proteins with SignalP," in *Protein function prediction: Methods and protocols, methods in molecular biology*. Ed. D. Kihara (New York, NY: Springer New York), pp 59–pp 73. doi: 10.1007/978-1-4939-7015-5_6

Novo-Uzal, E., Gutiérrez, J., Martínez-Cortés, T., and Pomar, F. (2014). Molecular cloning of two novel peroxidases and their response to salt stress and salicylic acid in the living fossil *Ginkgo biloba*. *Ann. Bot.* 114, 923–936. doi: 10.1093/aob/mcu160

Nveawiah-Yoho, P., Zhou, J., Palmer, M., Sauve, R., Zhou, S., Howe, K. J., et al. (2013). Identification of proteins for salt tolerance using a comparative proteomics analysis of tomato accessions with contrasting salt tolerance. *J. Am. Soc Hortic. Sci.* 138, 382–394. doi: 10.21273/JASHS.138.5.382

Oliveira, D. M., Mota, T. R., Salatta, F. V., Sinzker, R. C., Končitíková, R., Kopečný, D., et al. (2020). Cell wall remodeling under salt stress: Insights into changes in polysaccharides, feruloylation, lignification, and phenolic metabolism in maize. *Plant Cell Environ.* 43, 2172–2191. doi: 10.1111/pce.13805

Pailles, Y., Awlia, M., Julkowska, M. M., Passone, L., Zemmouri, K., Negrão, S., et al. (2020). Diverse traits contribute to salinity tolerance of wild tomato seedlings from the Galapagos islands. *Plant Physiol.* 182, 534–546. doi: 10.1104/pp.19.00700

Qin, Q. (2003). Discovery and characterization of a class of fungal endoglucanase inhibitor proteins from higher plants. DOCTOR OF PHILOSOPHY, The University of Georgia. Available at: https://getd.libs.uga.edu/pdfs/qin_qiang_200305_phd.pdf.

Quinet, M., Angosto, T., Yuste-Lisbona, F. J., Blanchard-Gros, R., Bigot, S., Martinez, J.-P., et al. (2019). Tomato fruit development and metabolism. *Front. Plant Sci.* 10. doi: 10.3389/fpls.2019.01554

Rivero, R. M., Mestre, T. C., Mittler, R., Rubio, F., Garcia-Sanchez, F., and Martinez, V. (2014). The combined effect of salinity and heat reveals a specific physiological, biochemical and molecular response in tomato plants. *Plant Cell Environ.* 37, 1059–1073. doi: 10.1111/pce.12199

Rui, Y., and Dinneny, J. R. (2020). A wall with integrity: surveillance and maintenance of the plant cell wall under stress. *New Phytol.* 225 (4), 1428–1439. doi: 10.1111/nph.16166

San, C. H., and Jamet, E. (2015). *WallProtDB*, a database resource for plant cell wall proteomics. *Plant Methods* 11 (1), 2. doi: 10.1186/s13007-015-0045-y

Sedbrook, J. C., Carroll, K. L., Hung, K. F., Masson, P. H., and Somerville, C. R. (2002). The *Arabidopsis SKU5* gene encodes an extracellular glycosyl phosphatidylinositol–anchored glycoprotein involved in directional root growth. *Plant Cell* 14, 1635–1648. doi: 10.1105/tpc.002360

Singh, J., Sastry, E. V. D., and Singh, V. (2012). Effect of salinity on tomato (*Lycopersicon esculentum* mill.) during seed germination stage. *Physiol. Mol. Biol. Plants* 18, 45–50. doi: 10.1007/s12298-011-0097-z

Szklarczyk, D., Franceschini, A., Wyder, S., Forslund, K., Heller, D., Huerta-Cepas, J., et al. (2015). STRING v10: protein-protein interaction networks, integrated over the tree of life. *Nucleic Acids Res.* 43, 447–452. doi: 10.1093/nar/gku1003

Wang, J., Sun, W., Kong, X., Zhao, C., Li, J., Chen, Y., et al. (2020). The peptidyl-prolyl isomerases FKBP15-1 and FKBP15-2 negatively affect lateral root development by repressing the vacuolar invertase VIN2 in *Arabidopsis*. *Planta* 252, 52. doi: 10.1007/s00425-020-03459-2

Wolf, S. (2017). Plant cell wall signalling and receptor-like kinases. *Biochem. J.* 474, 471–492. doi: 10.1042/BCJ20160238

Wolf, S. (2022). Cell wall signaling in plant development and defense. *Annu. Rev. Plant Biol.* 73, 323–353. doi: 10.1146/annurev-arplant-102820-095312

Wolf, S., Hématy, K., and Höfte, H. (2012). Growth control and cell wall signaling in plants. *Annu. Rev. Plant Biol.* 63, 381–407. doi: 10.1146/annurev-arplant-042811-105449

Yan, J., He, H., Fang, L., and Zhang, A. (2018). Pectin methylesterase31 positively regulates salt stress tolerance in. *Arabidopsis. Biochem. Bioph. Res. Co.* 496, 497–501. doi: 10.1016/j.bbrc.2018.01.025

Zaki, H. E. M., and Yokoi, S. (2016). A comparative *in vitro* study of salt tolerance in cultivated tomato and related wild species. *Plant Biotechnol. (Tokyo).* 33 (5), 361–372. doi: 10.5511/plantbiotechnology.16.1006a

Zörb, C., Geifus, C. M., and Dietz, K. J. (2019). Salinity and crop yield. *Plant Biol.* 1, 31–38. doi: 10.1111/plb.12884

Advantages of publishing in Frontiers

OPEN ACCESS
Articles are free to read for greatest visibility and readership

FAST PUBLICATION
Around 90 days from submission to decision

HIGH QUALITY PEER-REVIEW
Rigorous, collaborative, and constructive peer-review

TRANSPARENT PEER-REVIEW
Editors and reviewers acknowledged by name on published articles

Frontiers
Avenue du Tribunal-Fédéral 34
1005 Lausanne | Switzerland

Visit us: www.frontiersin.org
Contact us: frontiersin.org/about/contact

REPRODUCIBILITY OF RESEARCH
Support open data and methods to enhance research reproducibility

DIGITAL PUBLISHING
Articles designed for optimal readership across devices

FOLLOW US
@frontiersin

IMPACT METRICS
Advanced article metrics track visibility across digital media

EXTENSIVE PROMOTION
Marketing and promotion of impactful research

LOOP RESEARCH NETWORK
Our network increases your article's readership